INFORMATION TO USERS

This manuscript has been reproduced from the microfilm master. UMI films the text directly from the original or copy submitted. Thus, some thesis and dissertation copies are in typewriter face, while others may be from any type of computer printer.

The quality of this reproduction is dependent upon the quality of the copy submitted. Broken or indistinct print, colored or poor quality illustrations and photographs, print bleedthrough, substandard margins, and improper alignment can adversely affect reproduction.

In the unlikely event that the author did not send UMI a complete manuscript and there are missing pages, these will be noted. Also, if unauthorized copyright material had to be removed, a note will indicate the deletion.

Oversize materials (e.g., maps, drawings, charts) are reproduced by sectioning the original, beginning at the upper left-hand corner and continuing from left to right in equal sections with small overlaps. Each original is also photographed in one exposure and is included in reduced form at the back of the book.

Photographs included in the original manuscript have been reproduced xerographically in this copy. Higher quality 6" x 9" black and white photographic prints are available for any photographs or illustrations appearing in this copy for an additional charge. Contact UMI directly to order.

UMI

A Bell & Howell Information Company
300 North Zeeb Road, Ann Arbor MI 48106-1346 USA
313/761-4700 800/521-0600

UNIVERSITY OF OKLAHOMA
GRADUATE COLLEGE

INVESTIGATIONS INTO THE NEURODEGENERATIVE MODE OF ACTION OF DIHYDROXYTETRAHYDROQUINOLINE DERIVATIVES

A Dissertation
SUBMITTED TO THE GRADUATE FACULTY
in partial fulfillment of the requirements for the
degree of

Doctor of Philosophy

By
RUSSELL J. LEWIS
Norman, Oklahoma
1997

INVESTIGATIONS INTO THE NEURODEGENERATIVE MODE OF ACTION OF DIHYDROXYTETRAHYDROQUINOLINE DERIVATIVES

A DISSERTATION APPROVED FOR THE
DEPARTMENT OF CHEMISTRY AND BIOCHEMISTRY

BY

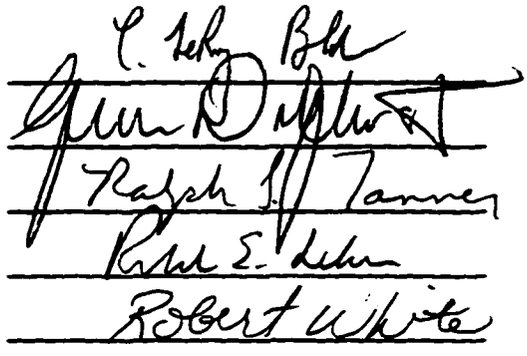

Acknowledgments

First and foremost, I would like to thank Dr. C. LeRoy Blank for his insight and guidance in my research. I could not have hoped for a better boss or friend. You were always there to talk to and bounce ideas off of. Your views on science and, more importantly, life were exciting. You always went above and beyond the call of duty. In this fast-paced and selfish world in which we live, it is nice to know someone who has not forgotten what is actually important. Dr. Blank, I will truly miss interacting with you on a daily basis.

While there are too many cherished friendships to mention here, a select few need to be addressed. Special thanks to Kris Wise, Mike, Eric, and Faith Lewis, Merlin "Duke" Kesselring, Steve "I must ride" and Denise, Jennifer "sunshine", Diane and John, and Barley and Hops, who stood by me through thick and thin and were willingly shared their ideas, and lack thereof, whenever and wherever needed. Friends like you are hard to come by...Thank you all very much.

I would like to thank Professors C.L. Blank, R.E. Lehr, G. Dryhurst, R. White, J. Robertson, and R. Tanner for serving on my Graduate Committee. Furthermore, the assistance obtained from Analytical Services has always been top-notch and greatly appreciated. I would like to thank the front office for their help and the Department of Chemistry and Biochemistry for its financial support.

My parents...what can I say. With out you, none of this would have been possible. Thank you for your love, patience, understanding, patience, moral support, and patience. While the verdict is still out, it is looking more and more as if I was worth raising after all...maybe. A mere thank you seems inadequate to express my gratitude, but I'm sure you know my feelings. And dad, the car analogies actually work.

"Happy is the man who has broken the chains which hurt the mind, and has given up worrying once and for all."

-Ovid

This dissertation, and all the work involved is dedicated to my father,

Mikal D. Lewis

my mother,

Roberta Kesselring

and my nephew,

Casey R. Lewis

Table of Contents

Chapter 1: Introduction

I. Introduction 1

II. Neurotransmission 2

A. The Neuron 2

B. Neurotransmitters 5

1. Catecholamines 6

2. Serotonin 9

III. Neurodegenerative Diseases & Other Mental Disorders 12

1. Alzheimer's Disease 12

2. Parkinson's Disease (PD) 13

3. Schizophrenia 14

4. Affective Disorders 15

IV. Neurotoxins 16

1. 6-Hydroxydopamine 17

2. MPTP 19

3. 5,7-Dihydroxytryptamine 21

V. Purpose of Dissertation Research 22

Chapter 2: Synthesis of 3-Aminomethyl-6,7-dihydroxy-1,2,3,4-tetrahydroquinoline & 3-Amino-6,8-dihydroxy-1,2,3,4-tetra-hydroquinoline

I. Introduction 25

II. Synthetic Summaries 27

A. Synthesis of 3-Aminomethyl-6,7-dihydroxy-1,2,3,4-tetrahydroquinoline Dihydrobromide 27
B. Synthesis of 3-Amino-6,8-dihydroxy-1,2,3,4-tetrahydroquinoline Dihydrobromide 32
III. Experimental 37
A. General Methods 37
B. Synthesis of 3-Aminomethyl-6,7-dihydroxy-1,2,3,4-tetrahydroquinoline Dihydrobromide 37
1. Dimethyl-3,4-dimethoxybenzylidenemalonate 37
2. Dimethyl-3,4-dimethoxybenzylmalonate 38
3. Dimethyl-4,5-dimethoxy-2-nitrobenzylmalonate 38
4. 3-Carboxymethyl-6,7-dimethoxy-1,2,3,4-tetrahydro-2-oxoquinoline 39
5. 3-Carboxamide-6,7-dimethoxy-1,2,3,4-tetrahydro-2-oxoquinoline 39
6. 3-Aminomethyl-6,7-dimethoxy-1,2,3,4-tetrahydroquinoline 40
7. 3-Aminomethyl-6,7-dihydroxy-1,2,3,4-tetrahydroquinoline • 2HBr 41
C. Synthesis of 3-Amino-6,8-dihydroxy-1,2,3,4-tetrahydroquinoline Hydrobromide 41
1. 4-(3,5-Dimethoxybenzylidene)-2-phenyl-5-oxazolone 41
2. Methyl-2-benzoylamino-3-(3,5-dimethoxyphenyl)-2-propenoate 42
3. Methyl-2-benzoylamino-3-(3,5-dimethoxyphenyl)propanoate 42
4. Methyl-2-benzoylamino-3-(3,5-dimethoxy-2-nitrophenyl)propanoate 43

5. 3-Benzoylamino-6,8-dimethoxy-1,2,3,4-tetrahydro-2-oxoquinoline 44
6. 3-Benzylamino-6,8-dimethoxy-1,2,3,4-tetrahydroquinoline 45
7. 3-Amino-6,8-dimethoxy-1,2,3,4-tetrahydroquinoline 45
8. 3-Amino-6,8-dihydroxy-1,2,3,4-tetrahydroquinoline•2HBr 46
IV. NMR Spectra and Assignments 47

Chapter 3: Basic Chromatography and Electrochemistry

I. Introduction 78
II. Chromatography 79
A. Migration of Solutes 79
B. Chromatographic Efficiency 81
C. Column Resolving Power 83
III. Electrochemistry 84
A. Electrochemical Detection 84
B. Voltammetry 87
IV. Conclusions 91

Chapter 4: Neurotoxicity

I. Introduction 92
II. Background 93
III. Experimental Design and Methods 96
A. Chemicals and Solutions 96
1. Chemicals 96
2. Stock Neurotransmitter and Metabolite Solutions 96
3. External Standard 98
4. Homogenization Solution 98

5. Isotonic Saline Solution 99
6. Toxin Solution Preparation 100
B. Chromatography 100
1. Chromatographic System 100
2. Mobile Phase 101
3. System Cleaning Procedure 102
4. Column Washing Procedure 102
5. Column Packing 103
6. Chromatographic Separation and Parameters 104
7. Calculation of Results 106
C. Experimental Procedures 107
1. LD_{50} 107
2. Intracerebroventricular Injection 109
3. Depletion 109
IV. Results and Discussion 111
A. LD_{50} 111
B. Depletion Studies 113
1. (±, +, and -)-6,7-ADTQ Investigations 113
2. 6,7-ADTQ, 6,7-AMDTQ, and 6,8-ADTQ Investigations 117
C. Behavioral Effects 120
V. Conclusions 121

Chapter 5: Mode of Action I : Uptake Interaction

I. Introduction 123
II. Background 124
III. Experimental Methods 129
A. Chemicals and Solutions 129

1. Chemicals 129
2. Homogenization Solution 130
3. Na^+ Tris-Krebs Buffer Solution 130
4. Li^+ Tris-Krebs Buffer Solution 131
5. Neurotransmitter Solution 132
6. Toxin Solution Preparation 133
7. Bicinconinic Acid Reagent 133
B. Methods and Procedures 134
1. Brain Removal 134
2. Preparation of Synaptosomes 135
3. Uptake/Blockade 136
4. Protein Analysis 137
IV. Results and Discussion 138
A. K_m Values for Transmitter Systems Tested 138
B. Uptake Blockade by 6,7-ADTQ and its Enantiomers 139
C. Toxin Uptake Blockade by Racemic 6,7-ADTQ, 6,7-AMDTQ, and 6,8-ADTQ 143
V. Conclusions 148

Chapter 6: Mode of Action II: Ease of Oxidation & Acid/Base Properties

I. Introduction 150
II. Experimental 152
A. Chemicals and Solutions 152
1. Chemicals 152
2. Toxin Solution for pK_a Studies 153
3. pK_a Buffer Solutions 153

B. Methods and Procedures 153
1. Ease of Oxidation 153
2. pK_a Determinations 154
3. pK_a Calculations 156
III. Results and Discussion 158
A. Ease of Oxidation 158
1. Formal Redox Potentials 158
2. Thermodynamic Considerations 159
B. Determination of the pK_a Values of Oxidized Toxin 160
1. 6,7-ADTQ 160
2. 6,7-AMDTQ 162
3. 6,8-ADTQ 164
4. 6-HDA 166
IV. Conclusions 168

Chapter 7: Mode of Action III: Autoxidation & Reactive Oxygen Species

I. Introduction 169
II. Background on Methods 171
III. Experimental 175
A. Chemicals and Solutions 175
1. Chemicals 175
2. Autoxidation Buffer 176
3. Toxin Solution 176
4. Fe^{2+} Stock Solution 176
5. Cu^{2+} Stock Solution 176
6. Fe^{2+}/EDTA Complex Solution 177

7. Catalase Solution 177
8. Superoxide Dismutase Solution 177
9. Diethylenetriaminepentacetic Acid (DTPA) Solution 178
10. Hydrogen Peroxide Solution 178
B. Autoxidation, Oxygen Electrode 178
1. Oxygen Electrode 178
2. Kinetic Measurements, Toxin Concentration Effects 178
3. Kinetic Measurements, Oxygen Concentration Effects 179
4. Kinetic Measurements, pH Effects 179
5. Toxin Autoxidation in Absence and Presence of Metal ions, Complexing Agents, & Enzymes 179
C. Autoxidation, Spectrophotometry 181
IV. Results 183
A. 6,7-ADTQ 183
B. 6,7-AMDTQ 193
C. 6,8-ADTQ 201
D. 6-HDA 209
V. Discussion 217
A. Rates of Autoxidation 217
1. Toxin Autoxidation Rates 217
2. Effects of SOD, Catalase, and H_2O_2 219
3. Role of Metal Ions in Autoxidation 221
4. Effects of Fe^{2+}/EDTA 224
B. Production of H_2O_2 From Autoxidation 224
1. Toxin effects 225
2. DTPA Effects 226
3. Metal Ion Effects 226

VI. Conclusions 229

Chapter 8: Mode of Action IV: Disruption of Mitochondrial Oxidative Phosphorylation

I. Introduction 231

II. Background 232

III. Methods and Materials 237

A. Chemicals and Solutions 237

1. Chemicals 237

2. Homogenization Buffer 237

3. Mitochondrial Incubation Buffer 238

4. Mitochondrial Substrate Solution 238

5. ADP Stock Solution 239

6. Toxin Stock Solution 239

B. Experimental 240

1. Animals 240

2. Liver Homogenate 240

3. Isolation of mitochondria 241

4. RCR Ratio, P/O Ratio & State 4 Rate 242

IV. Results and Discussion 244

A. 6,7-ADTQ 244

B. 6,7-AMDTQ 247

C. 6,8-ADTQ 251

D. 6-HDA 254

E. Toxin Effects on Mitochondria, A Toxin Comparison 258

1. Respiratory Control Ratios (RCR) 258

2. P/O Ratios 260

3. State 4 Respiration Rates 261

V. Conclusions 263

References 266

List of Tables

Table 2-1. Proton NMR signal assignments for 2 in $CDCl_3$. 49

Table 2-2. Proton NMR signal assignments for 3 in $CDCl_3$. 51

Table 2-3. Proton NMR signal assignments for 4 in $CDCl_3$. 53

Table 2-4. Proton NMR signal assignments for 5 in $CDCl_3$. 55

Table 2-5. Proton NMR signal assignments for 6 in DMSO-d6. 57

Table 2-6. Proton NMR signal assignments for 7 in $CDCl_3$. 59

Table 2-7. Proton NMR signal assignments for 8 in D_2O. 61

Table 2-8. Proton NMR signal assignments for 10 in $CDCl_3$. 63

Table 2-9. Proton NMR signal assignments for 11 in $CDCl_3$. 65

Table 2-10. Proton NMR signal assignments for 12 in $CDCl_3$. 67

Table 2-11. Proton NMR signal assignments for 13 in $CDCl_3$. 69

Table 2-12. Proton NMR signal assignments for 14 in $CDCl_3$. 71

Table 2-13. Proton NMR signal assignments for 15 in $CDCl_3$. 73

Table 2-14. Proton NMR signal assignments for 16 in $CDCl_3$. 75

Table 2-15. Proton NMR signal assignments for 17 in D_2O. 77

Table 4-1. 6,7-ADTQ effects on mouse whole brain neurotransmitter levels. 94

Table 4-2. 6,7-ADTQ effects on whole mouse brain neurotransmitter levels following pretreatment with desipramine and amfonelic acid. 95

Table 4-3. Stock neurotransmitter and metabolite solution preparation. 97

Table 4-4. External standard solution preparation. 98

Table 4-5. Homogenization solution preparation. 99

Table 4-6. Amounts of internal standard stock solutions used in preparation of the homogenization solution. 99

Table 4-7. Mobile phase preparation. 101

Table 4-8. LC tubing wash procedures. 102
Table 4-9. LC column wash procedure. 103
Table 4-10. Calculation of Results 106
Table 4-11. LD_{50} values in mice 112
Table 4-12. Whole mouse brain CNS neurotransmitter depletions 114
Table 4-13. Whole mouse brain CNS neurotransmitter depletions 114
Table 4-14. Survivability of mice 7 days after (±, +, and -)-6,7-ADTQ injection. 115
Table 4-15. Mouse whole brain neurochemical levels 7 days after treatment with "maximum usable" doses of (±)-, R-(+)-, and S-(-)-6,7-ADTQ. 116
Table 4-16. Mouse whole brain neurochemical levels 7 days after treatment with "maximum usable" doses of 6,7-ADTQ analogs. 118
Table 4-17. Mouse whole brain neurotransmitter effects of 6,7-ADTQ analogs and similar toxins at 7 days. 119
Table 5-1. Homogenization solution preparation. 130
Table 5-2. Na^+ Tris-Krebs buffer preparation. 131
Table 5-3. Li^+ Tris-Krebs buffer preparation. 132
Table 5-4. Bicinconinic acid reagent preparation. 134
Table 5-5. K_m values for NE, DA, and 5-HT uptake systems in rat brain synaptosomes. 138
Table 5-6. K_i values for 6,7-ADTQ and optical isomers. 142
Table 5-7. K_i values for 6,7-ADTQ, 6,7-AMDTQ, 6,8-ADTQ, and 6-HDA. 143
Table 6-1. Generation and sample period for oxidized toxins. 155
Table 6-2. Redox potentials for 6,7-ADTQ analogs and 6-HDA. 158
Table 7-1. Fe^{2+}/EDTA solution preparation. 177
Table 7-2. 6,7-ADTQ autoxidation reaction orders with respect to individual components. 188

Table 7-3. 6,7-ADTQ autoxidation, initial rate of oxygen consumption. 189
Table 7-4. 6,7-ADTQ autoxidation, H_2O_2 and $\bullet O_2^-$ produced. 190
Table 7-5. 6,7-AMDTQ autoxidation reaction orders with respect to individual components. 197
Table 7-6. 6,7-AMDTQ autoxidation, initial rate of oxygen consumption. 198
Table 7-7. 6,7-AMDTQ autoxidation, H_2O_2 and $\bullet O_2^-$ produced. 199
Table 7-8. 6,8-ADTQ autoxidation reaction orders with respect to individual components. 205
Table 7-9. 6,8-ADTQ autoxidation, initial rate of oxygen consumption. 206
Table 7-10. 6,8-ADTQ autoxidation, H_2O_2 and $\bullet O_2^-$ produced. 207
Table 7-11. 6-HDA autoxidation reaction orders with respect to individual components. 213
Table 7-12. 6-HDA autoxidation, initial rate of oxygen consumption. 214
Table 7-13. 6-HDA autoxidation, H_2O_2 and $\bullet O_2^-$ produced. 215
Table 7-14. A toxin comparison of autoxidation reaction orders and rate constants. 218
Table 8-1. Homogenization buffer preparation. 238
Table 8-2. Mitochondrial substrate solution preparation. 239
Table 8-3. 6,7-ADTQ effects on mitochondrial function. 244
Table 8-4. 6,7-AMDTQ effects on mitochondrial function. 248
Table 8-5. 6,8-ADTQ effects on mitochondrial function. 252
Table 8-6. 6-HDA effects on mitochondrial function. 255
Table 8-7. RCR values of various toxins. 258
Table 8-8. P/O values of various toxins. 260
Table 8-9. State 4 respiration rates of various toxins. 262
Table 8-10. pK_a values of oxidized toxins and standard uncoupling agents. 264

List of Figures

Figure 1-1. A typical neuron using dopamine (DA) as a transmitter. 4
Figure 1-2. Catecholamine biosynthesis. 7
Figure 1-3. Dopamine catabolic pathways. 8
Figure 1-4. Norepinephrine catabolic pathways. 9
Figure 1-5. Serotonin biosynthesis. 10
Figure 1-6. Serotonin catabolic pathways and biosynthesis of melatonin. 11
Figure 2-1. Proton NMR spectum of 2 in $CDCl_3$. 48
Figure 2-2. Proton NMR spectum 3 in $CDCl_3$. 50
Figure 2-3. Proton NMR spectum of 4 in $CDCl_3$. 52
Figure 2-4. Proton NMR spectum of 5 in $CDCl_3$. 54
Figure 2-5. Proton NMR spectum of 6 in DMSO-d6. 56
Figure 2-6. Proton NMR spectum of 7 in $CDCl_3$. 58
Figure 2-7. Proton NMR spectum of 8•2HBr in D_2O. 60
Figure 2-8. Proton NMR spectum of 10 in $CDCl_3$. 62
Figure 2-9. Proton NMR spectum of 11 in $CDCl_3$. 64
Figure 2-10. Proton NMR spectum of 12 in $CDCl_3$. 66
Figure 2-11. Proton NMR spectum of 13 in $CDCl_3$. 68
Figure 2-12. Proton NMR spectum of 14 in $CDCl_3$. 70
Figure 2-13. Proton NMR spectum of 15 in $CDCl_3$. 72
Figure 2-14. Proton NMR spectum of 16 in $CDCl_3$. 74
Figure 2-15. Proton NMR spectum of 17•2HBr in D_2O. 76
Figure 3-1. Chromatographic elution profile. 80
Figure 3-2. Representative cyclic voltammogram. 87
Figure 3-3. Hydrodynamic voltammograms for two oxidizable compounds. 91

Figure 4-1. A typical LCEC chromatogram for a brain sample..... 105
Figure 4-2. LD_{50} determination and calculation for 6,8-ADTQ..... 111
Figure 4-3. Mouse whole brain neurotransmitter depletions by (±,+,and-)-6,7-ADTQ..... 116
Figure 4-4. Whole mouse brain depletion by 6,7-ADTQ, 6,7-AMDTQ, and 6,8-ADTQ. 118
Figure 5-1. 5-HT K_m determination using a Lineweaver-Burk plot..... 139
Figure 5-2. K_i determination using a modified Lineweaver-Burk double reciprocal plot. 140
Figure 5-3. K_i determination using an IC_{50} approach for S-(-)-6,7-ADTQ blockade of NE..... 141
Figure 5-4. 6,8-ADTQ effects on NE uptake..... 144
Figure 5-5. 6,8-ADTQ effects on DA uptake 145
Figure 6-1. Oxidation of 6,7-ADTQ showing probable forms of the oxidized toxin. 152
Figure 6-2. UV-VIS spectra of ox-6,7-ADTQ at various pH values. 161
Figure 6-3. pK_a determination for ox-6,7-ADTQ. 162
Figure 6-4. UV-VIS spectra of ox-6,7-AMDTQ at various pH values..... 163
Figure 6-5. pK_a determination for ox-6,7-AMDTQ. 164
Figure 6-6. pK_a determination for ox-6,8-ADTQ. 165
Figure 6-7. UV-VIS spectra of ox-6-HDA at various pH values..... 166
Figure 6-8. pK_a determination for ox-6-HDA. 167
Figure 7-1. Typical autoxidation oxygen trace. 172
Figure 7-2. UV-VIS spectra of 6,7-ADTQ autoxidation at pH 5.4 and 25°C. 185
Figure 7-3. Toxin concentration effects on 6,7-ADTQ autoxidation. 186
Figure 7-4. Oxygen concentration effects on 6,7-ADTQ autoxidation. 187
Figure 7-5. The effects of pH on 6,7-ADTQ autoxidation rate. 187

Figure 7-6. UV-VIS spectra of 6,7-AMDTQ autoxidation at pH 7.4 and 25°C. 194
Figure 7-7. Toxin concentration effects on 6,7-AMDTQ autoxidation. 195
Figure 7-8. Oxygen concentration effects on 6,7-AMDTQ autoxidation. 196
Figure 7-9. The effects of pH on 6,7-AMDTQ autoxidation. 196
Figure 7-10. UV-VIS spectra of 6,8-ADTQ autoxidation at pH 7.4 and 37°C. 202
Figure 7-11. Toxin concentration effects on 6,8-ADTQ autoxidation. 203
Figure 7-12. Oxygen concentration effects on 6,8-ADTQ autoxidation. 204
Figure 7-13. The effects of pH on 6,8-ADTQ autoxidation. 204
Figure 7-14. UV-VIS spectra of 6-HDA autoxidation at pH 7.4 and 37°C. 210
Figure 7-15. Toxin concentration effects on 6-HDA autoxidation. 211
Figure 7-16. Oxygen concentration effects on 6-HDA autoxidation. 212
Figure 7-17. The effects of pH on 6-HDA autoxidation. 212
Figure 7-18. Rates of autoxidation of the quinoline agents and 6-HDA. 218
Figure 7-19. Possible autoxidation mechanisms of 6-HDA. 220
Figure 7-20. A toxin comparison of the rates of autoxidation in the presence of 100 μM Fe^{2+} in % controls. 222
Figure 7-21. A toxin comparison of the rates of autoxidation in the presence of 10 μM Cu^{2+} in % controls. 222
Figure 7-22. A toxin comparison of the rates of autoxidation in the presence of 10^{-3} M DTPA in % controls. 223
Figure 7-23. Oxygen consumed during autoxidation leading to the production of H_2O_2. 226
Figure 7-24. Oxygen consumed during toxin autoxidation, in the presence of 10^{-4} M Fe^{2+}, leading to the production of H_2O_2. 228
Figure 7-25. Oxygen consumed during autoxidation, in the presence of 10^{-4} M Fe^{2+}/EDTA, leading to the production of H_2O_2. 229

Figure 8-1. Typical O_2 trace showing stimulated and non-stimulated mitochondrial respiration. 233
Figure 8-2. Typical effects of an inhibitor on ADP stimulated respiration. 235
Figure 8-3. The effects of an uncoupler on non-ADP stimulated respiration. 236
Figure 8-4. 6,7-ADTQ effects on RCR. 245
Figure 8-5. 6,7-ADTQ effects on P/O ratio. 246
Figure 8-6. 6,7-ADTQ effects on state 4 rate. 246
Figure 8-7. 6,7-AMDTQ effects on RCR. 249
Figure 8-8. 6,7-AMDTQ effects on P/O ratio. 250
Figure 8-9. 6,7-AMDTQ effects on state 4 rate. 250
Figure 8-10. 6,8-ADTQ effects on RCR. 252
Figure 8-11. 6,8-ADTQ effects on P/O ratio. 253
Figure 8-12. 6,8-ADTQ effects on state 4 rate. 253
Figure 8-13. 6-HDA effects on RCR. 256
Figure 8-14. 6-HDA effects on P/O ratio. 256
Figure 8-15. 6-HDA effects on state 4 rate. 257

List of Schemes

Scheme 2-1. Synthesis of dimethyl-3,4-dimethoxybenzylidenemalonate 27

Scheme 2-2. Synthesis of dimethyl-3,4-dimethoxybenzylmalonate 28

Scheme 2-3. Formation of dimethyl-4,5-dimethoxy-2-nitrobenzylmalonate 28

Scheme 2-4. Synthesis of 3-Carboxymethyl-6,7-dimethoxy-1,2,3,4-tetrahydro-2-oxoquinoline 29

Scheme 2-5. Synthesis of 3-carboxamide-6,7-dimethoxy-1,2,3,4-tetrahydro-2-oxoquinoline 30

Scheme 2-6. Synthesis of 3-aminomethyl-6,7-dimethoxy-1,2,3,4-tetrahydroquinoline 31

Scheme 2-7. Synthesis of 3-aminomethyl-6,7-dihydroxy-1,2,3,4-tetrahydroquinoline•2HBr 31

Scheme 2-8. Formation of 4-(3,5-dimethoxybenzylidene)-2-phenyl-5-oxazolone 32

Scheme 2-9. Synthesis of methyl-2-benzoylamino-3-(3,5-dimethoxyphenyl)-2-propenoate 32

Scheme 2-10. Formation of methyl-2-benzoylamino-3-(3,5-dimethoxyphenyl)propanoate 33

Scheme 2-11. Synthesis of methyl-2-benzoylamino-3-(3,5-dimethoxy-2-nitrophenyl)propanoate 34

Scheme 2-12. Formation of 3-benzoylamino-6,8-dimethoxy-1,2,3,4-tetrahydro-2-oxoquinoline 34

Scheme 2-13. Formation of 3-benzylamino-6,8-dimethoxy-1,2,3,4-tetrahydroquinoline 35

Scheme 2-14. Synthesis of 3-amino-6,8-dimethoxy-1,2,3,4-tetrahydroquinoline 35

Scheme 2-15. Formation of 3-amino-6,8-dihydroxy-1,2,3,4-tetrahydroquinoline•2HBr 36

List of Abbreviations

Ac	acetyl
ACh	acetylcholine
AD	Alzheimer's disease
6-ADA	6-aminodopamine
α-6-ADA	α-methyl-6-aminodopamine
A.D.	aldehyde dehydrogenase
ADTQ	3-amino-6,7-dihydroxy-1,2,3,4-tetrahydroquinoline
A.I.	various aldehyde intermediates
app	apparent
A.R.	aldehyde reductase
b	broad
CNS	central nervous system
COMT	catechol-O-methyltransferase
CV	cyclic voltammetry
CSF	cerebrospinal fluid
d	doublet
DA	dopamine
dd	doublet of a doublet
ddd	doublet of a doublet of a doublet
DβH	dopamine-β-hydroxylase
5,6-DHI	5,6-dihydroxyindole
5,6-DHT	5,6-dihydroxytryptamine
5,7-DHT	5,7-dihydroxytryptamine
DMSO	dimethylsulfoxide

DOPA	3,4-dihydroxyphenylalanine
DOPAC	3,4-dihydroxyphenylacetic acid
EC	electrochemical detection
EPI	epinephrine
EPIN	epinine
eV	electron volt(s)
FAB	fast atom bombardment
g	gram
GABA	γ-aminobutyric acid
h	hour
HPLC	high performance liquid chromatography
6-HDA	6-hydroxydopamine
6-HDAQ	6-hydroxydopamine-*p*-quinone
5-HIAA	5-hydroxyindoleacetic acid
5-HT	5-hydroxytryptamine
5-HTPP	5-hydroxytryptaphan
HVA	homovanillic acid
Hz	hertz
J	NMR coupling constant
LSV	linear sweep voltammetry
m	multiplet
MAO	monoamine oxidase
M	molar
Me	methyl
mg	milligram
MHz	megahertz
min	minute(s)

mL	milliliter
µL	microliter
mol	mole
mmol	millimole
µmol	micromole
nmol	nanomole
MPTP	1-methyl-4-phenyl-1,2,3,6-tetrahydropyridine
$MPDP^+$	1-methyl-4-phenyl-2,3-dihydropyridinium
MPP^+	1-methyl-4-phenylpyridinium
MS	mass spectroscopy
3-MT	3-methoxytryptamine
NE	norepinephrine
NM	metanephrine
NMR	nuclear magnetic reasonance
N-MET	N-methylserotonin
PD	Parkinson's disease
Ph	phenyl
R	alkyl
s	singlet
t	triplet
TH	tyrosine hydroxylase
THF	tetrahydrofuran
UV-VIS	ultra-violet and visible spectrophotometry

Abstract

Preliminary testing of a dihydroxyquinoline derivative, 3-amino-6,7-dihydroxy-1,2,3,4-tetrahydroquinoline (6,7-ADTQ), showed substantial serotonergic depletion in mouse whole brain, but with only moderate selectivity. This preliminary finding warranted further examination of this type of novel neurotoxin. Thus, we synthesized two additional derivatives, 3-aminomethyl-6,7-dihydroxy-1,2,3,4-tetrahydroquinoline (6,7-AMDTQ) and 3-amino-6,8-dihydroxy-1,2,3,4-tetrahydroquinoline (6,8-ADTQ). We then investigated these neurotoxins in an attempt to establish a relationship between the physical and/or chemical nature of these toxins and their neurodegenerative abilities. The importance of chirality in this class of neurotoxins was also investigated. The extent of neuronal destruction afforded by these toxins was measured as their ability to elicit long-term depletion of endogenous transmitters. Two of the three agents elicited 5-HT depletions equal to or greater than that attainable using generally accepted 5-HT neurotoxins. From initial depletion studies, we found no advantage in employing enantiomers over that of the racemic agent. The uptake blockade interaction of the toxic agents with NE, DA, and 5-HT transport sites appears to be competitive in nature, with K_i values ranging from 14 to 280 μM and an apparent facilitation of uptake for NE and DA with 6,8-ADTQ. Investigation of autoxidation showed that oxidation rates of 6,7-analogs were rapid and increased in the presence of metal ions, while the 6,8- analog showed an overall slower rate and no significant rate change upon addition of metal ions. Examination of reactive O_2 species produced during autoxidation showed the majority of O_2 consumed during oxidation led to the production of H_2O_2. This H_2O_2 generally decreased with an increase in metal ion concentration, presumably as a result of $\bullet OH$ production *via* Fenton mechanisms. Pathways leading to the production of $\bullet O_2^-$ appeared to be negligible. Mitochondrial oxidative phosphorylation effects indicate primarily an uncoupling of oxidative phosphorylation by these agents.

Synthesis and Neurodegenerative Mode of Action of Dihydroxytetrahydroquinoline Derivatives

Introduction

Chapter 1

I. Introduction

The brain is the most complex organ in the human body. It contains 10^{10} - 10^{12} neurons, each typically making thousands of connections with other neurons. These multiple interconnections between neurons result in the ability to feel and show emotions and are responsible for the cognizant understanding of what you are reading right now. The brain is the origin of all qualities which embody and define humanity.

The laboratory of Dr. C. LeRoy Blank has long been interested in chemically induced neurotoxicity in the brain. Neurotoxins, chemicals that destroy nerve cells, can be used for a wide variety of neuro-applications. They are particularly useful in producing animal models of neurochemical disorders. Additionally, these chemicals can be used to elucidate the function of specific regions and tracts in the brain. By more fully understanding the actions of neurotoxic chemicals, we may obtain insight into the phenomena collectively known as neurodegeneration. This chapter briefly discusses neurotransmission, neuroanatomy, neurotransmitters, mental disorders resulting from neuron and/or neurotransmitter abnormalities, and neurotoxins.

II. Neurotransmission

A. The Neuron[1-5]

While not the most abundant cells in the central nervous system, neurons are the most important. The fundamental role of a neuron is "communication", i.e., the receiving, integrating, and transmission of neuronal signals. Many characteristics of a given nerve cell in the central nervous system (CNS), including its size, shape, cellular components, and connections, is directly related to its specific function in the brain.

Neurons communicate through the use of electrical and chemical signals. Neurons release neurotransmitters at a site of contact with another neuron called a synapse (see Figure 1-1). At this synapse, there is a functionally specific region of the membrane on the presynaptic neuron where one or more neurochemical transmitters are released. The neurotransmitter(s) diffuse(s) across the synaptic cleft (20-40 nm) and binds to receptor(s) on the postsynaptic neuron. The binding of a neurotransmitter to a receptor causes an electrical signal in the postsynaptic cell which is propagated through that cell and subsequently causes the release, or repression of release, of a

neurotransmitter(s) at the succeeding synapse. The final event in neurotransmission at a single synapse is the termination of neurotransmitter-induced receptor activation. This is predominantly accomplished through a mechanism known as reuptake, whereby released neurotransmitters are selectively returned to the cytoplasm of the presynaptic nerve terminal *via* selective uptake sites. Once inside the nerve terminal the neurotransmitter can be repackaged into vesicles for future neurotransmission or can be metabolically inactivated. Termination of receptor activation may also occur by neurotransmitter metabolism in the synaptic cleft and/or diffusion away from receptor sites.

The neuron is primarily comprised of three basic parts: dendrites, a cell body, and an axon. In order to accommodate many incoming synaptic connections, neurons may have a highly branched network of dendrites (see Figure 1-1). Dendrites are neuronal processes which receive synaptic input from other neurons. They have receptors and other components designed to convert chemical transmissions into electrical signals. Dendrites integrate these electrical signals with other incoming signals and pass the integrated result to the cell body.

The cell body of a neuron, often referred to as the soma, is responsible for the synthesis of essential enzymes and proteins. It contains the nucleus, endoplasmic reticulum, lysosomes, mitochondria and other cellular components required for normal cell functions. The soma plays a large role in the integration of electrical signals coming from the dendrites. Furthermore, the soma may also have many incoming synapses, by which it directly receives chemical information.

The axon is a long, thin neuronal process which is responsible for sending outgoing electrical information to the synapse (see Figure 1-1). At the base of the axon, called the axon hillock, the integrated electrical signals from the dendrites and the soma form an all-or-nothing electrical signal called the action potential. This action potential travels down the axon to the presynaptic nerve terminal and triggers a calcium dependent release of neurotransmitters.

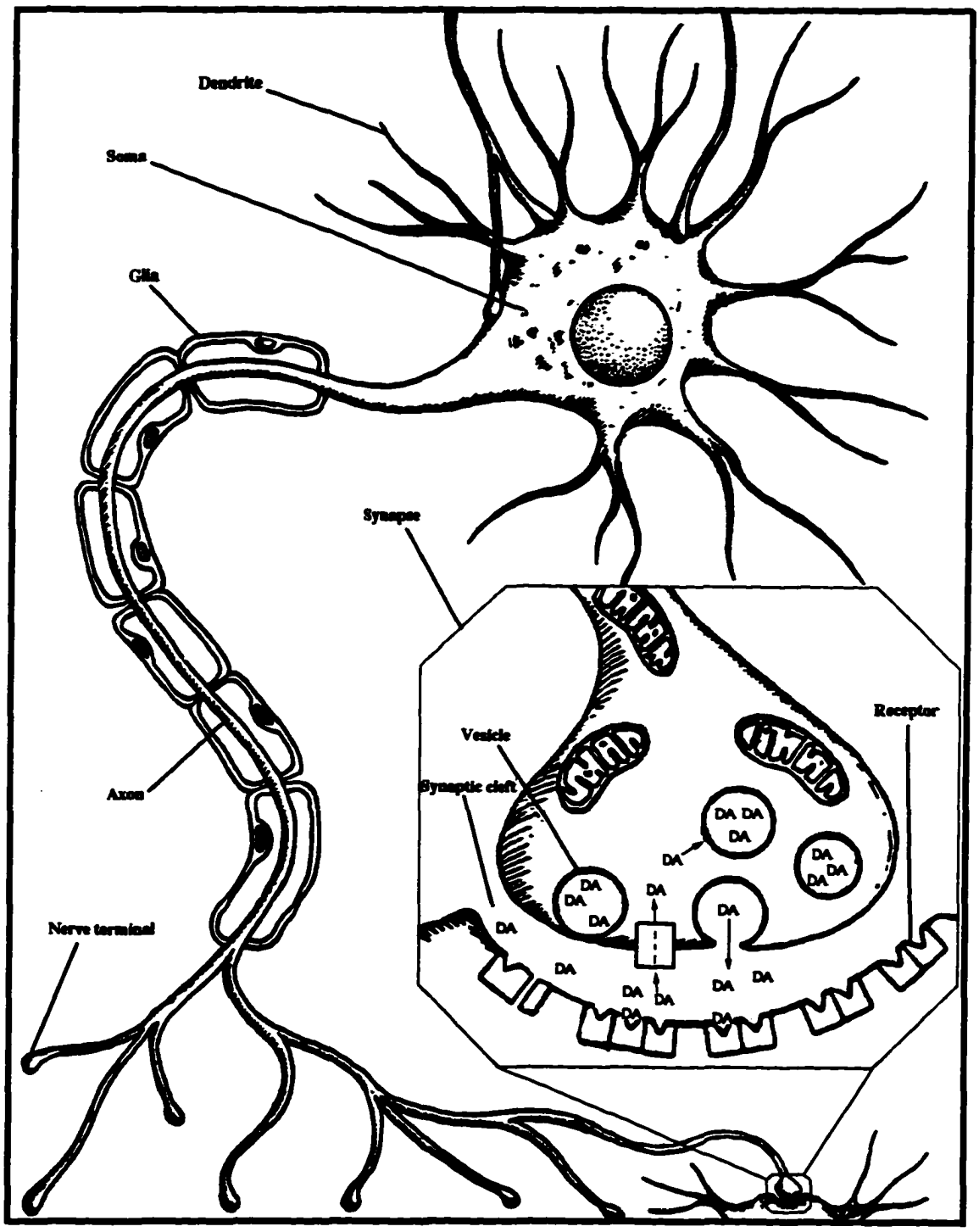

Figure 1-1. A typical neuron using dopamine (DA) as a transmitter.[6]

The presynaptic nerve terminal possesses both neurotransmitter reuptake sites and autoreceptors. Autoreceptors , among other things, can regulate neurotransmitter release.

A neuron contains only one axon; however, an axon may be branched, giving rise to multiple nerve terminals.

The neurotransmission process described above is primarily pertinent to neurotransmitters evoking an excitatory electrical change in the postsynaptic membrane potential *via* ion-channel linked receptors. However, neurotransmitters can also evoke electrical inhibition. Additionally, they can also regulate cellular function by a different means than an electrical event. Some neurotransmitters, when released, activate second messenger linked receptors coupled to G proteins. Activation of this type of receptor can result in the indirect regulation of neuron growth, metabolism, gene expression, and structural effects, along with or in addition to activation of ion channels. Therefore, neurotransmission may either integrate and pass on information or modify the cellular interworkings of a neuron.

In the brain, there are also non-neuronal cells that support the nervous system and are broadly classified as glial cells or glia. Glial cells line the internal and external surfaces of the brain, act as a boundary between blood vessels and neurons, wrap around axons forming myelin, surround synapses, and fill the spaces between neurons.

While this is a very brief discussion of the neuron and the neurochemical transmission process, many comprehensive overviews exist[1-5] which are not only enlightening, but also exciting to read.

B. Neurotransmitters

Neurotransmitters are the chemical substances which, when released by neurons, provide communication. There are many chemicals in the brain which have been identified as putative neurotransmitters. However, to be considered a neurotransmitter, a chemical must meet some very exacting criteria. A neurochemical must be localized in the presynaptic terminal and must be released upon axon stimulation in quantities sufficient

enough to evoke a response at postsynaptic receptors. Appropriate precursor enzymes for anabolism and catabolism of the neurotransmitter must also be localized in the presynaptic nerve terminal or vicinity. There must exist a mechanism by which inactivation of the released, extracellular neurotransmitter can occur. Furthermore, when exogenously supplied, the neurochemical should evoke a similar response to that of the endogenously released compound. Chemicals which meet all of these criteria are called neurotransmitters. Compounds which meet some, but not all, of the above criteria are called putative neurotransmitters. Of the many known and putative neurotransmitters in the brain, our current research efforts have been focused on the catecholaminergic and serotonergic neurotransmitters.

1. Catecholamines

The catecholaminergic neurotransmitters consist of dopamine (DA), norepinephrine (NE), and epinephrine (EPI). These transmitters are shown in Figure 1-2. They all contain a catechol ring with an ethylamine side chain. The biosyntheses of these neurotransmitters, which all begin with L-tyrosine, are also presented in Figure 1-2. L-Tyrosine is an amino acid that is obtained through the diet. The first step, the conversion of L-tyrosine to L-3,4-dihydroxyphenylalanine (L-DOPA) *via* tyrosine hydroxylase (TH), represents the rate limiting step in the syntheses of these compounds. Through the action of L-aromatic amino acid decarboxylase (L-AAAD), L-DOPA is converted to dopamine (DA). In dopaminergic neurons this represents the final step in the synthetic pathway. In noradrenergic and adrenergic neurons, dopamine-β-hydroxylase (DβH) converts DA to norepinephrine (NE). And, in adrenergic neurons, phenethanolamine-N-methyltransferase (PNMT) adds a methyl group to the amine of NE to produce epinephrine (EPI). These neurotransmitters are packaged in vesicles to await release during neurotransmission. The catabolic pathways for DA and NE are shown in Figures 1-3 and 1-4, respectively.

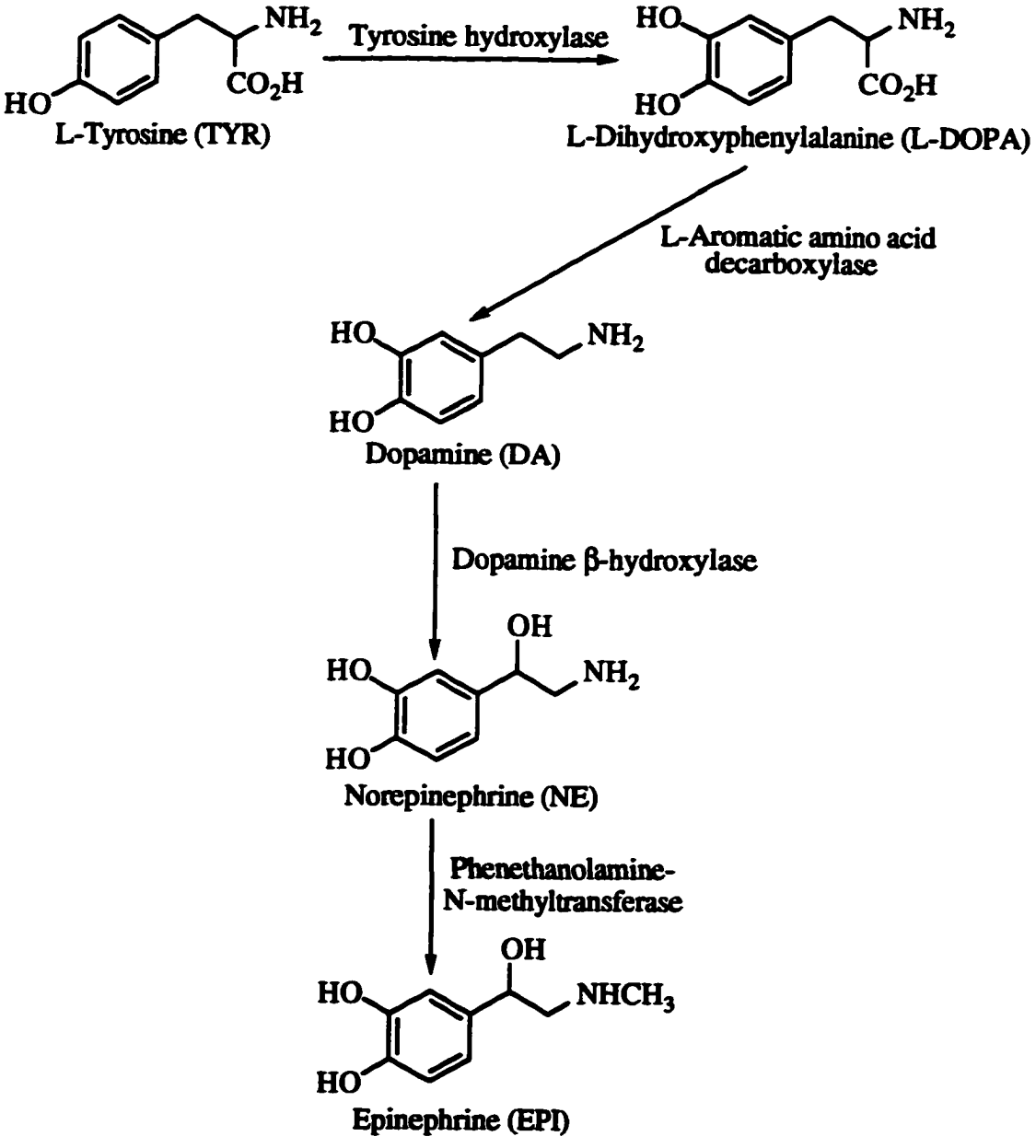

Figure 1-2. Catecholamine biosynthesis.

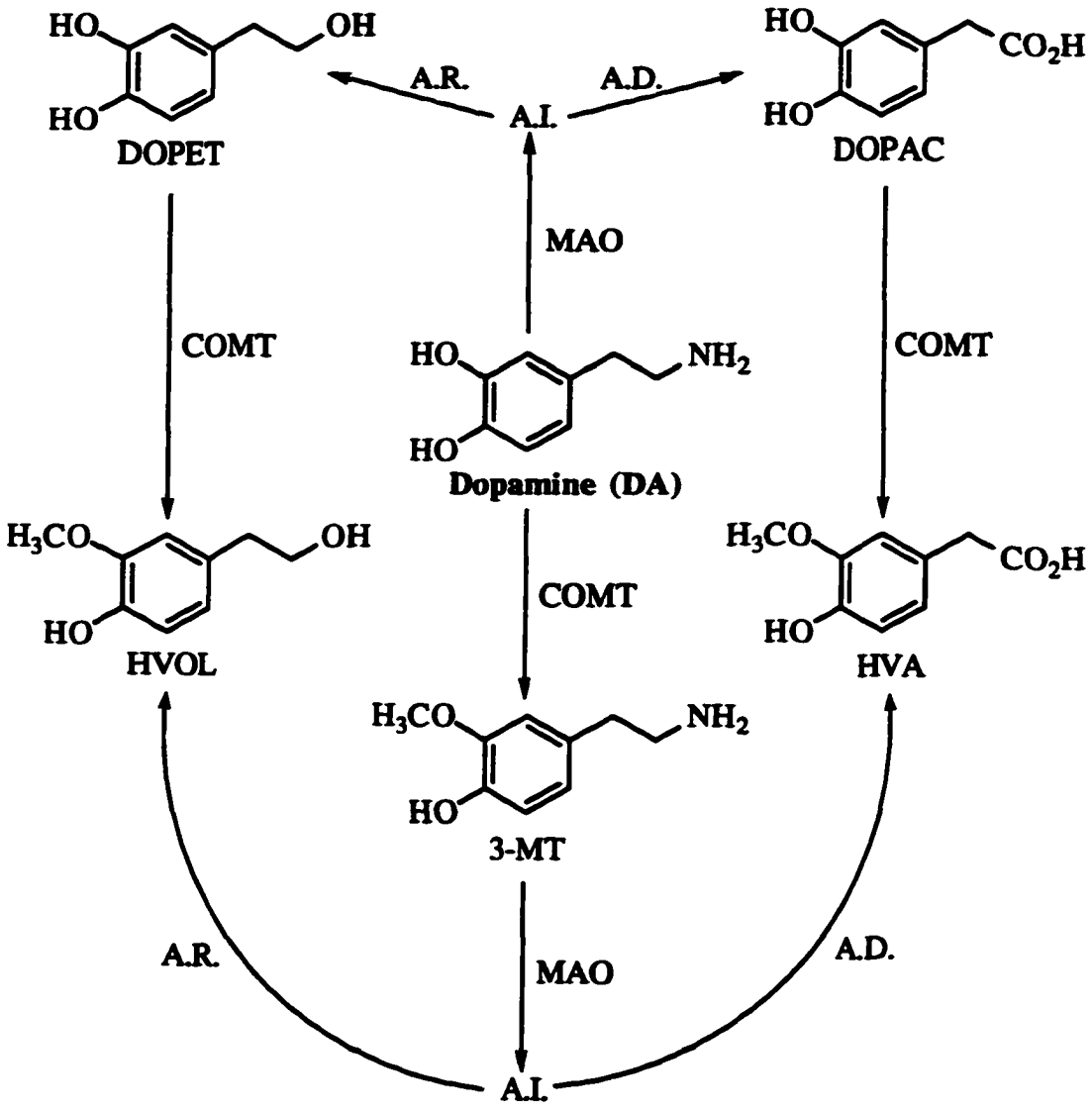

Figure 1-3. Dopamine catabolic pathways.

Abbreviations: MAO, monoamine oxidase; COMT, catechol-O-methyltransferase, A.R., aldehyde reductase; A.D., aldehyde dehydrogenase; A.I., various aldehyde intermediates.

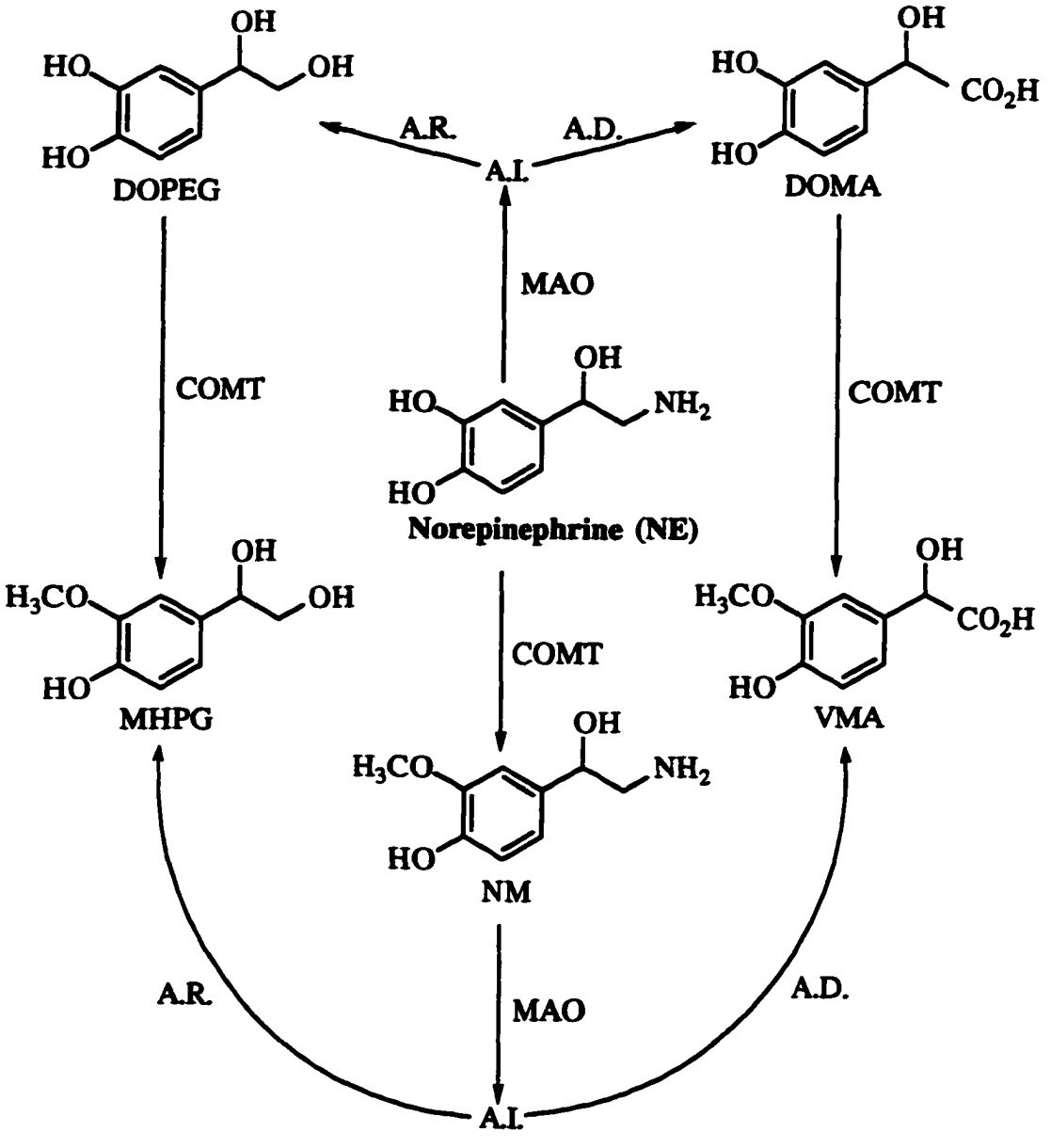

Figure 1-4. Norepinephrine catabolic pathways.

2. Serotonin

5-Hydroxytryptamine (5-HT), also known as serotonin, possesses an indole structure and is the transmitter used in serotonergic neurotransmission. Serotonin and its biosynthetic pathway are shown in Figure 1-5. L-Tryptophan (TRP), an amino acid obtained from the diet, represents the starting point in the synthesis of 5-HT. TRP is

converted to L-5-hydroxytryptophan (5-HTP) by tryptophan-5-hydroxylase. This represents the rate limiting step in the synthesis of 5-HT. L-aromatic amino acid decarboxylase then converts 5-HTP to 5-HT. The catabolism of 5-HT is shown in Figure 1-6. While there are multiple possibilities for metabolic products, the primary metabolite of 5-HT is 5-hydroxyindoleacetic acid (5-HIAA). Metabolic products of neurotransmitters generally possess no neuronal activity. However, in the pineal gland, 5-HT is further metabolized to melatonin (MEL) which is believed to regulate, among other things, circadian cycles.[2,3] The biosynthetic pathway for MEL is also shown in Figure 1-6.

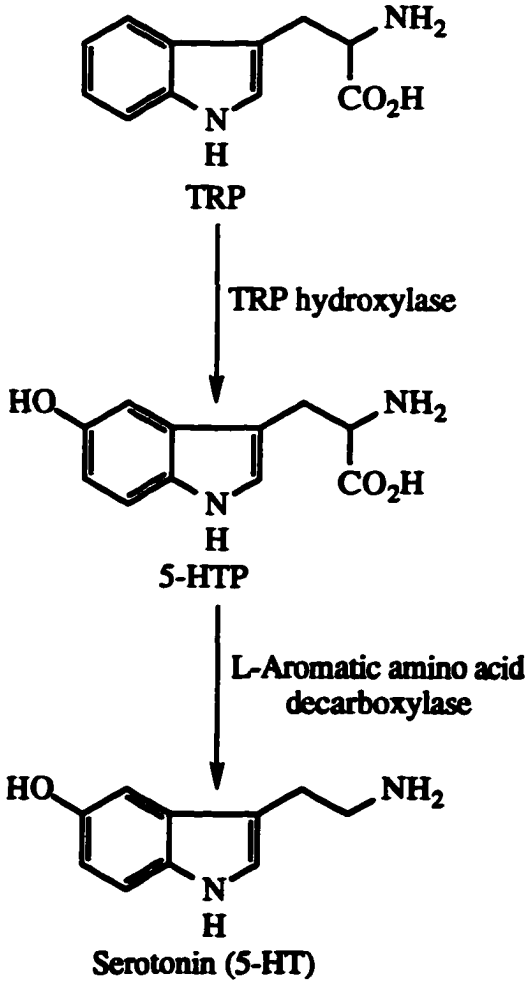

Figure 1-5. Serotonin biosynthesis.

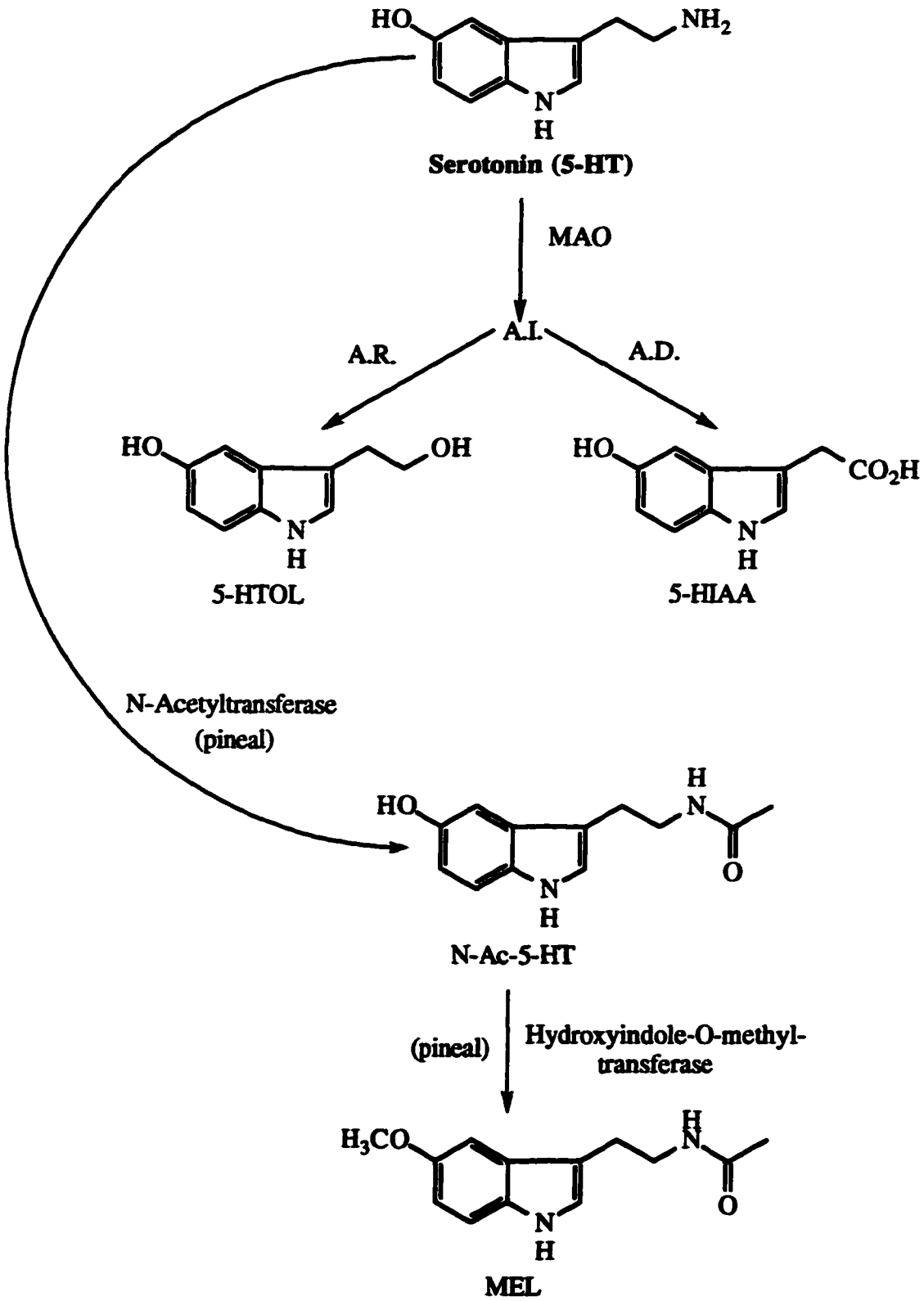

Figure 1-6. Serotonin catabolic pathways and biosynthesis of melatonin.

In spite of the fact that neurons containing the above described transmitters only constitute 3-5% of the total neurons in the brain, these neurotransmitter systems have been implicated, either directly or indirectly, in many neurodegenerative and psychiatric disorders such as Parkinson's disease, Alzheimer's disease, schizophrenia, sleep disorders, mania, depression, and aggression. The following section will briefly describe a few select mental disorders and their currently accepted associations with neurotransmitter system deficits and/or abnormalities.

III. Neurodegenerative Diseases & Other Mental Disorders

Neurodegenerative diseases and other mental disorders have increasingly become a major focus of the neuroscience community. This is understandable when we consider that 10-20 percent of the population over the age of 65 experience some form of dementia[7] and 1-2 percent develop Parkinson's Disease.[8] Furthermore, the prevalence of other mental disorders is extraordinarily high, with approximately 6 million Americans suffering from affective disorders like depression and/or mania, 14 million from various phobias, and 2 million from schizophrenia.[9] While the actual causes of most mental disorders still remain a mystery, the neurotransmitter and neuronal changes that accompany them are beginning to be unraveled.

1. Alzheimer's Disease

Alzheimer's disease is characterized by severe mental impairment and, with time, loss of motor function. Alzheimer's disease begins with memory impairment of recent events along with loss of the ability to plan multi-step tasks.[7] As the disease progresses, there are disturbances in attention, language skills, visiospatial skills, and motor skills.

These disturbances are accompanied by a change in personality which is characterized by irritability, depression, and psychosis.[10] In the final stages of the disease, which occurs approximately 5-10 years after appearance of the initial symptoms, there is a severe impairment of all mental and motor functions.[7]

At the anatomical level, Alzheimer's disease (AD) is initially characterized by cell loss in the cerebral cortex. As the disease progresses, cell loss is seen throughout many subcortical regions of the brain.[11] The pathology of AD is marked by amyloid deposits and neurofibrillary tangles and plaques. While many different neuronal types are affected in AD, some neuronal populations are affected more than others. For example, the cholinergic system, which uses acetylcholine (ACh) as its neurotransmitter and has been implicated in learning and memory,[2,12] shows a high degree of neuronal loss. Degeneration of NE containing nerve cells has also been observed,[12] which may explain some of the behavioral changes that accompany AD. Additionally, cell death in the serotonergic system occurs in this disease. The observed emotional disturbances in AD may be associated with the cell loss in the serotonergic system.

While many transmitter systems are affected in an Alzheimer's brain, the above described systems display the greatest degree of the observed degeneration. Perhaps it is not the loss of any one specific neuronal population, but rather the combination of neuronal losses that yields the symptomology and pathology of Alzheimer's Disease.

2. Parkinson's Disease (PD)[5]

Parkinson's Disease (PD) is characterized by rigidity, resting tremors, and bradykinesia and can be accompanied by dementia and depression.[8] The pathology of PD is marked by degeneration of neurons, predominately in the substantia nigra, and the presence of Lewy bodies, i.e., cytoplasmic spherical inclusions containing neurofilaments. The major neurotransmitter system affected in PD is the dopaminergic system.[13] Clinical signs of PD begin to appear only after 70-80 percent of the

dopaminergic neurons in the substantia nigra are lost.[14] While it appears that the substantia nigra neurons are the most affected, all DA systems ultimately show massive cell loss. And, it is the nigrostriatal DA cell loss that is thought to result in the motor impairment seen in PD. There is also NE cell loss in PD, although this generally occurs to a much lesser extent than DA cell loss.[14] However, the degree of NE loss seems to be higher in patients which display dementia.[12] Additionally, cell loss in the serotonergic system[12] is observed, and this may explain the depression that often accompanies PD. While many more neuronal systems are affected in PD than has been mentioned above, it is the loss in the dopaminergic system which is most characteristic of and most severe in PD. The widespread use of L-DOPA, a precursor of DA, in the treatment of PD is based on observed DA cell loss.

3. Schizophrenia[5]

Schizophrenia is characterized by delusions with no basis in fact, as well as thought which is deranged in content and form. Common symptoms displayed by schizophrenics include delusions that their thoughts are controlled by others, that everyone knows their thoughts, and that people are spying on them and trying to hurt them. Thoughts and ideas are random and illogical. Communication and speech may be disjointed and repetitive. Hallucinations, generally auditory, may occur with schizophrenia patients. The lack of ability to feel emotion may also be displayed by schizophrenics.

Schizophrenia has been suggested to be associated with an overstimulation of the dopaminergic system.[3] Additionally, hypoactive 5-HT systems have been implicated in schizophrenia, stemming from studies demonstrating that the concentrations of 5-HIAA in the cerebrospinal fluid is lower in schizophrenics than in normal patients.[5] Furthermore, 5-HT precursor supplements have been reported to partially alleviate symptoms of schizophrenia.[3,5]

4. Affective Disorders[5]

Affective disorders, including depression and/or mania, are marked by extreme changes in mood. Major depression is characterized by an intense feeling of despair and worry, loss of concentration, and low self-worth.[3] This is generally accompanied by physical changes such as decreased libido, insomnia, and weight loss.[5] Mania, which is less common than depression, is characterized by euphoria, hyperactivity, impaired judgment, uncontrollable speech, irritability, and insomnia.[5]

There are several lines of evidence which implicate both the serotonergic[3,15,16] and noradrenergic[3,17] systems in affective disorders and, in particular, depression. While there is no neuron loss associated with simple depression, reduction in 5-HT, NE, and related metabolites has been found in such patients.[15,17] Furthermore, tricyclic antidepressants, which block the uptake of 5-HT and/or NE, have been significant in treating depression.[5] These observations form the basis for the "biogenic amine hypothesis" of affective disorders.

From this brief overview of a select few neurodegenerative and other mental disorders we can see the complexity and severity of such conditions. It is difficult in all cases to state absolutely whether the disorder is caused by a change in the transmitter system(s) or whether the change in the transmitter system(s) is caused by the disorder. However, in either case, there needs to be more investigation and evaluation of all systems involved before we can truly understand what is actually occurring and why.

IV. Neurotoxins

Understanding how the brain works is a difficult and perplexing task. However, one of the easiest ways to connect pharmacological, behavioral, and physiological phenomena in vertebrates with a particular neuronal pathway in the brain is to first, produce an effect; second, inactivate the neuron subpopulation thought to control the observed effect; and third, reexamine the effect and identify any resulting changes. Physical lesioning was the best technique for many years in the removal and/or inactivation of suspected neuronal tracts in question. However, electrolytic and surgical lesions are inadequate for use with the complex and interwoven nervous tissues found in the CNS of vertebrates. These types of lesions in CNS tissues may provide complete removal of a given tract, but the associated selectivity is typically non-existent. An alternative to this non-selective lesioning is afforded by the use of a chemical neurotoxin. This is the only method which offers substantial cellular selectivity.

A neurotoxin is a molecule that causes neuronal destruction. This destruction may be axonal degeneration or total cell death, but in either case denervation occurs.[2] Neurotoxins, while being employed in many facets of the neuroscience community for various purposes, are particularly useful in producing animal models of neurodegenerative diseases. When a toxin produces behavioral and physiological changes similar to a neurodegenerative disease, that agent can provide critical insight into the underlying mechanism of the disorder and, thus, implicate potentially beneficial treatments. This is exemplified by the novel treatments of Parkinson's Disease derived from the understanding of the mechanism of action of MPTP (see below).

1. 6-Hydroxydopamine

6-Hydroxydopamine (6-HDA) is probably the best-known and most heavily studied neurotoxin. It was essentially the first toxin of its kind to be introduced to the scientific community. Following its identification by Senoh and coworkers[18] in 1959 as a DA by-product, 6-HDA was shown to cause peripheral NE depletions when systemically administered.[19,20] Ultrastructural evidence soon followed showing that the peripheral NE depletions actually corresponded to nerve terminal destruction.[21]

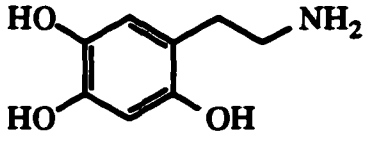

6-Hydroxydopamine (6-HDA)

After 6-HDA was shown to cause peripheral neuronal degeneration, its effects on the brain began to be investigated. Since 6-HDA is highly polar, it does not cross the blood-brain barrier[22] and, hence, must be administered directly into the brain. 6-HDA, administered intracerebroventricularly in mice at low doses (3 nmol) results in a reduction in whole brain NE levels by approximately 30% while apparently not affecting any other transmitter systems.[23] However, at higher doses 6-HDA becomes less selective and begins to destroy DA neurons as well. This is exemplified, following a 60 nmol injection, by a reduction in whole mouse brain NE levels to 40% of controls and DA levels to 86% of controls.[24] When 6-HDA is injected directly into the substantia nigra it produces significant dopaminergic neuronal degeneration and has been used to produce animal models that exhibit a very similar symptomology and pathology to that of Parkinson's Disease.

The mechanism by which 6-HDA elicits neurodegeneration has been extensively studied, and many 6-HDA reviews exist in the literature.[25-30] In order for 6-HDA to

elicit neurodegeneration, it must first be accumulated in the neuron. Toxin accumulation occurs by selective uptake at endogenous reuptake, or transport, sites. This uptake has been shown to be a requirement for 6-HDA toxicity in that neurodegeneration can be blocked by specific uptake blocking agents.[31,32] It is generally accepted that the selective uptake of 6-HDA, as well as other neurotoxins, is the most important characteristic associated with its neurotoxic selectivity. Another important characteristic believed to be associated with the toxicity of 6-HDA is its ability to readily undergo autoxidation, i.e., non-enzymatic oxidation by molecular oxygen. Many mechanisms of action have been proposed for 6-HDA, but the vast majority begin with neuronal accumulation and toxin autoxidation.

One school of thought on 6-HDA toxicity involves neuronal damage *via* reactive oxygen species.[33-38] 6-HDA has been shown to produce superoxide and hydrogen peroxide as byproducts of autoxidation, and it is possible for these species to directly damage the neuron.[39-41] Additionally, autoxidation of 6-HDA has been shown to produce the extremely reactive and damaging hydroxyl radical, •OH.[33,42,43] This •OH production, however, is most likely due to the interaction of hydrogen peroxide with trace metal ions *via* Fenton chemistry.[44-48] In support of the reactive oxygen species theory, free radical scavenging agents have shown at least some protection against 6-HDA induced neurotoxicity.[43,49]

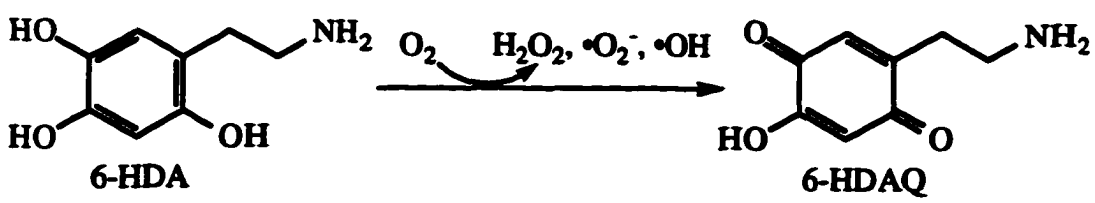

6-HDA 6-HDAQ

There are a number of other possible mechanisms by which 6-HDA may elicit neurodestruction. 6-HDA, upon oxidation, forms a corresponding para-quinone species

(6-HDAQ). This p-quinone has reactive electrophilic sites which can undergo nucleophilic attack by sulfhydryl moieties of cellular components such as enzymes and other proteins.[27,50-56] In this way 6-HDA can bind, and even cross-link, essential proteins and enzymes rendering them inactive. 6-HDA and its p-quinone have also been shown to disrupt mitochondrial oxidative phosphorylation.[57-60] By this mechanism, the cell is rapidly depleted of essential high energy phosphates. Furthermore, 6-HDA could effect neurodegeneration by disrupting both cellular and mitochondrial calcium homeostasis,[43,49,61-64] creating hypoxic conditions in the neuron, depleting neuronal antioxidant reserves,[34,43,50] releasing intraneuronal iron from ferritin for participation in •OH production,[65] and/or inducing apoptosis.[66]

2. MPTP

1-Methyl-4-phenyl-1,2,3,6-tetrahydropyridine (MPTP) is a highly selective dopaminergic neurotoxin.[67] MPTP originated not from the scientific community but from a "garage chemist" making illicit drugs. MPTP was a by-product in the attempted preparation of a synthetic heroin. This chemist accidentally applied too much heat during the synthesis, which inadvertently produced significant amounts of MPTP. This accident was realized only after a number of heroin addicts in northern California began appearing in emergency rooms displaying parkinsonian symptoms nearly identical to that of Idiopathic Parkinson's Disease.[68]

Since its discovery, a great deal of research has been undertaken on MPTP.[67,69] While not innately toxic, MPTP is oxidized to the toxic species, 1-methyl-4-phenylpyridinium (MPP^+), in the body. In other words, MPTP requires bioactivation. MPTP, being a lipophilic molecule, can cross the blood-brain barrier. Once inside the brain, MPTP is oxidized to 1-methyl-4-phenyl-2,3-dihydropyridinium ($MPDP^+$), by MAO-B.[67,70,71] $MPDP^+$ is then converted to the MPP^+, presumably *via* autoxidation.[29] It is speculated that the transformation of MPTP to MPP^+ occurs

predominately in astrocytes. MPP^+ then diffuses to the extracellular matrix where it is avidly taken up by dopaminergic neurons[70] due to its high affinity for the dopaminergic transport site. Once inside the DA neuron, MPP^+ appears to accumulate in mitochondria. This accumulation is driven by the electrochemical gradient that exists between the inner and outer regions of the mitochondria.[67,72] MPP^+ then acts by inhibiting oxidative phosphorylation at the level of complex I,[72,73] resulting in a large decrease in ATP production. This depletion of ATP has been observed both *in vitro*[74] and *in vivo*.[75]

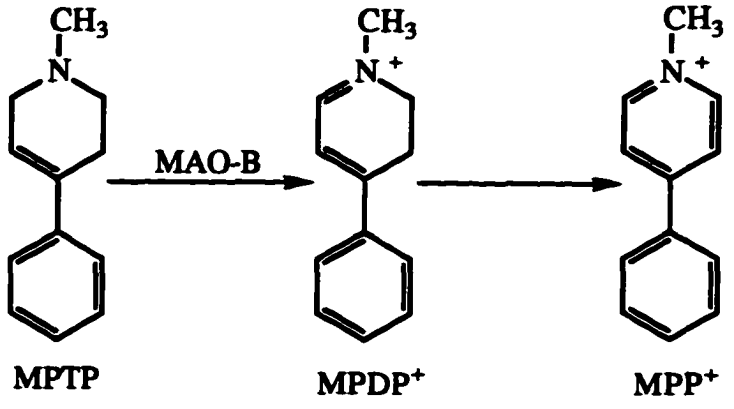

MPTP $MPDP^+$ MPP^+

The ability of MPTP to induce Parkinsonian symptoms in primates and, to a lesser extent, rodents has given the scientific community an excellent model of this disease. Understanding the mechanism by which MPTP produces neurodegeneration has provided some insight into the possible events which occur in Idiopathic PD and, thus, has indirectly provided some candidates for ameliorative pharmacological intervention. For example, from the observation that MPTP-induced parkinsonism can be blocked by MAO-B inhibitors,[71] clinical studies have subsequently shown that early treatment of human patients with an MAO-B inhibitor slows the progression of PD and delays the need for levodopa treatment.[76,77] Additionally, the possibility of mitochondrial dysfunction in patients with PD, which has now been demonstrated,[78] was only pursued following discovery of the MPP^+ inhibition of oxidative phosphorylation.

3. 5,7-Dihydroxytryptamine

5,7-Dihydroxytryptamine (5,7-DHT), an analog of serotonin (5-HT), is a well known and widely used neurotoxin.[29,30] This compound, when administered directly into the brain, produces neurodegeneration of serotonergic nerves and/or nerve terminals. At low doses, 5,7-DHT is relatively selective for 5-HT neurons and can produce up to a 25% depletion of 5-HT in mouse whole brain.[79] At moderate to high doses, 5,7-DHT can produce up to 30-35% 5-HT depletions in mouse whole brain.[23,79] At moderate to high doses, however, 5,7-DHT also elicits NE neurodegeneration.[23,79,80] However, these NE effects can be partially blocked with appropriate uptake blocking agents. DA depletions have also been reported.[80,81] The moderate selectivity of this 5-HT analog is attributed to its ability to act as a substrate at 5-HT transport sites.[26]

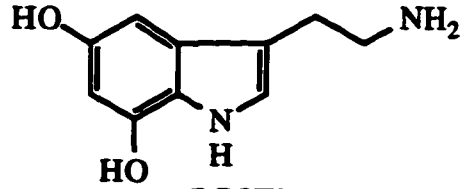

5,7-DHT

Although the mechanism of action of 5,7-DHT has not yet been elucidated, it is known that uptake is essential.[30] Furthermore, it is believed that autoxidation is a prerequisite for 5,7-DHT toxicity. Oxidation of 5,7-DHT, as well as oxidative formation of this toxin from 5-HT, have been extensively studied.[82-84] One theory on 5,7-DHT toxicity is that neurodegeneration is elicited by the free radicals and reactive oxygen species produced during autoxidation. It has been shown, for example, that superoxide and hydrogen peroxide are produced during 5,7-DHT autoxidation.[85] In support of the free radical theory, partial protection from 5,7-DHT toxicity has been demonstrated upon

pretreatment with free radical scavenging agents.[86,87] Another possible mechanism of action stems from the formation of reactive quinone intermediates. These intermediates can react with nucleophiles such as proteins and enzymes thereby rendering essential neuronal functionalities useless.[87-89]

It has recently been shown that 5,7-DHT is oxidized by a radical mechanism leading to the highly toxic 5-hydroxytryptamine-4,7-dione,[84,85] among other products. Additionally, it has been proposed that it is this oxidation product that elicits degeneration.[84,85] Interestingly, while the oxidative action of MAO is not required for 5-HT degeneration, it is required for the 5,7-DHT induced NE degeneration. And, by inhibiting MAO activity, NE degeneration by 5,7-DHT can be reduced or eliminated.[88]

5,6-Dihydroxytryptamine (5,6-DHT), a structural analog of 5,7-DHT, came into use as a serotonin neurotoxin about the same time as 5,7-DHT. 5,6-DHT has been extensively studied and used.[26,30,82,88,90-92] However, due to its lower potency and higher lethality, it is no longer used to the same extent as 5,7-DHT and, therefore, will not be discussed any further.

V. Purpose of Dissertation Research

Neurotoxins are very important research tools in the field of neurochemistry, particularly in the study of neurodegenerative diseases.[93] There are a number of such neurotoxins which have been used in CNS investigations and, particularly, to produce animal models of various mental disorders. While there are many neurotoxins, few provide good neuronal selectivity. And, while there have been many new neurotoxins recently discovered or developed and tested,[70,94-100] the most commonly used catecholaminergic and indolaminergic toxins today are still 6-HDA and 5,7-DHT. Considering the non-specific destructive tendencies exhibited by existing toxins, the need

for development of neurotoxins which are highly selective and very complete in the destruction of a given transmitter system remains.

The research presented in the following chapters encompasses the synthesis and the chemical and biological characterization of a series of dihydroxytetrahydroquinoline derivatives. The impetus of this project was two-fold. The first was to produce new agents which were very selective for and toxic to a specific transmitter system, preferably the serotonergic system. Previous studies had suggested that this series of compounds could possibly be potent serotonergic neurotoxins.[23] The second was to investigate the mode of action of the developed toxins, by which we might be able to (1) use the knowledge gained from these studies to develop even more selective and more potent neurotoxins, and (2) more completely understand the mode of action(s) of other toxins which have been heavily studied but not yet completely understood.

A previous report by L. Lin[23] showed that a fixed side chain catecholamine derivative, 3-amino-6,7-dihydroxy-1,2,3,4-tetrahydroquinoline (6,7-ADTQ), was capable of eliciting substantial 5-HT depletions. We, thus, decided to more thoroughly investigate this type of compound by designing and characterizing various ADTQ analogs in an attempt to find more selective and potent serotonergic agents. The specific compounds investigated included the enantiomers of 6,7-ADTQ and two analogs, namely 3-aminomethyl-6,7-dihydroxy-1,2,3,4-tetrahydroquinoline (6,7-AMDTQ) and 3-amino-6,8-dihydroxy-1,2,3,4-tetrahydroquinoline (6,8-ADTQ). The enantiomers were investigated to evaluate the biological relevance of toxin stereochemistry. The rational for 6,7-AMDTQ design was to increase in bulkiness of the 3-position substitution of the parent species in an attempt to enhance the selectivity for serotonergic neurons and decrease the selectivity for catecholaminergic neurons. The rational for 6,7-AMDTQ design was to give the parent agent a similar hydroxy configuration as displayed by the classic serotonergic toxin 5,7-DHT.

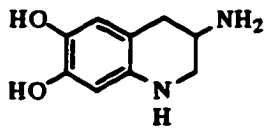

6,7-ADTQ

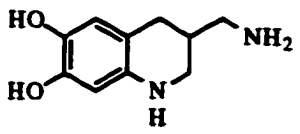

6,7-AMDTQ

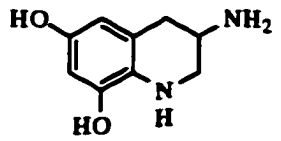

6,8-ADTQ

The following chapters describing and discussing the investigations undertaken are entitled:

Chapter 2

Synthesis of 3-Aminomethyl-6,7-dihydroxy-1,2,3,4-tetrahydroquinoline and 3-Amino-6,8-dihydroxy-1,2,3,4-tetrahydroquinoline

Chapter 3

Basic Chromatography and Electrochemistry

Chapter 4

Neurotoxicity

Chapter 5

Mode of Action I: Uptake Interactions

Chapter 6

Mode of Action II: Ease of Oxidation & Acid/Base Properties

Chapter 7

Mode of Action III: Autoxidation and Reactive Oxygen Species

Chapter 8

Mode of Action IV: Disruption of Mitochondrial Oxidative Phosphorylation

Synthesis of 3-Aminomethyl-6,7-dihydroxy-1,2,3,4-tetrahydroquinoline & 3-Amino-6,8-dihydroxy-1,2,3,4-tetrahydroquinoline

Chapter 2

I. Introduction

Neurotoxins, such as 6-hydroxydopamine (6-HDA) and 5,7- and 5,6-dihydroxy-tryptamine (5,7- and 5,6-DHT), have been employed for more than 25 years to study behavioral, physiological, and pharmacological phenomena associated with specific neuronal pathways. While highly specific when compared to surgical or electrolytic methods, such chemical toxins still exhibit a high degree of non-target tissue destruction. Considering this, it is not surprising that there has been an on-going search for agents

which exhibit higher degrees of selectivity and toxicity toward specific neuronal populations. Additionally, the mode of action by which 6-HDA and related neurotoxins elicit toxicity has, for the most part, eluded researchers. Therefore, the relentless effort to elucidate the mechanism by which these type of agents elicit neurodegeneration continues.

With the above in mind, we have designed fixed side chain analogs of 6-HDA with hopes to (1) provide neurotoxins which are superior to those in use and (2) more completely determine the destructive mode(s) of action of such agents. With a more complete understanding of how toxins elicit neurodestruction, the alleviation and/or postponement of onset of neurodegenerative disorders might be achieved. This rationale has already been realized through new treatments of Idiopathic Parkinson's Disease derived from the understanding of the mode of action of MPTP.[67]

This chapter describes the synthesis of two putative neurotoxic agents, 3-aminomethyl-6,7-dihydroxy-1,2,3,4-tetrahydroquinoline (**8**) and 3-amino-6,8-dihydroxy-1,2,3,4-tetrahydroquinoline (**17**) starting from easily available dimethoxy-benzaldehydes.

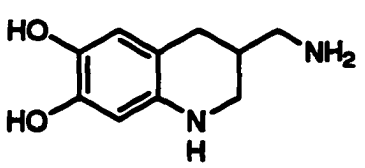

8

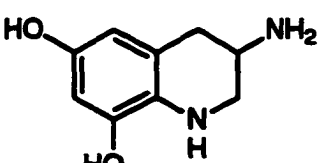

17

II. Synthetic Summaries

This section provides a brief outline of the synthetic steps involved in the production of 3-aminomethyl-6,7-dihydroxy-1,2,3,4-tetrahydroquinoline dihydrobromide (**8**•2HBr or 6,7-AMDTQ•2HBr) and 3-amino-6,8-dihydroxy-1,2,3,4-tetrahydroquinoline dihydrobromide (**17**•2HBr or 6,8-ADTQ•2HBr). The details of each of the synthetic steps are presented in the following experimental section, while NMR spectra of the intermediates and the final products, along with their associated peak assignments, appear in the final section, NMR Spectra and Assignments.

A. Synthesis of 3-Aminomethyl-6,7-dihydroxy-1,2,3,4-tetrahydroquinoline Dihydrobromide

The first step in the synthesis of 3-amino-6,7-dihydroxy-1,2,3,4-tetrahydroquinoline dihydrobromide was the condensation of 3,4-dimethoxybenzaldehyde, **1**, with dimethylmalonate in the presence of piperidine and benzoic acid. This reaction is an example of a Knoevenagel condensation of an aldehyde and an enolizable compound, base catalyzed by an amine. The condensed product **2** was obtained in a yield of 88% and the associated proton NMR spectrum was in agreement with literature reports.[101,102]

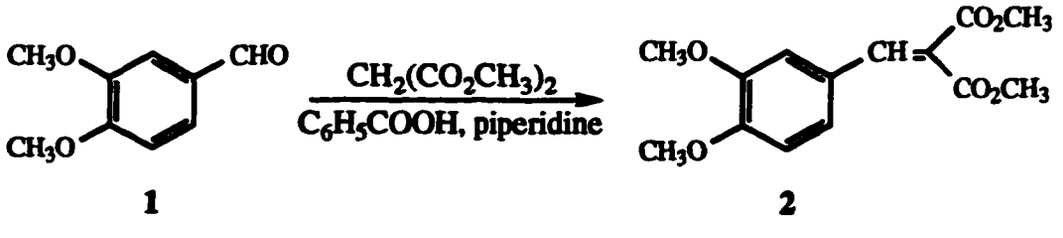

1 **2**

Scheme 2-1. Synthesis of dimethyl-3,4-dimethoxybenzylidenemalonate, **2**.

Reduction of the benzylidene derivative **2** was accomplished through catalytic hydrogenation using palladium on carbon as a catalyst. This reaction proceeded at a moderate rate and resulted in a clean product **3** with a yield of 86%. The proton NMR spectrum agreed with previous literature reports.[101,102]

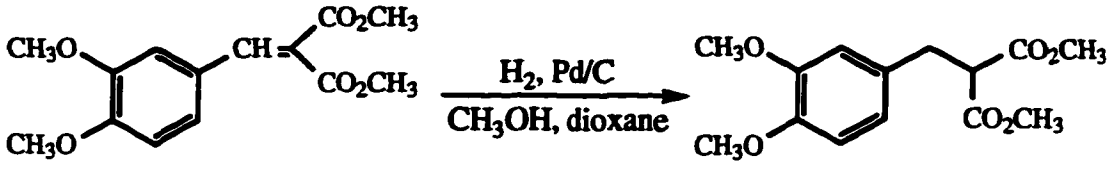

2 **3**

Scheme 2-2. Synthesis of dimethyl-3,4-dimethoxybenzylmalonate, **3**.

The regioselective ring nitration of dimethyl-3,4-dimethoxybenzylmalonate **3** was realized using fuming nitric acid at 0°C. Due to the aromatic ring being highly activated, this nitration resulted in product **4** in quantitative yield (100%).

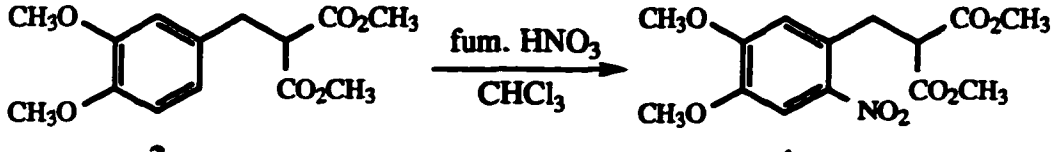

3 **4**

Scheme 2-3. Formation of dimethyl-4,5-dimethoxy-2-nitrobenzylmalonate, **4**.

The tetrahydroquinoline derivative **5** was produced by catalytic hydrogenation of **4**, using palladium on carbon as a catalyst. Reduction of the nitro group to the corresponding amine allowed for intramolecular cyclization of the side chain *via*

nucleophilic substitution, i.e., attack by the amine on the electron deficient carbonyl carbon. This reaction proceeded rapidly and resulted in a clean product **5** with a yield of 72%.

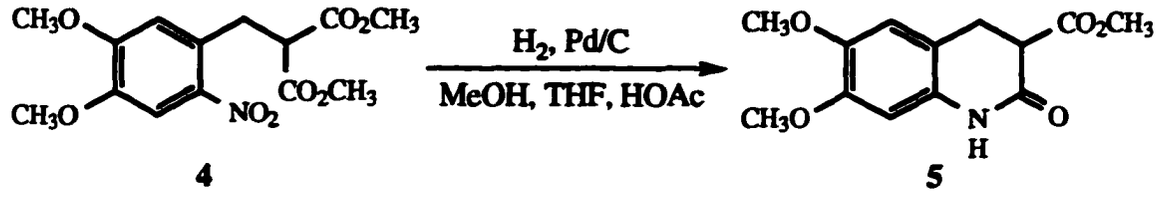

4 **5**

Scheme 2-4. Synthesis of 3-Carboxymethyl-6,7-dimethoxy-1,2,3,4-tetrahydro-2-oxoquinoline, **5**.

The next step involved the production of the carboxamide **6** from the methylester **5**. While seemingly straightforward, this step proved to be challenging. The conversion was attempted using many different methods, most resulting in unsuccessful reactions. Reagents and reaction conditions attempted included (1) ammonium hydroxide and ammonium chloride at atmospheric pressure, (2) condensed ammonia with ammonium chloride in a sealed, pressure-resistant vessel with heat, (3) saturated ammonia solution in a sealed, pressure-resistant vessel with heat, and (4) Me_2AlNH_2 at atmospheric pressure conditions. All these attempts yielded the amide from the methylester, but the major product formed was 3-carboxamide-6,7-dimethoxy-2-hydroxyquinoline (**6a**), the oxidized form of **6**, and small amounts, if any, of the desired product **6**.

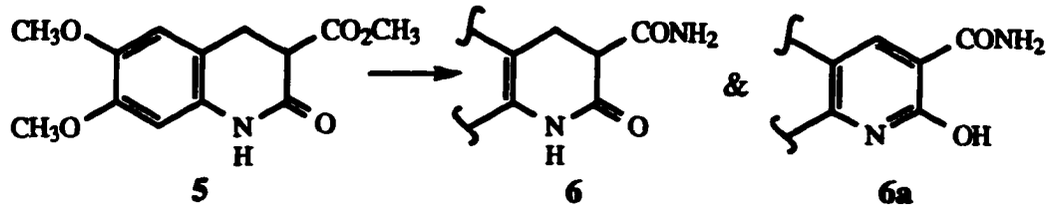

5 **6** **6a**

Attempts to determine the problem(s) with these reactions led us to studies using pure, desired product **6**. Exposing **6** to the same reaction conditions in which it was formed resulted in a time dependent conversion to the oxidized product **6a**. Thus, the time for the reaction was optimized to allow for maximal formation of **6** while limiting the follow-up oxidation reaction.

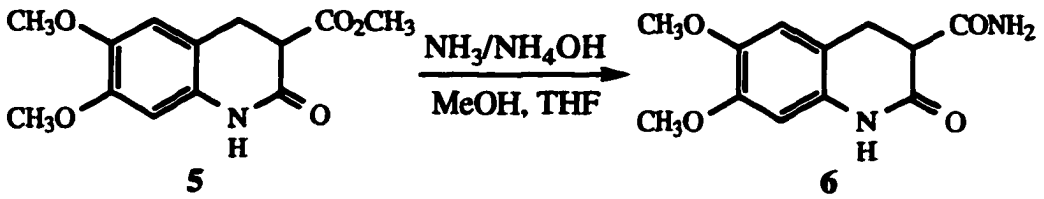

5 **6**

Scheme 2-5. Synthesis of 3-carboxamide-6,7-dimethoxy-1,2,3,4-tetrahydro-2-oxoquinoline, **6**.

The reagents and reaction conditions ultimately employed were ammonia and ammonium hydroxide with a high ammonia pressure and an elevated temperature. The major product under these conditions remained **6a**; however, due to solubility differences in methanol, the desired product was isolable. While this reaction was neither fast nor efficient, the product was obtained in a yield of 24%.

Conversion of the two amide functionalities of **6** to their corresponding amines was achieved *via* diborane reduction. The reaction proceeded at a moderate rate and was followed by hydrolysis of the borate complex with dilute hydrochloric acid. This resulted in a relatively pure (~95%) diamine **7** in a yield of 88%. Further purification using silica gel column chromatography was not useful due to the fact that the diamine degraded while on the column.

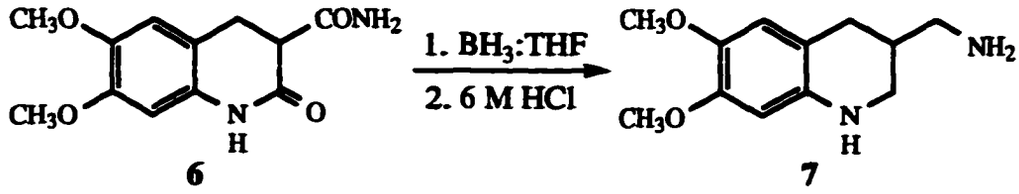

6 7

Scheme 2-6. Synthesis of 3-aminomethyl-6,7-dimethoxy-1,2,3,4-tetrahydroquinoline, **7**.

The final step in this synthesis was the cleavage of the methyl ethers to their corresponding hydroxy functionalities. An excess of 48% hydrobromic acid under reflux conditions in a pressure vessel produced the desired product. With minor workup, a light tan solid, **8**•2HBr, was obtained in high purity with a yield of 74%.

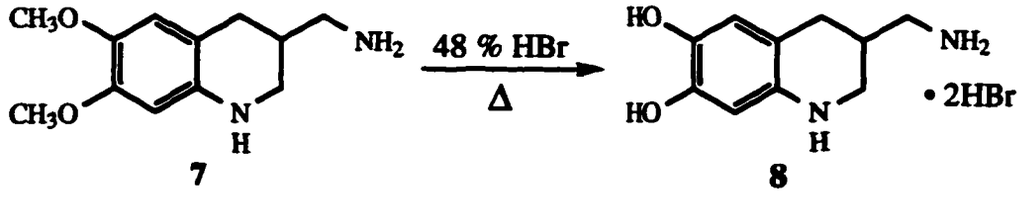

7 **8**

Scheme 2-7. Synthesis of 3-aminomethyl-6,7-dihydroxy-1,2,3,4-tetrahydroquinoline•2HBr, **8**•2HBr.

The synthesis of 3-aminomethyl-6,7-dihydroxy-1,2,3,4-tetrahydroquinoline dihydrobromide (**8**•2HBr) was completed with an overall yield of 9%. The ammonolysis reaction provided the poorest yield in this synthetic pathway and was the major contributor to the low overall yield. The ring-formation reaction shown in Scheme 2-4, however, proved to be a useful and efficient general method for the production of tetrahydroquinoline ring structures.

B. Synthesis of 3-Amino-6,8-dihydroxy-1,2,3,4-tetrahydroquinoline Dihydrobromide

The first step in the synthesis of 3-amino-6,8-dihydroxy-1,2,3,4-tetrahydroquinoline dihydrobromide was the formation of the oxazolone from the corresponding aldehyde. This was accomplished by condensing 3,5-dimethoxybenzaldehyde, **9**, with hippuric acid in the presence of powdered sodium acetate and acetic anhydride. This reaction gave a yellow crystalline product, **10**, with an 86% yield.

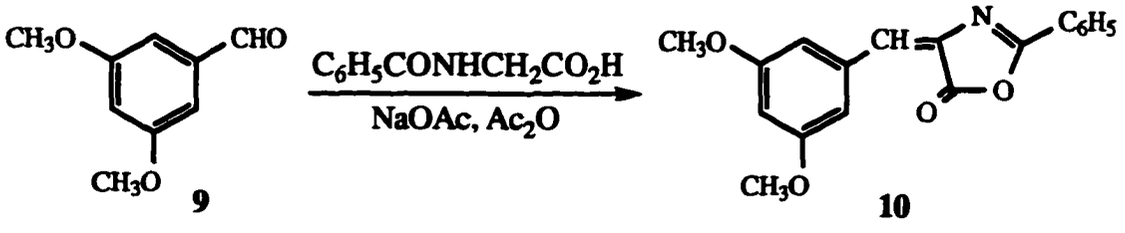

Scheme 2-8. Formation of 4-(3,5-dimethoxybenzylidene)-2-phenyl-5-oxazolone, **10**.

Opening of the azlactone ring and addition of the desired methoxy group was achieved by basic methanolysis. The reaction afforded a white crystalline product, **11**, in a yield of 88%.

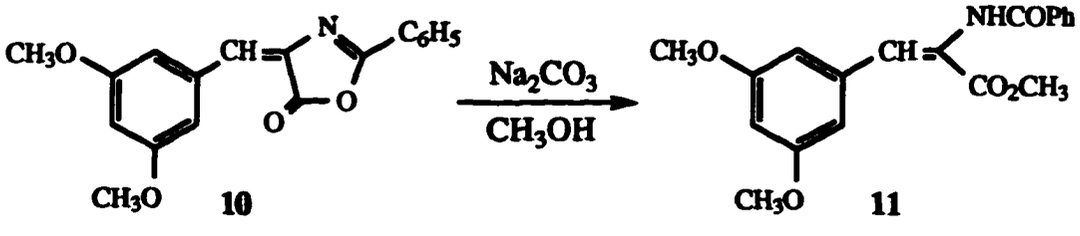

Scheme 2-9. Synthesis of methyl-2-benzoylamino-3-(3,5-dimethoxyphenyl)-2-propenoate, **11**.

Reduction of the vinyl moiety was accomplished through hydrogenation, using palladium on carbon as a catalyst. The reaction progressed at a moderate rate and gave a clean product in quantitative yield (100%).

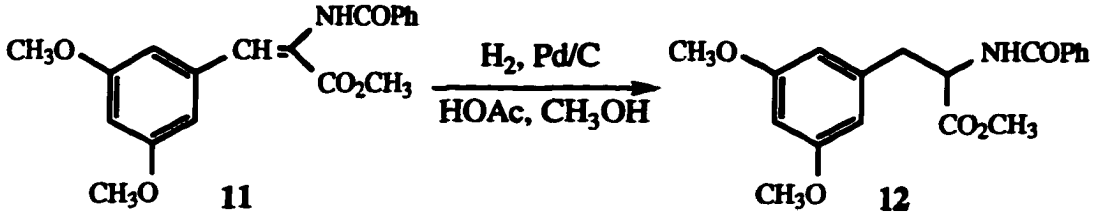

Scheme 2-10. Formation of methyl-2-benzoylamino-3-(3,5-dimethoxyphenyl)propanoate, **12**.

A typical attempt at nitration of the aromatic ring of **12** employed fuming nitric acid with chloroform as the solvent. The nitration of **12**, however, proved quite perplexing. Using a 6-fold mole excess of fuming nitric acid and a reaction temperature of 0°C, a yield of 16% was obtained for nitrated product **13** following silica gel column purification. Attempts to optimize this reaction with regards to the amount of fuming nitric acid (2- to 6-fold mole excess), nature of the solvent (chloroform, acetic acid, and a mixture of these), and the reaction temperature (-78 to 25°C) were undertaken. But, each of these alternatives resulted in a lesser yield than the original reaction. Since all of these fuming nitric acid reactions resulted in large amounts of uncharacterizable product(s), some milder nitration conditions were attempted. These included (1) ammonium nitrate and trifluoroacetic anhydride, which led to multiple side products but no discernible desired product, and (2) tetranitromethane with pyridine, reported to nitrate tyrosine in good yield, but which only provided the desired product **13** in an 8% yield in the current

case. Following this string of unsuccessful attempts, we employed a 2- to 4-fold excess of 70.4% nitric acid with acetic acid as the solvent and reaction temperatures ranging from -10 to 25°C. These conditions appeared to be reasonably promising with yields ranging between 10 to 19%. Ultimately, by applying simplex optimization, maximal yield was achieved using a 4-fold excess of 70.4% nitric acid in acetic acid at 15°C. The reaction, under these conditions, was neither clean nor efficient, resulting in a yield of only 19% after purification.

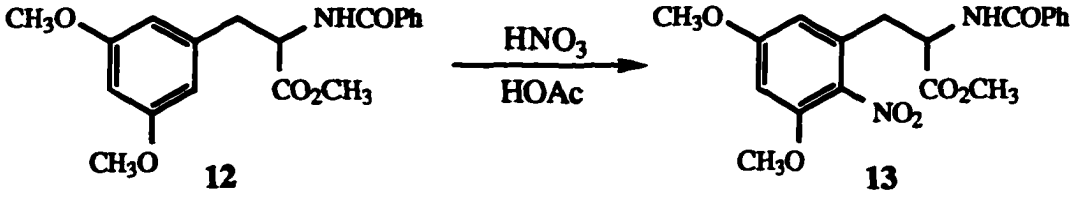

Scheme 2-11. Synthesis of methyl-2-benzoylamino-3-(3,5-dimethoxy-2-nitrophenyl)propanoate, **13**.

Catalytic hydrogenation, using palladium on carbon, resulted in reduction of the nitro group to its corresponding amine, which subsequently underwent intramolecular cyclization to afford the lactam derivative **14**. This reaction gave a clean product with a 90% yield.

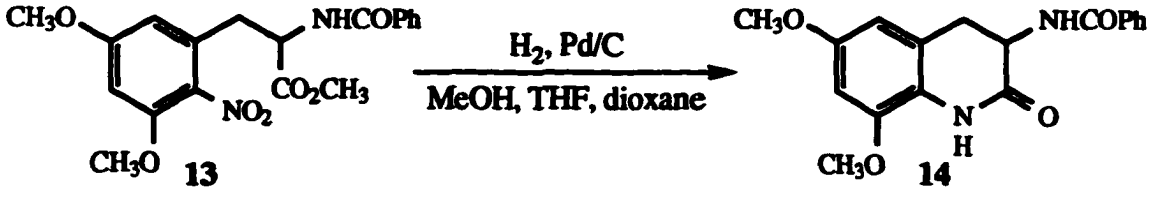

Scheme 2-12. Formation of 3-benzoylamino-6,8-dimethoxy-1,2,3,4-tetrahydro-2-oxoquinoline, **14**.

The amide functionalities of **14** were converted to their corresponding amines through a diborane reduction. The time required for reduction was substantial because the benzoyl amide functionality, due to its characteristically low electrophilicity, underwent reduction at a much slower rate than did the ring amide. The product obtained from this reaction was not clean and, thus, was purified by silica gel column chromatography, resulting in a yield of 90% for **15**.

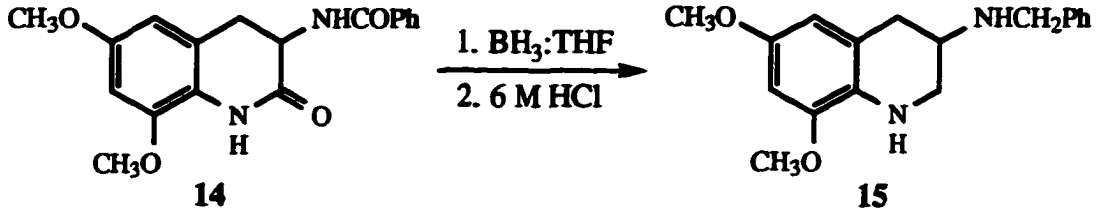

14 **15**

Scheme 2-13. Formation of 3-benzylamino-6,8-dimethoxy-1,2,3,4-tetrahydroquinoline, **15**.

N-debenzylation was achieved through catalytic hydrogenation, using palladium on carbon. The reaction was slow and resulted in some uncharacterizable by-products. Utilizing silica gel column chromatography, **16** was obtained in an 83% yield.

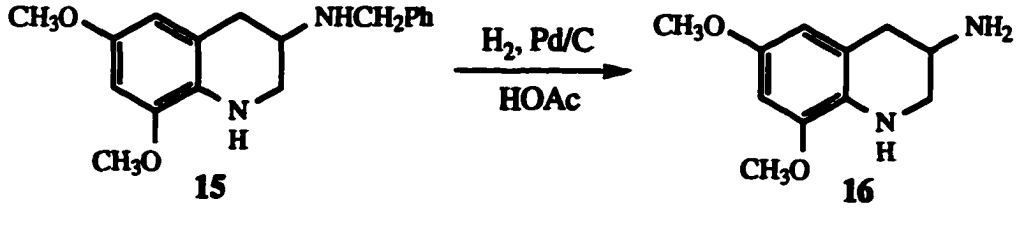

15 **16**

Scheme 2-14. Synthesis of 3-amino-6,8-dimethoxy-1,2,3,4-tetrahydroquinoline, **16**.

Deprotection of the methyl ethers employed an excess of 48% hydrobromic acid under reflux conditions in a sealed, pressure-resistant vessel. A considerable amount of time was required for this reaction to reach completion, with the 8-methoxy cleavage requiring a five-fold longer period of time than what was needed for the 6-methoxy cleavage. This reaction required 26 hours. Stopping the reaction before this time resulted in a mixture of the dihydroxy and 8-monomethoxy products. This reaction gave the desired product **17** with a satisfactory purity and a yield of 86%.

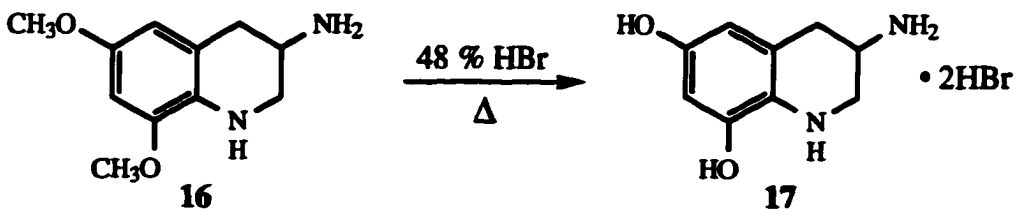

16 **17**

Scheme 2-15. Formation of 3-amino-6,8-dihydroxy-1,2,3,4-tetrahydroquinoline•2HBr, **17**•2HBr.

The complete synthesis of 3-amino-6,8-dihydroxy-1,2,3,4-tetrahydroquinoline dihydrobromide, **17**•2HBr, gave an overall yield of 8%. The aromatic ring nitration was the major stumbling block in the pathway. Many different reaction conditions for this nitration were tried, but the optimal yield obtained was only 19%. However, considering that the complete synthesis required 8 steps, we were reasonably satisfied with an overall 8% yield.

III. Experimental

A. General Methods

Tetrahydrofuran (THF) was refluxed over calcium hydride and freshly distilled prior to use. Acetic anhydride was distilled from phosphorus pentoxide. Methanol was refluxed over Mg turnings and iodine, distilled, and stored over 4Å, 8-12 mesh molecular sieves. Ethyl acetate was refluxed over sodium and benzophenone and freshly distilled prior to use. All other chemicals and reagents were purchased and used without further purification.

Proton NMR spectra were acquired using a Varian XL-300 MHz spectrometer. While the location of peaks and their associated splitting constants are presented in this section, actual spectra for each intermediate and associated peak assignments are presented in the next and final section, entitled NMR Spectra and Assignments. Mass spectra were recorded using a VG-ZAB-E instrument.

B. Synthesis of 3-Aminomethyl-6,7-dihydroxy-1,2,3,4-tetrahydroquinoline Dihydrobromide

1. Dimethyl-3,4-dimethoxybenzylidenemalonate (2)

To a 500 mL round bottomed flask, fitted with a water condenser, was added 3,4-dimethoxybenzaldehyde 1 (16.6 g, 100 mmol), dimethylmalonate (12.54 mL, 110 mmol), benzoic acid (0.3 g, 2.5 mmol), and piperidine (0.93 mL, 9.4 mmol). This mixture was heated at 85°C, with continuous stirring, for 1.2 h. The reaction solution

was allowed to cool to room temperature followed by addition of cold methanol (75 mL), at which time crystals began to form. The reaction mixture was cooled in an ice bath for 30 min. The crystalline product was collected by suction filtration, washed with cold methanol (2 x 10 mL) followed by hexane (3 x 30 mL) and allowed to air dry. The white crystalline product was obtained in a yield of 88%.

^{1}H NMR ($CDCl_3$): δ = 7.68 (s, 1H), 7.05 (d, J = 8.2 Hz , 1H), 6.97 (1, 1H), 6.85 (d, J = 8.3, 1H), 3.89 (s, 3H), 3.85 (s, 6H), 3.82 (s, 3H).

2. Dimethyl-3,4-dimethoxybenzylmalonate (3)

The benzylidene derivative **2** (20.4 g, 87 mmol) was dissolved in a mixture of hot methanol (50 mL) and dioxane (100 mL), and degassed with nitrogen. 10% palladium on carbon (5 g) was added and hydrogenation was carried out at 60 psi in a Parr shaker apparatus for 8 h. The reaction mixture was then filtered through a bed of Celite, the deposited carbon washed with hot methanol (2 x 10 mL), and the filtrate solvent stripped to give a tan oil. This reaction afforded a yield of 86% for **3**.

^{1}H NMR ($CDCl_3$): δ = 6.75-6.68 (m, 3H), 3.81 (s, 3H), 3.80 (s, 3H), 3.60 (s, 6H), 3.61 (t, J = 7.8, 1H), 3.13 (d, J = 7.8, 2H).

3. Dimethyl-4,5-dimethoxy-2-nitrobenzylmalonate (4)

Fuming nitric acid (16.3 mL, 354 mmol) was added dropwise to a solution of dimethyl-3,4-dimethoxybenzylmalonate **3** (16.6 g, 58.9 mmol) dissolved in chloroform (160 mL) at 0°C under a nitrogen atmosphere. The reaction was stirred at 0°C for 4 h. The reaction mixture was neutralized and washed with a saturated sodium hydroxide solution followed by water. The organic layer was dried with Na_2SO_4, followed by rotory evaporation to give a yellow solid in quantitative yield (100%).

^{1}H NMR ($CDCl_3$): δ = 7.63 (s, 1H), 6.78 (s, 1H), 3.96-3.93 (m, 1H), 3.92 (s, 6H), 3.69 (s, 6H), 3.49 (d, J = 7.5 Hz, 2H).

4. 3-Carboxymethyl-6,7-dimethoxy-1,2,3,4-tetrahydro-2-oxoquinoline (5)

The nitrophenyl derivative **4** (1.2 g, 3.67 mmol) was dissolved in a mixture of warm THF (15 mL) and methanol (60 mL). After cooling to room temperature, 10% palladium on carbon (200 mg) and glacial acetic acid (0.6 mL) were added. The hydrogenation vessel was pressurized to 40 psi of hydrogen in a Parr shaker apparatus. The reaction was stopped after 6 h at room temperature, bubbled with nitrogen gas, diluted with warm THF (50 mL), filtered through a bed of Celite, and the residue washed successively with hot THF (2 x 10 mL) and hot chloroform (2 x 10 mL). The combined filtrate was stripped of sovent to yield a sticky solid. This was dissolved in 50 mL of chloroform, and the mixture was washed with a saturated sodium bicarbonate solution followed by water. The organic layer was separated, and the solvent was stripped. The product was dissolved in hot methanol (10 mL) and then cooled to 0°C, with a white precipitate forming during the cooling. The precipitate was collected by suction filtration and washed with cold methanol (2 x 5 mL). The collected product was obtained in a 72% yield.

^{1}H NMR ($CDCl_3$): δ = 7.69 (bs, 1H), 6.68 (s, 1H), 6.31 (s, 1H), 3.83 (s, 6H), 3.74 (s, 3H), 3.60 (dd, J = 8.4 & 6.3 Hz, 1H), 3.30 (dd, J = 15.9 & 8.4 Hz, 1H), 3.05 (dd, J = 15.9 & 6.3 Hz, 1H).

MS (70 eV-DIP) m/z (relative intensity): 265 (M^+, 21), 206 (100).

MS (FAB) m/z (relative intensity): 266 (M+1, 100), 265 (98), 206 (54).

5. 3-Carboxamide-6,7-dimethoxy-1,2,3,4-tetrahydro-2-oxoquinoline (6)

The methylester derivative **5** (200 mg, 0.755 mmol), methanol (8 mL), and THF (8 mL) were added to a pressure bottle and heated to effect dissolution. The solution was cooled to 0°C, degassed with argon, and ammonium hydroxide (4 mL) was added. The solution was saturated with ammonia gas, and the pressure bottle was sealed and heated

to 65°C for 22 h. A white precipitate formed as the reaction proceeded. The solution was cooled to room temperature, and the precipitate was collected by suction filtration. Further purification by silica gel chromatography was unsuccessful due to instability of the product. A yield of 24% was obtained.

^{1}H NMR (DMSO-d^6): δ = 9.97 (bs, 1H), 7.43 (s, 1H), 7.07 (s, 1H), 6.81 (s, 1H), 6.49 (s, 1H), 3.69 (s, 3H), 3.67 (s, 3H), 3.28 (dd, J = 9.9 & 6.6 Hz, 1H), 3.08 (dd, J = 15.9 & 9.9 Hz, 1H), 2.88 (dd, J = 15.9 & 6.6 Hz, 1H).

MS (70 eV-DIP) m/z (relative intensity): 250 (M^+, 32), 206 (100).

MS (12 eV-DIP) m/z (relative intensity): 250 (M^+, 30), 206 (100).

MS (FAB) m/z (relative intensity): 251 (M+1, 100), 250 (63), 206 (81).

6. 3-Aminomethyl-6,7-dimethoxy-1,2,3,4-tetrahydroquinoline (7)

The carboxamide compound **6** (100 mg, 0.40 mmol) was placed in a pear-shaped side arm flask equipped with a water condenser and maintained under a nitrogen atmosphere. The reaction flask was lowered to 0°C, and BH_3:THF (1 M, 9.6 mL, 9.6 mmol) was added dropwise. The solution was heated at reflux for 3.5 h with continuous stirring. The reaction mixture was hydrolyzed with 6 M HCl until the evolution of hydrogen subsided, stirred for a further 30 min, and cooled. The solution was basified with a saturated sodium hydroxide solution to pH 10-11 and extracted with chloroform (4 x 50 mL). The organic extracts were combined, dried using Na_2SO_4, and the organic solvent stripped to yield a thick oil. Any purification by column chromatography is not recommended due to instability of the product. The reaction gave a pure product with a yield of 88%.

^{1}H NMR ($CDCl_3$): δ = 6.50 (s, 1H), 6.09 (s, 1H), 3.76 (s, 6H), 3.33 (dd, J = 10.8 & 3.3 Hz, 1H), 2.94 (dd, J = 10.8 & 8.7 Hz, 1H), 2.76 (dd, J = 15.9 & 5.1 Hz, 1H), 2.69 (dd, J = 7.2 & 2.4 Hz, 2H), 2.39 (dd, J = 15.9 & 8.7 Hz, 1H), 2.00-1.86 (m, 1H).

MS (70 eV-DIP) m/z (relative intensity): 222 (M^+, 100), 192 (12), 190 (70).

7. 3-Aminomethyl-6,7-dihydroxy-1,2,3,4-tetrahydroquinoline • 2HBr (8 • 2HBr)

Dimethoxy derivative **7** (80 mg, 0.37 mmol) was placed in a pressure bottle, and the bottle was flushed with argon. Hydrobromic acid (48%, 1.4 mL, 25.9 mmol) was added, the bottle was sealed, and the mixture was heated at reflux for 8 h. The solution was lyophilized, and the resultant crude solid was repeatedly washed with ether (6 x 1 mL) and acetonitrile (6 x 1 mL) in an alternating fashion until the organic layer remained clear. A light tan solid was isolated in a 74% yield.

^{1}H NMR (D_2O); δ = 6.79 (s, 1H), 6.75 (s, 0.5H, part. exch.), 3.67 (bd, J_{app} = 11.1, 1H), 3.19-3.03 (m, 3H), 2.94 (dd, J = 15.6 & 3.9 Hz, 1H), 2.59 (dd, J = 15.6 & 10.8 Hz, 1H), 2.54-2.44 (m, 1H).

MS (12 eV-DIP) m/z (relative intensity): 194 (M^+, 76), 176 (26).

C. Synthesis of 3-Amino-6,8-dihydroxy-1,2,3,4-tetrahydroquinoline Hydrobromide

1. 4-(3,5-Dimethoxybenzylidene)-2-phenyl-5-oxazolone (10)

3,5-dimethoxybenzaldehyde **9** (17 g, 102 mmol), hippuric acid (19.25 g, 107 mmol), anhydrous sodium acetate (8.39 g, 102 mmol) and acetic anhydride (50 mL, 530 mmol) were added to a 250 mL round bottomed flask equipped with a water condenser fitted with a drying tube. The reaction mixture was heated at 85°C with continuous stirring for 2.5 h, during which time the color of the solution turned from white to a bright yellow. The mixture was cooled, and cold ethanol (65 mL) was added, upon which a yellow crystalline product appeared. The mixture was further cooled. The

mixture was then filtered with suction, and the solid product was washed with cold ethanol (2 x 25 mL), with boiling water (3 x 20 mL), and, finally, with ice-cold ether (5 mL). The yield was 86%.

^{1}H NMR ($CDCl_3$): δ = 8.14 (bd, J_{app} = 6.9 Hz, 2H), 7.63-7.49 (m, 3H), 7.40 (d, J = 2.4 Hz, 2H), 7.15 (s, 1H), 6.65 (t, J = 2.4 Hz, 1H), 3.87 (s, 6H).

2. Methyl-2-benzoylamino-3-(3,5-dimethoxyphenyl)-2-propenoate (11)

The azlactone compound **10** (26.3 g, 85 mmol), anhydrous sodium carbonate (26.82 g, 255 mmol), and methanol (263 mL, dry) were added to a 500 mL round bottomed flask equipped with a water condenser fitted with a drying tube. The contents were refluxed for 45 min during which time the yellow color of the reaction mixture disappeared. The mixture was filtered hot, and the captured solid washed with hot methanol (2 x 15 mL). The combined filtrate was cooled in the refrigerator for a minimum of 3 h. A white crystalline product formed and was collected by filtration and washed with 1:1 methanol:water (2 x 10 mL). The yield was 88%.

^{1}H NMR ($CDCl_3$): δ = 7.85 (bd, J_{app} = 7.2 Hz, 2H), 7.70 (bs, 1H), 7.56-7.43 (m, 3H), 7.36 (s, 1H), 6.64 (d, J = 2.1 Hz, 2H), 6.40 (t, J = 2.1 Hz, 1H), 3.85 (s, 3H), 3.65 (s, 6H).

3. Methyl-2-benzoylamino-3-(3,5-dimethoxyphenyl)propanoate (12)

Propene derivative **11** (9.89 g, 29 mmol) was dissolved in hot THF (55 mL). To this solution was added methanol (55 mL), 10% palladium on carbon (1.50 g) and glacial acetic acid (0.75 mL). Hydrogenation was carried out at 60 psi for 10 h in a Parr shaker apparatus. The reaction solution was filtered through a thick layer of Celite. The filtering agent was washed with hot methanol:chloroform (1:3, 3 x 10 mL). Solvent was removed, yielding an oil which turned into a white solid upon drying with an oil pump vacuum. This reaction was quantitative (100% yield).

^{1}H NMR ($CDCl_3$): δ = 7.73 (d, J = 7.8 Hz, 2H), 7.52-7.38 (m, 3H), 6.59 (d, J = 7.2 Hz, 1H), 6.33 (t, J = 2.4 Hz, 1H), 6.26 (d, J = 2.4 Hz, 2H), 5.06 (dt, J = 7.5 & 5.4 Hz, 1H), 3.77 (s, 3H), 3.69 (s, 6H), 3.25-3.12 (m, 2H)

4. Methyl-2-benzoylamino-3-(3,5-dimethoxy-2-nitrophenyl)propanoate (13)

Initial attempted syntheses

a) The propanoate derivative **12** (1 g, 2.9 mmol) was dissolved in chloroform (10 mL), and the mixture was purged with nitrogen. To this solution, fuming nitric acid (128 µL, 17.5 mmol) was added dropwise. The reaction was stirred at 0°C for 9 h. The workup of the mixture was the same as that described below for the most successful conditions. These conditions gave a yield of 16%.

b) The propanoate derivative **12** (50 mg, 0.146 mmol) was dissolved in chloroform (100 µL), and the mixture was purged with nitrogen. To this solution were added ammonium nitrate (11.9 mg, 0.146 mmol) and trifluoroacetic acid (73 µL, 0.51 mmol). The reaction was stirred at room temperature for 1 h. The workup of the mixture was the same as that described below for the most successful conditions. These conditions gave a yield of 3%.

c) In a round bottomed flask equipped with a condenser fitted with a drying tube, the starting material (105 mg, 0.307 mmol) was dissolved in $CHCl_3$ (3 mL). To this solution were added ethanol (1 mL, 100%), pyridine (50 µL) and tetranitromethane (0.4 g). The mixture was heated at reflux for 4 h. At the completion of the reaction, 6 M HCl (20 mL) was added, and the reaction mixture was extracted with EtOAc. The organic layer was dried with Na_2SO_4, and the solvent was stripped to yield a violet solid. The crude product was purified using preparative TLC and afforded an 8% yield.

Final, most successful synthesis

The propanoate derivative **12** (3.41 g, 9.9 mmol) was dissolved in glacial acetic acid (136 mL), and the solution was purged with nitrogen. The nitrating agent, 70.4% nitric acid (2.25 mL, 39.6 mmol) mixed with glacial acetic acid (4 mL), was added dropwise to the solution. The reaction was stirred at 15°C for 24 h, after which the mixture was neutralized with a sodium hydroxide solution to a neutral pH. Chloroform (50 mL) was added, and the layers were allowed to separate. The chloroform layer was dried with Na_2SO_4, and the solvent was removed to give a blackish product which was purified by column chromatography (SiO_2, 75:25 $CHCl_3$:EtOAc, 40 g SiO_2/g crude product). The yield of the nitrated product following column purification was 18.6%. ^1H NMR ($CDCl_3$): δ = 7.78 (bd, J_{app} = 6.9 Hz, 2H), 7.51-7.38 (m, 3H), 7.10 (d, J = 7.0 Hz, 1H), 6.43 (d, J = 2.4 Hz, 1H), 6.39 (d, J = 2.4 Hz, 1H), 4.98 (ddd, J = 9.3 & 7.1 & 5.1 Hz, 1H), 3.83 (s, 3H), 3.77 (s, 3H), 3.76 (s, 3H), 3.23 (dd, J = 14.4 & 5.1 Hz, 1H), 3.03 (dd, J = 14.4 & 9.3 Hz, 1H).

5. 3-Benzoylamino-6,8-dimethoxy-1,2,3,4-tetrahydro-2-oxoquinoline (14)

The nitro compound **13** (4.25 g, 10.9 mmol) was dissolved in a hot mixture of methanol (140 mL), THF (6 mL), and 1,4-dioxane (120 mL). The solution was degassed with nitrogen and cooled to room temperature. Palladium on carbon (10%, 682 mg) and glacial acetic acid (3.25 mL) were added, and hydrogenation was carried out at 65 psi for 48 h in a Parr shaker apparatus. The solution was degassed with nitrogen and filtered through a bed of Celite. The deposited charcoal was washed with hot chloroform (2 x 10 mL), and the combined filtrate was stripped of the solvent leaving a thick oil. The oil was dissolved in chloroform (50 mL), and the resulting solution was washed with a 5% sodium bicarbonate solution, followed by water. The organic layer was separated

and dried with Na_2SO_4, and the solvent was removed to give an off-white solid. The yield was 90%.

^1H NMR ($CDCl_3$): δ = 7.86 (bd, J_{app} = 6.9 Hz, 2H), 7.71 (bs, 1H), 7.54-7.41 (m, 3H), 7.33 (d, J = 4.3 Hz, 1H), 6.39 (d, J = 2.7 Hz, 1H), 6.37 (d, J = 2.1 Hz, 1H), 4.66 (ddd, J = 14.1 & 6.3 & 4.4 Hz, 1H), 3.84 (s 3H), 3.78 (s, 3H), 3.69 (dd, J = 15.3 & 6.3 Hz, 1H), 2.83 (dd, J = 15.3 & 14.1 Hz, 1H).

6. 3-Benzylamino-6,8-dimethoxy-1,2,3,4-tetrahydroquinoline (15)

To the quinoline product **14** (893 mg, 2.7 mmol) in a 300 mL round bottomed flask equipped with a water condenser and a dropping funnel was added BH_3:THF (1 M, 44 mL, 44 mmol), dropwise, at room temperature under a nitrogen atmosphere. The solution was heated at reflux for 3 h and then cooled. The reaction mixture was hydrolyzed with 6 M HCl until no more hydrogen evolved. Water was added until all the salts dissolved. The mixture was stirred for an additional 30 min and then cooled. THF was stripped from the mixture. The reaction mixture was basified with a saturated sodium hydroxide solution to pH 10-11 and extracted with chloroform (4 x 50 mL). The organic extracts were combined, dried with Na_2SO_4, filtered, and the solvent was removed to give a thick brown oil which was purified by column chromatography (SiO_2, 90:10 $CHCl_3$:MeOH). The yield of purified **15** was 90%.

^1H NMR ($CDCl_3$): δ = 7.38-7.22 (m, 5H), 6.28 (d, J = 2.4 Hz, 1H), 6.17 (J = 2.4 Hz, 1H), 3.89 (s, 2H), 3.78 (s, 3H), 3.72 (s, 3H), 3.36 (bt, J_{app} = 7.2 Hz, 1H), 3.15-3.08 (m, 2H), 2.95 (dd, J = 16.5 & 3.9 Hz, 1H), 2.69 (dd, J = 16.5 & 7.5 Hz, 1H).

MS (70 eV-DIP) m/z (relative intensity): 298 (M^+, 100), 192 (88).

7. 3-Amino-6,8-dimethoxy-1,2,3,4-tetrahydroquinoline (16)

N-Benzylamine derivative **15** (532 mg, 1.79 mmol) was dissolved in glacial acetic acid (13.3 mL). The solution was degassed with nitrogen, and 10% palladium on

carbon (107 mg) was added. Hydrogenation was carried out at 65 psi for 98 h in a Parr shaker apparatus. The solution was filtered through a bed of Celite, the carbon powder washed with hot chloroform (2 x 10 mL), and the filtrate solvent was removed to yield an oil. This oil was dissolved in chloroform (100 mL), washed with a 10% sodium hydroxide solution, and washed with water. The organic layer was isolated and dried with Na_2SO_4, and the solvent was removed to give a gummy solid which was purified by column chromatography (SiO_2, 90:10 $CHCl_3$:MeOH). The purified product was obtained in an 83% yield.

^1H NMR ($CDCl_3$): δ = 6.28 (d, J = 2.4 Hz, 1H), 6.16 (d, J = 2.7 Hz, 1H), 3.78 (s, 3H), 3.71 (s, 3H), 3.39-3.32 (m, 1H), 3.30 (bd, J_{app} = 11.7 Hz, 1H), 3.06-2.95 (m, 2H), 2.46 (dd, J = 16.2 & 6.3 Hz, 1H).

MS (70 eV-DIP) m/z (relative intensity): 208 (M^+, 100), 193 (34), 192 (23).

8. 3-Amino-6,8-dihydroxy-1,2,3,4-tetrahydroquinoline•2HBr (17•2HBr)

The dimethoxy compound **16** (232 mg, 1.12 mmol) was placed in a pressure bottle. The bottle was flushed with argon, followed by addition of an excess of 48% hydrobromic acid (3.0 mL). The mixture was heated at reflux for 26 h. The solution was lyophilized, and the solid obtained was repeatedly washed with ether (6 x 1 mL) and acetonitrile (6 x 1 mL) in an alternating fashion until the organic wash solvents remained clear. A tan solid product was obtained with a yield of 86%.

^1H NMR (D_2O); δ = 6.38 (d, J = 2.7 Hz, 0.5H, part. exch.), 6.3 (d, J = 2.4 Hz, 1H), 3.98-3.88 (m, 1H) [alternatively, this multiplet could be reported as 3.93 (dddd, J = 9.9, 9.6, 5.3, & 3.5 Hz, 1H)], 3.83 (ddd, J = 12.3 & 3.5 & 1.7 Hz, 1H), 3.42 (dd, J = 12.3 & 10.2 Hz, 1H), 3.23 (bdd, J_{app} = 16.8 & 5.4 Hz, 1H), 2.94 (dd, J = 16.8 & 9.3 Hz, 1H).

MS (70 eV-DIP) m/z (relative intensity): 180 (M^+, 100), 164 (22), 82 (53), 80 (55).

IV. NMR Spectra and Assignments

This section contains the 300 MHz proton NMR spectra and associated signal assignments for the compounds discussed above in sections II and III.

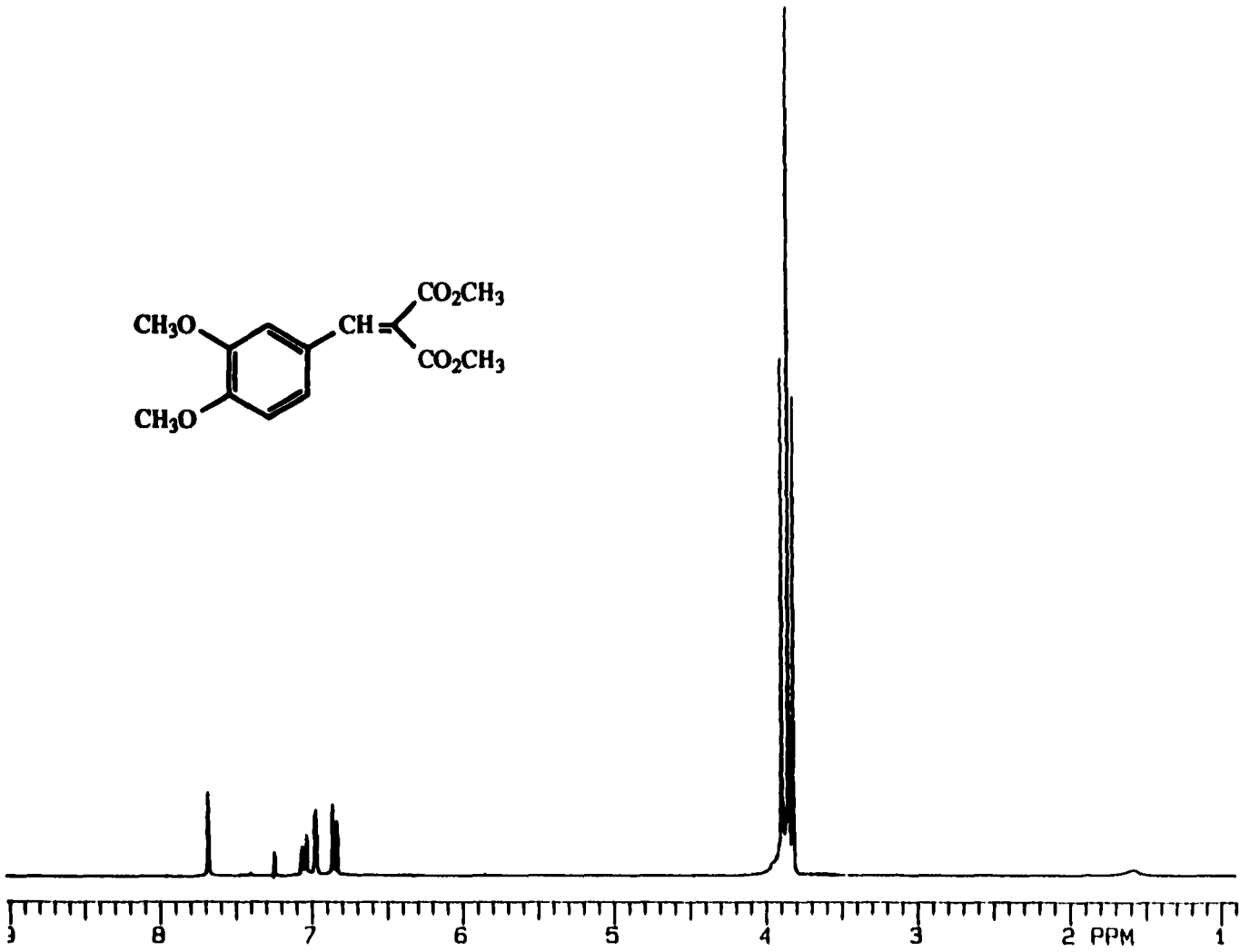

Figure 2-1. Proton NMR spectum of **2** in $CDCl_3$.

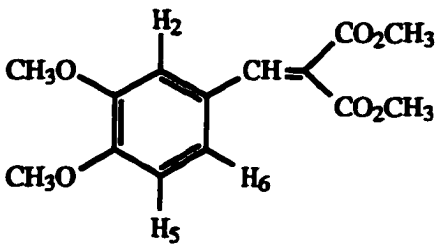

2

Table 2-1. Proton NMR signal assignments for **2** in $CDCl_3$.

Proton(s)	Multiplicity	Chemical shift, δ (ppm)	Coupling constant, J (Hz)
=CH	s	7.68	-
H-6	d	7.05	8.2
H-2	s	6.97	-
H-5	d	6.85	8.3
-OMe	s	3.89	-
$-CO_2Me$'s	s	3.85	-
-OMe	s	3.82	-

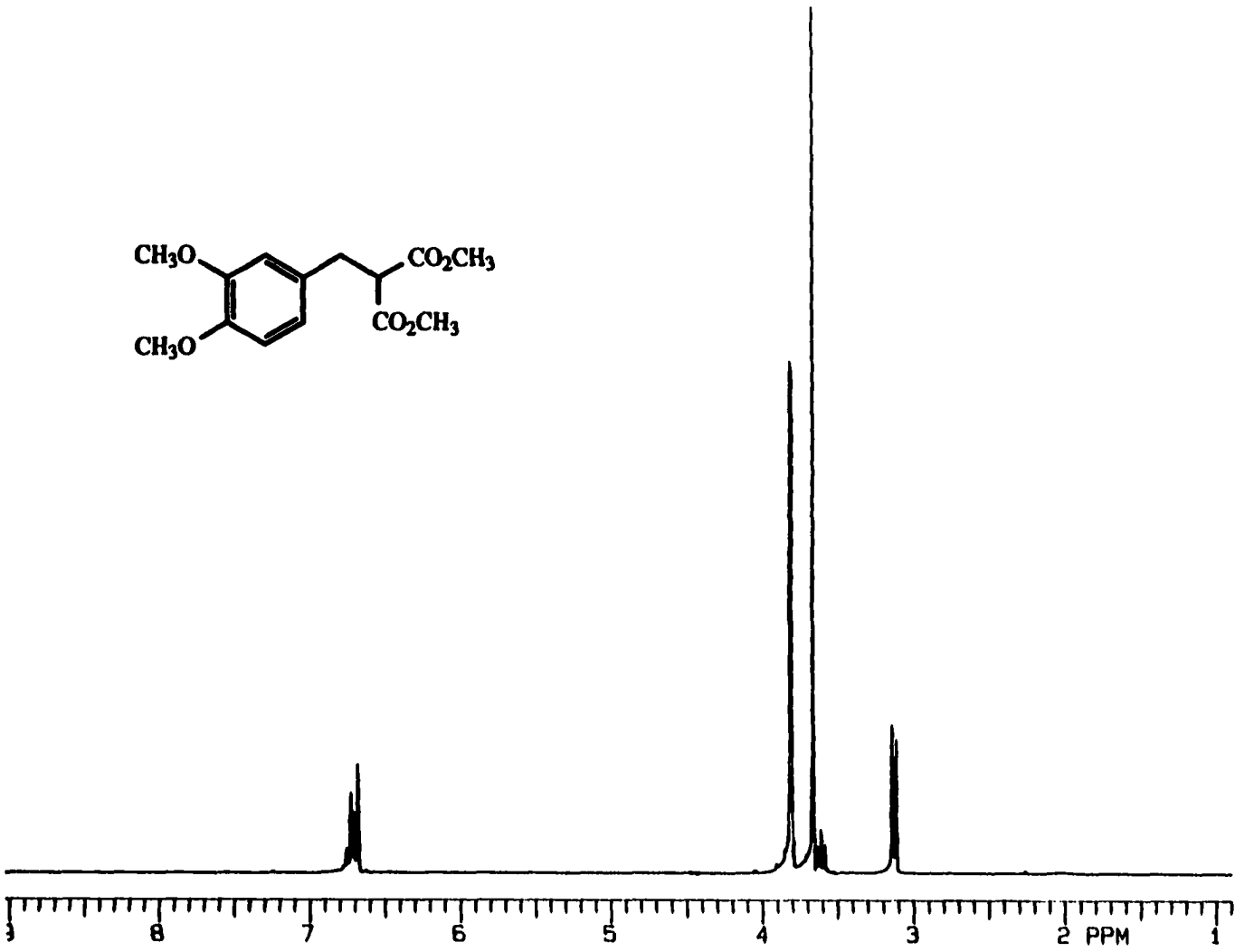

Figure 2-2. Proton NMR spectum of **3** in $CDCl_3$.

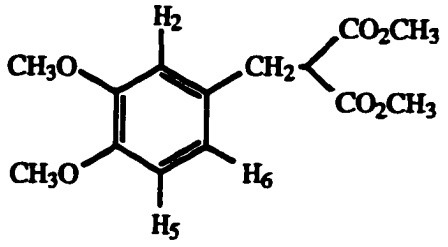

3

Table 2-2. Proton NMR signal assignments for **3** in $CDCl_3$.

Proton(s)	Multiplicity	Chemical shift, δ (ppm)	Coupling constant, J (Hz)
H-2, H-5, & H-6	m	6.75-6.68	-
-OMe	s	3.81	-
-OMe	s	3.80	-
$-CO_2Me$'s	s	3.66	-
-CH	t	3.61	7.8
$-CH_2$	d	3.13	7.8

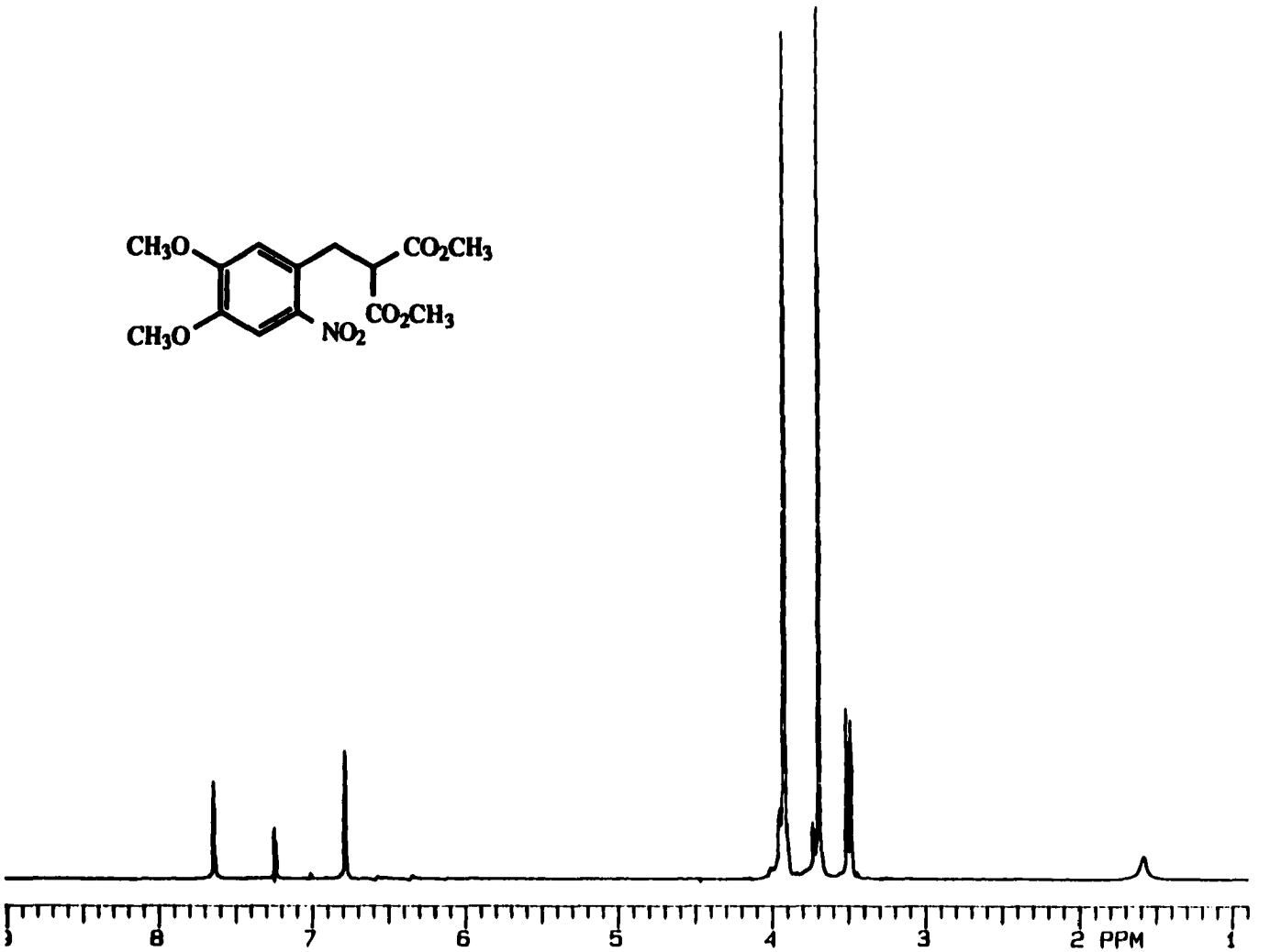

Figure 2-3. Proton NMR spectum of **4** in $CDCl_3$.

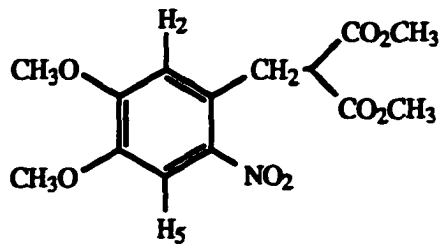

4

Table 2-3. Proton NMR signal assignments for **4** in $CDCl_3$.

Proton(s)	Multiplicity	Chemical shift, δ (ppm)	Coupling constant, J (Hz)
H-5	s	7.63	-
H-2	s	6.78	-
-CH*	m	3.96-3.93	-
-OMe's	s	3.92	-
-CO_2Me's	s	3.69	-
-CH_2	d	3.49	7.5

* One would a priori expect to see a triplet for -CH. Unfortunately, we were unable to resolve the actual pattern due in part to a coincidental overlap of these peaks with those of the -OMe's at δ = 3.92.

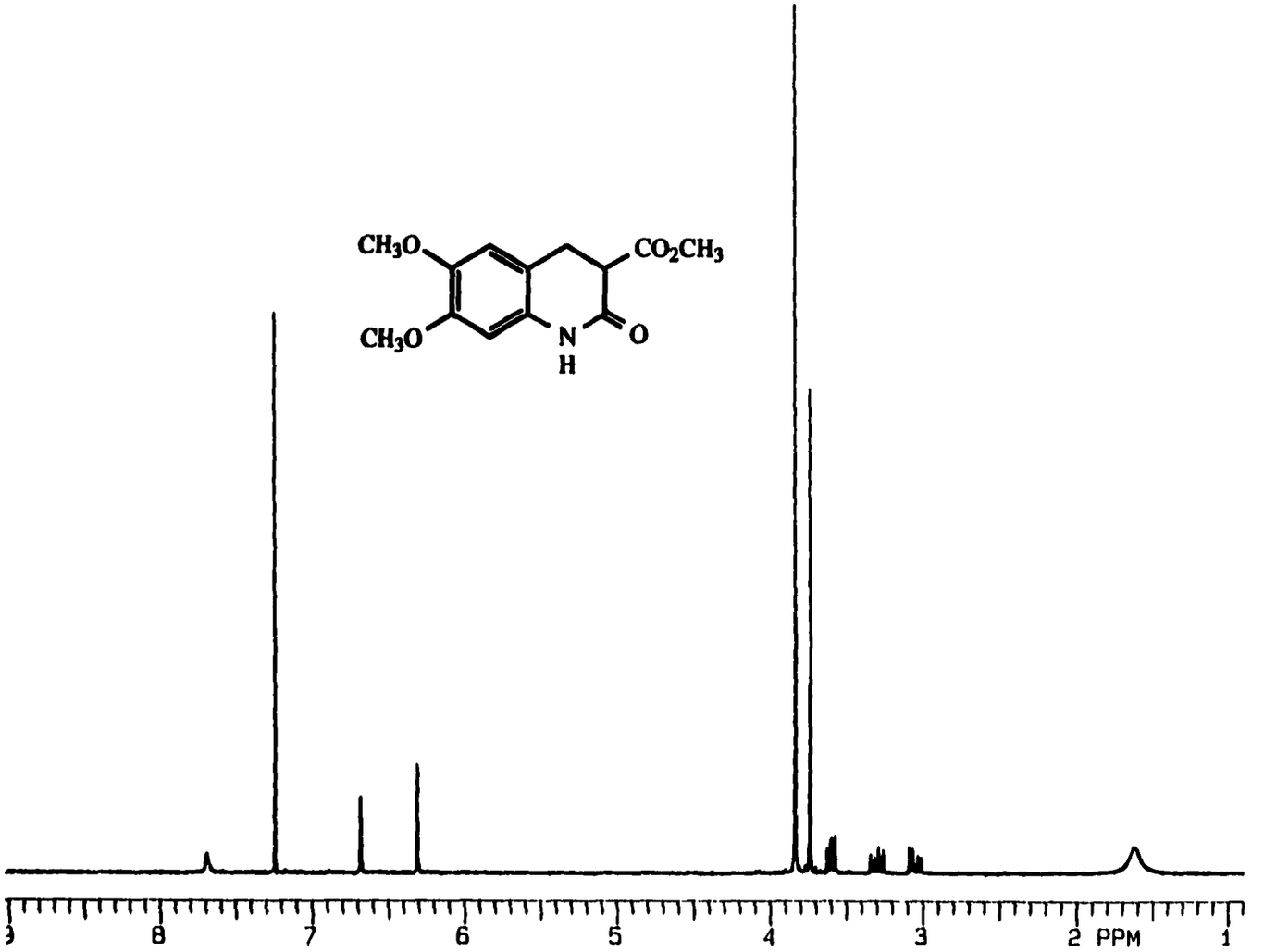

Figure 2-4. Proton NMR spectum of **5** in $CDCl_3$.

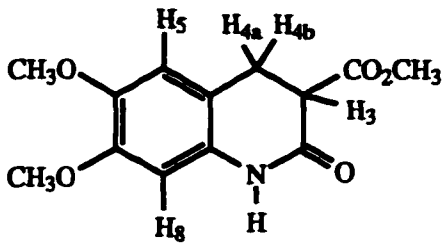

5

Table 2-4. Proton NMR signal assignments for **5** in $CDCl_3$.

Proton(s)	Multiplicity	Chemical shift, δ (ppm)	Coupling constant, J (Hz)
-NH	bs	7.69	-
H-8	s	6.68	-
H-5	s	6.31	-
-OMe's	s	3.83	-
$-CO_2Me$	s	3.74	-
H-3	dd	3.60	8.4, 6.3
H-4a	dd	3.30	15.9, 8.4
H-4b	dd	3.05	15.9, 6.3

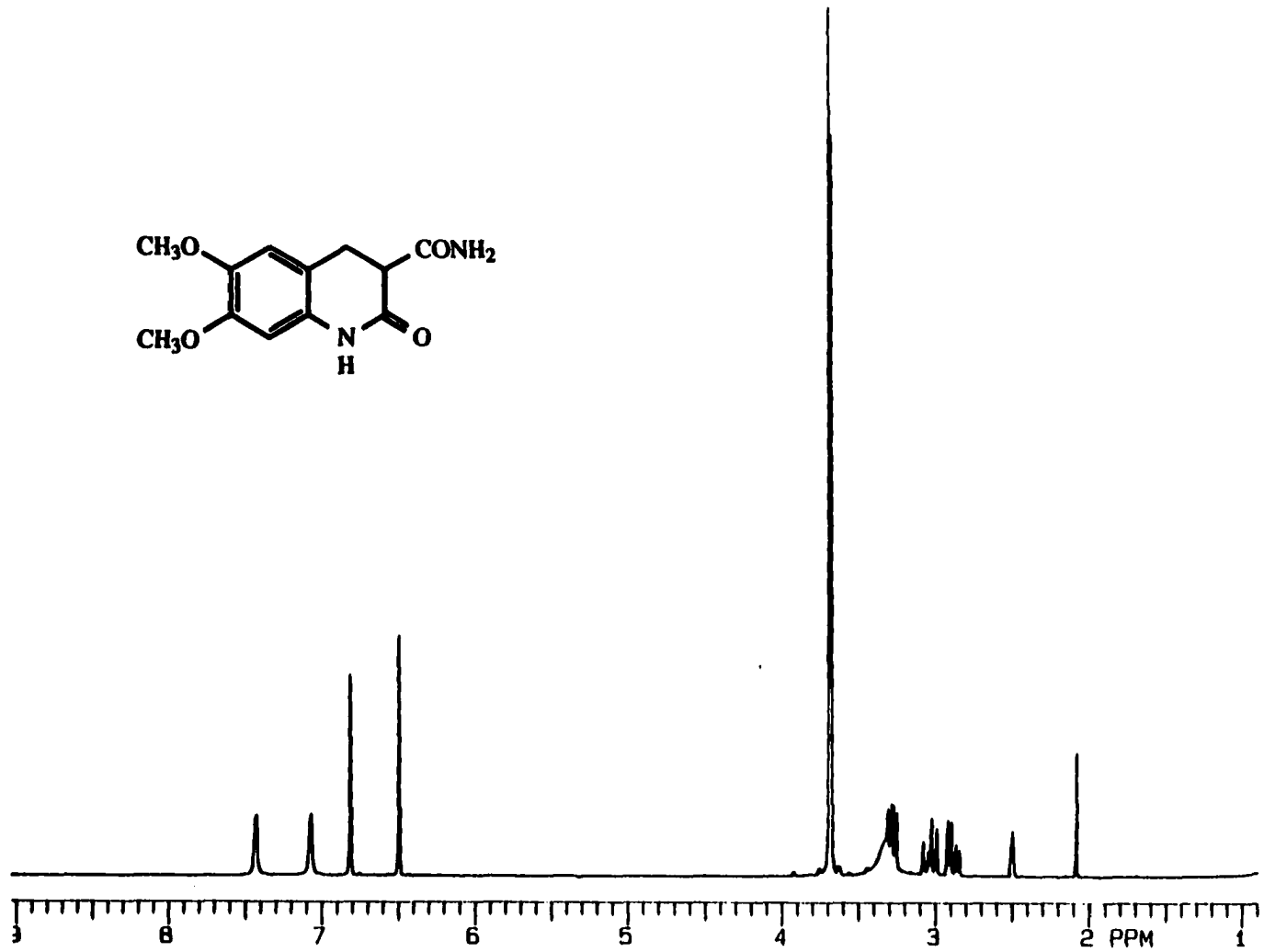

Figure 2-5. Proton NMR spectum of **6** in DMSO-d^6.

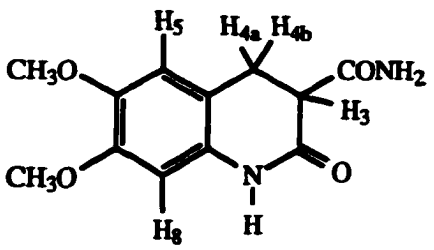

6

Table 2-5. Proton NMR signal assignments for **6** in DMSO-d^6.

Proton(s)	Multiplicity	Chemical shift, δ (ppm)	Coupling constant, J (Hz)
-$CONH_2$	bs	9.97	-
-NH	s	7.43	-
-$CONH_2$	s	7.07	-
H-8	s	6.81	-
H-5	s	6.49	-
-OMe	s	3.69	-
-OMe	s	3.67	-
H-3	dd	3.28	9.9, 6.6
H-4a	dd	3.03	15.9, 9.9
H-4b	dd	2.88	15.9, 6.6

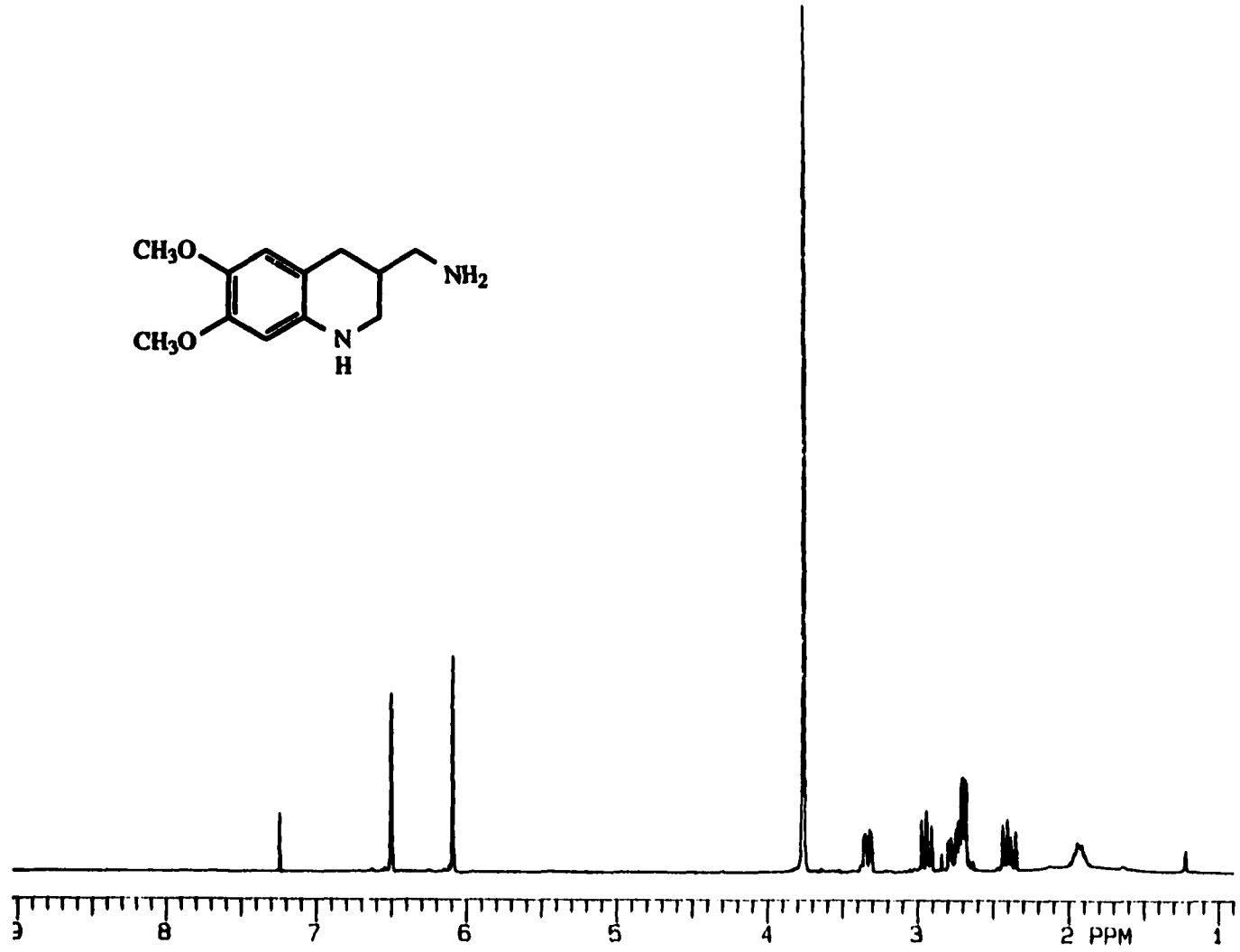

Figure 2-6. Proton NMR spectum of 7 in $CDCl_3$.

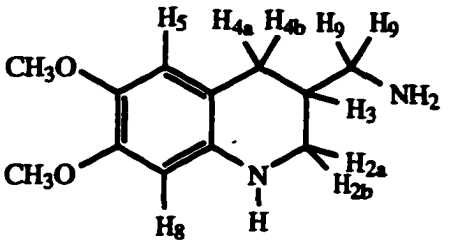

7

Table 2-6. Proton NMR signal assignments for **7** in $CDCl_3$.

Proton(s)	Multiplicity	Chemical shift, δ (ppm)	Coupling constant, J (Hz)
H-5	s	6.50	-
H-8	s	6.09	-
-OMe's	s	3.76	-
H-2a	dd	3.33	10.8, 3.3
H-2b	dd	2.94	10.8, 8.7
H-4a	dd	2.76	15.9, 5.1
H-9*	dd	2.69	7.2, 2.4
H-4b	dd	2.39	15.9, 8.7
H-3	m	2.00-1.86	-

* One would a priori expect to see a doublet for $-CH_2$ (H-9); however, we observed a doublet of doublets. This is most likely a result of the H-9 protons being diastereotopic. Since they are diastereotopic, we would expect to see two doublet of doublets. But, their chemical shifts may be so similar that a non-first order spectrum is observed.

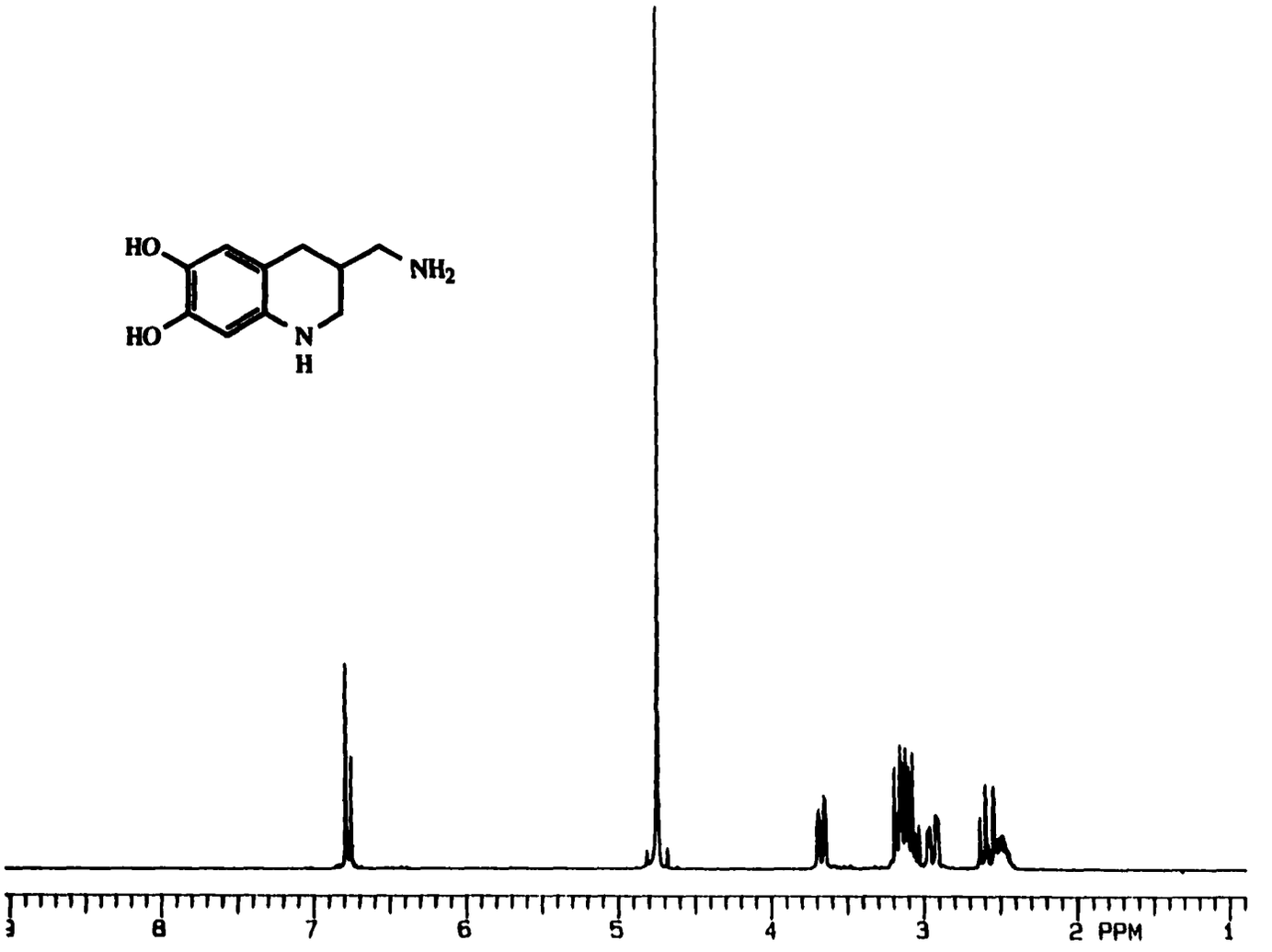

Figure 2-7. Proton NMR spectum of **8**•2HBr in D_2O.

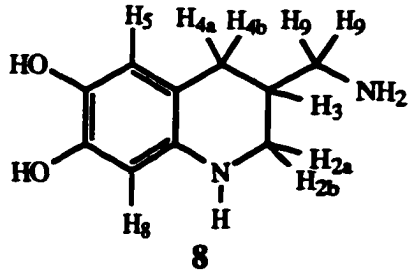

8

Table 2-7. Proton NMR signal assignments for **8** in D_2O.

Proton(s)	Multiplicity	Chemical shift, δ (ppm)	Coupling constant, J (Hz)
H-5	s	6.79	-
H-8	s	6.75	-
H-2a*, **	bd	3.67	J_{app} = 11.1
H-2b** & H-9	m	3.19-3.03	-
H-4a*, **	bdd	2.94	15.6, 3.9
H-4b**	dd	2.59	15.6, 10.8
H-3	m	2.54-2.44	-

* COSY shows there to be a long range coupling between H-2a and H-4a which is obscured in the broad doublet seen at δ = 3.67 and the broad doublet of doublets at δ = 2.94.

** Equatorial protons, in general, are more deshielded than axial protons and have a greater potential for long range coupling; therefore, it is presumed that H-2a and H-4a are equatorial and H-2b and H-4b are axial.

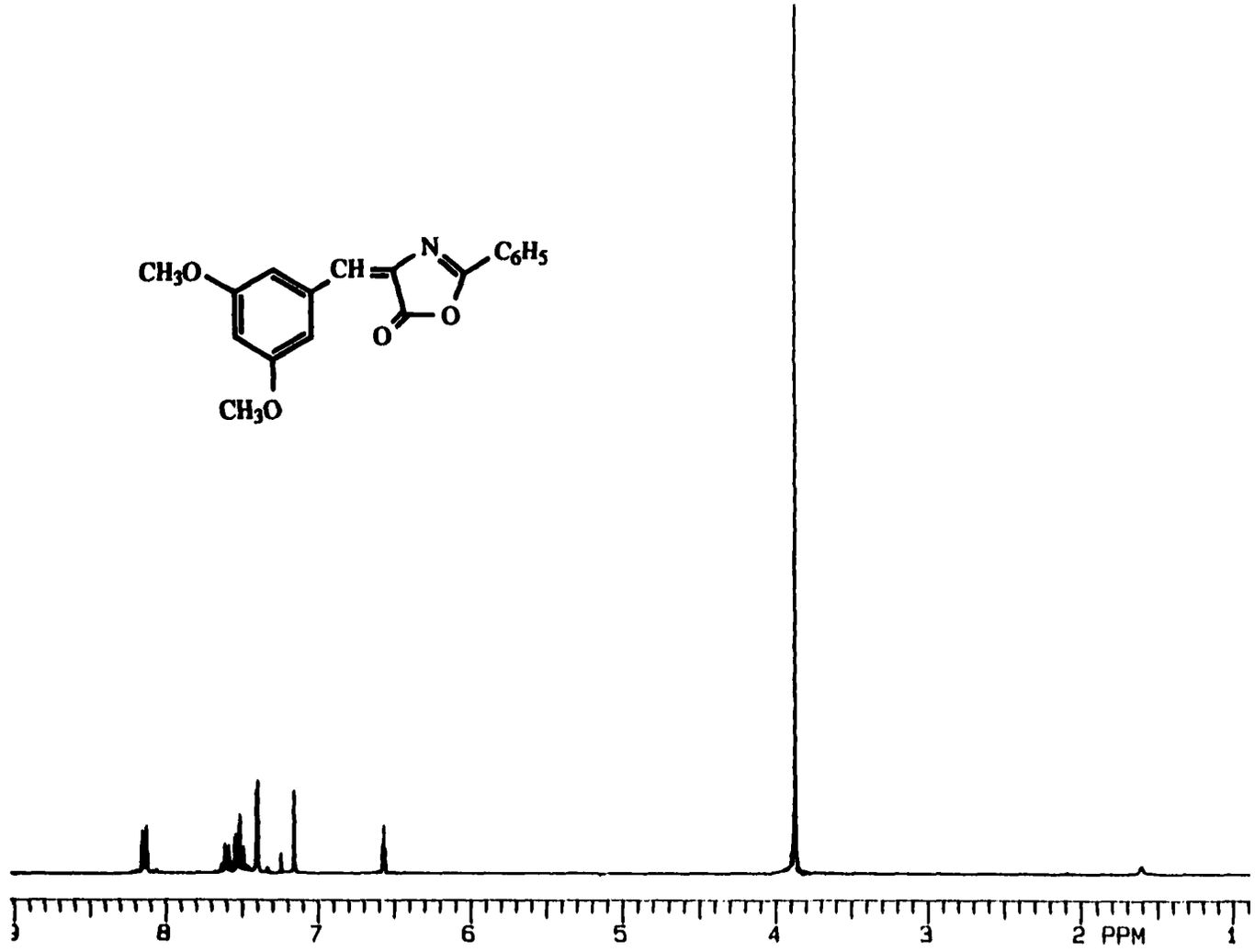

Figure 2-8. Proton NMR spectum of **10** in $CDCl_3$.

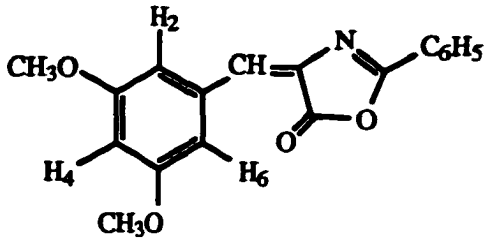

10

Table 2-8. Proton NMR signal assignments for **10** in $CDCl_3$.

Proton(s)	Multiplicity	Chemical shift, δ (ppm)	Coupling constant, J (Hz)
C_6H_5 (ortho)	bd	8.14	$J_{app} = 6.9$
C_6H_5 (meta, para)	m	7.63-7.49	-
H-2 & H-6	d	7.40	2.4
=CH	s	7.15	-
H-4	t	6.65	2.4
-OMe's	s	3.87	-

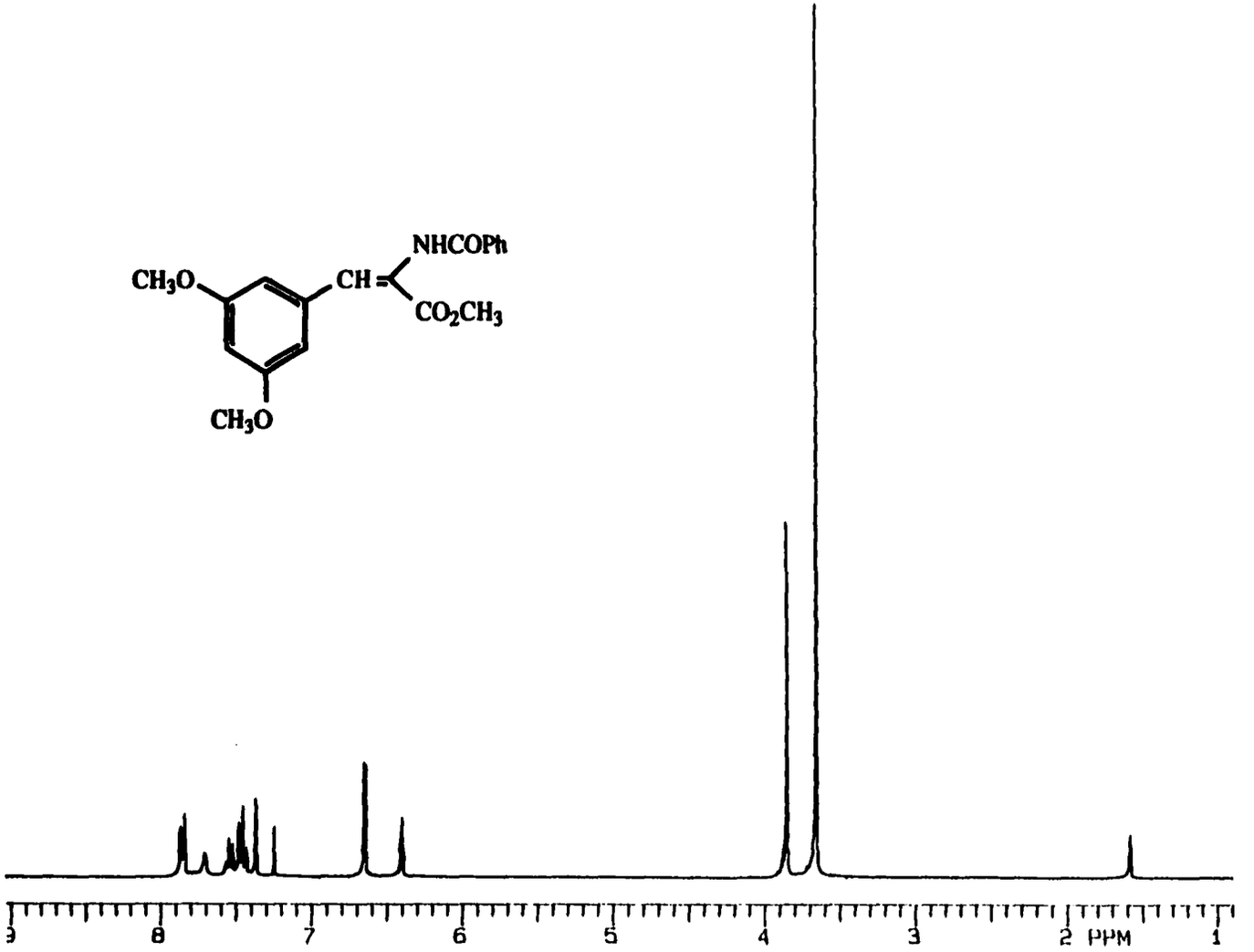

Figure 2-9. Proton NMR spectum of **11** in $CDCl_3$.

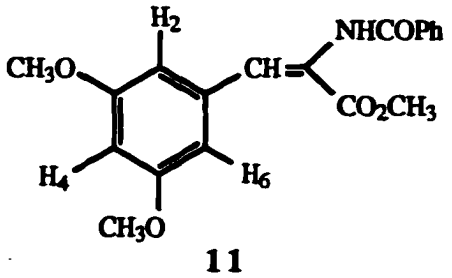

11

Table 2-9. Proton NMR signal assignments for **11** in $CDCl_3$.

Proton(s)	Multiplicity	Chemical shift, δ (ppm)	Coupling constant, J (Hz)
C_6H_5 (ortho)	bd	7.85	J_{app} = 7.2
-NH	bs	7.70	-
C_6H_5 (meta, para)	m	7.56-7.43	-
=CH	s	7.36	-
H-2 & H-6	d	6.64	2.1
H-4	t	6.40	2.1
$-CO_2Me$	s	3.85	-
-OMe's	s	3.65	-

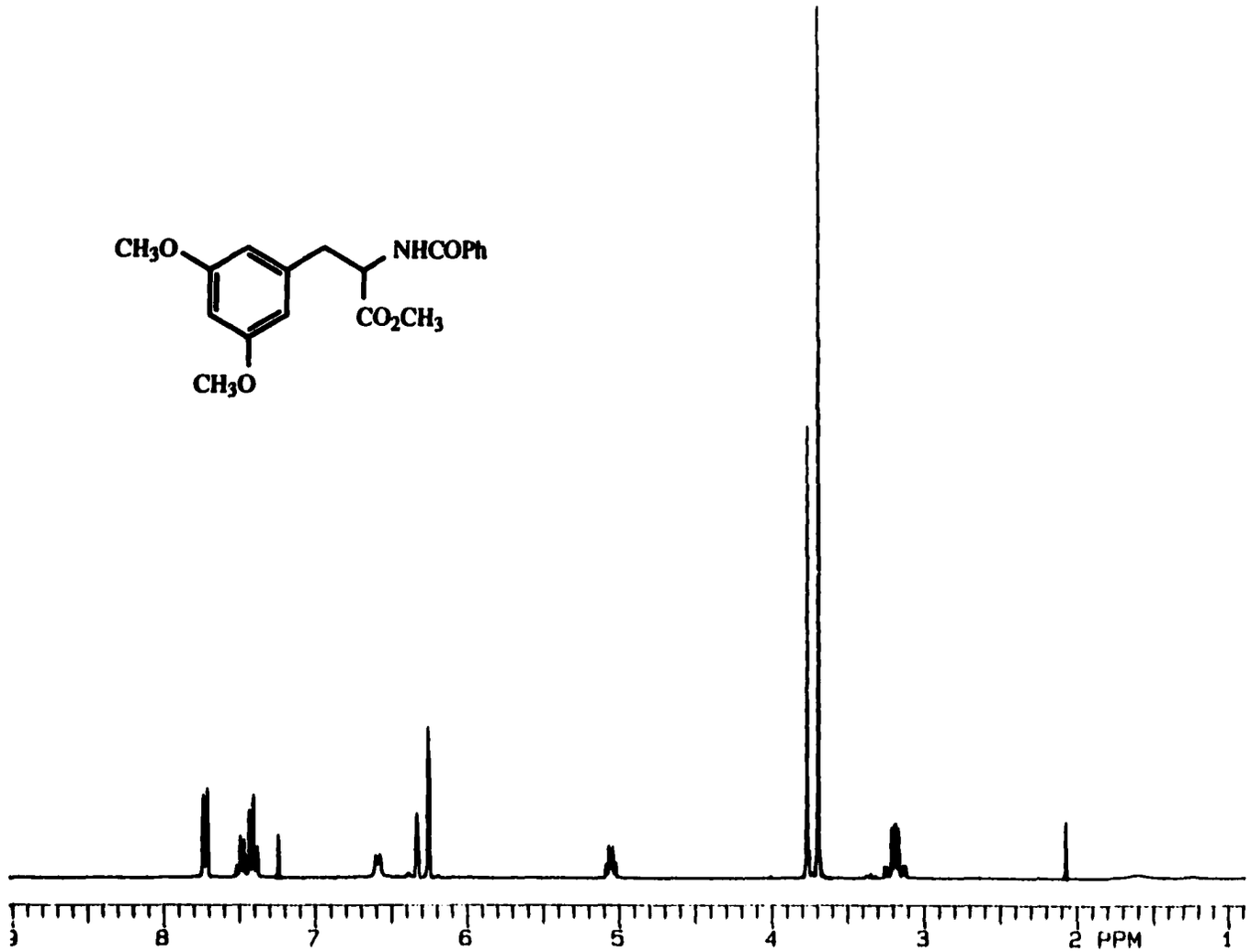

Figure 2-10. Proton NMR spectum of **12** in $CDCl_3$.

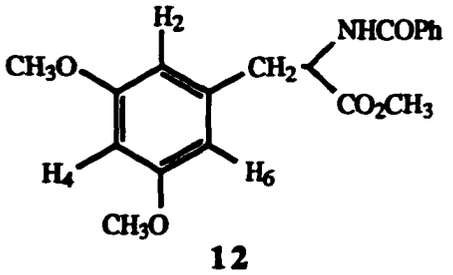

12

Table 2-10. Proton NMR signal assignments for **12** in $CDCl_3$.

Proton(s)	Multiplicity	Chemical shift, δ (ppm)	Coupling constant, J (Hz)
C_6H_5 (ortho)	d	7.73	J_{app} = 7.8
C_6H_5 (meta, para)	m	7.52-7.38	-
-NH	bd	6.59	7.2
H-4	t	6.33	2.4
H-2 & H-6	d	6.26	2.4
-CH*	dt	5.06	7.5, 5.4
$-CO_2Me$	s	3.77	-
-OMe's	s	3.69	-
$-CH_2$	m	3.25-3.12	-

* Upon cursory inspection, -CH appears as a doublet of doublets. But, with rigorous examination, it is actually observed to be an overlapping doublet of triplets.

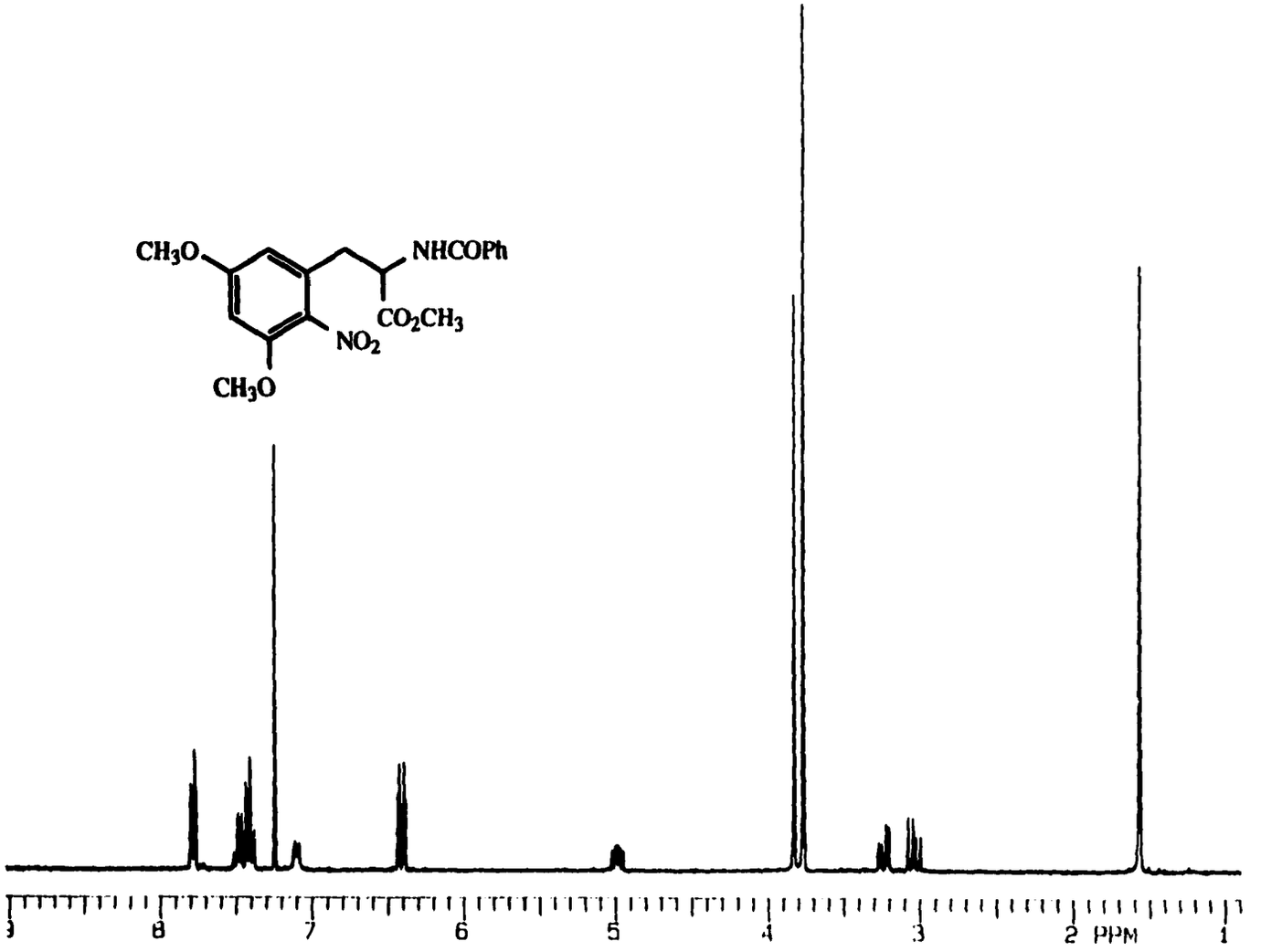

Figure 2-11. Proton NMR spectum of **13** in $CDCl_3$.

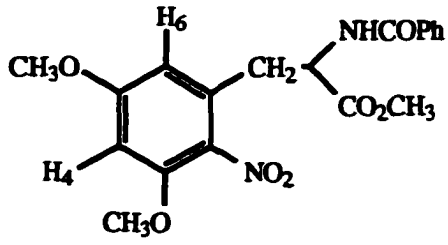

13

Table 2-11. Proton NMR signal assignments for **13** in $CDCl_3$.

Proton(s)	Multiplicity	Chemical shift, δ (ppm)	Coupling constant, J (Hz)
C_6H_5 (ortho)	bd	7.78	J_{app} = 6.9
C_6H_5 (meta, para)	m	7.51-7.38	-
-NH	d	7.1	7.0
H-4	d	6.43	2.4
H-6	d	6.39	2.4
-CH	ddd	4.98	9.3, 7.1, 5.1
$-CO_2Me$	s	3.83	-
-OMe	s	3.77	-
-OMe	s	3.76	-
$-CH_2$*	dd	3.23	14.4, 5.1
$-CH_2$*	dd	3.03	14.4, 9.3

* One would expect a priori to see a simple doublet for $-CH_2$; however, we observed a doublet of doublets for each of the $-CH_2$ protons. This is most likely a result of the $-CH_2$ protons being diastereotopic. Since they are diastereotopic, we would expect to see two doublet of doublets.

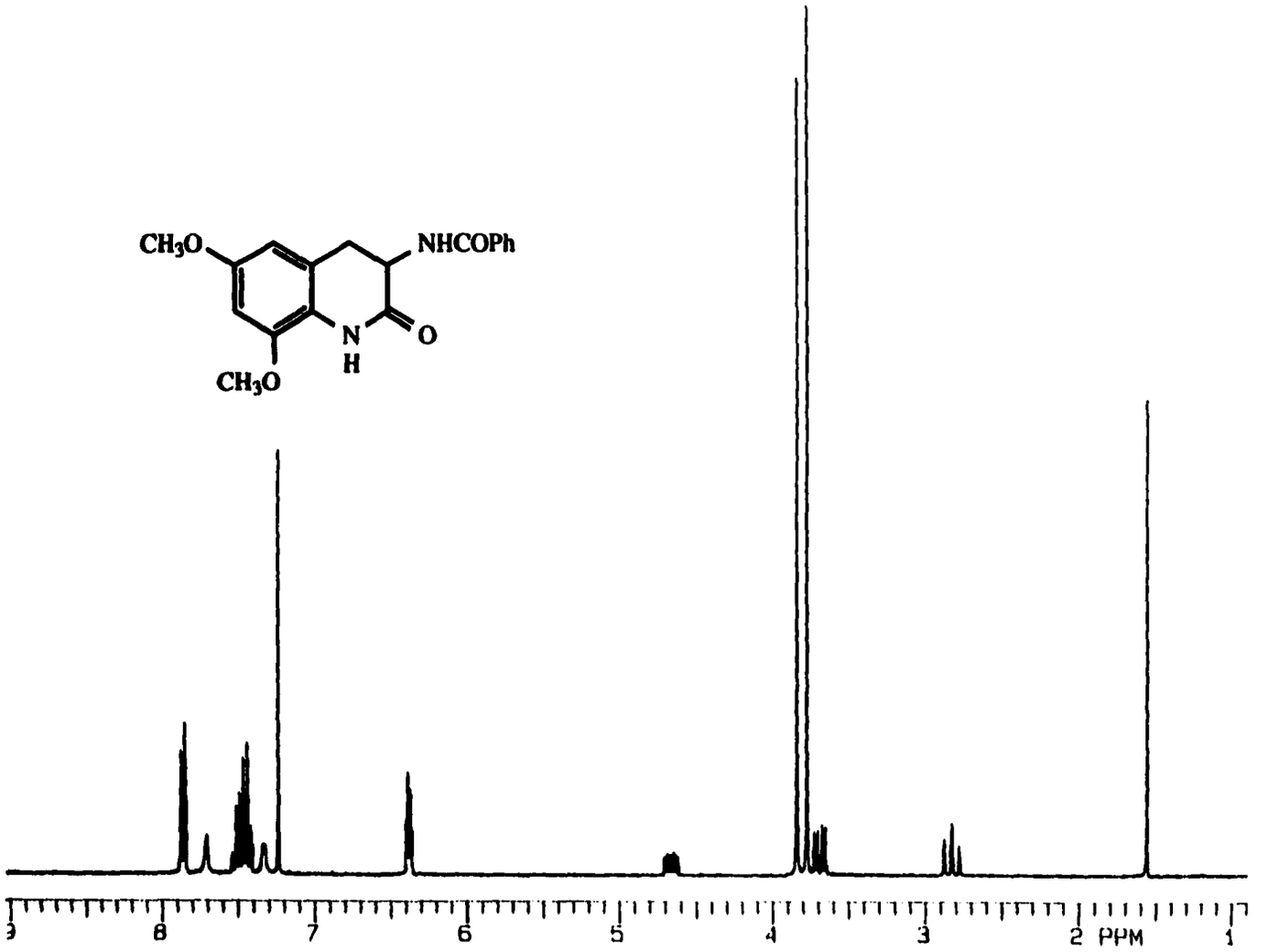

Figure 2-12. Proton NMR spectum of **14** in $CDCl_3$.

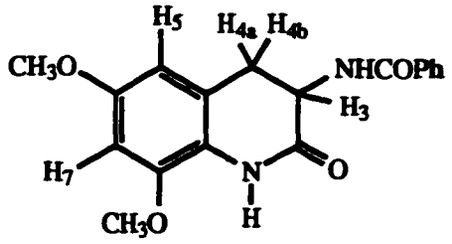

14

Table 2-12. Proton NMR signal assignments for **14** in $CDCl_3$.

Proton(s)	Multiplicity	Chemical shift, δ (ppm)	Coupling constant, J (Hz)
C_6H_5 (ortho)	bd	7.86	$J_{app} = 6.9$
Ar-NH	bs	7.71	-
C_6H_5 (meta, para)	m	7.54-7.41	-
PhCONH	d	7.33	4.3
H-5	d	6.39	2.7
H-7	d	6.37	2.1
H-3	ddd	4.66	14.1, 6.3, 4.4
-OMe	s	3.84	-
-OMe	s	3.78	-
H-4a	dd	3.69	15.3, 6.3
H-4b	dd	2.83	15.3, 14.1

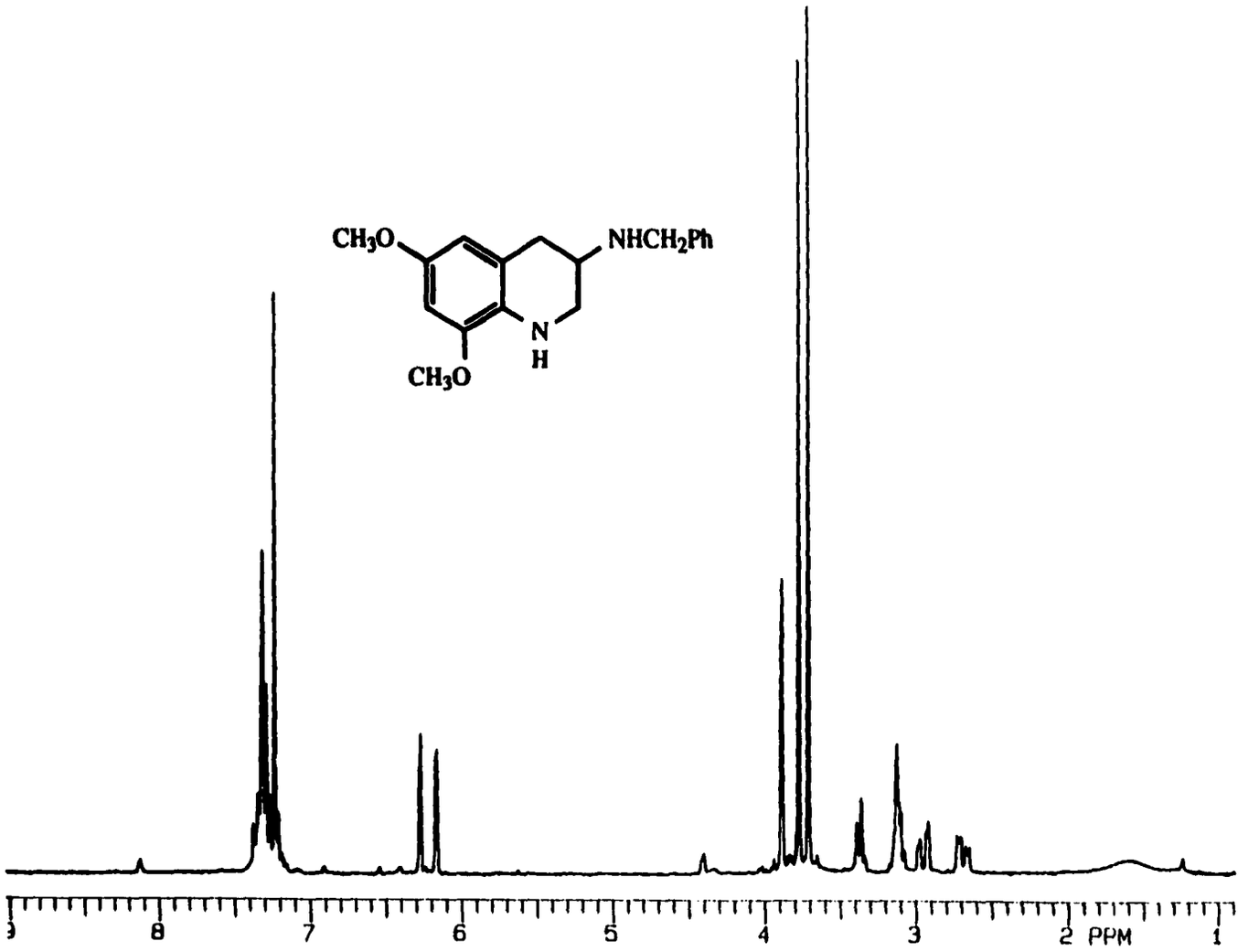

Figure 2-13. Proton NMR spectum of **15** in $CDCl_3$.

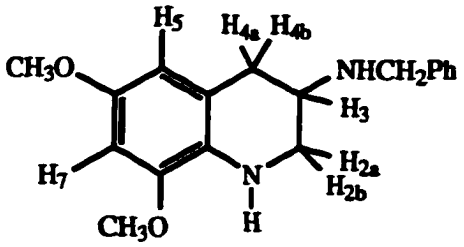

15

Table 2-13. Proton NMR signal assignments for **15** in $CDCl_3$.

Proton(s)	Multiplicity	Chemical shift, δ (ppm)	Coupling constant, J (Hz)
C_6H_5	m	7.38-7.22	-
H-5	d	6.28	2.4
H-7	d	6.17	2.4
Ph-CH_2	s	3.89	-
-OMe	s	3.78	-
-OMe	s	3.72	-
H-4a	bt	3.36	J_{app} = 7.2
H-3 & H-4b	m	3.15-3.08	-
H-2a	dd	2.95	16.5, 3.9
H-2b	dd	2.69	16.5, 7.5

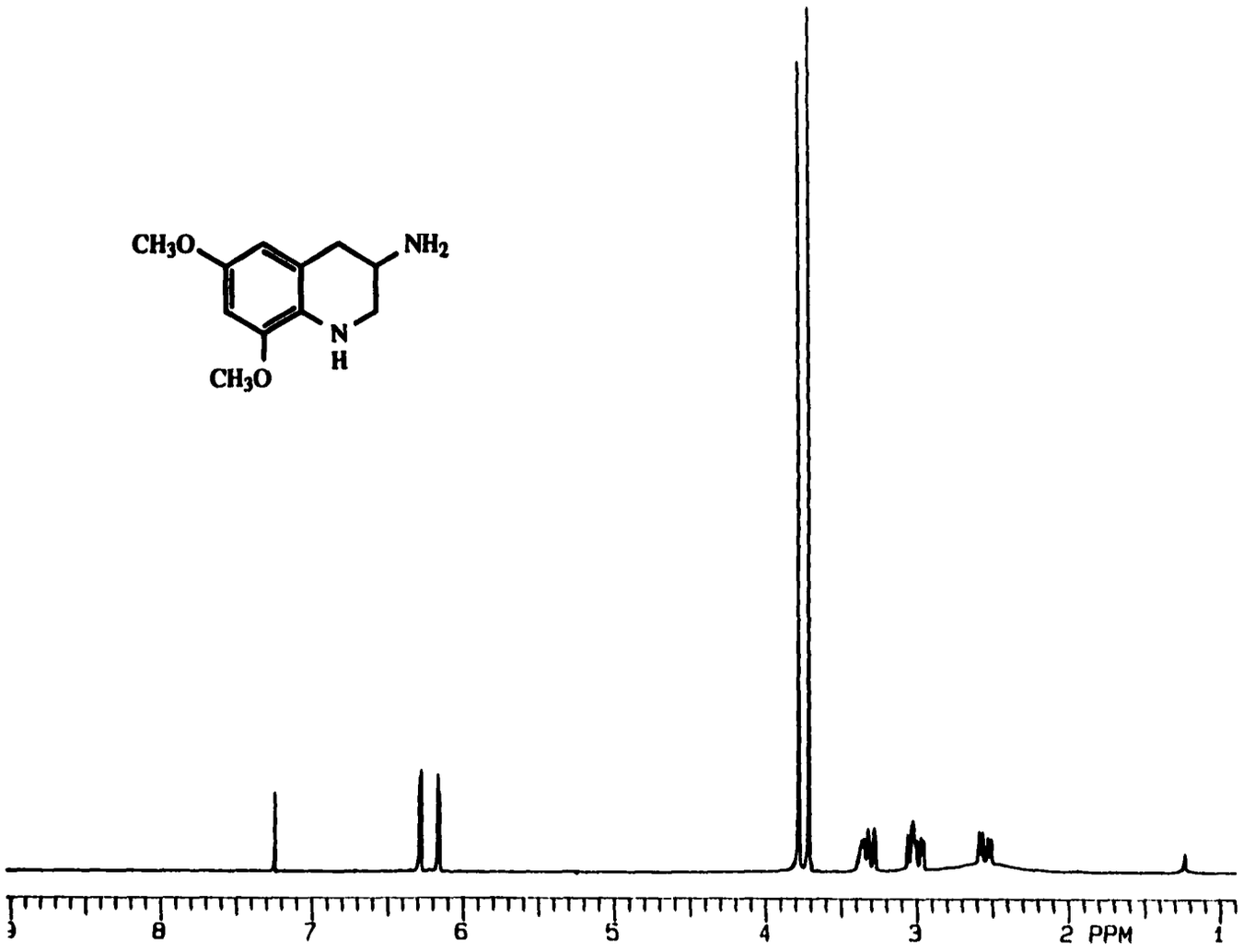

Figure 2-14. Proton NMR spectum of **16** in $CDCl_3$.

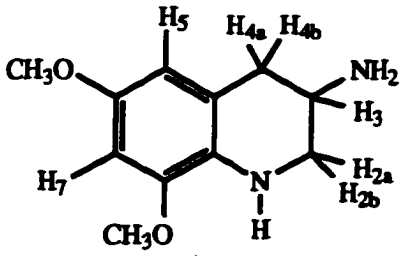

16

Table 2-14. Proton NMR signal assignments for **16** in $CDCl_3$.

Proton(s)	Multiplicity	Chemical shift, δ (ppm)	Coupling constant, J (Hz)
H-5	d	6.28	2.4
H-7	d	6.16	2.7
-OMe	s	3.78	-
-OMe	s	3.71	-
H-3	m	3.39-3.32	-
H-4a	bd	3.30	11.7
H-2a & H-4b	m	3.06-2.95	-
H-2b	dd	2.46	16.2, 6.3

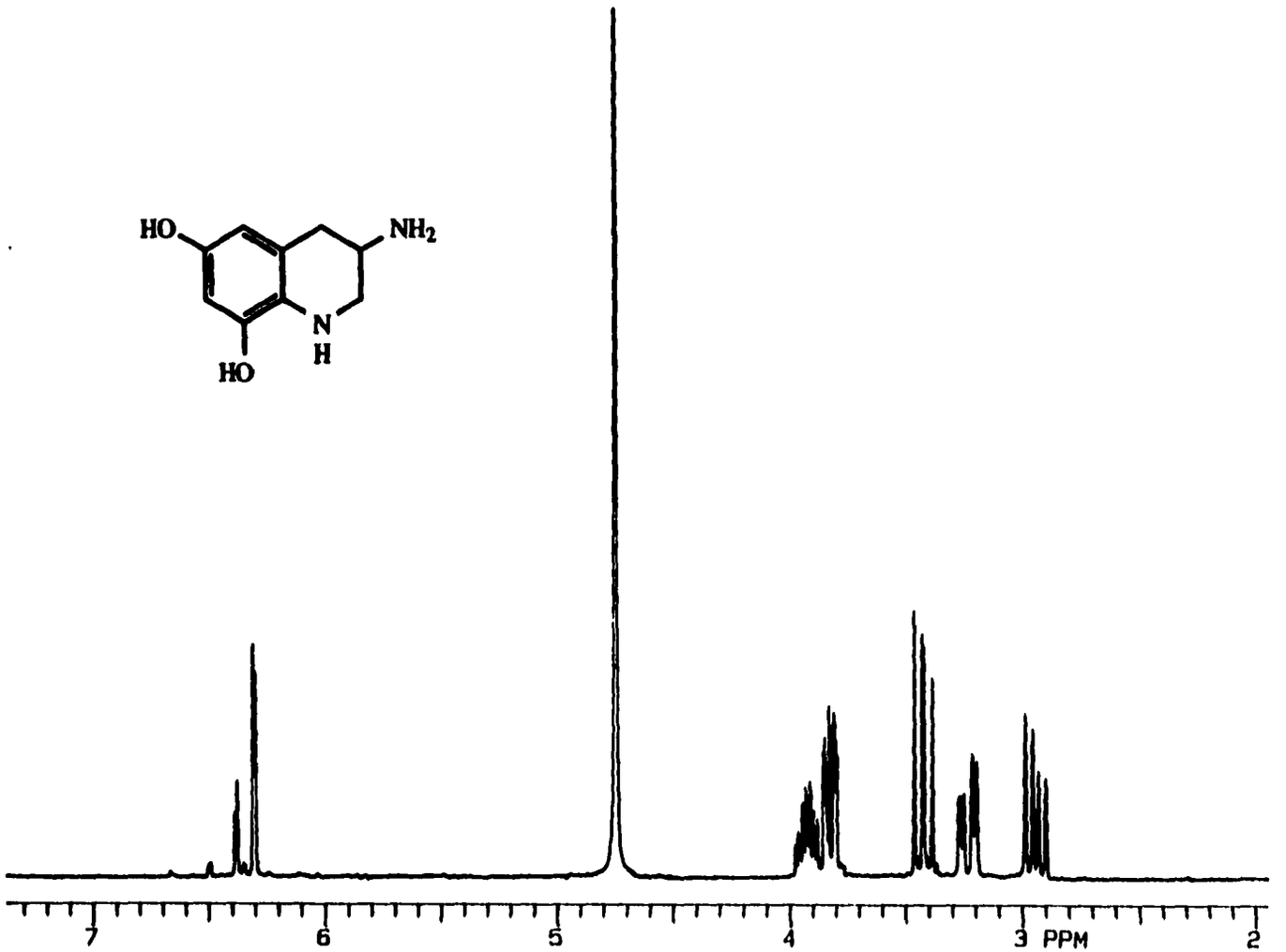

Figure 2-15. Proton NMR spectum of 17•2HBr in D_2O.

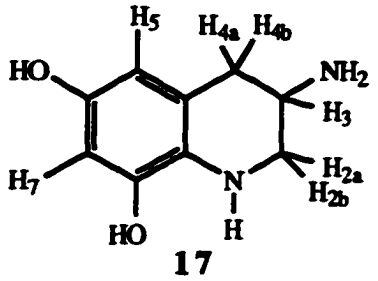

17

Table 2-15. Proton NMR signal assignments for **17** in D_2O.

Proton(s)	Multiplicity	Chemical shift, δ (ppm)	Coupling constant, J (Hz)
H-5	d	6.38	2.7
H-7	d	6.30	2.4
H-3***	dddd	3.93	9.9, 9.6, 5.3, 3.5
H-2a*‡	ddd	3.83	12.3, 3.5, 1.7**
H-2b‡	dd	3.42	12.3, 10.2
H-4a‡	bdd	3.23	16.8, 5.4
H-4b‡	dd	2.94	16.8, 9.3

* Alternatively, H-2a could be simply reported as a multiplet at 3.85-3.80.

** J = 1.7 Hz is presumed to be a long range coupling of H-2a to H-4a which is obscured in the broad doublet of doublets seen at δ = 3.23. This long range coupling is verified by COSY.

*** Alternatively, H-3 could be simply reported as a multiplet at 3.98-3.88.

‡ Equatorial protons, in general, are more deshielded than axial protons and have a greater potential for long range coupling; therefore, it is presumed that H-2a and H-4a are equatorial while H-2b and H-4b are axial.

Basic Chromatography and Electrochemistry

Chapter 3

I. Introduction

In the field of neuroscience, it is frequently useful to have the ability to quantitate neurotransmitters and related metabolites in the CNS. Many different methods can be used to accomplish this, yet none possess the simplicity, ease, high sensitivity, versatility, and rapidness exhibited by high performance liquid chromatography (HPLC) coupled with electrochemical detection (EC). This combination, commonly known as LCEC, was first developed in the laboratory of R.N. Adams at the University of Kansas

in the early 1970's. Since that time, LCEC has become the most widely used tool for the routine separation and determination of neurochemicals.

In order to be applicable to EC detection, a compound must possess electrochemical activity. Therefore, it is important to determine whether a given neurochemically related species can or does exhibit electroactivity. If such activity exists, it is often of interest to determine the specific nature of its electrochemical characteristics. The initial electrochemical characterization of a species most generally employs cyclic voltammetry or linear sweep voltammetry. Using these techniques, basic information, such as the associated formal potential(s), and in-depth information, such as the nature and rate(s) of follow-up reaction(s), can be determined. This chapter covers pertinent aspects of chromatographic separation, electrochemical detection, and the fundamentals of cyclic voltammetry and linear sweep voltammetry.

II. Chromatography

A. Migration of Solutes

Chromatographic separation is based upon the extent to which different solutes partition between a stationary phase and a mobile phase. The partition coefficient, K, describes the degree to which a solute resides in the stationary phase versus the mobile phase and is defined as:

$$K = \frac{C_S}{C_M} \qquad \text{equation 3-1}$$

where C_S is the molar concentration of the solute in the stationary phase and C_M is the molar concentration in the mobile phase.

The time required between the injection of a sample and the elution of a solute is called the retention time, t_R. The time required for the elution of an unretained species is called the dead time, t_O. Retention time reflects the partitioning of a solute between the two phases, while the dead time reflects the dead volume of the column.

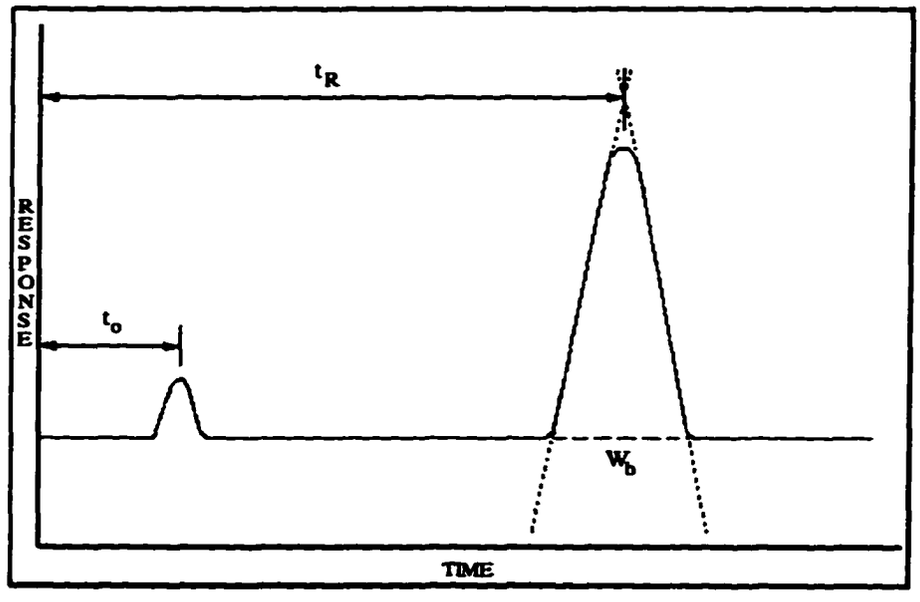

Figure 3-1. Chromatographic elution profile.

These two parameters are used to find the capacity factor, k', which provides a measure of the migration rate, or degree of retention, of a given solute under a given set of chromatographic conditions, and is defined as:

$$k' = \frac{(t_R - t_O)}{t_O} = K\left(\frac{V_{stationary}}{V_{mobile}}\right) \qquad \text{equation 3-2}$$

where $V_{stationary}$ is the volume of the stationary phase and V_{mobile} is the volume of the mobile phase. Since the capacity factor takes into account the dead time as well as the retention time, it is relatively independent of alterations in column length and/or diameter. This parameter provides a rapid assessment of the effects of different eluting solvents and/or packing materials on solute retention.

Another important parameter is the selectivity factor, α. The selectivity factor is a measure of how well a column separates two analytes, A and B. It is defined as:

$$\alpha = \frac{K_B}{K_A} = \frac{k'_b}{k'_a} \qquad \text{equation 3-3}$$

where B is the more strongly retained analyte, or $k'_b > k'_a$ and $\alpha > 1$. The selectivity factor is used to calculate the resolving power of a column for two analytes and will be discussed later in this chapter.

B. Chromatographic Efficiency

Chromatographic efficiency is a measure of the band broadening that occurs as an analyte passes through the column. By simple inspection of the chromatogram in Figure 3-1, it is apparent that the shape of an eluting peak is reminiscent of a Gaussian, or normal probability curve. The associated band broadening can be viewed as the result of a random-walk phenomenon and diffusion processes.

While a complete discussion of the random-walk theory is beyond the scope of this text, a brief description is as follows. A solute molecule undergoes thousands of

transfers, during its elution, between the stationary and mobile phases. Due to statistical probability, the time a molecule spends in either phase is variable. Therefore, the time spent in a given phase may be relatively brief or long. Noting that a molecule only moves through a column while in the mobile phase, some molecules will travel more rapidly because they reside in the mobile phase for a greater-than-average period of time, while others will travel more slowly due to their greater-than-average time spent in the stationary phase. The outcome of these individual random processes is a symmetrical distribution of solute velocities around the mean analyte velocity. Thus, the degree of band broadening derived from the random-walk phenomena is dependent on the frequency and length of these random processes, as well as the total time during which they are allowed to occur, i.e., the time spent in the column.

Diffusion is another major contributor to band broadening. Diffusion occurs from a point of higher concentration to a point of lesser concentration. Molecules at the center of a chromatographic band, where the concentration is highest, will diffuse toward the edges of the band, where the concentration is lowest. And, since diffusion is concentration dependent, half of the diffusion occurs in the direction of the flow and half occurs against the flow.

As a result of these two phenomena, band broadening increases as the solute moves through the column. Hence, it is apparent that the degree of band broadening is directly proportional to the time spent on the column.

The efficiency of a chromatographic column is quantitatively expressed as either the plate height, H, or the number of theoretical plates, N. The plate height is defined as:

$$H = \frac{L}{N} \qquad \text{equation 3-4}$$

where L is the length of the column, while the number of theoretical plates is defined as:

$$N = \left(\frac{t_R}{\sigma}\right)^2 = 16\left(\frac{t_R}{W_b}\right)^2 = 5.55\left(\frac{t_R}{W_{1/2}}\right)^2 \qquad \text{equation 3-5}$$

where t_R is the solute retention time, σ is the standard deviation of the solute band, W_b is the width of the peak at its base ($W_b=4\sigma$), and $W_{1/2}$ is the width of the peak at half height. Since N is a dimensionless parameter, the dimensions of t_R and σ or W, normally measured as either time or distance, need to be the same.

C. Column Resolving Power

Resolution, R_S, is the quantitative measure of the separation of two analytes. It is defined as the distance between the centers of two analyte peaks divided by the average of the two base widths:

$$R_S = \frac{2(t_2 - t_1)}{W_1 + W_2} \qquad \text{equation 3-6}$$

An equation for R_S incorporating the number of theoretical plates, the selectivity, and the capacity factor of the more strongly retained component is:

$$R_S = \frac{\sqrt{N}}{4}\left(\frac{\alpha - 1}{\alpha}\right)\left(\frac{k'_b}{1 + k'_b}\right) \qquad \text{equation 3-7}$$

III. Electrochemistry

A. Electrochemical Detection

While an in-depth discussion of electrochemical detection in LCEC is beyond the scope of this chapter, there exists numerous literature and text reviews on the theory, function and various applications of this technique.[103-115]

For a compound to be amenable to electrochemical detection, it must have the ability to accommodate the loss or gain of one or more electrons. In other words, a compound must be electrochemically active. While there exists many different types of electrochemical detectors, most are amperometric in design. Amperometric detectors oxidize or reduce only a small fraction (1-5%) of the desired species as it flows across the surface of the electrode.

The current produced by the gain or loss of electrons from a chemical species at the electrode surface is called faradaic current:

$$i = \frac{\partial Q}{\partial t} \qquad \text{equation 3-8}$$

where i is the current in amps, Q is the charge in coulombs, and t is the time in seconds. The amount of charge is described by Faraday's law:

$$Q = nFN \qquad \text{equation 3-9}$$

where n is the number of equivalents per mole, F is Faraday's constant (96,485 C eq^{-1}), and N is the number of moles. The instantaneous faradaic current at an electrode surface is, thus, given by:

$$i = \frac{\partial Q}{\partial t} = nF\left(\frac{\partial N}{\partial t}\right) = (9.65 \times 10^4) \times (\text{equivalents converted per second}) \quad \text{equation 3-10}$$

The measured current at an amperometric detector is proportional to the diffusional flux, J_R, of the species to the electrode surface and the electrode area, A.

$$\left(\frac{i}{nF}\right) = \left(\frac{\partial N}{\partial t}\right) = AJ_R(x=0,t) \quad \text{equation 3-11}$$

In fact, the rate of conversion of the electroactive species at the electrode surface, i.e., current, is controlled by both the kinetics of electron transfer and the diffusion-driven flux of the substrate from the bulk of the solution to the electrode surface. In the normal amperometric detector, however, a sufficient overpotential is supplied to the working electrode so that the electron transfer kinetics become extremely rapid. Thus, the rate becomes diffusion controlled. Under these conditions, the current simply becomes a function of the flux at the electrode surface as shown in equations 3-11 and 3-13. The flux is proportional to the concentration gradient at the electrode surface according to Fick's first law, which assumes one-dimensional diffusion at a planar electrode:

$$J_R(x=0,t) = D_R\left(\frac{\partial C_R(x,t)}{\partial x}\right)_{x=0} \quad \text{equation 3-12}$$

where D_R is the diffusion coefficient of species R and $\partial C/\partial x$ is the concentration gradient. This equation can be combined with equation 3-11 to obtain a revised expression for the current at an electrode surface:

$$i = nFAD_R\left(\frac{\partial C_R(x,t)}{\partial x}\right)_{x=0} \qquad \text{equation 3-13}$$

Equation 3-13 completely describes the observed current for a one-dimensional, diffusion controlled process. Unfortunately, the situation for an electrochemical detector is a little more complex. The flowing stream across the electrode surface adds convection to the simple diffusion controlled delivery of the electroactive species to the surface of the electrode. Additionally, the physical dimension of the channel depth is very small which further restricts the above discussion by eliminating the assumption of semi-infinite linear diffusion. Taking all of these and other factors into account, Weber and Purdy[116] have presented a fairly rigorous derivation for the current observed at an amperometric LCEC electrode which is:

$$i = 1.467nFC_R W_e\left(\frac{D_R L}{b}\right)^{2/3}\left(\frac{U}{W_c}\right)^{1/3} \qquad \text{equation 3-14}$$

where C_R is the bulk concentration of electroactive species R, W_e is the width of the electrode, L is the length of the electrode, U is the average volume flow rate of the solution, and W_c and b are the width and depth of the flow channel, respectively. Expressions for other amperometric LCEC electrodes and cell designs may be found elsewhere.[107,116,117]

B. Voltammetry

A commonly employed method used to investigate the electrochemical characteristics of an electroactive species is cyclic voltammetry (CV). In cyclic voltammetry, current is monitored as a function of applied potential, with the potential being scanned in one direction followed by a scan in the opposite direction. A cyclic voltammogram, i.e., current-potential curve, may be viewed as the electrochemical equivalent of a spectrum produced in spectrophotometry. A representative cyclic voltammogram is shown in Figure 3-2. Basic electrochemical characteristics which may be determined using CV are the reduction peak potential, the oxidation peak potential, the reversibility of a system, the number of electrons involved in the oxidation and/or reduction reaction(s), and the diffusion coefficient(s).[107,118]

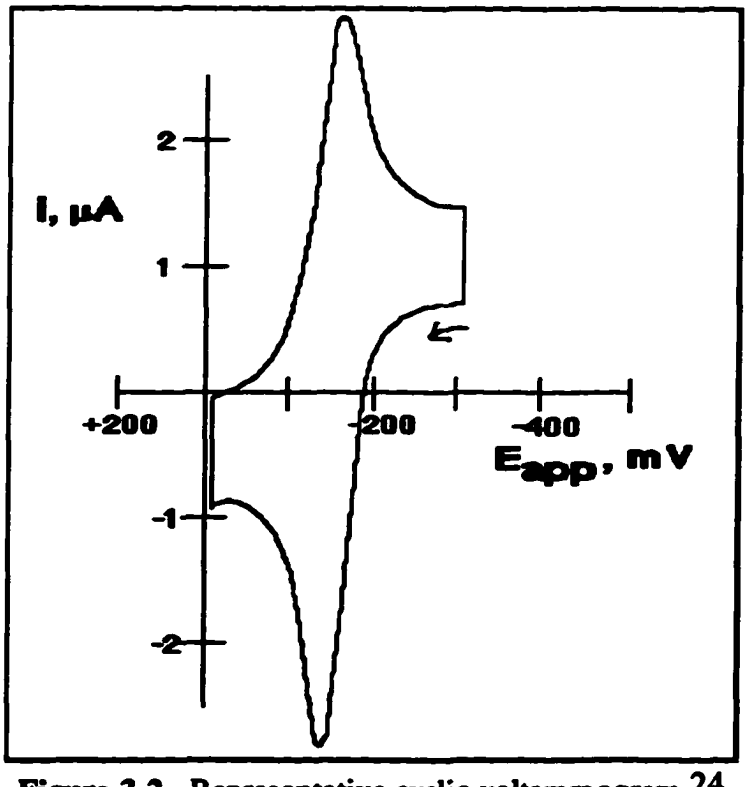

Figure 3-2. Representative cyclic voltammogram.[24]

Cyclic voltammetric peak separation, ΔE_p, serves as one criterion for the determination of electrochemical reversibility. For a reversible system, i.e., a system with facile electron transfer characteristics,

$$\Delta E_p = E_{pa} - E_{pc} = \frac{58}{n} mV \qquad \text{equation 3-15}$$

where E_{pa} is the anodic peak potential, E_{pc} is the cathodic peak potential, and n is the number of electrons involved in the redox process. For example, a reversible two-electron system is expected to have ΔE_p = 29 mV. Furthermore, if the system is reversible and the products stable, the magnitude of the anodic peak current should equal to that of the cathodic peak current. The formal redox potential, $E^{\circ\prime}$, in a reversible system can be readily obtained from cyclic voltammetry. Two common methods used for $E^{\circ\prime}$ are:

$$E^{\circ\prime} = \frac{\left(E_{pa} + E_{pc}\right)}{2} \qquad \text{equation 3-16}$$

and

$$E^{\circ\prime} = E@0.8517 i_p \qquad \text{equation 3-17}$$

where equation 3-17 can be used for either the anodic or cathodic peak.

As electrochemical systems approach quasi-reversibility, the potential separation between the anodic and cathodic peaks increases. In a system where either the anodic or the cathodic current becomes negligible, that system is said to be electrochemically irreversible. The quasi- and ir-reversible cases are much more complex than the reversible case, since the observed current becomes dependent on charge transfer

kinetics, in addition to thermodynamics and diffusion. Detailed descriptions of these more complex cases are available elsewhere.[107,119,120]

Linear sweep voltammetry (LSV) is similar to CV. However, in LSV, the potential is scanned only once in one direction. Thus, LSV information can be obtained from a CV by simply examining only the initial potential sweep. Reversibility can be assessed from this unidirectional sweep, since a reversible system conforms to the equation:

$$\left|E_p - E_{\frac{p}{2}}\right| = \frac{56.5}{n} mV \qquad \text{equation 3-18}$$

where $E_{p/2}$ is the potential at $i = i_p / 2$. The diffusion coefficient, D, the number of electrons involved, n, the bulk concentration, C^*, or the area of the electrode, A, can each be determined from the peak current in a reversible system as:

$$i_p = 0.4463nFAC^*\left(\frac{nF}{RT}\right)v^{1/2}D^{1/2} \qquad \text{equation 3-19}$$

or

$$i_p = \left(2.69\times10^5\right)n^{3/2}Av^{1/2}D^{1/2}C^* \qquad @\ 25°C \quad \text{equation 3-20}$$

if all other parameters in the equation are known. The appropriate units for the parameters are A in cm^2, D in cm^2/sec, v in V/sec, C^* in mol/cm^3, and i in amps. Equations 3-19 and 3-20 apply to planar electrodes under diffusion controlled conditions. However, spherical electrodes, such as a hanging drop mercury electrode, can be treated in a similar manner, yielding:

$$i_p = i(plane) + (0.725 \times 10^5)\frac{nADC^*}{r_o} \qquad \text{equation 3-21}$$

where r_0 (cm) is the radius of the spherical electrode, i(plane) is the current described in equations 3-19 and 3-20, and the other parameters are as defined above. The treatment of LSV for quasi- and ir-reversible systems differs from that of reversible systems and is covered in-depth elsewhere.[107]

Knowledge of the oxidation potential of various species contained in a sample for LCEC analysis may allow one to choose an applied potential which will maximize sensitivity and selectivity for the desired components. At a sufficient overpotential, the oxidation current for a given electrochemically active species becomes governed by mass transport and, therefore, is relatively independent of potential. However, undesirable noise is generally found to be proportional to the potential. Thus, the optimal potential for a species is that which is large enough to maximize the signal, but is small enough so that it does not introduce any more noise than is absolutely necessary. Furthermore, if one is attempting analysis of a desired compound A in the presence of a chromatographically overlapping, undesired compound B, potential selection may be of some help. For example, if compound A has a formal potential significantly less than compound B, an applied potential may be chosen where only A is oxidized. This approach achieves electrochemical selectivity. This situation is illustrated in Figure 3-3, which shows hydrodynamic voltammograms of the hypothetical compounds A and B.

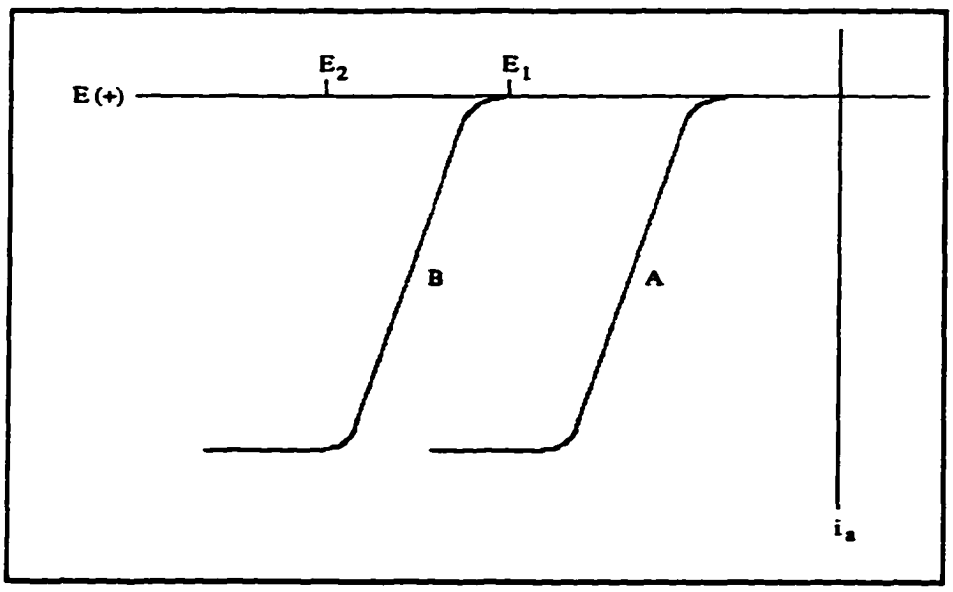

Figure 3-3. Hydrodynamic voltammograms for two oxidizable compounds.

A hydrodynamic voltammogram is a plot of the current produced as a function of the applied electrode potential. At potential E_2 in Figure 3-3, both A and B can undergo oxidation. However, by selecting potential E_1, compound A can be selectively oxidized in the presence of B. A notable characteristic of a hydrodynamic voltammogram is the $E_{1/2}$, defined as the potential at which $i = i_{max} / 2$. The $E_{1/2}$ is equal to the $E^{o'}$ for a species of concern if the species is electrochemically reversible.

IV. Conclusions

While the preceding discussions are rather rudimentary in nature, more extensive details can be found, for the interested reader, in multiple references (LC[103,106,121-123] and EC[105,107,111,118-120]). However, it is hoped that this brief introduction to these essential topics will be helpful in the understanding of the following chapters.

Neurotoxicity

Chapter 4

I. Introduction

Neurotoxins have been used extensively in the study of neuronal function(s). 6-Hydroxydopamine (6-HDA) and 1-methyl-4-phenyl-1,2,3,6-tetrahydropyridine (MPTP), for example, have frequently been employed in investigations of the noradrenergic and dopaminergic systems, respectively, due to the moderate to high degree of potency and concomitant selectivity which they exhibit towards these systems. However, comparably effective neurotoxins for serotonergic systems have not been available, particularly for the mouse. 5,7-Dihydroxytryptamine (5,7-DHT) is the most widely used 5-HT neurotoxin. But, doses producing even modest 5-HT depletion are,

unfortunately, accompanied by poor selectivity. Furthermore, 5,7-DHT has only been shown to, at most, produce minimal (approx. 30%) serotonin depletions in mouse whole brain.[23,79] Therefore, it is not surprising that there is an on-going search for more potent and selective 5-HT neurotoxins.

A previous report by L. Lin[23] had shown that a fixed side chain catecholamine derivative, 3-amino-6,7-dihydroxy-1,2,3,4-tetrahydroquinoline (6,7-ADTQ), was capable of eliciting 5-HT depletions of approximately 50%. We, thus, decided to more thoroughly investigate this compound. Additionally, we designed and characterized various ADTQ analogs in an attempt to find more selective and potent serotonergic agents. The specific compounds investigated included the enantiomers of 6,7-ADTQ and two analogs, namely 3-aminomethyl-6,7-dihydroxy-1,2,3,4-tetrahydroquinoline (6,7-AMDTQ) and 3-amino-6,8-dihydroxy-1,2,3,4-tetrahydroquinoline (6,8-ADTQ). This chapter examines the lethality, potency, and selectivity of these neurotoxic agents. It also briefly covers some of the associated behavioral effects of the agents.

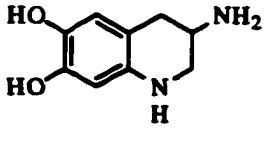

6,7-ADTQ

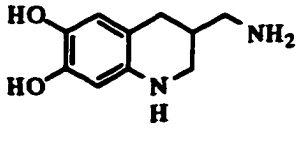

6,7-AMDTQ

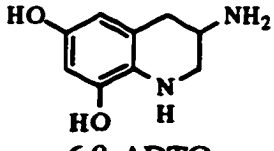

6,8-ADTQ

II. Background

Neurotransmitter depletion studies are frequently employed to evaluate the degree of neuronal destruction and/or degeneration elicited by a toxic agent. While absolute proof of destruction or degeneration requires electron microscopic or histochemical verification, these techniques were not accessible for the current studies. However, 6-HDA and many of its analogs have previously been shown, using such techniques, to

produce neuronal degeneration.[21,24,124,125] Due to the similarity in chemical structures between the quinoline analogs and 6-HDA and its congeners, as well as the fact that the quinoline analogs produce long term depletions of neurotransmitters, we believe that depletion measurements reasonably reflect the degree of degeneration afforded by these toxins.

Early studies of a racemic mixture of 6,7-ADTQ by L.A. Lin[23] briefly examined both the toxicity and selectivity afforded by this toxin. Two doses of 25 μg of the free base, separated by 24 hours, were administered intracerebroventricularly (i.c.v.) to mice. The mice were then sacrificed 9 days after the first treatment. The results of these studies are shown in Table 4-1.

Table 4-1. 6,7-ADTQ effects on mouse whole brain neurotransmitter levels.

	Neurotransmitter Levels[23] (% controls ± SEM)			
Compound	NE	DA	5-HT	N
Controls	100 ± 5	100 ± 6	100 ± 4	6
6,7-ADTQ	61 ± 7	87 ± 3	52 ± 6	9

Treated group received two doses of 25 μg 6,7-ADTQ, i.c.v., separated by 24 hours.

From this initial data it appeared that there were very little DA effects and only moderate NE effects when compared to existing NE and DA toxins. However, the ability of 6,7-ADTQ to elicit a 48% depletion of 5-HT was judged significant considering that the widely used 5-HT toxins, 5,7-DHT and 5,6-DHT, were capable of producing no more than 30-35% depletions in mouse whole brain.[23,79] But, 6,7-ADTQ clearly exhibited a lack of selectivity. In an attempt to circumvent this problem, Lin incorporated

NE and DA transport blocking agents. Amfonelic acid was used to block uptake by DA neurons, and desipramine was used to block uptake by NE neurons.[5,23] The results of this modified examination of 6,7-ADTQ are shown in Table 4-2. By employing these uptake blockers, Lin was able to eliminate virtually all the DA effects and over 50% of the NE effects, while not significantly altering the 5-HT depletion.

Table 4-2. 6,7-ADTQ effects on whole mouse brain neurotransmitter levels following pretreatment with desipramine and amfonelic acid.

	Neurotransmitter Levels[23] (% controls ± SEM)			
Compound(s)	NE	DA	5-HT	N
Controls	100 ± 3	100 ± 3	100 ± 3	9
Desip., Amfo., 6,7-ADTQ	84 ± 6*	95 ± 4	72 ± 3***	9
6,7-ADTQ	56 ± 3***	92 ± 3	70 ± 1***	17
5,7-DHT[a]	82 ± 3***	99 ± 1	71 ± 6***	16

Significant differences compared to control values (*t* test): $*P < 0.05$, $***P < 0.001$.
Animals were treated with 12.5 μg 6,7-ADTQ on days one and two. Pretreated animals received a mixture of 25 mg/kg desipramine and 50 mg/kg amfonelic acid, i.p., one hour prior to toxin treatment. Sacrifice occurred on day 9 following treatment.
[a] data from Lin[23]; toxin amount 25 μg.

While 6,7-ADTQ alone was found to lack somewhat in selectivity, it was shown, at the higher dose, to be capable of producing more complete 5-HT depletions than can be obtained with 5,7-DHT.[23,79] Using uptake blockers and a lower dose, 6,7-ADTQ elicited selectivity comparable to that reported for 5,7-DHT. Lin's work, thus, showed that 6,7-ADTQ offered some promise as a serotonergic toxin. This prompted us to design and investigate some analogs of this toxin.

III. Experimental Design and Methods

A. Chemicals and Solutions

1. Chemicals

All aqueous solutions employed 18 MΩ distilled/deionized water which was prepared by passing distilled water through a Milli-Q Reagent Water System (Millipore, Continental Water Systems, El Paso, TX).

6,7-AMDTQ and 6,8-ADTQ were prepared by Russell J. Lewis. The racemic and enantiomeric forms of 6,7-ADTQ were prepared by Charles A. Francis.[6]

The chemicals listed below were purchased through Sigma Chemical Company (St. Louis, Mo.) in high purity and used without any further purification.

sodium chloride

sodium hypochlorite

diethylamine

citric acid monohydrate

sodium octylsulfate

$Na_2EDTA \cdot 2H_2O$

neurotransmitters, metabolites, and chromatographic internal standards are listed in Table 4-3.

2. Stock Neurotransmitter and Metabolite Solutions

A stock solution for an individual compound was prepared by dissolving an appropriate amount of the compound in 25 mL of degassed 10^{-3} M HCl. This was then divided into ca. fifty 1.5 mL plastic storage vials and frozen at -80°C until needed. The

amounts used in these preparations, along with the resultant concentrations, are shown below in Table 4-3 for the pertinent chemicals.

Table 4-3. Stock neurotransmitter and metabolite solution preparation.

Compound	Salt Form	Amount of Salt Used (mg)	Concentration (mM)
NE	•HCL	7.16	1.393
EPI	free base	4.71	1.028
DOPAC	acid form	4.63	1.101
NM	•HCl	7.06	1.285
DA	•HCl	5.44	1.147
5-HIAA	acid form	6.79	1.421
HVA	acid form	4.94	1.085
3-MT	•HCl	5.53	1.086
5-HT	creatinine sulfate	11.58	1.142
N-MET	oxalate	8.22	1.173
EPIN	•HCl	5.04	0.990

3. External Standard

The external standard was prepared by mixing the appropriate volume of the individual stock solutions listed below in Table 4-4 and diluting the mixture to 25 mL with degassed 10^{-3} M HCl. This solution was prepared 30 min before use and kept on ice. Excess solution was discarded within 5 h of preparation.

Table 4-4. External standard solution preparation.

Compound	Stock Solution Used (μL)	External Std. Conc. (nmol/mL)
NE	53.8	2.998
EPI	24.3	0.999
DOPAC	22.7	1.000
NM	38.9	1.999
DA	130.8	6.001
5-HIAA	52.8	3.001
HVA	69.1	2.999
3-MT	69.1	3.002
5-HT	109.5	5.002

4. Homogenization Solution

The homogenization solution was a pH 4.75 mixture containing 0.50 M acetate and 0.40 M $NaClO_4$. The solution contained the LCEC internal standards N-MET and EPIN for convenience and was prepared as sequentially outlined below in Table 4-5 using the amounts of internal standards specified in Table 4-6. This solution was made

just prior to use and was kept on ice. Excess solution was discarded within 5 h of preparation.

Table 4-5. Homogenization solution preparation.

Compound	Amount
water	90 mL
glacial acetic acid	2.94 mL
$NaClO_4$	4.90 g
adjust to pH 4.75 with NaOH	
add x µL internal standard (see Table 4-6 below)	
dilute to final volume of 100 mL	

Table 4-6. Amounts of internal standard stock solutions used in preparation of the homogenization solution.

Internal Standard	Amounts of Stock Solution Used (µL)	Final Conc. (nmol/mL)
N-MET	213	2.500
EPIN	253	2.505

5. Isotonic Saline Solution

Isotonic saline was prepared by dissolving 0.90 g sodium chloride in 100 mL water and stored at 2°C until needed, and discarded after 1 week.

6. Toxin Solution Preparation

A carefully limited amount of toxin was weighed and transferred to a 1 mL glass ampule that was preflushed with argon or O_2-free nitrogen. An appropriate amount of deaerated isotonic saline solution was added to obtain the desired concentration, and the ampule was flushed with argon or nitrogen again. The ampule was then capped using a crimp cap with a rubber septum. This method minimized the amount of required toxin while maintaining an oxygen free environment for the stock toxin solution. The toxin was stable in excess of 8 hrs.

B. Chromatography

1. Chromatographic System

The LCEC system utilized was made up of a Milton Roy minipump, a Royal pressure gauge, an Alltech Mark III pulse dampener, a model 7125 Rheodyne injector with a 10 μL injection loop, and a 7.5 cm x 4.6 mm (i.d.) column with 3 μ C-18 Adsorbosphere stationary phase from Alltech. The column was packed in-house with a Haskel (Burbank, CA) column packer at a pressure of 7200 psi. The chromatographic system was fitted with a specially designed 1 mm diameter glassy carbon electrochemical detector (Bioanalytical Systems, BAS, West Lafayette, IN) contained in a thin-layer flow-through cell. The reference electrode was a BAS model MW 2021 Ag/AgCl. A BAS LC-4B potentiostat was employed for potential control and current monitoring, and chromatograms were recorded on a Fisher series 5000 Recordall strip chart recorder. All chromatographic tubing was stainless steel, typically 0.006" i.d., except between the column and detector, which was a short piece of 0.005" i.d. teflon tubing. Typical chromatographic conditions were: 1.8-2.1 mL/min flow rate, 0.5 sec time constant, 1-5 nA full scale, and applied potential of 800 mV vs. Ag/AgCl.

2. Mobile Phase

The liquid chromatography mobile phase contained 0.10 M citric acid, 0.085% (v/v) diethylamine, 0.05 mM EDTA, 0.255 mM sodium octylsulfate, and 5% (v/v) acetonitrile. The pH was adjusted to 2.50 with NaOH. The detailed preparation is sequentially outlined below in Table 4-7. Fresh mobile phase was prepared at least monthly. This mobile phase provided for separation of the 11 desired compounds in ca. 8 min.

Table 4-7. Mobile phase preparation.

Compound	Amount
water	1400 mL
diethylamine	1.7 mL
$Na_2EDTA \cdot 2H_2O$	37.16 mg
citric acid monohydrate	42.2 g
sodium octylsulfate	118.64 mg
adjust to pH 2.50 with NaOH	
water	500 mL
filter through 0.45 μ aqueous filter	
filtered acetonitrile	100 mL
degas with nitrogen for 15 min	

3. System Cleaning Procedure

Occasionally, the internal surfaces of the metallic components in the LCEC flow stream experienced deterioration leading to excessive background current and/or spurious chromatographic peaks. This usually could be corrected by cleaning the chromatographic system. In this procedure, all items down stream from and including the column were first removed to avoid damage. The specified amounts of solutions listed below in Table 4-9 were then sequentially pumped through the remaining system components. Following the final wash, the column and associated downstream items were reattached and the system was ready for operation. This procedure normally corrected the high background and/or spurious peak problems.

Table 4-8. LC tubing wash procedures.

Solution	Volume
water	200 mL
Dilute soap/water solution	200 mL
water	200 mL
8 M nitric acid	200 mL
water	200 mL
mobile phase	200 mL

4. Column Washing Procedure

With multiple injections of crude brain homogenates, a column may deteriorate, resulting in a diminished number of theoretical plates and a loss of separation. Flipping the column, i.e., changing the inlet to the outlet and vice versa, generally remedied this

problem. However, if this did not work, washing the column sometimes rectified the loss in column efficiency. Prior to engaging in this procedure, all components downstream from the column were removed from the LC system. The individual solvents and associated amounts, which were subsequently used to regenerate a column, are listed below in sequence in Table 4-9.

Table 4-9. LC column wash procedure.

Solution	Volume
water	50 mL
40:60 acetonitrile:water	100 mL
acetonitrile	100 mL
chloroform	100 mL
hexane	100 mL
chloroform	100 mL
acetonitrile	100 mL
40:60 acetonitrile:water	100 mL
water	50 mL
mobile phase	1000 mL

5. Column Packing

The Haskel (Burbank, CA) column packing unit consisted of a reciprocating plunger pump with an outlet:inlet pressure amplification of 122:1. The packing material was prepared as a 5-20% slurry (w/v) in HPLC grade acetone. For a typical 4.6 mm i.d. column, ca. 0.18 g of 3 μ C-18 Adsorbosphere particles were employed per cm of

column to be packed. For example, 1.35 g of Adsorbosphere packing, suspended in 20-25 mL acetone, was used for a 7.5 cm column. The slurry was sonicated for 10-15 min prior to packing to ensure dispersal of packing material. After placing the slurry in the column packer slurry reservoir, 300 mL of acetone were added to the solvent reservoir. The column was packed at 6000-7200 psi until most of the solvent acetone had been consumed. The packing process required anywhere from 7 to 25 min. The column was then removed from the packing unit, assembled, and flushed with 40:60 acetonitrile:water for one hr. If not used immediately, the column ends were capped, and the column was stored at 4°C.

6. Chromatographic Separation and Parameters

We achieved a clean separation of 11 compounds, including 9 neurotransmitters and metabolites and 2 internal standards, with detection limits in the high femtomole to low picomole range. The typical elution time for an injection was between 7-9 min. A representative chromatogram for a processed brain sample is shown in Figure 4-1. The chromatographic parameters for each of the peaks shown in Figure 4-1 is presented in Table 4-11.

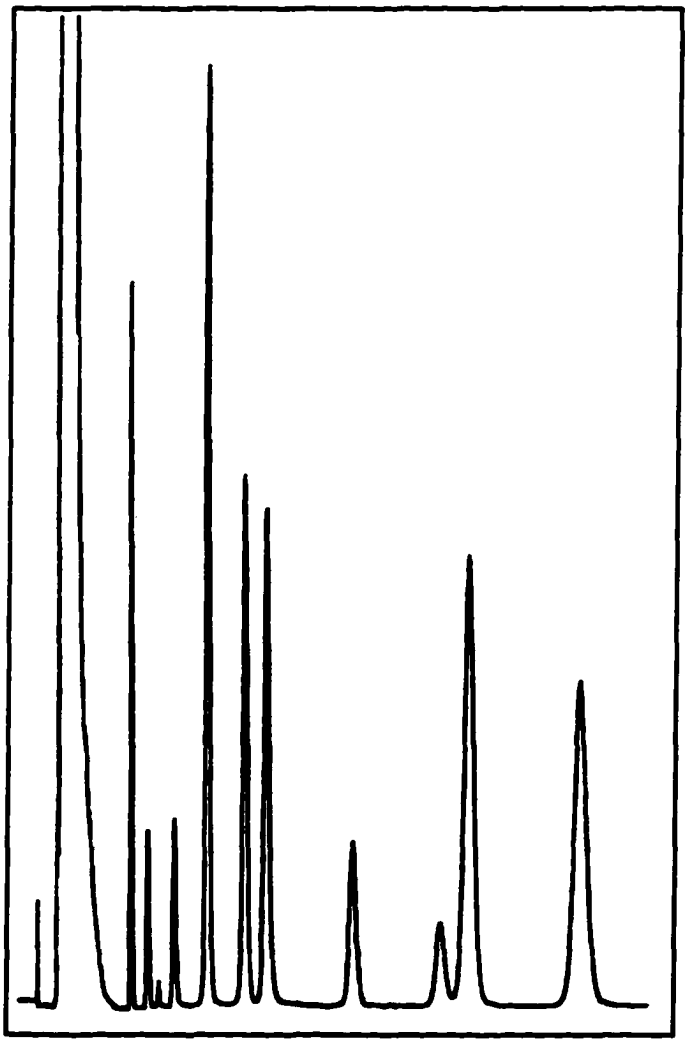

Figure 4-1. A typical LCEC chromatogram for a brain sample. From left to right, the peaks observed represent: the injection spike, the solvent front, NE, EPI, NM, DOPAC, DA, EPIN, 5-HIAA, HVA, 3-MT, 5-HT, and N-MET. The full-scale of the vertical axis was 5 nA, and the time required for elution of the final peak was 7.8 min.

Table 4-10. Experimentally determined chromatographic parameters using above described conditions.

Solute	t_r (min)	k'	N
NE	0.94	1.61	12787
EPI	1.2	2.32	10605
NM	1.34	2.70	10024
DOPAC	1.61	3.46	9329
DA	2.13	4.87	9013
EPIN	2.69	6.43	8984
5-HIAA	3.01	7.30	8973
HVA	4.33	10.96	9211
3-MT	5.67	14.65	8880
5-HT	6.10	15.85	8333
N-MET	7.79	20.52	8703

7. Calculation of Results

Tissue concentrations of neurotransmitters and metabolites were calculated directly from the ratio of the peak height of the compound of concern in a sample to that of the internal standard in the same sample. This is mathematically expressed for the determination of the 5-HT concentration in a single sample as:

$$5-HT\left(\frac{\text{nmol}}{\text{g tissue}}\right)=\frac{\left(\frac{PH_{5-HT}}{PH_{int.std.}}\right)_{sample}(\text{nmol } 5-HT \text{ in ext.std.})}{\left(\frac{PH_{5-HT}}{PH_{int.std.}}\right)_{ext.std.}(\text{wt. of brain sample, g})}$$

where $PH_{5\text{-}HT}$ is the peak height of 5-HT, $PH_{int.std.}$ is the peak height of the internal standard, and nmol is the total nanomole of 5-HT in the 500 µL external standard. The

internal standard used for catecholamines was EPIN, while N-MET was used for indolamines. Final results for a group of similarly treated animals were expressed as the mean ± SEM. Different test groups were compared using Student's two-tailed t-test.[126,127]

Typical whole mouse brain control values obtained for individual neurochemicals, using the above described LCEC approach, were (nmol/g, mean ± SEM): NE, 2.98 ± 0.08; EPI, 0.91 ± 0.00; NM, 0.10 ± 0.02; DOPAC, 0.78 ± 0.05; DA, 8.19 ± 0.20; 5-HIAA, 1.65 ± 0.06; HVA, 1.16 ± 0.04; 3-MT, 1.00 ± 0.05; 5-HT, 4.50 ± 0.06.

C. Experimental Procedures

1. LD_{50}

The LD_{50} is defined as the dosage of an agent at which 50% of treated animals die. While traditionally this value was determined by treating a large number of animals at several fixed doses, this method is time consuming, expensive, and wasteful with respect to animal life. Alternative, statistically valid, techniques for the determination of LD_{50} values, which require fewer animals and less time, are the approaches known collectively as the Dixon up/down method.[128-130]

The Dixon up/down approaches employ a staircase bioassay in which the dose for a given animal in the procedure is based on the observed response of the animal treated immediately before it. In an LD_{50} study, there are only two responses: live or dead. The result is observed at a predetermined time. For example, if a test animal is alive at the predetermined time following treatment, the next animal is treated at a higher dose; however, if the animal dies before the predetermined time is reached, the next animal is treated at a lower dose. For this method to work, however, two criteria must first be met. The doses must be equally spaced on a log scale and this spacing must be chosen close to

log σ, where σ is the standard deviation of the threshold distribution. While it is required that the spacing be close to log σ, error in this estimation by as much as 50% does not effect the results dramatically.

In order to minimize the amount of time spent on an LD_{50} study, three animals were typically injected at any one time period. The three included one at the desired dose in μg, one at log (dose) + 0.1, and one at log (dose) - 0.1. If the middle animal lived, the results for the middle and the high dose animals were used in the data set, while the low dose result was discarded. If the middle animal died, the results for the middle and low dose animals were used, while the high dose result was discarded. In this fashion, one can complete an LD_{50} study in half the normal time. The volume of the individual, unilateral intraventricular injections never exceeded 5 μL. Results from animals with heavy bleeding, i.e., those experiencing a medial sinoidal vein puncture during injection, were discarded from the data set. Results from animals that engaged in self-mutilation were treated as if the animals had died. Animals remaining alive at the end of 1 h were sacrificed by cervical dislocation. All animal brains were removed from the skull and dissected following death to verify that the injected toxin was delivered to the ventricular system. If the injection did not reach the ventricular system, the results for the corresponding animals were not included in the final data set.

Calculation of an LD_{50} from the Dixon approach depends on whether one employs N=6 or N>6 animals in the data set. Since we wanted to shorten the time and minimize the number of animals needed for such studies, we initially decided to see if the less extensive data set would yield results which reasonably corresponded to those of the more extensive data set. Using 6,8-ADTQ, t=1 h, and N=11, we subjected the initial 6 results to the shorter approach and the entire data set to the longer approach.[128-130] In both cases we obtained the same 85 μg (free base) for LD_{50}. Thus, the shorter, N=6, approach was employed for all subsequent LD_{50} determinations.

2. Intracerebroventricular Injection

In order to reproducibly inject mice intracerebroventricularly (i.c.v.), a specific procedure was developed and followed. The animal was weighed, anesthetized in an ether chamber, and placed upright on a surgical table. The thumb and middle finger of one hand were placed on the lateral posterior portions of the skull, while the index finger was placed on the dorsal posterior portion of the skull. Holding the animal in this way immobilized the head of the mouse and, simultaneously, allowed for the immobilization of the animal's body with the palm of the same hand.

With the other hand, the tip of the needle of a prefilled syringe was placed ca. 3 mm posterior from the back of the eyes and ca. 3 mm lateral from the midline. The syringe was held at an angle of approximately 35° lateral, measured from the mid-sagital plane. The needle was inserted through the scalp and skull, and into the brain to the desired depth. The depth of injection into the brain was held at a constant 4 mm though the use of a piece of Teflon tubing, cut to an appropriate length and fitted over the end of the injection needle. The toxic agent was slowly injected over the course of ca. 7-10 sec. This slow injection promoted delivery of the toxin into the ventricular region and minimized undesirable movement up the needle track and out of the brain.

3. Depletion

ICR:Hsd male mice (Harlan Sprague-Dawley, Madison, WI) weighing 30-37 g were used for all depletion studies. After weighing, the animals were anesthetized in an ether chamber. Bilateral injections were carried out using a model 80330 10 μL Hamilton syringe (Fisher Scientific, Pittsburg, PA) with the total volume never exceeding 3.5 μL. Control animals were routinely injected with equivalent volumes of saline. Animals were sacrificed on day 7 following injection using exposure to 7.0 kW of microwave irradiation for 150 msec, delivered by a New Japan Radio model NJE-2603-10kW

unit.[131-134] To ensure reproducible heating of brain tissue, a water load was irradiated 1 min prior to each animal sacrificed.[122]

Brains were removed and weighed, with individual brain weights generally ranging from 450-525 mg. Each brain was placed in a 10 mL ground glass homogenization mortar, and 1 mL of homogenization solution was added. For external standards, 500 μL of stock external standard was used in place of the brain. Homogenization involved 20 complete up/down strokes employing the highest rpm setting possible using a model 143 Dyna-mix motor (Fisher Scientific, Dallas, TX), outfitted with a Duall 22 (Kontes Glass Co., Vineland, NJ) ground glass tissue grinder/homogenizer. The homogenate was transferred to a 1 mL polycarbonate centrifuge vial and centrifuged in a type 25 rotor using a model L8-80 Beckman Ultracentrifuge at 21,000 rpm (50,000 x g) for 60 min at 4°C. The supernatant was then transferred to a 1.5 mL plastic storage vial and frozen at -80°C until the time of analysis. The samples were individually thawed and filtered 15 min prior to LCEC analysis utilizing a model 926 bench top centrifuge (Fisher Scientific, Dallas, TX) and a model MF5500 BAS (Bioanalytical Systems Inc., West Lafayette, IN) microfiltration apparatus with 0.45 μ RC55 nitrocellulose membrane filters.

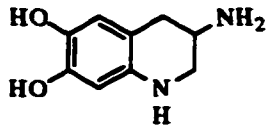

6,7-ADTQ

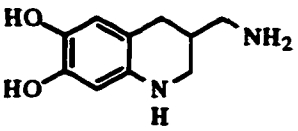

6,7-AMDTQ

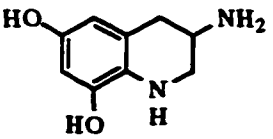

6,8-ADTQ

IV. Results and Discussion

A. LD_{50}

The LD_{50} for each of the quinoline analogs was assessed using the N=6 Dixon approach[129] and an experimental time of 1 hour. A typical investigation is shown below for 6,8-ADTQ, along with calculation of the LD_{50}, in Figure 4-2.

LD_{50} for 6,8-ADTQ								
Toxin dose, μg	log(dose)	Results of Test (X = dead; O = living)						
120	2.08		X					
95	1.98	O		X				
76	1.88				X			O
60	1.78					O		

$\log (LD_{50}) = x_f + kd = 1.88 + 0.500(0.1) = 1.93$, where

x_f = log (final test dose)
d = log (spacing of doses)
k = tabulated value for maximum likelihood estimate (Dixon and Mood[129])

LD_{50} = antilog(1.93) = 85 μg

Figure 4-2. LD_{50} determination and calculation for 6,8-ADTQ.

Comparable LD_{50} investigations were performed for each of 6,7-ADTQ, 6,7-AMDTQ, and 6,8-ADTQ. The results of these investigations, along with previously reported results for 6-HDA and 5,7-DHT, are presented in Table 4-11.

Table 4-11. LD_{50} values in mice.

LD_{50} Values in Mice at 1 hour		
Compound	$LD_{50} \pm$ s.d. (μg)	$LD_{50} \pm$ s.d. (nmol)
6,7-ADTQ	37 ± 3	206 ± 17
6,7-AMDTQ	48 ± 5	247 ± 26
6,8-ADTQ	85 ± 11	472 ± 61
6-HDA[24]	134 ± 7	793 ± 43
5,7-DHT[89]	52	271

s.d. was calculated from tabulated estimated errors as determined by Dixon.[128]

From these results, we see that the LD_{50} values for 6,7-ADTQ and 6,7-AMDTQ are similar, as one might expect from the structural similarities. Interestingly, however, 6,8-ADTQ exhibits an LD_{50} approximately twice that of its 6,7-analogs. While the LD_{50} values for all the quinoline derivatives are lower than that for 6-HDA, the values for the 6,7-analogs were quite comparable to that reported for 5,7-DHT.

For 6-HDA and its analogs, a one hour LD_{50} had been shown to be a reasonable representation of the "long term", i.e., 7-14 day, LD_{50}. Thus, one hour was initially chosen for the quinoline LD_{50} studies presented here. However, it was found during the

subsequent depletion studies, much to our surprise, that the one hour LD_{50} was not a good representation of the 7 day LD_{50} with these toxins. In fact, many of the animals treated at doses near the LD_{20}, while living past 1 hour, died in the five days following treatment. Nonetheless, a one hour $LD_{15\text{-}20}$[128] generally proved to be a reasonable first guess for the seven day depletion studies. And, ultimately, the amount of toxin used in the final depletion experiments was adjusted based on observed mortality rates in the initial depletion experiments.

B. Depletion Studies

1. (±, +, and -)-6,7-ADTQ Investigations

Stereochemistry can significantly alter the biological activity of a compound.[135,136] We, thus, investigated the effects of chirality on the neurotoxic properties of 6,7-ADTQ. The initial intent was to compare the potency and selectivity of the agents for 5-HT degeneration under conditions approaching maximal effects for each individually. Thus, we attempted to adjust the dose of each to maximize its effects while maintaining reasonable survivability in the seven day experiment. Reasonable survivability, defined as that which would be practically useful for others in routine studies, was taken to be on the order of, or slightly greater than, 50%. The corresponding dose is called the "maximum usable" dose.

For the racemic and enantiomeric forms of 6,7-ADTQ, we began with a dose of 111 nmol for each, which was considered a conservative estimate based on the one hour LD_{50} studies. The results of this study are shown in Table 4-12.

Table 4-12. Whole mouse brain CNS neurotransmitter depletions 7 days after 111 nmol of (±, +, and -)-6,7-ADTQ.

Compound	Neurotransmitter Levels (% controls ± SEM)			
	NE	DA	5-HT	N
Controls	100 ± 4	100 ± 3	100 ± 1	8
(±)-6,7-ADTQ	60 ± 6***	75 ± 5***	68 ± 4***	6
R-(+)-6,7-ADTQ	45 ± 2***	76 ± 5***	73 ± 1***	5
S-(-)-6,7-ADTQ	44 ± 2***	82 ± 17	51 ± 1***	2

Significant differences compared to control values (*t* test): ***$P < 0.001$.

From these equidose results, it was apparent that the S-(-)-6,7-ADTQ was more potent in effecting 5-HT degeneration than either the R-(+)-6,7-ADTQ or the parent racemic mixture. But, the survival rate for mice injected with S-(-)-6,7-ADTQ was only 16%. Thus, we decided to lower the dose of all three species to 83 nmol and repeat the experiment, as shown in Table 4-13.

Table 4-13. Whole mouse brain CNS neurotransmitter depletions 7 days after 83 nmol of (±, +, and -)-6,7-ADTQ.

Compound	Neurotransmitter Levels (% controls ± SEM)			
	NE	DA	5-HT	N
Controls	100 ± 3	100 ± 3	100 ± 4	7
(±)-6,7-ADTQ	48 ± 2***	79 ± 5**	69 ± 5**	7
R-(+)-6,7-ADTQ	52 ± 3***	81 ± 4**	73 ± 3***	9
S-(-)-6,7-ADTQ	49 ± 2***	79 ± 6**	65 ± 7**	3

Significant differences compared to control values (*t* test): **$P < 0.01$, ***$P < 0.001$.

Under these new, but still equivalent dosage, conditions, the S-(-)-6,7-ADTQ continued to appear more potent with respect to its 5-HT effects. However, the individual 5-HT results were notably not significantly different. And, more importantly, the survival rate for the S-(-)-6,7-ADTQ group was only 25%.

At this juncture, the difficulty associated with extrapolating a one hour LD_{50} value to a seven day LD_{50} value was obvious. Thus, we injected another group of animals with only 55 nmol of S-(-)-6,7-ADTQ and stopped to examine our knowledge of 7 day survivability. The results are shown below in Table 4-14.

Table 4-14. Survivability of mice 7 days after (±, +, and -)-6,7-ADTQ injection.

Compound	Amount used (nmol)	% Alive at 7 days
(±)-6,7-ADTQ	111	43 %
	83	58 %
R-(+)-6,7-ADTQ	111	21 %
	83	75 %
S-(-)-6,7-ADTQ	111	16 %
	83	25 %
	55	75 %

Thus, based on the results in Table 4-15, we were ready to compare the "maximum usable" effects of each of the agents. The doses indicated for this study were 83 nmol for both (±)- and R-(+)-6,7-ADTQ and 55 nmol for S-(-)-6,7-ADTQ. An examination of the mouse brain effects under these conditions yielded the results shown below in Figure 4-4 for the neurotransmitters and in Table 4-16 for all the measured endogenous neurochemicals.

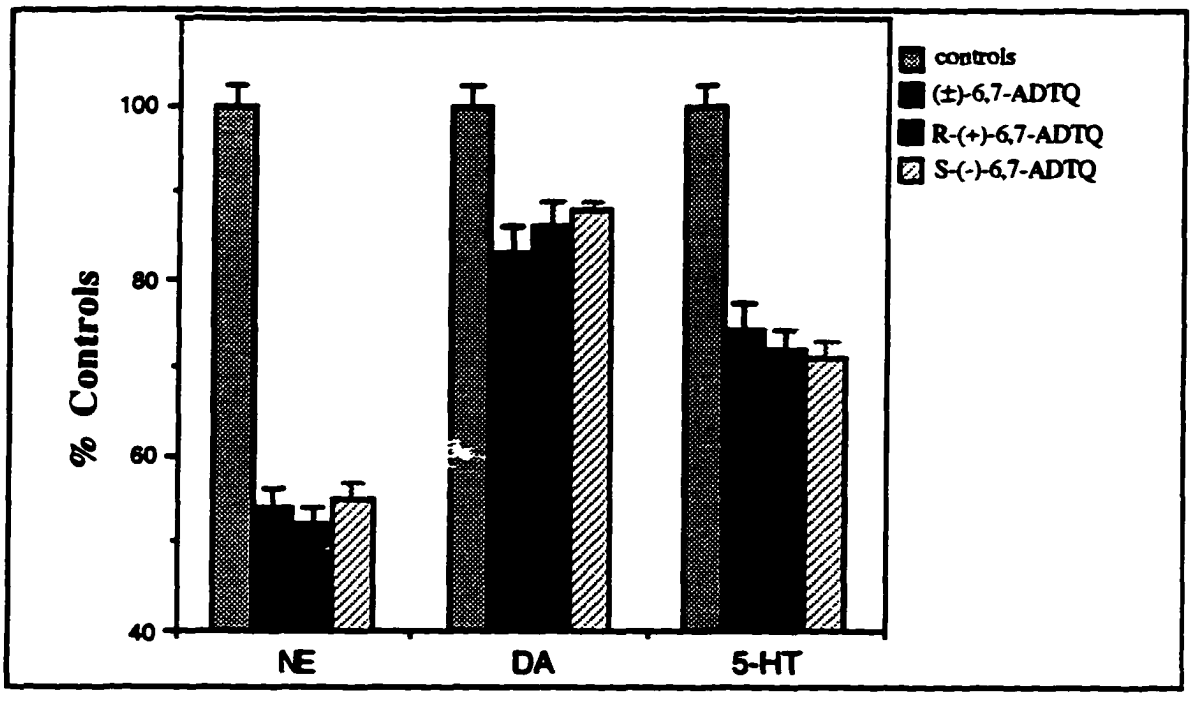

Figure 4-3. Mouse whole brain neurotransmitter depletions by (±,+,and-)-6,7-ADTQ.

Table 4-15. Mouse whole brain neurochemical levels 7 days after treatment with "maximum usable" doses of (±)-, R-(+)-, and S-(-)-6,7-ADTQ.

		Neurotransmitter Levels, % controls ± SEM					
Compd	N	NE	DA	5-HT	DOPAC	HVA	5-HIAA
(±)-6,7-ADTQ	11	54 ± 2***	83 ± 3***	74 ± 3***	92 ± 5	113 ± 5*	100 ± 5
R-(+)-ADTQ	14	52 ± 2***	86 ± 3***	72 ± 2***	90 ± 4	113 ± 5	87 ± 3*
S-(-)-ADTQ	16	55 ± 2***	88 ± 3***	71 ± 3***	83 ± 4**	112 ± 6	82 ± 3***

Significant differences compared to control values (*t* test): $*P < 0.05$; $**P < 0.01$, $***P < 0.001$. 6,7-ADTQ, 83 nmol; R-(+)-6,7-ADTQ, 83 nmol; S-(-)-6,7-ADTQ, 55 nmol. Typical mouse whole brain control transmitter values were (nmol/g tissue, mean ± SEM): NE, 2.98 ± 0.08; DA, 8.19 ± 0.2; 5-HT, 4.5 ± 0.06.

Employing the "maximum usable" dose for each of these species, we observed no discernible and/or significant effects with respect to neurotransmitter depletions.

Summarization of all the results obtained for the racemic and enantiomeric forms of 6,7-ADTQ are, thus, quite straightforward. When employed at equivalent doses, the S-(-)-enantiomer is both more lethal and more potent in its 5-HT degenerative effects than either the R-(+)- enantiomer or the racemic mixture. Simultaneously, at equivalent doses, no significant differences were observed for the effects of any of these three species on non-5-HT systems. When the dose of each species was adjusted to a "maximum usable" value, there was no discernible differences in the depletion effects on any of NE, DA, or 5-HT. Thus, overall, there is no substantial advantage to utilization of either enantiomers over that of the parent racemic mixture in neurotoxic investigations.

2. 6,7-ADTQ, 6,7-AMDTQ, and 6,8-ADTQ Investigations

Initial efforts on 6,7-AMDTQ and 6,8-ADTQ concentrated on finding an appropriate dose to employ for "maximum usable" comparisons to the 6,7-ADTQ. The one hour LD_{50} results strongly indicated that equivalent doses would be inappropriate for these two species. For 6,7-AMDTQ, we initially employed 156, 78, 52 nmol. These doses yielded 7 day survival rates of 4%, 18%, and 89%, respectively. Thus, we selected 52 nmol as the "maximum usable" dose. For 6,8-ADTQ, two attempts at 333 nmol yielded 7 day survival rates of 45% and 40%; thus, this value was selected for this toxin.

The effects of 6,7-AMDTQ, 6,8-ADTQ, and 6,7-ADTQ, each at its "maximum usable" dose, on mouse whole brain neurotransmitter levels 7 days following i.c.v. injection are shown in Figure 4-4. The corresponding effects on all measured endogenous neurochemicals are presented in Table 4-16. All toxins employed for these studies were, notably, racemic mixtures.

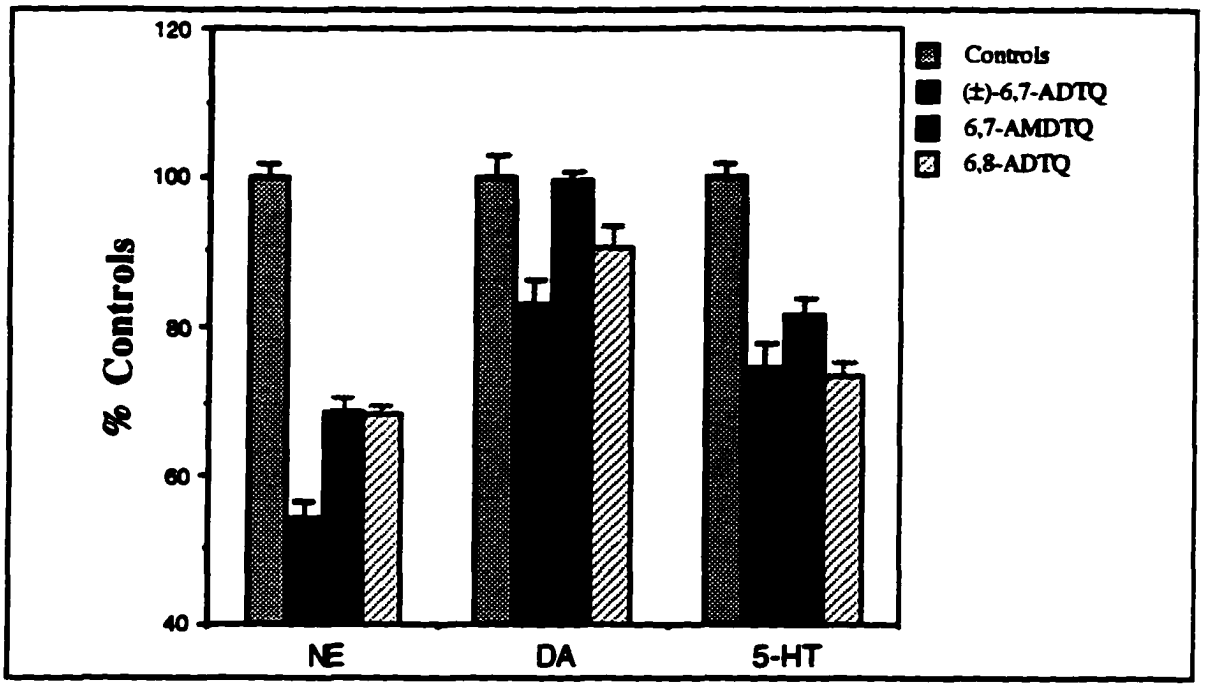

Figure 4-4. Whole mouse brain depletion by 6,7-ADTQ, 6,7-AMDTQ, and 6,8-ADTQ.

Table 4-16. Mouse whole brain neurochemical levels 7 days after treatment with "maximum usable" doses of 6,7-ADTQ analogs.

	Neurotransmitter Levels, % controls ± SEM						
Compd	N	NE	DA	5-HT	DOPAC	HVA	5-HIAA
(±)-6,7-ADTQ	11	54 ± 2***	83 ± 3***	74 ± 3***	92 ± 5	113 ± 5*	100 ± 5
6,7-AMDTQ	17	68 ± 2***	100 ± 1	81 ± 2***	87 ± 2*	104 ± 5	86 ± 4*
6,8-ADTQ	16	68 ± 1***	91 ± 3*	73 ± 2***	88 ± 3*	118 ± 4**	68 ± 2***

Significant differences compared to control values (*t* test): $*P < 0.05$; $**P < 0.01$, $***P < 0.001$. Toxin amounts used were: 6,7-ADTQ, 83 nmol; 6,7-AMDTQ, 52 nmol; and 6,8-ADTQ, 333 nmol. Typical mouse whole brain control transmitter values were (nmol/g tissue, mean ± SEM): NE, 2.98 ± 0.08; DA, 8.19 ± 0.2; 5-HT, 4.5 ± 0.06.

These results indicate that the examined toxins are only able to elicit ca. 30% 5-HT degeneration under the "maximum usable" conditions. This was somewhat disappointing. However, there were also some encouraging aspects. For example, both 6,7-AMDTQ and 6,8-ADTQ exhibited lesser effects on NE and DA degeneration than did the parent 6,7-ADTQ. Thus, these analogs are more selective than 6,7-ADTQ.

To facilitate comparisons between the quinoline analogs currently examined and the established 6-HDA and 5-HT standards, we have shown neurotransmitter depletions produced by each in mouse whole brain 7 days following treatment with the agent in Table 4-17. The dose used in each case was at or near the "maximum usable" value.

Table 4-17. Mouse whole brain neurotransmitter effects of 6,7-ADTQ analogs and similar toxins at 7 days.

Compound	dose, nmol	Neurotransmitter Levels (% controls ± SEM)[a]			
		NE	DA	5-HT	N
(±)-6,7-ADTQ	83	54 ± 2***	83 ± 3***	74 ± 3***	11
6,7-AMDTQ	52	68 ± 2***	100 ± 1	81 ± 2***	17
6,8-ADTQ	333	68 ± 1***	91 ± 3*	73 ± 2***	16
6-HDA[b]	300	35 ± 6***	71 ± 6**	88 ± 3*	6
5,7-DHT[c]	129	82 ± 3***	99 ± 1	70 ± 6***	16

[a] Significant differences compared to control values (*t* test): $*P < 0.05$; $***P < 0.001$.

[b] data from Su Ma et al.[24]

[c] data from Lin[23]

From a noradrenergic viewpoint, the quinoline analogs fall short of matching the abilities of 6-HDA. However, from a serotonergic viewpoint, the 6,7-ADTQ and 6,8-ADTQ are equally as potent as 5,7-DHT. And, at higher doses, 6,7-ADTQ has been shown capable of producing 48% 5-HT depletions (see Table 4-1), which is substantially more than maximal 5-HT depletions of 30% reported for 5,7-DHT.

6,7-AMDTQ and 6,8-ADTQ are more selective than 6,7-ADTQ in that they cause lesser degenerative effects on the noradrenergic and dopaminergic systems. But, 5,7-DHT is clearly more innately selective than all the quinoline adducts. Fortunately, L. Lin has demonstrated that, by incorporating appropriate uptake blocking agents, NE and DA depletions produced by 6,7-ADTQ can be substantially blocked. Thus, it is not unreasonable to assume that the lesser NE and DA effects elicited by 6,7-AMDTQ and 6,8-ADTQ could also be similarly blocked, possibly to an even greater extent. As such, we would predict that uptake blocking agents could be used with all the quinoline congeners to eliminate these selectivity problems. The reader should also be reminded that the results presented here are from intracerebroventricular administration of the toxic agents. And, selectivity is a function of many different factors, including the site at which the toxin is administered. Thus, selectivity could additionally be enhanced by simply injecting the agent directly into a brain region containing the desired nerve ending and/or cell bodies to be destroyed.

C. Behavioral Effects

At the doses indicated in the depletion study, mice treated with 6,7-ADTQ, 6,7-AMDTQ, and, to a lesser degree, 6,8-ADTQ exhibited extreme hyperactivity upon recovery from anesthesia, which took approximately 1 min. Treated animals would initially be motionless, with their backs arched and their tails erect. Then, suddenly, they

would jump 6 to 10 times in rapid succession, straight up 4 to 6 inches. This was followed by many interesting behavioral effects such as: rapid running around the sides of the cage; lying on the side or back and rubbing the head on the sides and bottom of the cage; rolling along the head-tail axis; lying on the back with limbs extended straight out, accompanied by occasional body and head tremors; and, periodically, appearing to experience extended seizures lasting 20 to 40 sec each. Such phases of high activity would last 5 to 10 min and would be followed by a 2 to 4 min period in which the animal would lay prone and upright, appearing entirely limp. These alternating episodes of high and low activity would continue for up to 1 day.

V. Conclusions

6,7-ADTQ, its enantiomers, and its analogs were investigated to determine their potential utility as serotonergic neurotoxins. Examinations of the enantiomers of 6,7-ADTQ revealed the S-(-)-enantiomer, at equivalent doses, to be more potent than the R-(+)-enantiomer. However, the S-(-)-enantiomer was also more lethal. When the dose of the S-(-)-enantiomer was reduced to compensate for this lethality, it unfortunately displayed no significant advantage in neurodegenerative capabilities over the R-(+)-enantiomer or the racemic mixture. But, both 6,7-ADTQ and 6,8-ADTQ produced substantial depletions in mouse whole brain 5-HT levels. These depletions are at least comparable to those produced in mouse brain by 5,7-DHT[23,79] at "maximum usable" doses. Furthermore, at higher dose levels, 6,7-ADTQ produced 5-HT depletions greater than any previously reported for 5,7-DHT. But, these quinoline compounds were inherently less selective than 5,7-DHT. However, Lin has shown that the non-specific destruction can be substantially blocked with appropriate uptake blocking agents, thereby eliminating the selectivity problems.

Considering all of the above factors, we conclude that both 6,7-ADTQ and 6,8-ADTQ, if employed with appropriate NE and DA uptake blocking agents, would be at least equally potent in their neurodegenerative effects on the mouse brain serotonergic system as the standard 5,7-DHT.

Mode of Action I : Uptake Interaction

Chapter 5

I. Introduction

Neurotransmitter uptake, or transport, sites are present in nerve terminal membranes and bear the primary responsibility for inactivation of released transmitters. Uptake sites, therefore, play a key functional role at many synapses.[137] Uptake sites are also believed to be the primary site of action of many drugs. For example, cocaine acts, at least in part, by blocking the uptake of DA, thereby increasing the extracellular concentration of this neurotransmitter.[5] Other psychostimulants, such as amphetamines, act in a similar manner.[5] The ability of tricyclic antidepressants to inhibit catecholamine

and/or indolamine transmitter reuptake led to the "biogenic amine hypothesis" of affective disorders.[3] In addition to drugs exerting their effects *via* uptake blockade, pharmacologically active agents may also gain access to the cytoplasm of the neuron through these highly selective transport sites and, once inside, elicit other effects.

It is known that 6-HDA and related analogs must be accumulated inside the neuron to subsequently elicit degenerative effects. This requirement is also accepted for MPP^+, the toxic metabolite of MPTP, 5,6- and 5,7-DHT, and most other neurotoxins. The mechanism by which these compounds gain access to the cytoplasm involves selective recognition and transport by the relevant neurotransmitter uptake sites. This requirement is easily demonstrated by the elimination of neurotoxicity upon incorporation of appropriate uptake blocking agents prior to administration of the toxin. Selective transport is, thus, unquestionably a primary factor involved in the selective degeneration exhibited by a given agent. On the other hand, Ma and coworkers,[24] investigating eight analogs of 6-HDA, have shown that no direct correlation exists between the degree of toxin-transporter interaction and the observed degeneration which occurs in affected neurotransmitter systems.

II. Background

Toxin affinities for and interactions with various neurotransmitter transport sites are generally determined by the extent to which the toxin interferes with the uptake of radiolabeled neurotransmitters. This is normally accomplished *in vitro* utilizing synaptosomes, which possess much of the functional viability characteristics inherent of *in vivo* nerve endings from which they are derived.[138-140] Synaptosomes are isolated *via* tissue homogenization followed by purification using a sucrose gradient centrifugation technique.[136,138,139,141,142]

The interaction of substrates with uptake, or transport, sites are remarkably similar to those of substrates and enzymes, and, therefore, can be mathematically treated using enzyme kinetic models. A modified version of the Michaelis-Menten equation is the Briggs-Haldane equation:

$$v_o = \frac{V_{max}[S]}{K_m + [S]} \qquad \text{equation 5-1}$$

where v_0 is the initial velocity of uptake, V_{max} is the saturated or maximal uptake velocity, [S] is the substrate concentration, and K_m is the Michaelis-Menten constant. Taking the reciprocal of equation 5-1 leads to the Lineweaver-Burk equation:

$$\frac{1}{v_o} = \frac{K_m + [S]}{V_{max}[S]} = \left(\frac{K_m}{V_{max}}\right)\frac{1}{[S]} + \frac{1}{V_{max}} = \frac{1}{V_{max}}\left(\frac{K_m}{[S]} + 1\right) \qquad \text{equation 5-2}$$

Thus, if $1/v_0$ is plotted against 1/[S], one obtains a straight line with a slope of K_m/V_{max} and a Y-intercept of $1/V_{max}$. K_m is an important parameter which is characteristic of the specific substrate-transporter interaction. It is also of interest to note that, when $v_0 = V_{max} / 2$, $K_m = [S]$.

In the presence of an inhibitor, the uptake velocity becomes dependent upon both the substrate and inhibitor concentrations. Modifying equation 5-2 to accommodate a competitive inhibitor, we obtain:

$$\frac{1}{v_i} = \frac{1}{V_{max}}\left(\frac{K_m}{[S]}\left(1+\frac{[I]}{K_i}\right)+1\right) \qquad \text{equation 5-3}$$

where v_i is the uptake velocity in the presence of the inhibitor, [I] is the inhibitor concentration, and K_i is an equilibrium constant for the interaction of the inhibitor with the transporter. The corresponding equations for noncompetitive and uncompetitive interactions are, respectively:

$$\frac{1}{v_i} = \frac{1}{V_{max}}\left(1+\frac{[I]}{K_i}\right)\left(\frac{K_m}{[S]}+1\right) \qquad \text{equation 5-4}$$

and

$$\frac{1}{v_i} = \frac{1}{V_{max}}\left(\frac{K_m}{[S]}\left(1+\frac{[I]}{K_i}\right)\right) \qquad \text{equation 5-5}$$

The nature of the interaction of a given inhibitor and transporter combination normally is determined in a series of experiments, each employing a unique concentration of inhibitor, in which the transport velocity is measured as a function of the substrate concentration. The resultant data is plotted as $1/v_i$ vs. 1/[S] and compared to the theoretically expected plots for each of the competitive, noncompetitive, and uncompetitive cases. The theoretical plots are derived directly from equations 5-3 to 5-5 and appear as:

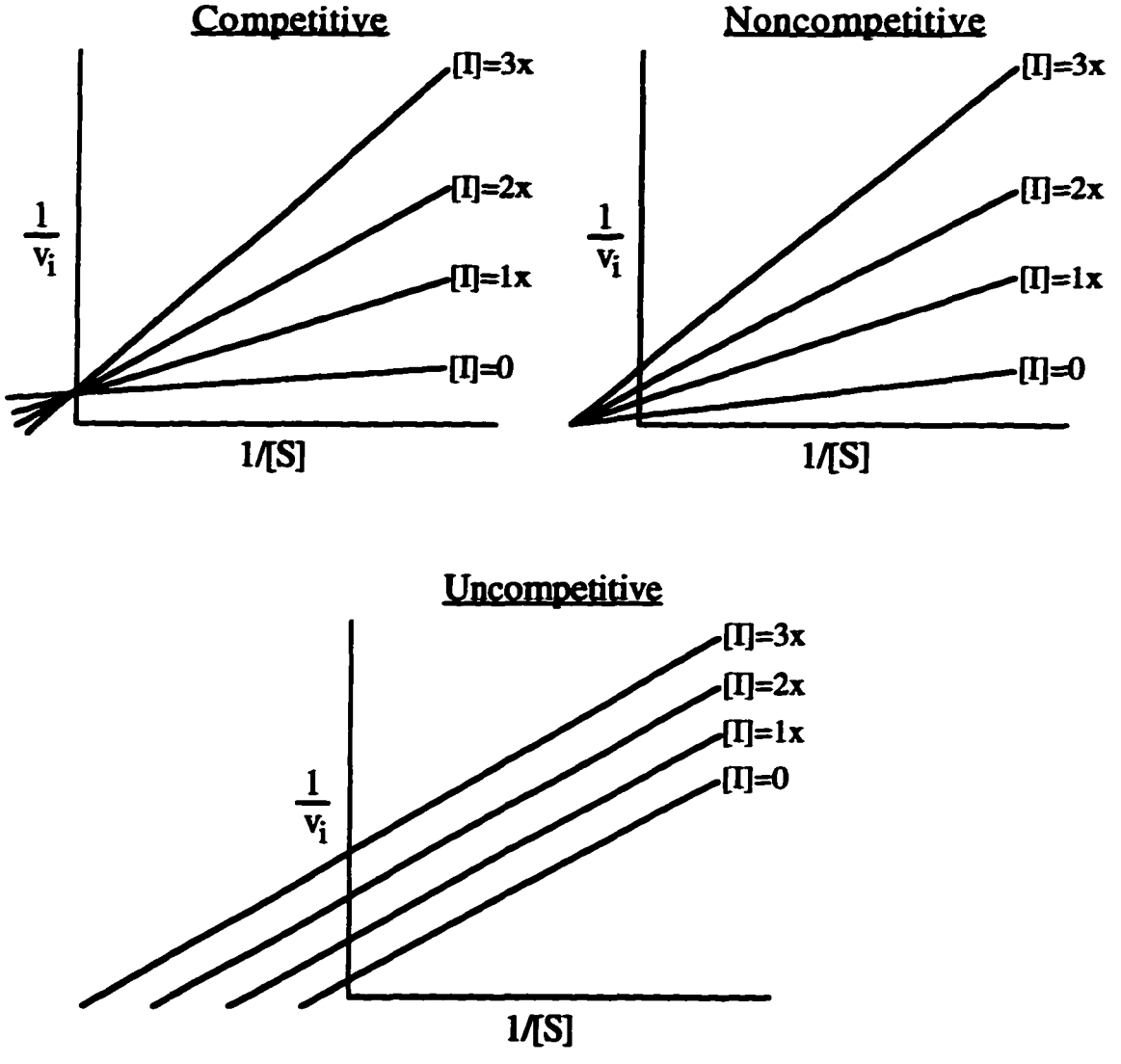

However, direct determinations of the K_m, K_i, and V_{max} values from a Lineweaver-Burk plot, such as that shown above, is inadvisable due to the inappropriate weighting of individual data points. For these determinations, a nonlinear least squares provides more reliable constants. In our case, we used NLLSQ, a program written by Dr. Enwall (University of Oklahoma), to obtain values of K_m, K_i, and V_{max}, as well as error estimates for each.[24] Thus, a normal sequence in the determination of the interaction of an inhibitor with a transport site involved (1) identification of the type of inhibition *via* a

Lineweaver-Burk double reciprocal plot, and (2) determination of the K_i value *via* fitting to the appropriate kinetic equation using NLLSQ.

In some cases, one may, a priori, know that a particular inhibitor/transporter interaction is competitive. In these cases, a shorter route to the K_i is available. Using a fixed concentration of substrate near the K_m, one measures the initial uptake velocity at varying concentrations of the inhibitor. The results are typically plotted as transport velocity, in % control units, vs. log[I] and yields an inverted S-shaped curve. The inhibitor concentration, [I], at which the transport rate is 50% of its control, or maximum, value is signified as the IC_{50}.[143] Using $v_i=v_o / 2$ and $[I]=IC_{50}$, combination and reduction of equations 5-2 and 5-3 yields:

$$IC_{50} = K_i\left(1+\frac{[S]}{K_m}\right) \qquad \text{equation 5-6}$$

or

$$K_i = \frac{K_m IC_{50}}{K_m + [S]} \qquad \text{equation 5-7}$$

Thus, K_i is directly accessible in an IC_{50} experiment through (1) determination of IC_{50}, (2) knowledge of the substrate concentration employed, and (3) prior knowledge of the K_m value. However, as was the case with the above Lineweaver-Burk discussion, fitting of all the data points with NLLSQ, rather than simple graphical extrapolation, is preferred to avoid improper weighting of any single data point. In this case, the data is fitted to the reciprocal of equation 5-3.

III. Experimental Methods

A. Chemicals and Solutions

1. Chemicals

All aqueous solutions employed 18 MΩ distilled/deionized water which was prepared by passing distilled water through a Milli-Q Reagent Water System (Millipore, Continental Water Systems, El Paso, TX).

Radiolabeled transmitters, ^{3}H-NE, ^{3}H-DA, and ^{3}H-5-HT, were purchased from DuPont NEN Research Products and stored under a nitrogen atmosphere in the refrigerator. EcoLite+ was purchased through ICN Biochemical, Inc.

The chemicals listed below were purchased through Sigma Chemical Company (St. Louis, Mo.) in high purity and used without any further purification. All other chemicals were obtained and used as described in previous chapters.

sucrose

TRIS buffer

iproniazid

potassium chloride

calcium chloride

lithium chloride

magnesium chloride

D-glucose

L-ascorbic acid

sodium carbonate

sodium bicarbonate

sodium tartrate

bicinconinic acid, disodium salt

ethylene glycol monomethyl ether (2-methoxyethanol)

2. Homogenization Solution

The homogenization solution used for the preparation of synaptosomes contained 0.32 M sucrose, 20 mM TRIS buffer, adjusted to pH 7.4 with HCl, and 10 μM iproniazid, an irreversible monoamine oxidase inhibitor. Component additions and solution adjustments performed sequentially as shown in Table 5-1. The prepared solution was stored at 4°C for up to 1 week, then discarded.

Table 5-1. Homogenization solution preparation.

Compound	Amount
sucrose	54.77 g
Tris Base	1.21 g
iproniazid	1.39 mg
add 490 mL water	
adjust to pH 7.40 with HCl	
dilute to 500 mL	

3. Na^+ Tris-Krebs Buffer Solution

The Na^+ Tris-Krebs buffer was employed in synaptosomal incubations. It contained 140 mM NaCl, 5 mM KCl, 2.5 mM $CaCl_2$, 1.2 mM $MgCl_2$, 10 mM D-glucose, 1 mM L-ascorbic acid, 20 mM TRIS buffer, and adjusted to pH 7.4 with HCl. Component additions and solution adjustments were performed sequentially as

given in Table 5-2. This solution was prepared 18 h prior to use and stored at 4°C, then discarded following the experiment.

Table 5-2. Na^+ Tris-Krebs buffer preparation.

Compound	Amount
NaCl	8.18 g
KCl	373 mg
$CaCl_2 \cdot 2H_2O$	368 mg
$MgCl_2 \cdot 6H_2O$	244 mg
D-glucose	1.80 g
L-ascorbic acid	176 mg
Tris Base	2.42 g
add 980 mL water	
adjust to pH 7.40 with HCl	
dilute to 1.00 L	

4. Li^+ Tris-Krebs Buffer Solution

For samples in which background, or zero, uptake was determined, Li^+ Tris-Krebs buffer was substituted for the Na^+ Tris-Krebs buffer. It contained 140 mM LiCl, 5 mM KCl, 2.5 mM $CaCl_2$, 1.2 mM $MgCl_2$, 10 mM D-glucose, 1 mM L-ascorbic acid, 20 mM TRIS buffer, and adjusted to pH 7.4 with HCl. Component additions and solution adjustments were performed sequentially as given in Table 5-3. This solution was prepared 18 h prior to use and stored at 4°C, then discarded following the experiment.

Table 5-3. Li^+ Tris-Krebs buffer preparation.

Compound	Amount
LiCl	5.93 g
KCl	373 mg
$CaCl_2 \cdot 2H_2O$	368 mg
$MgCl_2 \cdot 6H_2O$	244 mg
D-glucose	1.80 g
L-ascorbic acid	176 mg
Tris Base	2.42 g
add 980 mL water	
adjust to pH 7.40 with HCl	
dilute to 1.00 L	

5. Neurotransmitter Solution

The radiolabeled transmitters, ^{3}H-NE, ^{3}H-DA, and ^{3}H-5-HT, were mixed with their corresponding unlabeled transmitters in a molar ratio of between 1:10 to 1:15. A 0.10 mM HCl solution was used for dissolving unlabeled transmitter and the dilution of the transmitter mixture to the desired concentration. The radiolabeled transmitters possessed a specific activity of; NE, 9.0 mCi/mL; DA, 11.7 mCi/mL; and 5-HT, 25.4 mCi/mL. The labeled/unlabeled mixture was prepared just prior to the experiment and was used for a maximum of 2 h. The radiolabeled transmitters were stored at -20°C under a nitrogen atmosphere and were discarded within 2 months of their initial opening.

6. Toxin Solution Preparation

A carefully limited amount of toxin was weighed and transferred to a 1 mL glass vial that was preflushed with argon or O_2-free nitrogen. An appropriate amount of deaerated 10^{-4} M HCl was added to obtain the highest desired toxin concentration, and the vial was flushed with argon or nitrogen again. For an IC_{50} study, typical toxin incubation concentrations were $1x10^{-3}$, $3x10^{-4}$, $1x10^{-4}$, $3x10^{-5}$, $1x10^{-5}$, and $3x10^{-6}$. For a double reciprocal study, typical toxin incubation concentrations were 0.5, 1, and 1.5 times the K_i value for the toxin. The desired toxin concentrations were achieved by diluting the original stock solution with 10^{-4} M HCl. The toxin solutions were utilized and discarded within 1 h.

7. Bicinconinic Acid Reagent

Protein determinations for synaptosomal preparations employed the bicinconinic acid method of Smith et al.[144] The reagent contained 1% bicinconinic acid (BCA), 1.74% Na_2CO_3, 0.19% tartrate, 0.4% NaOH, 0.95% $NaHCO_3$. Component additions and solution adjustments were performed sequentially as shown in Table 5-4.

Table 5-4. Bicinconinic acid reagent preparation.

Compound	Amount
BCA-Na_2	2.5 g
Na_2CO_3 anhyd.	4.35 g
tartrate•Na_2•$2H_2O$	0.475 g
NaOH	1.00 g
$NaHCO_3$	2.375 g
add 225 mL water	
adjust to pH 11.25 with solid $NaHCO_3$	
dilute to 250 mL	

B. Methods and Procedures

1. Brain Removal

Male Sprague-Dawley rats weighing 300-400 g were anesthetized in a diethyl ether vapor chamber and sacrificed by decapitation. The rat head was placed on an absorbent towel. Holding the head securely, with the nose pointing away from the experimenter, the skin was removed from the top portion of the skull by cutting with scissors. Starting at the severed part of the neck, cutting proceeded forward below the ear and eye, and along the side of the skull to a point approximately 5 mm in front of the eye. This was repeated on the other side of the skull. Then, by cutting under the skin, the skin was freed from the skull. Scissors were then inserted into the *magnus foramanus*, i.e., the opening at the base of the skull, and the skull was cut down the

midline to a point somewhere between the eyes, being careful not to cut or gouge the brain with the lower half of the scissors. The skull was then cut between the eyes and the rostral-caudal midline using bone cutting forceps. At this point, the skull was opened by inserting the scissors into the midline cut and opening the scissors, thereby splitting the dorsal portion of the skull apart and exposing the brain. The brain was quickly removed and placed upright on a dissection glass kept over ice. With a scalpel, the brain was cut coronally downward between the cerebellum and the cerebral cortex. The cerebellum, medulla/pons, and all caudal tissue components were discarded. The brain was then bisected with a mid-sagittal cut and weighed. Typical brain weights were 1.3-1.6 g.

2. Preparation of Synaptosomes

The two dissected forebrain halves were placed in separate homogenization tubes, each containing ca. 10 mL of homogenization solution at 0°C. Homogenization employed a model 143 Dyna-mix stirrer (Fisher Scientific, Dallas, TX) outfitted with a model S-703 teflon pestle and model B-3103 tissue homogenizing mortar from A.H.T. Co. (Philadelphia, PA). Homogenization required 10 complete up/down strokes at 350 rpm, which corresponded to setting # 4. The homogenates were transferred to precooled, 10 mL plastic centrifuge tubes. Isolation and purification of synaptosomes was accomplished by centrifugation, always at 4°C, using a model RC-5B Sorvall Superspeed Centrifuge and a model SM-24 rotor, both from DuPont Instruments (Newtown, CT). The tissue homogenates were centrifuged at 3000 rpm (1000g) for 10 min, and the resultant pellets, containing cellular debris, were discarded. The supernatant was centrifuged again at 3000 rpm for 10 min, and the resultant pellets were again discarded. The supernatant was then centrifuged at 10000 rpm (12000g) for 20 min to isolate synaptosomes. This time the supernatant was discarded, and the resulting pellets were resuspended at 0°C in 1 mL of homogenization solution using a glass rod. The manually resuspended mixture was transferred to a single homogenization tube, the volume was

adjusted to ca. 3 mL, and the mixture was slowly subjected to 5 up-down strokes to ensure homogeneity of the synaptosomes. The synaptosomal preparation was then divided between the Na^+ and the Li^+ buffers, making the resultant synaptosomal buffer solutions equal in synaptosomal concentration.

3. Uptake/Blockade

250 μL aliquots of buffer/synaptosomal solution were added to 7.4 mL glass incubation vials and kept at 0°C until used. Incubation was carried out in a water shaker bath (Eberbach Corp., Ann Arbor, MI) and the temperature held constant at 37°C by employing a model 71A YSI (Yellow Springs, OH) Thermistep Temperature Controller. Between 8-12 vials were run at a time. Synaptosomal solutions were preincubated for 5 min in the water bath, at which time 20 μL of toxin was added, if toxin was being used. This was immediately followed by the addition of 20 μL of desired ^3H-transmitter which initiated the actual uptake experiment. This mixture was then incubated for 2 min. Uptake was terminated by the addition of 2 mL ice cold Li^+ buffer, and transferred immediately to an ice bath prior to filtering. The synaptosomal solution was then filtered through a Metricel GN-6 0.45 μm filter membrane using a model 1225 Millipore (Millipore, El Paso, TX) 12 port filtration apparatus. Each vial and membrane was rapidly washed two times with 2 mL Li^+ buffer.

The filters were carefully placed in scintillation vials and allowed to air dry overnight. The filters were then dissolved *via* the addition of 1 mL of 2-methoxyethanol (ethylene glycol monomethyl ether). Once dissolved, which took approximately 4-5 h, 4 mL of EcoLite+ scintillation cocktail was added, and the vial was capped and shaken 40 to 50 times to ensure complete homogeneity. The vials were then placed in plastic scintillation containers and stored in the dark for a minimum of 48 h to insure the absence of light-induced fluorescence and chemical-induced luminescence. The radioactivity (DPM) was determined by using a model LS 5801 Beckman liquid scintillation counter.

4. Protein Analysis

Protein concentration was determined using the bicinchoninic acid (BCA) method of Smith and coworkers.[144] BCA reagent (50 mL) was mixed with 1 mL of 4% $CuSO_4$ solution and allowed to stand for 2 h; this mixture turned candy apple green almost immediately. 100 μL of protein standard or sample was added to 2 mL of the BCA/$CuSO_4$ mixture and incubated at 39 ± 1°C in a water bath shaker for 30 min, then cooled to room temperature. Absorbance of the incubated solution was recorded at a wavelength of 562 nm using a model 8452A Hewlett-Packard spectrophotometer. All samples were run in triplicate. A protein calibration curve was obtained by plotting absorbance vs. concentration bovine serum albumin protein standard.

IV. Results and Discussion

A. K_m Values for Transmitter Systems Tested

K_m values for the three neurotransmitter transporters were initially determined to ensure the validity of the individual results. Typical K_m values obtained for NE, DA, and 5-HT in these uptake studies are presented in Table 5-5. These values agree well with those reported in the literature. The determination of a typical K_m value for 5-HT is exemplified graphically in Figure 5-1.

Table 5-5. K_m values for NE, DA, and 5-HT uptake systems in rat brain synaptosomes.

Neurotransmitter	Experimentally Determined K_m (nM)	Literature K_m (nM)
NE	588 ± 20	470[145] - 664[140,146]
DA	232 ± 12	209[147]
5-HT	97 ± 3	83[148] - 130[149]

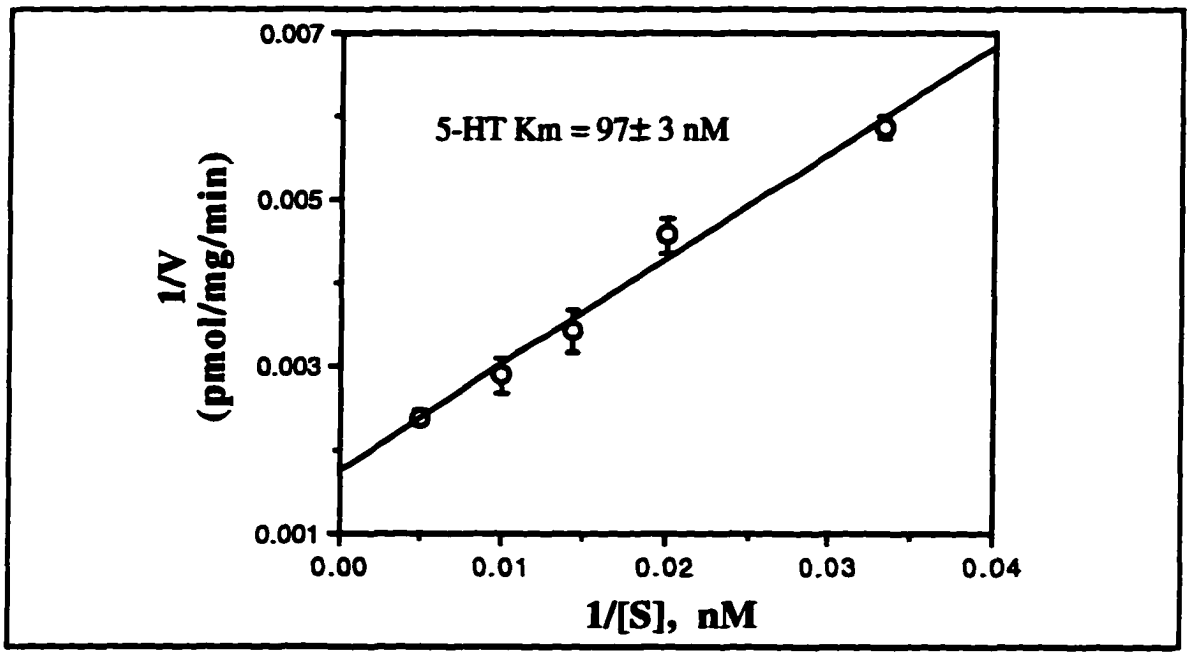

Figure 5-1. 5-HT K_m determination using a Lineweaver-Burk plot.

B. Uptake Blockade by 6,7-ADTQ and its Enantiomers

Uptake inhibition by 6,7-ADTQ and its enantiomers on the noradrenergic, dopaminergic, and serotonergic systems were initially investigated using a double reciprocal Lineweaver-Burk analysis. Employing a variety of inhibitor and substrate concentrations, the inhibition produced by 6,7-ADTQ and its stereoisomers was found to be competitive in nature for each of the neurotransmitters examined. A typical determination of the inhibition nature is given for the (±)-6,7-ADTQ blockade of NE uptake in Figure 5-2 below.

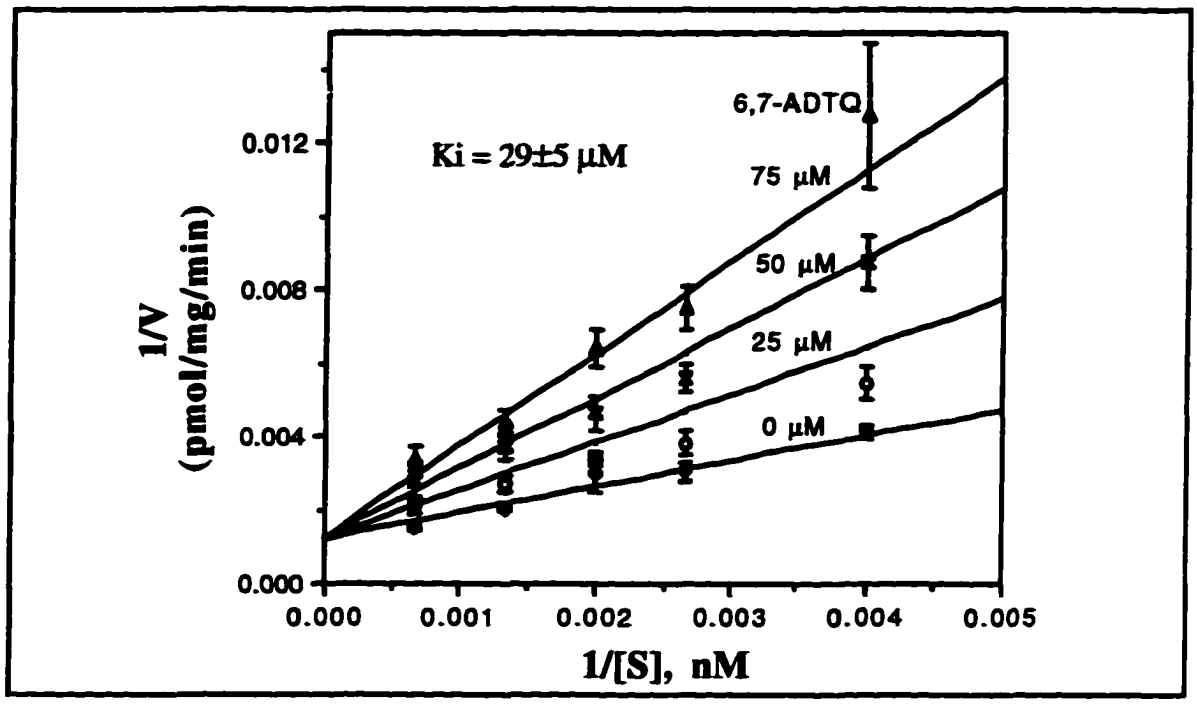

Figure 5-2. K_i determination using a modified Lineweaver-Burk double reciprocal plot.

In all such cases, the entire data set derived from multiple individual experiments was fitted using NLLSQ to each of the competitive, noncompetitive, and uncompetitive cases. The type of inhibition was then assessed as the fitted model providing the smallest error estimates for K_m, V_{max}, and K_i.

Once the nature of the inhibition was established to be competitive, an IC_{50} approach similar to that shown in Figure 5-3 for the S-(-)-6,7-ADTQ allowed more rapid and precise determination of the K_i value *via* a single experiment.

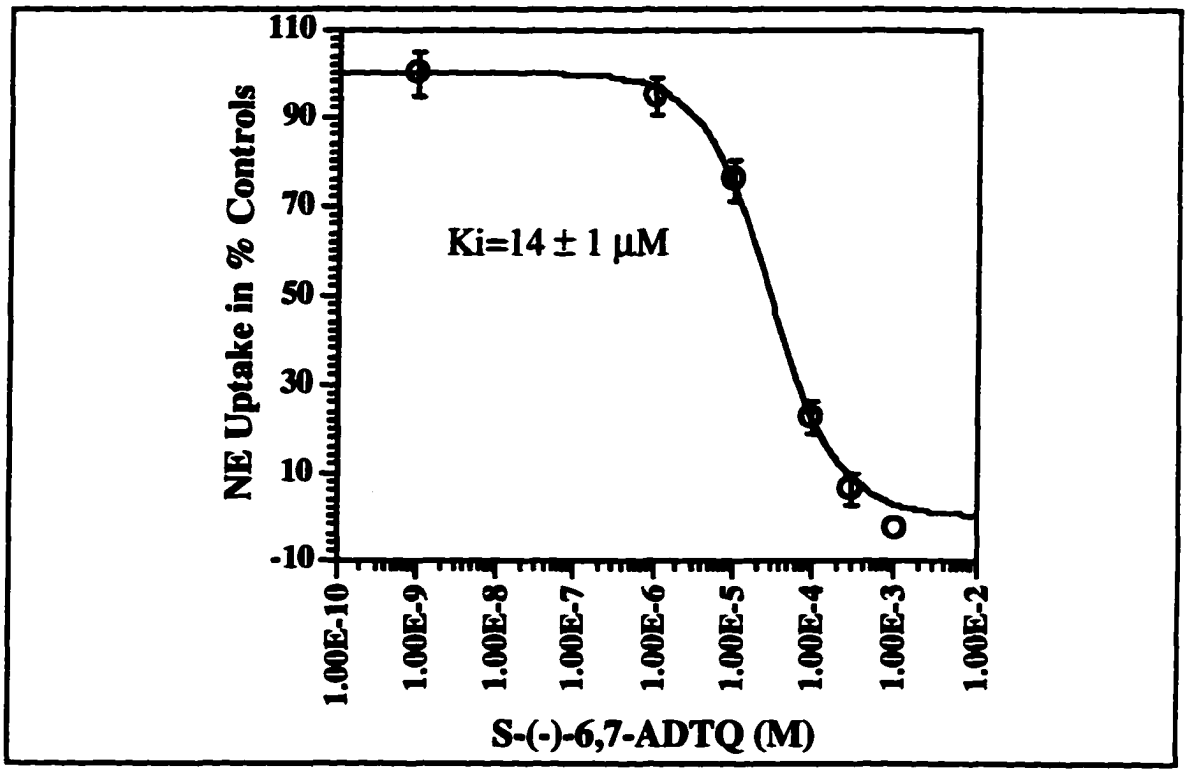

Figure 5-3. K_i determination using an IC_{50} approach for S-(-)-6,7-ADTQ blockade of NE. Concentration of NE used was 600 nM.

The K_i values obtained for uptake blockade of NE, DA, and 5-HT by 6,7-ADTQ and its enantiomers using this approach are summarized in Table 5-6. All the values were in the range of 10 to 100 μM, which indicates substantial interactions with the uptake sites. 6,7-ADTQ and its optical isomers showed their highest uptake affinities towards the noradrenergic system. And, in depletion studies, we saw that 6,7-ADTQ and its stereoisomers showed maximal depleting potency towards the noradrenergic system. On the other hand, 6,7-ADTQ and its enantiomers individually displayed comparable uptake interactions between the dopaminergic and serotonergic systems, while these agents elicited substantially more 5-HT depletion than they did DA depletion. This reinforces the conclusion by Su Ma et al.[24] that uptake is not the sole determining factor in depletion

potency and that selectivity of an agent cannot be quantitatively correlated to the degree of uptake inhibition exhibited in the affected transmitter systems.

Table 5-6. K_i values for 6,7-ADTQ and optical isomers.

Compound	Uptake interaction constant, K_i (μM)		
	NE	DA	5-HT
(±)-6,7-ADTQ	29 ± 5	74 ± 18	86 ± 17
R-(+)-6,7-ADTQ	33 ± 7	80 ± 13	84 ± 42
S-(-)-6,7-ADTQ	14 ± 1	48 ± 10	57 ± 34

Each value employed, typically, 6 data points with N=5 for each point and N=6 for background for each point.

The K_i results for the racemic agent and its optical isomers showed that the R-(+)-6,7-ADTQ exhibited similar uptake site affinities to that of the racemic 6,7-ADTQ. For the S-(-)-6,7-ADTQ, however, a general trend of lower K_i values was observed for each of the three transmitters when compared with either the R-(+)-6,7-ADTQ or the racemic 6,7-ADTQ. While these uptake interactions for S-(-)-6,7-ADTQ are only significantly greater for the NE and DA systems, the stronger interactions do qualitatively correlate with the observed stronger depletions for each of NE, DA, and 5-HT by this enantiomer.

C. Toxin Uptake Blockade by Racemic 6,7-ADTQ, 6,7-AMDTQ, and 6,8-ADTQ

Transporter affinities of racemic 6,7-ADTQ, 6,7-AMDTQ, and 6,8-ADTQ for the NE, DA, and 5-HT uptake proteins were approached using the same procedures outlined in the previous section. The 6,7-ADTQ/transmitter combination revealed the expected competitive inhibition mechanism and, therefore, the remaining analogs were assumed to possess the same competitive nature. The resulting K_i values for these agents, obtained using the IC_{50} approach, are presented in Table 5-7, along with the corresponding values for the catecholaminergic toxin 6-HDA.

Table 5-7. K_i values for 6,7-ADTQ, 6,7-AMDTQ, 6,8-ADTQ, and 6-HDA.

	Uptake interaction constant, K_i (μM)		
Compound	NE	DA	5-HT
6,7-ADTQ	29 ± 5	74 ± 18	86 ± 17
6,7-AMDTQ	---	261 ± 21	124 ± 55
6,8-ADTQ	---	---	114 ± 47
6-HDA	51 ± 1*	12 ± 0*	NA

Each value employed, typically, 6 data points with N=5 for each point and N=6 for background for each point. *values reported by Su Ma et al.[24]

Three transmitter/toxin combinations, however, yielded entirely unexpected results. First, the 6,7-AMDTQ effects on NE uptake were found to be not significantly different in multiple experiments using toxin concentrations varying between 1.0 μM and

1.0 mM. This was unexpected since 6,7-AMDTQ had clearly exhibited long term NE depleting effects in the previously reported studies. However, even more unusual results were obtained with the 6,8-ADTQ/NE and 6,8-ADTQ/DA investigations. As shown below in Figures 5-4 and 5-5, respectively, increasing concentrations of 6,8-ADTQ in the incubation mixture provided corresponding increases in uptake accumulation of the radiolabeled transmitter.

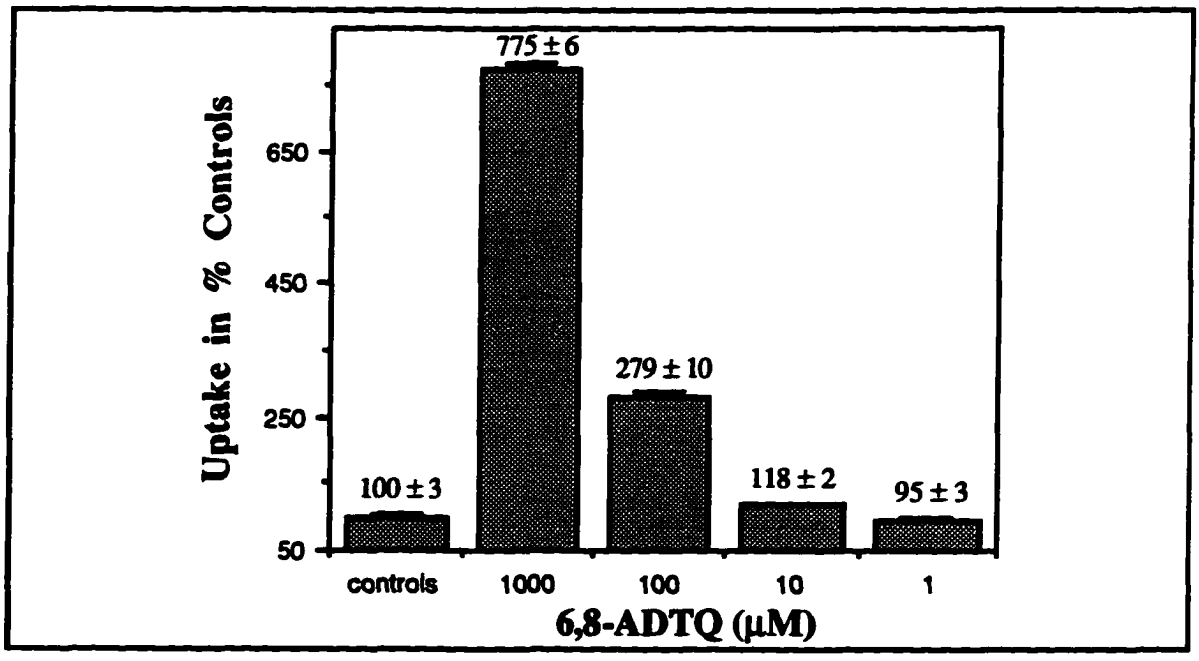

Figure 5-4. 6,8-ADTQ effects on NE uptake; [NE]=600 nM

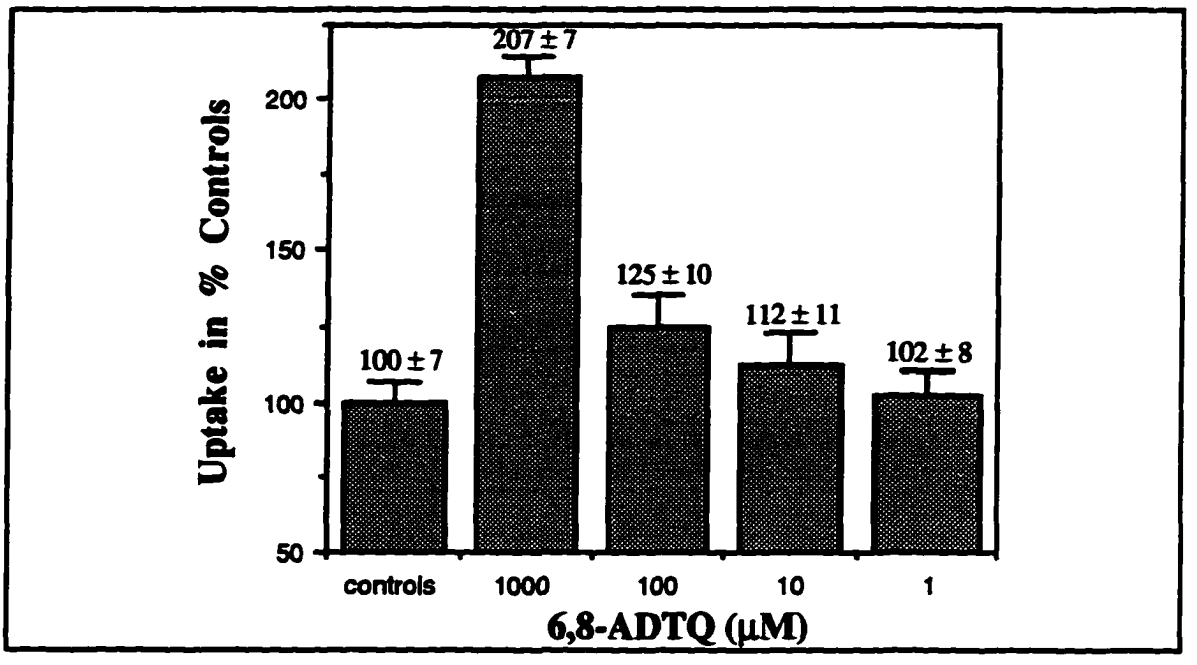

Figure 5-5. 6,8-ADTQ effects on DA uptake; [DA]=230 nM

Examination of the K_i values for an individual toxin, where obtained, allows at least a qualitative assessment of the import of the uptake interaction on the observed long term depletion of individual transmitters and, thus, the inherent selectivity of the toxin. In this regard, as already mentioned, the stronger interaction of 6,7-ADTQ with the NE transporter is qualitatively reflected in the more potent long term depletion of NE as seen in Table 4-16, compared to DA and 5-HT, by this toxin. However, the long term depletions of DA and 5-HT by 6,7-ADTQ do not correspond to their strength of interaction with the uptake sites. For 6,7-AMDTQ, the strength of interaction with the uptake sites qualitatively, but not quantitatively, corresponds to the observed DA and 5-HT long term depletion effects. However, the lack of any measurable interaction of 6,7-AMDTQ with the NE uptake site clearly did not correlate with the observed substantial long term depletion of NE by this toxin.

Comparisons between the observed long term depletion effects and the uptake K_i values for various toxins and a single transmitter could also reveal possible correlations. However, in the current studies of the three quinolines, this is considered inappropriate for two reasons. First, the unusual transporter interactions observed for 6,7-AMDTQ/NE, 6,8-ADTQ/NE, and 6,8-ADTQ/DA eliminate the possible use of these in such a comparison. Second, the long term depletion studies were performed, for reasons previously stated, at "maximum usable" doses for each toxin. Thus, comparisons between toxins would be inappropriate due to the lack of consistency in the employed dosages.

The apparent stimulation of uptake seen in the cases of 6,8-ADTQ/NE, 6,8-ADTQ/DA, and 6,7-AMDTQ/NE are difficult at this point to understand and interpret. Stimulated uptake, with increases to 400% of controls, has been reported in various long term investigations, however, which may be pertinent. These investigations, and their results, include:

(1) a 10 day treatment of rats with cocaine and/or pimozide, a D_2 receptor antagonist, by Parsons et al.,[150] which, when examined with microdialysis, revealed modest enhancement of DA uptake and release mediated by the D_2 autoreceptor;

(2) a single or 30 day oral administration of BY-1949, a benzodiazepine derivative by Nagafuji et al.,[151] which, when examined by normal synaptosomal uptake procedures at 30 min and 2 days following treatment, respectively, revealed 0 to 20% enhancements in glutamate and GABA transport which were presumed due to increases in the V_{max} observed for the low affinity isoform of Na^+,K^+-ATPase;

(3) administration of lead, triethyl lead, or tetraethyl lead to rats either in a single dose or continuously for 3 weeks by Komulainen et al.,[152] followed by

normal synaptosomal uptake examination 24 hrs after final treatment, yielded NE and DA uptake enhancements of 0 to 50% of controls;

(4) rats treated with lithium for 12 days or lithium for 10 days and allowed 2 days for withdrawal by Abluwalia and Singhal,[153] when examined thereafter, yielded synaptosomal uptakes of NE and DA which were elevated to as much as 400 and 250% of controls, respectively; and

(5) exposure of rats to hypoxia for 12 hr by Odarjuk et al.,[154] when examined 12 hr later, yielded elevated DA synaptosomal uptake to 150% of controls.

Unfortunately, all the above reviewed cases which reported substantial enhancements in synaptosomal uptake, such as those seen for our three anomalous toxin/transmitter combinations, employed days to weeks of treatment and/or at least 12 hr between single treatments and examination. No literature reports could be found in which, similar to our experiments, substantial enhancement of uptake was observed by simply adding an agent directly to the synaptosomal incubation *in vitro*. Substantial synthesis of transporter protein, leading to an increase in V_{max} for the uptake process, would require 12 to 36 hr. Such protein synthesis could explain virtually all the long term enhancements reported above and, indeed, was actually shown to be the case for the hypoxia study.[154] However, protein synthesis, and the corresponding V_{max} increase, clearly does not apply to our experimental paradigm.

Alternatively, a kinetically derived possible explanation of the observed enhancements in uptake would be associated with the K_m values. A substantial increase in the affinity of the uptake site for the substrate, witnessed by a substantial decrease in K_m, could lead to approximately two-fold increases in the measured uptake since we employed substrate concentrations approximately equal to the original K_m. This effect could explain what we observed with the 6,8-ADTQ/DA and 6,7-AMDTQ/NE combinations; but, it could not explain the 6,8-ADTQ/NE effects. And, while some[150] have suggested possible short term decreases in K_m due to phosphorylation of the uptake

protein, the only reported changes in K_m[154] were, in fact, increases to approximately 250% of controls, and these increases required a long term period for manifestation.

Non-kinetically derived explanations of the observed enhancements in uptake are possible. However, we consider these to be so speculative at present as to be inappropriate for discussion. In short, no factually supported reasonable explanation exists for the increased transport seen with the 6,8-ADTQ/DA, 6,8-ADTQ/NE, and 6,7-AMDTQ/NE combinations.

V. Conclusions

For the majority of combinations investigated, a substantial affinity has been demonstrated by the toxin for the uptake site of the transmitter system which experiences long term depletion effects. This supports the conclusion that the uptake site is the primary means by which the toxin gains access to the intracellular region of the affected neuron. It also supports the primary importance of toxin transport in its mode of destructive action. The necessity for uptake has even more pointedly been demonstrated for the long term depletion of NE and DA by 6,7-ADTQ, in that uptake blockade in these two cases effectively blocks the observed depletion afforded by this agent.

Among the enantiomeric forms of 6,7-ADTQ, the S-(-)-enantiomer was found to elicit more potent interactions with the various uptake sites, corresponding to the slightly more potent long term depletions provided by this stereoisomer.

Considering all the quinoline analogs for which K_i values were determined, it is obvious that selectivity, with respect to the long term depletions afforded these agents, is not solely determined by the strength of the toxin/transmitter uptake site interaction alone. Indeed, using such values would lead to quantitatively, and even qualitatively, incorrect

predictions of selectivity for long term depletions in the associated neurotransmitter systems.

The apparent stimulated uptake observed with the 6,8-ADTQ/DA and 6,7-AMDTQ/NE combinations may be explained by a short term decrease in K_m, mediated by phosphorylation of the transporter protein.[150] However, such an explanation for the 6,8-ADTQ/NE combination is usefully inadequate. And, the time scale of the current experiments is far too short to invoke meaningful alterations in the associated V_{max} values. Thus, overall, we view the apparent enhancements in transport seen with these combinations to simply be inexplicable at the current time.

Mode of Action II: Ease of Oxidation & Acid/Base Properties

Chapter 6

I. Introduction

The ease of oxidation of 6-hydroxydopamine (6-HDA) and its congeners has been repeatedly implicated in the neurodegenerative mode of action of these toxins.[25,28,30] Inherently low oxidation potentials thermodynamically allow these agents to be oxidized by molecular oxygen, which produces the superoxide radical, hydrogen peroxide, and the highly reactive hydroxyl radical. Production of these oxygen-derived cytotoxins, particularly the hydroxyl radical, is almost certainly a part of the mode of action of 6-HDA.

The thermodynamically driven autoxidation of 6-HDA and related analogs at physiological pH also produces quinone or quinoneimine products which have potential pertinence to the neurodegenerative process as well. Consideration of these quinoid products in the mode of action of the toxin, however, frequently ignores an important and thermodynamically controlled aspect, i.e., the state of protonation. Simple deprotonation could lead to excessive acidification of the intraneuronal milieu. Facile protonation and deprotonation, coupled with transport of both forms across the inner mitochondrial membrane, could seriously hamper oxidative phosphorylation. Additionally, the state of protonation affects the reactivity of these quinoid species toward nucleophilic attack and other follow-up chemical reactions; or, the state of protonation affects the fundamental stability of the quinoids.

There are, in fact, two fundamental locations on a typical oxidized 6-HDA analog which could reasonably be considered for protonation/deprotonation under physiological conditions. The first of these, the aliphatic amine, has been shown to have pK_a values, in the protonated state, of 9.5 to 10.5.[155-161] These relatively high pK_a values mean the majority of such groups would exist in the relatively unreactive protonated state at pH 7.4. Thus, these are generally considered to be of lesser importance. One the other hand, the second site of potential protonation/deprotonation is represented by the enolic hydroxyl group. This group exhibits pK_a values in the range of 4 to 7, which are considerably lower than the pK_a values of 8.5 to 11 exhibited by the phenolic protons of the reduced species from which they are derived. The lower pK_a values of these enolic protons makes it highly likely that their deprotonation is a substantial occurrence under physiological conditions.

Both oxidation and the likely protonated and deprotonated forms of the resulting quinoid species are depicted for 6,7-ADTQ, a typical 6-HDA related species, in Figure 6-1.

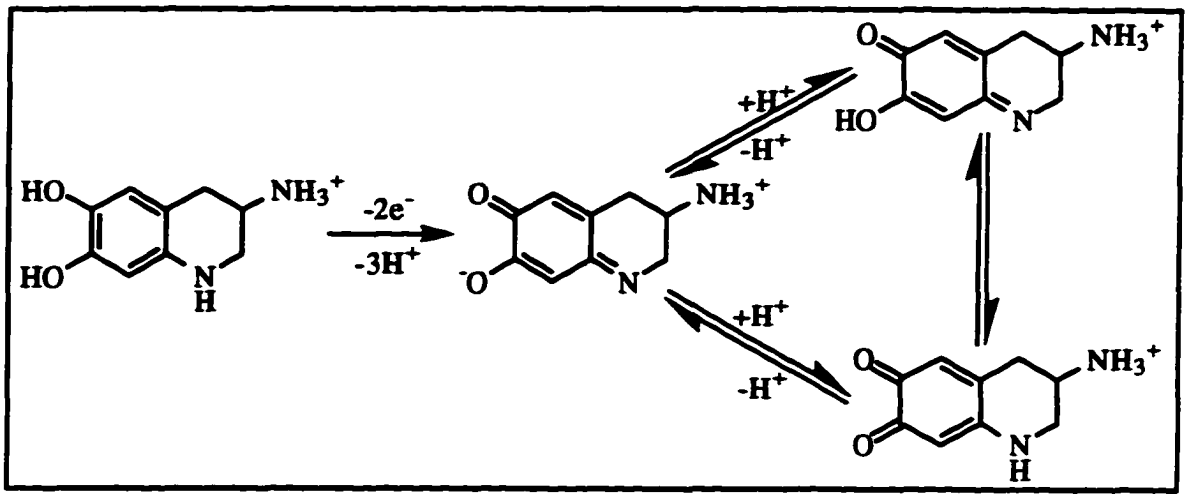

Figure 6-1. Oxidation of 6,7-ADTQ showing probable forms of the oxidized toxin.

The current chapter is concerned with the determination of two important thermodynamic properties of our quinoline derivatives: (1) ease of oxidation, and (2) pK_a of the enolic group of the oxidized quinoid species.

II. Experimental

A. Chemicals and Solutions

1. Chemicals

All chemicals listed below were purchased through Sigma Chemical Company (St. Louis, Mo.) in high purity and used without any further purification. Chemicals not listed below are listed in previous chapters.

6-hydroxydopamine (6-HDA) hydrobromide

potassium hydroxide (KOH)

potassium phosphate dibasic (anhydrous)

potassium phosphate monobasic monohydrate

All aqueous solutions employed 18 MΩ distilled/deionized water which was prepared by passing distilled water through a Milli-Q Reagent Water System (Millipore, Continental Water Systems, El Paso, TX).

2. Toxin Solution for pK_a Studies

Stock toxin solutions were made by dissolving the desired amount of toxin in an appropriate amount of degassed 10^{-3} M HCl, to yield a stock concentration of 10 mM. Typically 1.5 to 2 mL of stock solution were needed The stock toxin solution was stable in excess of 8 hr.

3. pK_a Buffer Solutions

The pH buffers were generally created by adding 0.10 M KH_2PO_4 to 0.10 M K_2HPO_4 until the desired pH was obtained. For lower pH values, HCl was added to 0.10 M KH_2PO_4, while for higher pH values, NaOH was added to 0.10 M K_2HPO_4. The 0.10 M KH_2PO_4 and 0.10 M K_2HPO_4 were prepared as separate solutions by dissolving 13.61 g $KH_2PO_4 \cdot H_2O$ and 17.42 g K_2HPO_4, respectively, in 1.0 L of water.

B. Methods and Procedures

1. Ease of Oxidation

The ease of oxidation of the agents was determined using cyclic voltammetry (CV). The $E^{o'}$ value for a 0.10 mM solution of the agent was measured in 0.10 M phosphate buffer at pH 7.4 and 22°C using a hanging drop mercury working electrode and an SCE reference electrode. The CV was obtained using a Great Plains Laboratories

(Norman, OK) potentiostat and was recorded on a model 2000 Omnigraphic X-Y recorder (Houston Instruments, Bellaire TX). The scan rate was 92.6 mV/sec. The $E^{o'}$ was determined as the average of the anodic and cathodic peak potentials.

2. pK_a Determinations

For the evaluation of the dissociation constant for the enolic group of the oxidized toxin, we incorporated UV-VIS spectroscopy. The spectra were recorded using a model 8452A Hewlett-Packard (Palo Alto, CA) spectrophotometer equipped with a temperature regulated cell held at 25°C. The formal concentration of the oxidized toxin was 100 μM in all experiments. A blank was periodically recorded and automatically subtracted from each spectrum. The blank contained all the same components as the oxidized toxin sample except the toxin.

To find the pK_a of the enolic proton on the oxidized quinoid form of our compounds, we first established appropriate conditions for each toxin under which the oxidized products were stable and, thus, could reproducibly be sampled. This was accomplished by following autoxidation of the toxin in an oxygen saturated 0.10 M phosphate buffer at various pH values using UV-VIS spectroscopy. In these initial experiments, we established both the pH at which a reasonably stable oxidation product could be generated and the time window or "sample period" in which it remained stable. The "sample period" was defined as the time period between completion of autoxidation and appearance of any significant follow-up reactions. Appearance of a significant follow-up reaction was arbitrarily determined as ≥ 3% change in the absorbance for any of the UV-VIS peaks observed for the oxidized toxin. The pH at which the oxidized toxin was generated and the "sample period" for each toxin are shown in Table 6-1.

Table 6-1. Generation and sample period for oxidized toxins.

Toxin	Generation pH*	Sample period** (min)
6,7-ADTQ	7.4	7-22
6,7-AMDTQ	8.4	3-10
6,8-ADTQ	5.4	14-17
6-HDA	7.4	5-18

* pH at which autoxidation was performed.

** time period following initiation of autoxidation in which oxidized toxin was stable.

To determine the pK_a, 50 μL of the stock 10.0 mM toxin was added to 150 μL of 0.010 M phosphate buffer at the appropriate pH, and oxidized with continuous oxygen saturation until the beginning of the "sample period". During the "sample period", 80 μL aliquots of the oxidized toxin solution were added to a quartz UV cell containing 1.920 mL of 0.10 M phosphate buffer (deoxygenated with Ar) having various pH values. The spectrum for each such combination was recorded within 5 sec following toxin introduction into the cell. The pH values used for observation of the oxidized quinoid spectra were approximately 1.5, 2.4, 2.9, 3.4, 3.9, 4.4, 4.9, 5.4, 5.9, 6.4, 6.9, 7.4, 7.9, 8.4, 9.4, and 10.

In order to ensure that the toxins remained in their reduced forms in the stock solutions for the duration of the experiment, stability controls were periodically examined. A stability control was prepared by adding 10 μL of a toxin stock solution to 1990 μL of 0.10 M phosphate buffer at pH 2.4. The pH value of 2.4 was selected since autoxidation of all the toxins is extremely slow at this pH; therefore, the form in which the toxin resided in the stock solution was subsequently directly observed in the corresponding UV-VIS spectrum.

3. pK_a Calculations

Dissociation constants for weak acids may be determined by monitoring the pH dependent UV-VIS absorbance changes of such species. Deprotonation of the enolic hydroxyl group of our oxidized toxins is, fortunately, accompanied by such absorbance changes. The theory associated with such determinations begins with a definition of the acid dissociation constant, K_a,

$$K_a = \frac{[H^+][tox^-]}{[Htox]} \qquad \text{equation 6-1}$$

where $[H^+]$ is the proton concentration in mol/L, $[tox^-]$ is the concentration of the deprotonated oxidized toxin in mol/L, and [Htox] is the concentration of the protonated oxidized toxin in mol/L. This can then be rearranged to:

$$[Htox] = \frac{[H^+][tox^-]}{K_a} \qquad \text{equation 6-2}$$

By mass balance considerations, we define:

$$[tox^-]_{Tot} = [Htox] + [tox^-] \qquad \text{equation 6-3}$$

The absorbance of a sample at a particular wavelength is the sum of the absorbances of the protonated and deprotonated forms of the oxidized toxin. Defining A_{Htox} to be the expected absorbance if the toxin was totally converted to its protonated form, and A_{tox^-} to be the expected absorbance if the toxin was totally converted to its deprotonated form, the observed absorbance A_i becomes:

$$A_i = \frac{A_{Htox}[Htox]}{[Htox]_{Tot}} + \frac{A_{tox^-}[tox^-]}{[tox^-]_{Tot}} \qquad \text{equation 6-4}$$

Substitution of equation 6-2 into the numerator of the first term and equation 6-3 into the denominator of both terms of equation 6-4 yields:

$$A_i = \frac{A_{Htox}[H^+][tox^-]}{([Htox]+[tox^-])K_a} + \frac{A_{tox^-}[tox^-]}{[Htox]+[tox^-]} \qquad \text{equation 6-5}$$

Then, by substituting equation 6-2 into the denominator of equation 6-5 and rearranging, one obtains:

$$A_i = \frac{A_{Htox}[H^+]+A_{tox^-}K_a}{[H^+]+K_a} \qquad \text{equation 6-6}$$

This final equation is fitted, using NLLSQ, to all the pH-absorbance data for a given oxidized toxin to yield the desired K_a value.

III. Results and Discussion

A. Ease of Oxidation

1. Formal Redox Potentials

The formal redox potential, E°', for each of the quinoline derivatives and the standard 6-HDA was determined as the average of the E_{pc} and E_{pa}, as described previously in Chapter 2. The results are presented in Table 6-2.

Table 6-2. Redox potentials for 6,7-ADTQ analogs and 6-HDA.

Toxins	E_{pa} (mV)	E_{pc} (mV)	ΔE_p (mV)	E°' (mV)
6,7-ADTQ	-132	-161	29	-147
6,7-AMDTQ	-166	-190	24	-178
6,8-ADTQ	-178	-201	23	-189
6-HDA	-196	-225	29	-212

- 10^{-4} M toxin, 23°C, working e'trode HDME, reference e'trode SCE, auxiliary e'trode Pt, scan rate 92.6 mV/sec, 0.10 M phosphate buffer at pH 7.4, solution degassed with Ar, solution under N_2 atmosphere throughout experiment.

The theoretical spread between the peak potentials for a reversible 2 electron system should be 29 mV. All compounds, thus, displayed ΔE values which were reasonably close to that expected for a reversible 2 electron redox system. The E°' for 6-HDA was -212 mV vs. SCE, which agrees well with reports from the literature.[24,25] The formal redox potentials determined for the quinoline analogs were found to be more

positive than that of 6-HDA, but fell well within the range of such values displayed by various 6-HDA analogs. For example, the $E^{o'}$ for 6-HDA is -212 mV vs. SCE, while that for α-methyl-6-aminodopamine, a known toxic analog of 6-HDA, is -123 mV vs. SCE.[24] Interestingly, while we expected 6,7-ADTQ and 6,7-AMDTQ to exhibit very similar $E^{o'}$ values, due to the structural similarities of their electroactive aromatic rings, their $E^{o'}$ values differed by 31 mV.

2. Thermodynamic Considerations

From a thermodynamic standpoint, the $E^{o'}$ values for the quinoline analogs and 6-HDA can be combined with the $E^{o'}$ value for molecular oxygen ($O_2 + 4H^+ + 4e^- \longrightarrow 2H_2O$, $E^{o'}$=0.753 V vs. NHE at 37°C, pH=7.4, and P_{O_2}=0.21). Such combinations show that, thermodynamically, the ratio of the oxidized to the reduced toxin should vary from 1.5×10^{23} for 6-HDA to 1.2×10^{21} for 6,7-ADTQ. The P_{O_2} value used in these combinations was arbitrarily chosen to be the atmospheric pressure of oxygen. But, even by employing P_{O_2} values 100 times lower, the oxidized-to-reduced ratios only decrease by a factor of 10. Thus, at reasonable levels of oxygen, these agents are strongly driven thermodynamically to their oxidized forms. However, *in vivo* toxin-molecular oxygen redox reactions do not occur in a redox vacuum.

Redox reactions occurring in the brain are most likely controlled by redox couples existing in substantial concentrations in the neuronal milieu. Ignoring subcellular locality and timing aspects, this overall CNS redox regulation could quite conceivably be associated with the ascorbate half-reaction, due to the high average concentration of 3 mM of this species in the brain.[162] Furthermore, McCreery et al.[163] have reported the existence of an extraneuronal CNS ascorbate redox "buffer" with a value of approximately -0.200 V vs. SCE. Employing this "buffer" value, an alternative thermodynamic analysis predicts ratios of oxidized-to-reduced toxin which fall between 2.5 for 6-HDA and 0.02 for 6,7-ADTQ, with ratios of 0.2 for 6,7-AMDTQ and 0.4 for

6,8-ADTQ. Using this approach, the ratios are much smaller than those found using the oxygen half-reaction. However, the agents are still thermodynamically driven, at least to some degree, to their oxidized forms. For comparative purposes, we applied the same CNS redox buffer approach to endogenous catecholamines. This yielded ratios which were 10^9 to 10^{12} times smaller than those found for the neurotoxic agents. Therefore, from a thermodynamic standpoint, it appears that the quinoline agents would be considerably oxidized in the brain, whereas endogenous transmitters would not.

B. Determination of the pK_a Values of Oxidized Toxin

1. 6,7-ADTQ

The pH dependent spectral changes seen with oxidized 6,7-ADTQ (ox-6,7-ADTQ) are shown in Figure 6-2. At pH 1.5 there is a band at 286 nm. As the pH increases, this band rapidly decreases and a new band appears and grows at 298 nm. At pH values above 6.4, this new band shifts to a shorter wavelength (λ_{max} = 294 nm), and is accompanied by a significant increase in absorbance. The band initially at 222 nm increases rapidly between pH 1.4 and 2.9 and again between pH 6 and 7.4. The band at 518 nm, barely visible at low pH, also rapid increases in absorption between pH 6 and 7.4. The rapid increase in absorbance of the 222 nm band between pH 1.4 and 2.9 may be a result of the deprotonation of the imine functionality. But, since this phenomenon was not physiologically relevant, we did not pursue it beyond this simple observation. The changes observed between pH 6 and 7.4 are due to the dissociation of the enolic proton of interest. Using the data from 518 nm, as shown in Figure 6-3, we found the pK_a of ox-6,7-ADTQ to be 6.61 ± 0.17. Analysis of the absorbance data from 222 nm and 294 nm, while providing less precision for the pK_a value, agreed with this result.

For the pH measurements described above, the toxin was preoxidized at pH 7.4 and 25°C, and sampled between 7-22 minutes.

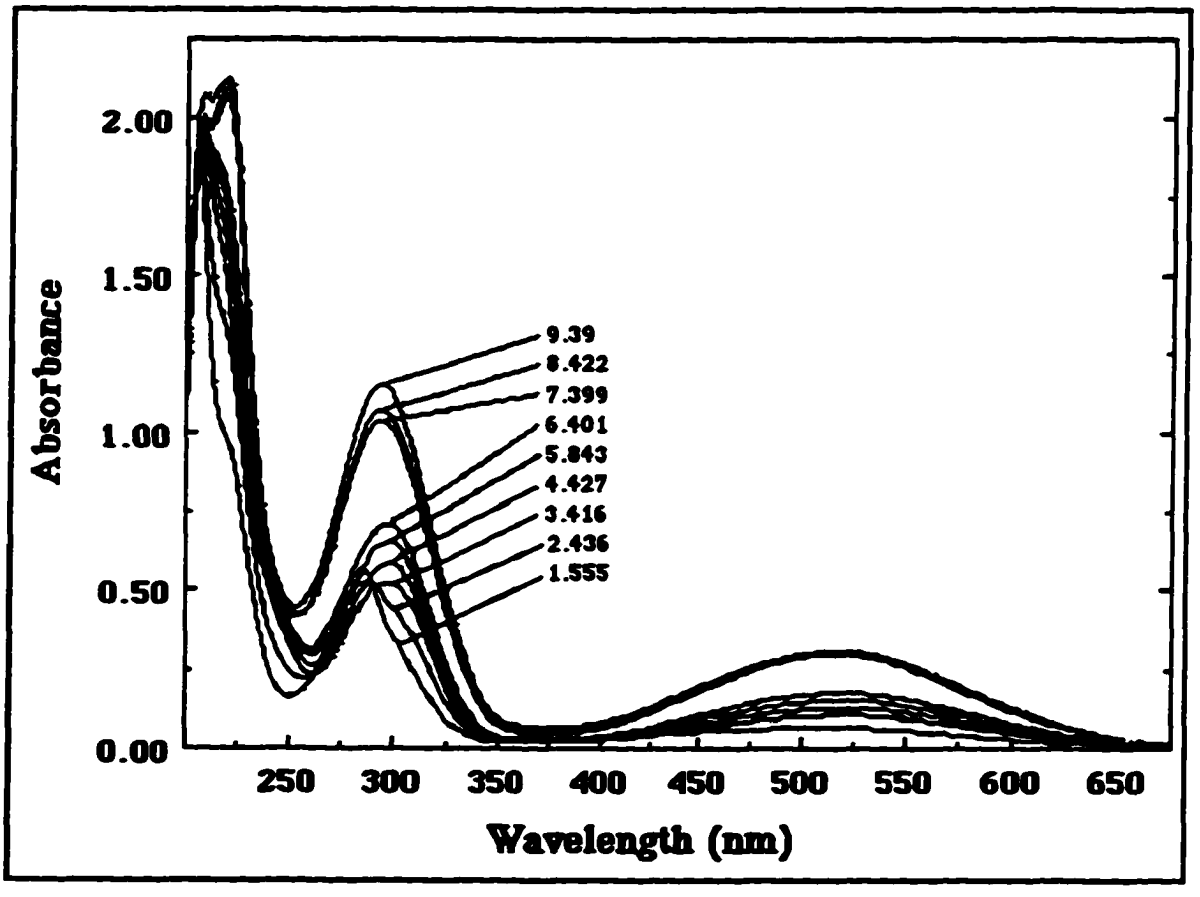

Figure 6-2. UV-VIS spectra of ox-6,7-ADTQ at various pH values. The pH values are written on the individual traces. The pH dependence of individual peaks are described in the text.

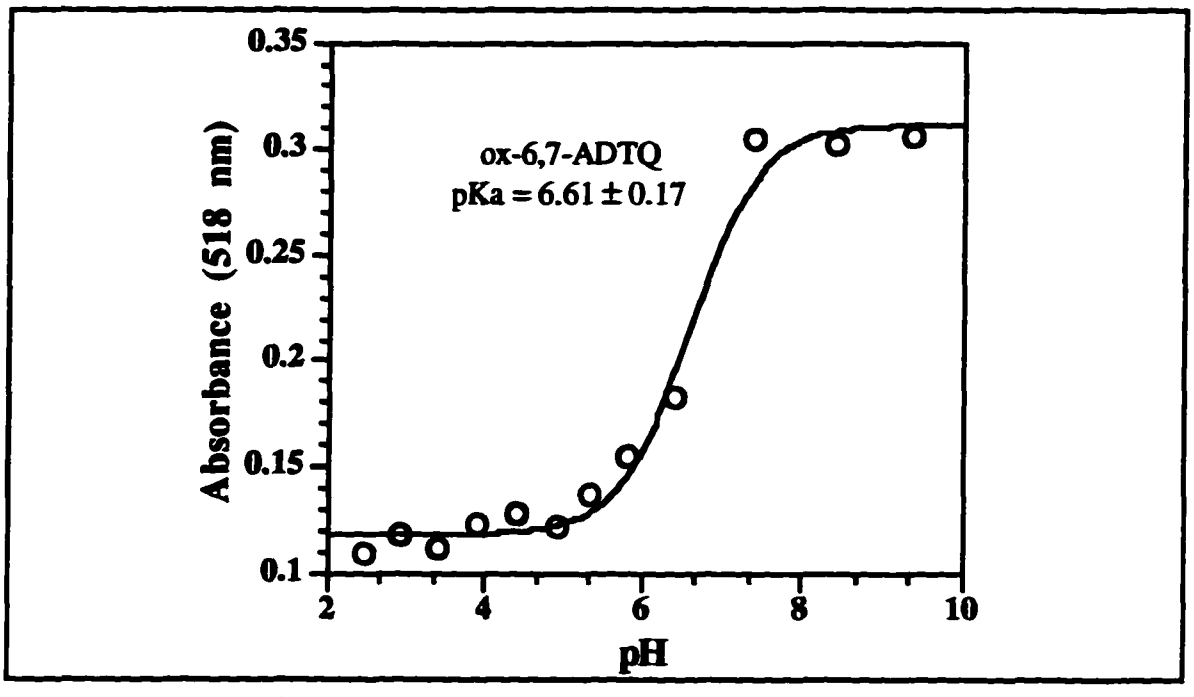

Figure 6-3. pK_a determination for ox-6,7-ADTQ.
Absorbance data at 518 nm was used and the toxin concentration was 100 μM.

2. 6,7-AMDTQ

The observed spectral changes with pH for the oxidized form of 6,7-AMDTQ (ox-6,7-AMDTQ) are shown in Figure 6-4. As can be seen in this figure, significant absorption changes occur at 218, 244, 300, 344, and 518 nm. Between pH 1.5 and 3, there is an absorbance increase in the bands at 518 nm and 218 nm. At these wavelengths, absorbance begins to decrease at pH values above 6.4. The band at 344 nm is non-existent below pH 5.4, but its absorbance begins to increase rapidly at pH values above that. This increase is paralleled by an increase at 244 nm and a decrease at 300 nm. The absorption band at 344 nm, however, is the only band that is absent at low pH values and appears as pH increases. Additionally, no other wavelength yielded as large an absorption change without interference from other parts of the spectrum.

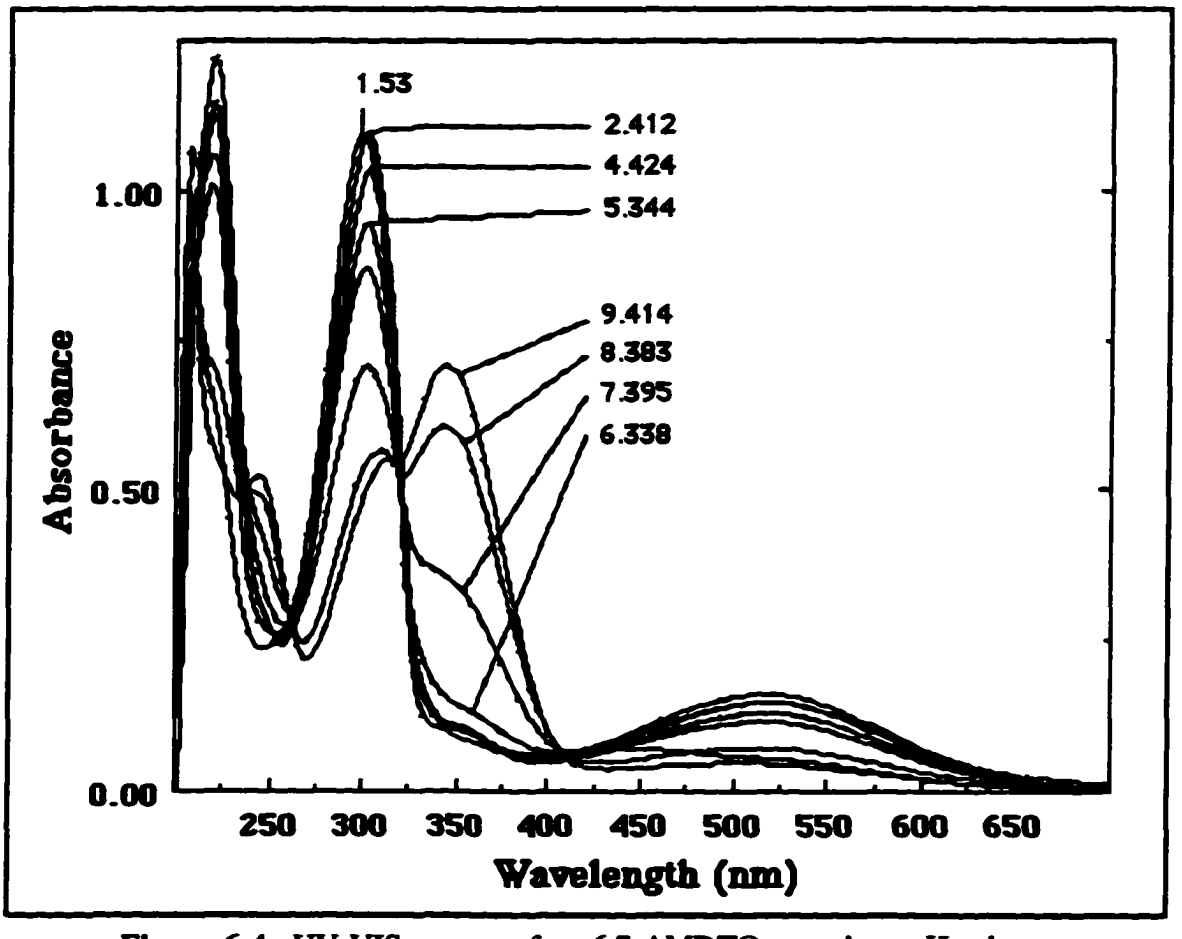

Figure 6-4. UV-VIS spectra of ox-6,7-AMDTQ at various pH values. The pH values are written on the individual traces. The pH dependence of individual peaks are described in the text.

Therefore, the absorbance changes at 344 nm were used to determine the enolic pK_a of ox-6,7-AMDTQ. As shown in Figure 6-5, the pK_a determined for ox-6,7-AMDTQ was 7.57 ± 0.03. The absorbance changes observed between pH 1.5 and 3 may be attributed to the deprotonation of the protonated imine group. But, since this change is not relevant at physiological pH values, this was not further investigated. For the above pH dependent measurements, the toxin was preoxidized at pH 8.4 and 25°C, and sampled between 3-10 minutes.

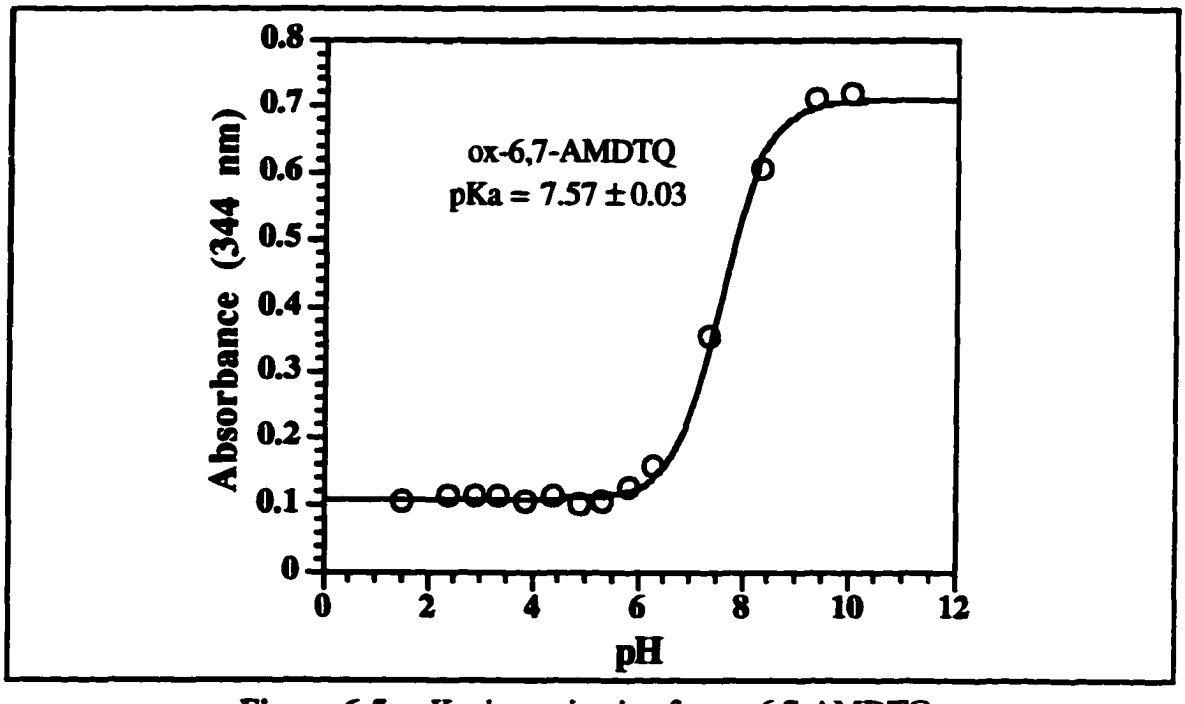

Figure 6-5. pKa determination for ox-6,7-AMDTQ.
Absorbance data at 344 nm was used and the toxin concentration was 100 μM.

3. 6,8-ADTQ

The pK_a determination for the enolic component of ox-6,8-ADTQ was difficult in that there was a very small time window between completion of autoxidation and subsequent polymerization in which to sample the oxidized toxin. Thus, for each pH measurement, a new batch of toxin was oxidized at pH 5.4 and 25°C, and sampled between 14-17 minutes. Furthermore, spectral changes with pH were minimal. The absorption band which yielded the best results was 460 nm. This band displayed an increase between pH 3 and 6, which is shown in Figure 6-6. The dissociation of the enolic proton most likely corresponds to this increase and was found to have a pK_a value of 4.32 ± 0.09.

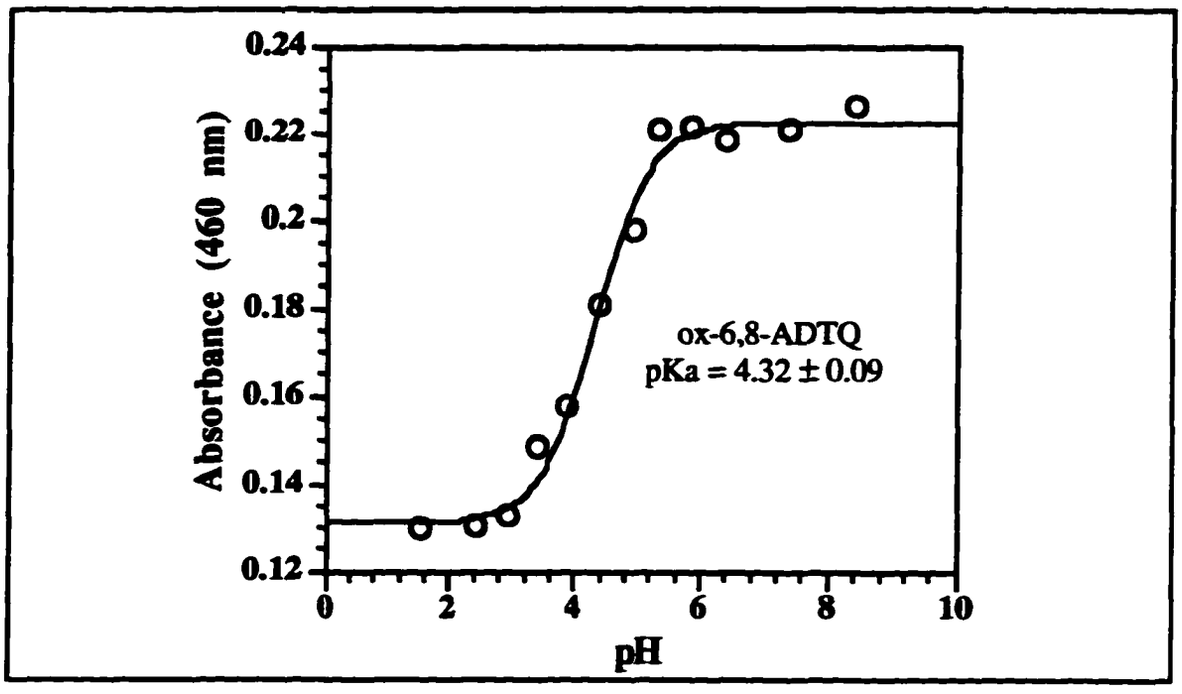

Figure 6-6. pK_a determination for ox-6,8-ADTQ.
Absorbance data at 460 nm was used and the toxin concentration was 100 μM.

At pH values higher than pH 8.4, the absorbance at 460 nm begins to decrease. This is believed to correlate with deprotonation of the protonated aliphatic amine. Absorption changes are generally not observed for deprotonation of the primary amine in these type of compounds, especially one so far removed from a conjugated system. However, a fitted pK_a value of 9.33 ± 0.32 was found, which is quite reasonable for such a process. Another plausible explanation is that the decreases observed at 460 nm are a result of a rapid follow-up reaction(s) at high pH. In preliminary studies determining the appropriate sample period for ox-6,8-ADTQ, we found these follow-up reactions substantially increased in rate with increasing pH.

4. 6-HDA

Spectra of the oxidized form of 6-HDA (ox-6-HDA or 6-HDAQ) at various pH values are shown in Figure 6-7. At pH 1.5, this species displayed bands at 206, 264, and 382 nm. With increasing pH, the band at 206 nm increased in absorption and shifted to longer wavelengths with a final absorption maxima at 212 nm. The band at 264 nm simultaneously decreased in absorbance and also shifted to longer wavelengths (268 nm), resulting in isobestic points at 243 nm and 276 nm. The band at 382 nm decreased rapidly and a new band appeared at 486 nm, which grew with increasing pH. Additionally, an isobestic point was found to exist between these two bands at 404 nm.

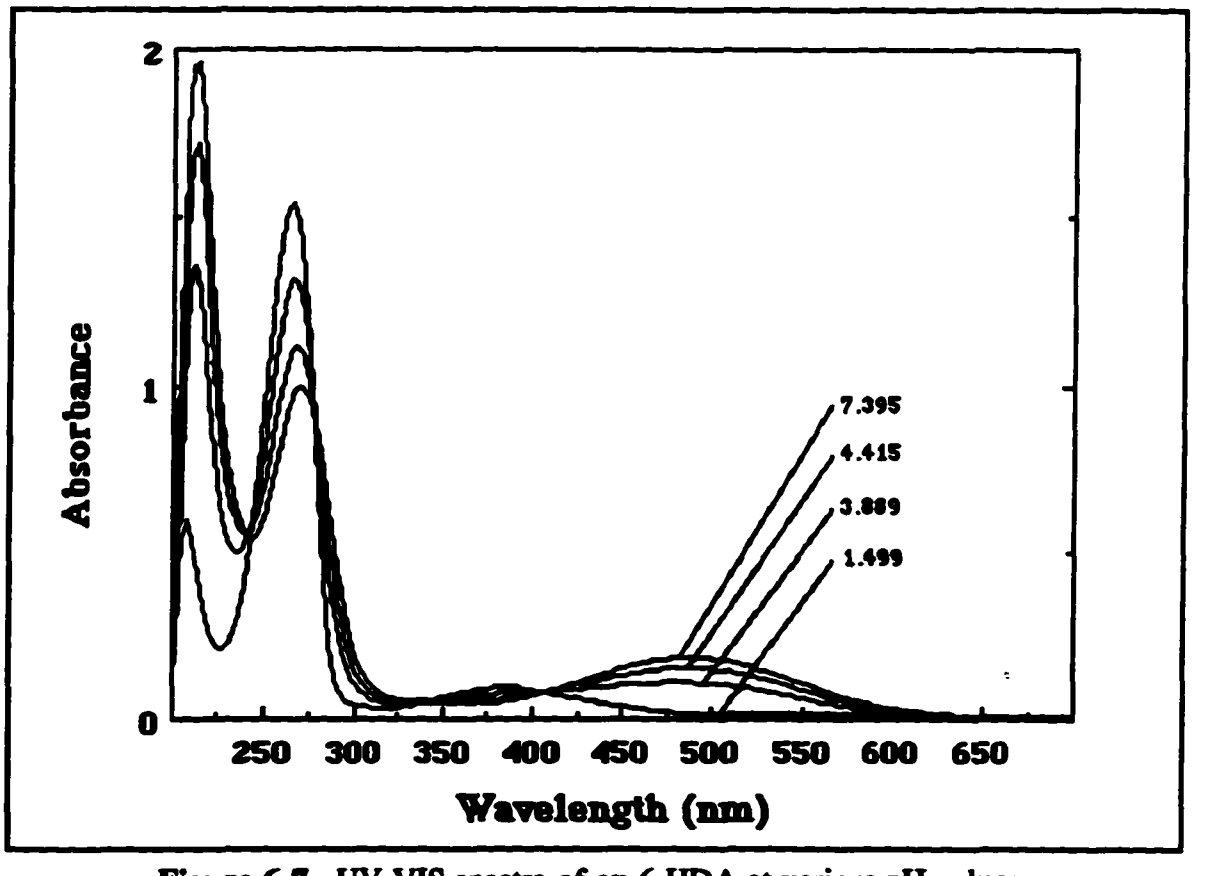

Figure 6-7. UV-VIS spectra of ox-6-HDA at various pH values. The pH values are written on the individual traces. The pH dependence of individual peaks are described in the text.

For the above discussed pH measurements, the toxin was preoxidized at pH 7.4 and 25°C, and sampled between 5-18 minutes.

In studies using 6-HDA, the absorbance at 486 nm is commonly monitored as an indicator of the oxidized form of this toxin.[34,38,164] The pH dependent increase in absorbance at 486 nm for ox-6-HDA is due to deprotonation of the enolic hydroxyl group, whereby creating a much more electron-rich conjugated system. As shown in Figure 6-8, the pK_a for ox-6-HDA was determined to be 3.87 ± 0.04. This value agrees well with those previously reported.[25,165]

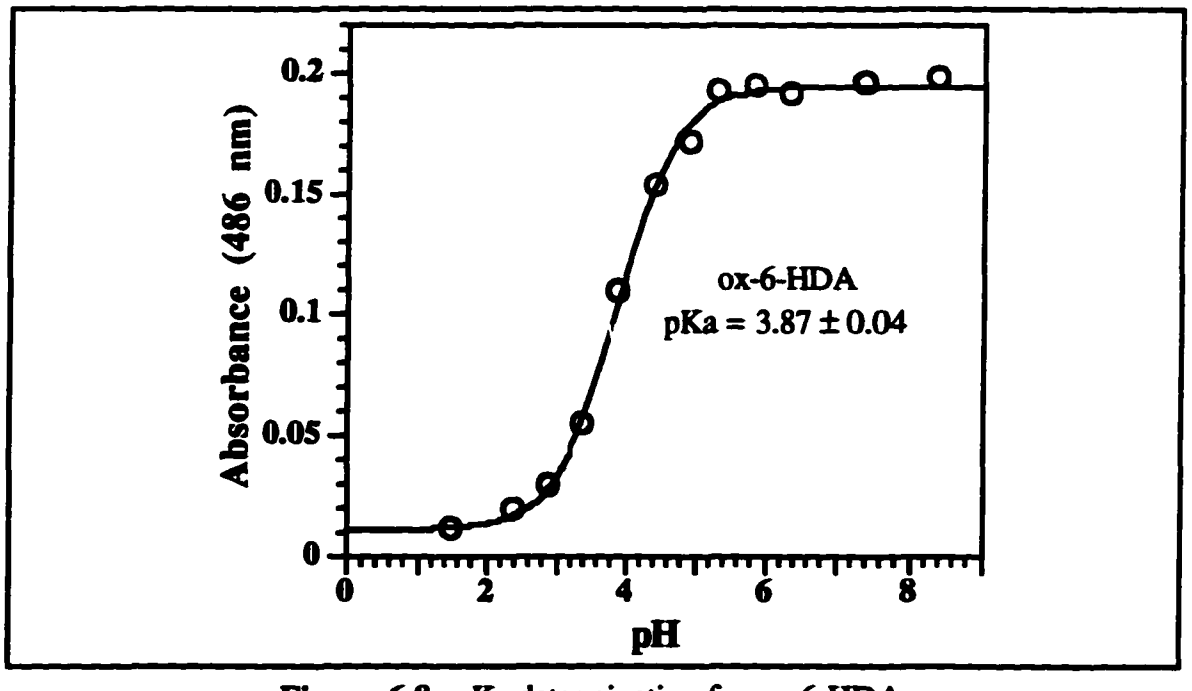

Figure 6-8. pK_a determination for ox-6-HDA.
Absorbance data at 486 nm was used and the toxin concentration was 100 μM.

IV. Conclusions

It is apparent from the redox studies that our toxins have the thermodynamic capability to readily undergo oxidation in the CNS. We believe this oxidation to be a prerequisite for the observed neuronal damage and/or degeneration elicited by these agents. Furthermore, the unique pK_a values of the enolic group of the oxidized toxins provide oxidation pathways, at physiological pH, which likely involve one more proton than the number of electrons.

The thermodynamic findings in this chapter suggest a few reasonable possibilities which could result in neurodegeneration. These include, but are not limited to: (1) the ease of toxin oxidation, which implicates a possible decreases in the intraneuronal supply of oxygen, a possible decrease in antioxidant defense system capabilities, and a possible production of reactive quinoid species; (2) the capability to reduce molecular oxygen, producing damaging reactive oxygen species; and (3) neuronal acidosis induced by unbalanced proton donation and acceptance during oxidation of the toxins by oxygen, resulting from the inherently low pK_a values of the enolic groups on the oxidized agents.

Mode of Action III: Autoxidation & Reactive Oxygen Species

Chapter 7

I. Introduction

The neurodegenerative effects imparted by 6-HDA and associated compounds are believed to be related to their ability to undergo rapid autoxidation, i.e., spontaneous non-enzymatic oxidation by molecular oxygen. Autoxidation of such compounds results in the production of quinones or quinoneimines and reduced oxygen species (H_2O_2, $\bullet O_2^-$, and $\bullet OH$). These two groups of autoxidation products represent two primary schools of thought which directly relate autoxidation to neurotoxicity.

The quinone or quinoneimine product(s) formed by autoxidation are very susceptible towards nucleophilic attack by sulfhydryl functionalities which exist in abundance in the neuronal milieu. Entities which contain sulfhydryl groups include essential proteins and enzymes, and molecules that contribute to antioxidant defense systems such as glutathione (GSH). Through binding of the electrophilic oxidized quinoid species to these thiols, crucial neuronal functionality may be compromised. 6-HDA and related compounds have been shown to react with sulfhydryl containing proteins and enzymes.[27,50-55] In the process of reacting with the nucleophile, the toxin is reduced to the hydroquinone form. Once reduced, the adduct can, again, undergo autoxidation. The oxidized adduct is also electrophilic and can further react with other nucleophiles, resulting in cross-linking of proteins and/or enzymes[51,52] to render them inactive. In addition, the oxidized forms of the toxins and/or adducts may be reduced directly by antioxidants like ascorbate. The newly reduced species are, of course, again susceptible to autoxidation. Multiple such oxidations by O_2 and reductions by antioxidants is commonly known as redox cycling. The ultimate outcome of redox cycling is the depletion of both intraneuronal oxygen and antioxidants. Thus, redox cycling is a viable mechanism for neurodegeneration in its own right.

It is well known that the generation of hydrogen peroxide, H_2O_2, superoxide radical, $\bullet O_2^-$, and the hydroxyl radical, $\bullet OH$, can result in cellular damage and/or destruction.[39-42,49,56,166,167] Not surprisingly, it has been shown that H_2O_2, $\bullet O_2^-$, and $\bullet OH$ are formed during the autoxidation of 6-HDA and related analogs.[33-38,43,164] H_2O_2 and $\bullet O_2^-$, in contrast to common beliefs, are not highly reactive agents. Additionally, neurons contain defense systems to combat such species, including the enzymes glutathione peroxidase and catalase for H_2O_2 and superoxide dismutase for $\bullet O_2^-$.[168] However, the brain contains metal ions in various chelated forms, and these metal ions, particularly iron, in the presence of H_2O_2 and $\bullet O_2^-$ lead to the production of hydroxyl radicals. These hydroxyl radicals, created through metal-catalyzed Fenton

and/or Haber-Weiss pathways,[44,45,48,169,170] are highly reactive and, thus, highly pertinent to the neurodegenerative process of many neurotoxins.

Our dihydroxytetrahydroquinoline compounds are structurally similar to 6-HDA and are hypothesized to act in a manner similar to 6-HDA. Therefore, a logical and important step in elucidating the mechanism(s) by which our compounds produce neurodegeneration was to investigate the inherent rates of autoxidation of these compounds under physiological conditions. Additionally, we wanted to determine the distribution of reactive oxygen species produced by the autoxidation process.

II. Background on Methods

The rate of autoxidation can be conveniently determined using either an oxygen electrode system or UV-visible (UV-VIS) spectroscopy. Using an oxygen electrode, toxin autoxidation is followed indirectly through the consumption of oxygen. Using UV-VIS spectroscopy, formation of the oxidized toxin can be followed directly. Additionally, reactions following the initial oxidation, but not necessarily involving oxygen consumption, may also be monitored by UV-VIS. However, spectra of follow-up products may obscure those of the initial oxidation products by which the process of autoxidation is being monitored.

Using UV-VIS spectroscopy, the apparent rate constant for autoxidation for a first order reaction, e.g., can be determined by monitoring the absorbance at a wavelength characteristic of the oxidized form of a toxin using:

$$\ln|A_\infty - A_t| = -kt + \ln|A_\infty - A_o| \qquad \text{equation 7-1}$$

where A_∞ is the absorbance at the completion of the reaction, A_0 is the absorbance at the beginning of the reaction, and A_i is the absorbance at any time t during the reaction. By rearranging equation 7-1, we obtain:

$$A_i = A_\infty - (A_\infty - A_0)10^{-kt(0.43429)} \qquad \text{equation 7-2}$$

By fitting the absorbance data, at a specific wavelength, to equation 7-2 using NLLSQ, the apparent rate constant can be determined.

When employing an oxygen electrode, the initial autoxidation rate can be determined from the slope of the linear portion of the oxygen trace following introduction of toxin to the reaction cell. A representative oxygen trace is shown in Figure 7-1.

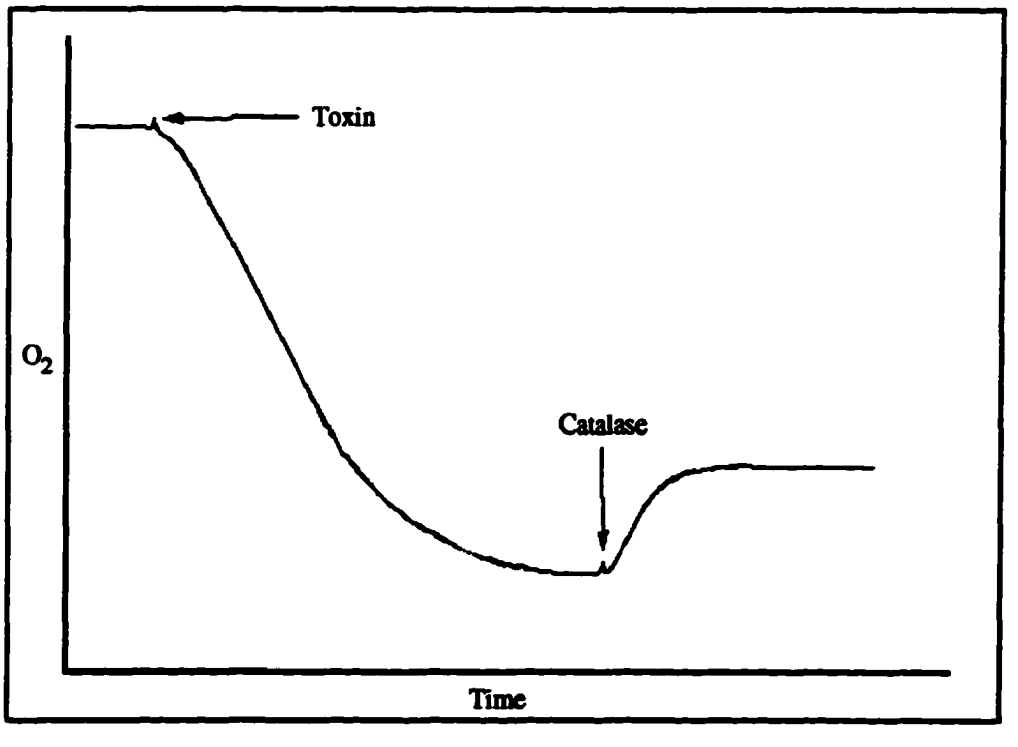

Figure 7-1. Typical autoxidation oxygen trace.

The effects of various metal ions, chelating agents, reactive oxygen species, and enzymes on the autoxidation reaction can be determined in the same fashion by administering the desired reactant prior to toxin introduction.

The H_2O_2 and $\bullet O_2^-$ which result from toxin autoxidation can also be determined utilizing the oxygen electrode. This is accomplished by introducing an appropriate enzyme following completion of autoxidation. To determine the production of H_2O_2 from autoxidation, catalase was used. Catalase breaks down H_2O_2 as:

$$H_2O_2 \xrightarrow{\text{cat.}} H_2O + 1/2\ O_2$$

The resulting oxygen liberated by catalase is, thus, equal to one-half of the oxygen consumed during autoxidation which led to the production of H_2O_2.

The production of superoxide can be determined in a similar way, using superoxide dismutase (SOD). SOD promotes dismutation of superoxide, $\bullet O_2^-$, as:

$$2\ O_2^{-\bullet} \xrightarrow{\text{SOD}} H_2O_2 + O_2^*$$

where O_2^* is singlet oxygen. Quantitation of $\bullet O_2^-$ using this method, however, is not quantitatively reliable since $\bullet O_2^-$ also spontaneously dismutates. Therefore, SOD provides $\bullet O_2^-$ values which are necessarily less than actual values. Nonetheless, this was considered a qualitatively useful tool.

Reaction orders and rate constants, as expressed in equation 7-3, can also be determined using an oxygen electrode system. The rate of autoxidation can be expressed as:

$$\text{rate} = k[\text{tox}]^x[O_2]^y[H^+]^z \qquad \text{equation 7-3}$$

By determining the rate of autoxidation while varying the toxin concentration and holding the oxygen concentration and pH constant, we can rewrite equation 7-3 as:

$$\text{rate} = k_T[\text{tox}]^x \qquad \text{equation 7-4}$$

Taking the log of both sides of equation 7-4 yields:

$$\log(\text{rate}) = x \log[\text{tox}] + \log(k_T) \qquad \text{equation 7-5}$$

Then, plotting the log(autoxidation rate) vs. log[toxin] yields the reaction order with respect to the toxin as the slope and the combined rate constant, k_T, as the y-intercept. A similar approach is used to determine the reaction orders and combined rate constants for oxygen and H^+.

The rate constant, as defined in equation 7-3, can be extracted from the above determined reaction orders and combined rate constants as follows:

$$\text{rate} = k_T[\text{tox}]^x$$

$$k_T = k[O_2]^y[H^+]^z$$

$$\log(k_T) = \log(k) + y \log[O_2] + z \log[H^+] \qquad \text{equation 7-6}$$

rearranging equation 7-6, we arrive at the solution for k:

$$\log(k) = \log(k_T) - y \log[O_2] - z \log[H^+] \qquad \text{equation 7-7}$$

where log (k_T) is the Y-intercept of the log(rate) vs. log[toxin] plot, y is the slope of the log(rate) vs. log[O_2] plot, z is the slope of the log(rate) vs. log[H^+] plot, and [O_2] and [H^+] are the concentrations used in the original toxin related experiments. This approach can also be carried out using the determined k_{O_2} and k_{H^+} combined rate constants, and would result in the same k value.

III. Experimental

A. Chemicals and Solutions

1. Chemicals

Chemicals listed below were purchased through Sigma Chemical Company (St. Louis, Mo.) in high purity and used without any further purification. All other chemicals are the same as in previous chapters.

ferrous chloride tetrahydrate ($FeCl_2 \cdot 4H_2O$)

cupric chloride tetrahydrate ($CuCl_2 \cdot 4H_2O$)

diethylenetriaminepentaacetic acid (DTPA)

catalase, 2000 units/mg

superoxide dismutase (SOD), 4000 units/mg

hydrogen peroxide, 30% (w/v)

All aqueous solutions employed 18 MΩ distilled/deionized water which was prepared by passing distilled water through a Milli-Q Reagent Water System (Millipore, Continental Water Systems, El Paso, TX).

2. Autoxidation Buffer

The pH buffers were generally created by adding 0.10 M KH_2PO_4 to 0.10 M K_2HPO_4 until the desired pH was obtained. For lower pH values, HCl was added to 0.10 M KH_2PO_4, while for higher pH values, NaOH was added to 0.10 M K_2HPO_4. The 0.10 M KH_2PO_4 and 0.10 M K_2HPO_4 were prepared as separate solutions by dissolving 13.61 g $KH_2PO_4 \cdot H_2O$ and 17.42 g K_2HPO_4, respectively, in 1.0 L of water.

3. Toxin Solution

Stock toxin solutions were made by dissolving the desired amount of toxin in an appropriate amount of degassed 10^{-3} M HCl to yield a stock concentration of 10 mM for the oxygen electrode studies and 12.5 mM for the spectroscopic studies. Typically, 1.5 to 2 mL of toxin solution were needed. The stock toxin solution was stable in excess of 8 hr.

4. Fe^{2+} Stock Solution

The Fe^{2+} stock solution was prepared by dissolving 80.96 mg ferrous chloride tetrahydrate ($FeCl_2 \cdot 4H_2O$) in 100 mL degassed water to yield a stock concentration of 4.072 mM. This was made 10 min prior to utilization. The stock was diluted 1:10 with water to obtain a 0.4072 mM Fe^{2+} secondary stock solution. These solutions were used for no more than 20 min following their preparation.

5. Cu^{2+} Stock Solution

The Cu^{2+} stock solution was prepared by dissolving 34.71 mg cupric chloride tetrahydrate ($CuCl_2 \cdot 4H_2O$) in 100 mL degassed water to yield a stock concentration of 0.40 mM. The stock was diluted 1:10 with water to obtain the 0.04072 mM Cu^{2+} secondary stock solution. These solutions were used for no more than 20 min following their preparation.

6. Fe^{2+}/EDTA Complex Solution

The Fe^{+}/EDTA solution was prepared 10 min prior to utilization and was used for no more than 20 min following its preparation. Component additions and solution adjustments were performed sequentially as shown in Table 7-1.

Table 7-1. Fe^{2+}/EDTA solution preparation.

Compound	Amount
$Na_2EDTA \cdot 2H_2O$	75.79 mg
add 90 mL water and make basic with KOH to dissolve EDTA	
adjust to pH 7.4	
$FeCl_2 \cdot 4H_2O$	80.96 mg
dilute to final volume of 100 mL	

7. Catalase Solution

The catalase stock solution was prepared by dissolving 4.072 mg catalase (2000 units/mg) in 1.0 mL water. This solution was prepared and stored at -20°C until use. Each sample was thawed once and frozen samples were discarded after 2 months.

8. Superoxide Dismutase Solution

The superoxide dismutase stock solution was prepared by dissolving 1.018 mg SOD (4000 units/mg) in 1.0 mL water. This solution was prepared and stored as individual 500 µL aliquots at -20°C until use for up to 2 months. Each aliquot was thawed once, used, and the remainder discarded.

9. Diethylenetriaminepentacetic Acid (DTPA) Solution

The DTPA stock solution was prepared by dissolving 16 mg DTPA in 1.0 mL water to yield a final stock concentration of 41 mM. This solution was prepared 30 min prior to utilization, used for no more than 8 h, and then discarded.

10. Hydrogen Peroxide Solution

Stock solution was prepared by diluting 1 mL of 30% H_2O_2 to 500 mL with water. This solution was prepared 10 min prior to utilization and used for no longer than 30 min following its preparation.

B. Autoxidation, Oxygen Electrode

1. Oxygen Electrode

A model 58 YSI dissolved oxygen meter outfitted with a model 5739 YSI dissolved oxygen probe (Yellow Springs Instrument Co., Yellow Springs, OH) was used to monitor changes in dissolved oxygen concentrations. The probe was equipped with a fresh membrane (0.001" standard YSI oxygen electrode membrane) and calibrated at least daily using an atmospheric calibration procedure. The reaction cell used for all experiments was a temperature regulated, water jacketed cell that fit tightly over the end of the O_2 probe. The volume of the cell, once in place, was 2.036 mL. All oxygen electrode reactions were conducted at 37°C.

2. Kinetic Measurements, Toxin Concentration Effects

To investigate the effect of toxin concentration on the initial rate of autoxidation, various volumes (25, 50, 75, and 100 μM) of 10 mM stock toxin solution were injected into the 2.036 mL oxygen electrode incubation cell filled with air saturated incubation

buffer. For these investigations, the initial oxygen concentration was held constant at 7.5 to 8.0 mg/L, the pH was fixed at 7.40, and no metal ions or complexing agents were added.

3. Kinetic Measurements, Oxygen Concentration Effects

The effect of oxygen concentration on the initial autoxidation rate was investigated by varying the initial oxygen concentration while keeping the pH and initial toxin concentration constant. The initial oxygen levels employed were approximately 5, 8, 10, and 15 mg/L. These oxygen levels were obtained by bubbling the incubation buffer with either oxygen or nitrogen gas for varying periods of time. For these studies, the initial toxin concentration was held constant at 196 μM, the pH was 7.40, and no metal ions or complexing agents were added.

4. Kinetic Measurements, pH Effects

The effects of pH on initial rate of oxidation was investigated by holding the initial oxygen and toxin concentration constant and varying the pH. pH values of 5.40, 6.40, 7.40, and 8.40 for the incubation buffer were used. These pH values were created by mixing 0.10 M KH_2PO_4 and 0.10 M K_2HPO_4 incubation buffers to the desired pH. The initial toxin concentration was 196 μM, the initial oxygen concentration was 7.5 to 8.0 mg/L, and no added metal ions or complexing agents were added.

5. Toxin Autoxidation in Absence and Presence of Metal ions, Complexing Agents, & Enzymes

Investigating the effects of various metal ions, complexing agents, and enzymes on the initial rate of toxin autoxidation, the toxin concentration was kept constant at 196 μM (40 μL stock), the buffer was air saturated to obtain constant oxygen levels at ca. 250 μM oxygen (7.5-8.0 mg oxygen/L), and the pH was fixed at 7.40. Catalase and

superoxide dismutase injections were performed, separately, upon completion of toxin oxidation, i.e., after oxygen consumption had reached a plateau, to investigate the production of H_2O_2 and $\bullet O_2^-$, receptively. For each given condition, the same experiment was generally run four times; three of these four were followed by a 50 μL injection of stock catalase solution yielding a 200 units/mL incubation concentration, and one was followed by a 50 μL injection of stock SOD solution yielding an incubation concentration of 100 units/mL. The incubation cell was rinsed and drained three times with fresh buffer between each experiment to avoid contamination.

In all experiments investigating the rates of oxidation, the toxin was the last component to be added. For an individual toxin autoxidation experiment, the toxin was first examined without any metal ion or complexing agent present. To investigate the effects of metal ions on autoxidation, the following experiments were used. A 50 μL aliquot of the 4.072 mM stock Fe^{2+} solution was injected into the incubation cell, resulting in an incubation concentration of 100 μM Fe^{2+}, followed by the addition of toxin. Using the 0.4072 mM stock Fe^{2+} solution, which yielded an incubation concentration of 10 μM Fe^{2+}, the previous experiment was repeated. The same experiment was conducted using (1) 50 μL of 4.072 mM stock Fe^{2+}/EDTA solution, yielding a 100 μM incubation concentration, (2) 0.4072 mM Cu^{2+} stock solution, giving a 10.0 μM incubation concentration, and (3) 0.041 mM Cu^{2+} stock solution, yielding a 1.00 μM incubation concentration.

In an effort to observe autoxidation in the absence of any trace metal ions, we incorporated DTPA into the incubation cell mixture. A 50 μL aliquot of 40.72 mM stock DTPA was added to the reaction cell, yielding a 1.0 mM incubation concentration, and allowed a one minute incubation prior to toxin introduction.

In order to investigate the effects of reactive oxygen species and enzyme interactions with toxin autoxidation, 31 μL of 17.65 mM stock hydrogen peroxide solution was added to the incubation cell prior to the toxin, giving a 268.7 μM H_2O_2

incubation concentration. The same experiment was conducted, separately, using 50 μL of stock catalase, yielding a 200 units/mL incubation concentration, and 50 μL of stock SOD, yielding a 100 units/mL incubation concentration.

C. Autoxidation, Spectrophotometry

The UV-VIS spectra were recorded using a model 8452A Hewlett-Packard (Palo Alto, CA) spectrophotometer equipped with a temperature regulated cell held at 37°C unless otherwise noted. The formal concentration of the toxin was 196 μM in all experiments. The buffer used was an oxygen saturated 0.10 M phosphate buffer at pH 7.4 unless otherwise noted. A blank was periodically recorded and automatically subtracted from each spectrum. The blank contained all solution components except the toxin.

A 2460 μL aliquot of buffer was added to a quartz cell and placed in the temperature regulated cell holder for 15 min to equilibrate. After temperature equilibration, the solution was bubbled with oxygen for 2 min. A 40 μL aliquot of 12.5 mM stock toxin solution was administered to the cell, the cell was shaken vigorously for 2 sec, the cell was placed back in the holder, and spectra were recorded as rapidly as possible. The reaction solution was reoxygenated for 30 sec at 3 to 5 min after the beginning of the experiment in order to ensure maintenance of pseudo first order conditions.

Following the initial toxin autoxidation study, we investigated the effects of SOD, catalase, and H_2O_2 on autoxidation rates. First, we collected a spectrum of the solution with the enzyme alone to examine the possible existence of conflicting absorption bands. We found no conflicting bands with SOD or catalase. Following this, we obtained spectra in the same manner as above from a solution consisting of 2410 μL buffer, 50 μL

stock SOD, catalase, or H_2O_2, and 40 μL stock toxin. Final concentrations were; SOD 100 units/mL, catalase 200 units/mL, and 268.7 μM H_2O_2. Buffer equilibration and oxygenation was as described immediately above.

In order to ensure that the toxins remained in their reduced forms in the stock solutions for the duration of the experiment, stability controls were periodically examined. A stability control was prepared by adding 10 μL of a toxin stock solution to 2490 μL of 0.10 M phosphate buffer at pH 2.4. The pH value of 2.4 was selected since autoxidation of all the toxins is extremely slow at this pH, and, therefore, the form in which the toxin resided in the stock solution was subsequently directly observed in the corresponding UV-VIS spectrum.

IV. Results:

Autoxidation and Reactive Oxygen Species

In the following studies, toxin autoxidation occurred so rapidly at 37°C that UV-VIS spectroscopy was not as useful in the determination of initial rates as was the oxygen electrode system. While monitoring autoxidation with an oxygen electrode is an indirect method, we were able to observe this reaction shortly after initiation, which we were unable to accomplish using UV-VIS. However, where possible, the oxygen electrode determined rates and rate changes were verified, to the best of our abilities, with the limited UV-VIS data.

A. 6,7-ADTQ

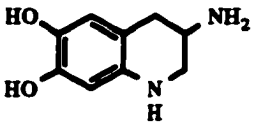

6,7-ADTQ, when put in an air saturated phosphate buffer at pH 7.4, rapidly formed a pinkish-purple colored solution. The UV-VIS spectrum of reduced 6,7-ADTQ initially shows a band at λ_{max} = 305 nm. At pH 7.4, 6,7-ADTQ autoxidation occurred too rapidly at both 37°C and 25°C to obtain a full sequence of spectra throughout the process. Thus, the autoxidation shown in Figure 7-2 was performed at the lower pH of 5.4. However, the spectra obtained at pH 5.4, notably, display the same band increases and decreases as do those at pH 7.4, just at a slower rate. During 6,7-ADTQ autoxidation at pH 7.4 there was an initial increase in absorption in the band at 305 nm.

This band shifted to shorter wavelengths and grew throughout autoxidation with a final band maxima at 294 nm. This increase corresponded to the appearance of new bands at 222 nm and 518 nm, which also grew throughout the autoxidation reaction. The spectrum of 6,7-ADTQ quinoneimine shows prominent bands at λ_{max} = 222, 294, and 518 nm. After the completion of autoxidation, these bands began to decrease in intensity, although slowly in comparison to their previous growth during autoxidation, and the overall baseline began to slowly increase. This general baseline increase in absorption throughout the spectrum corresponded to the appearance of a deep purple color and, with time, the formation of dark precipitates in the solution, presumably indicating polymerization. The same spectral changes occurred at both higher and lower pH values. But, the rate was much faster at higher pH values and much slower at lower pH values. Interestingly, autoxidation was even observed at pH 2.4, with an increase in absorption at 518 nm and 294 nm, although the rate was approximately 60 times slower than that at pH 7.4. Again, this autoxidation was followed by decreases in band maxima and a general baseline increase.

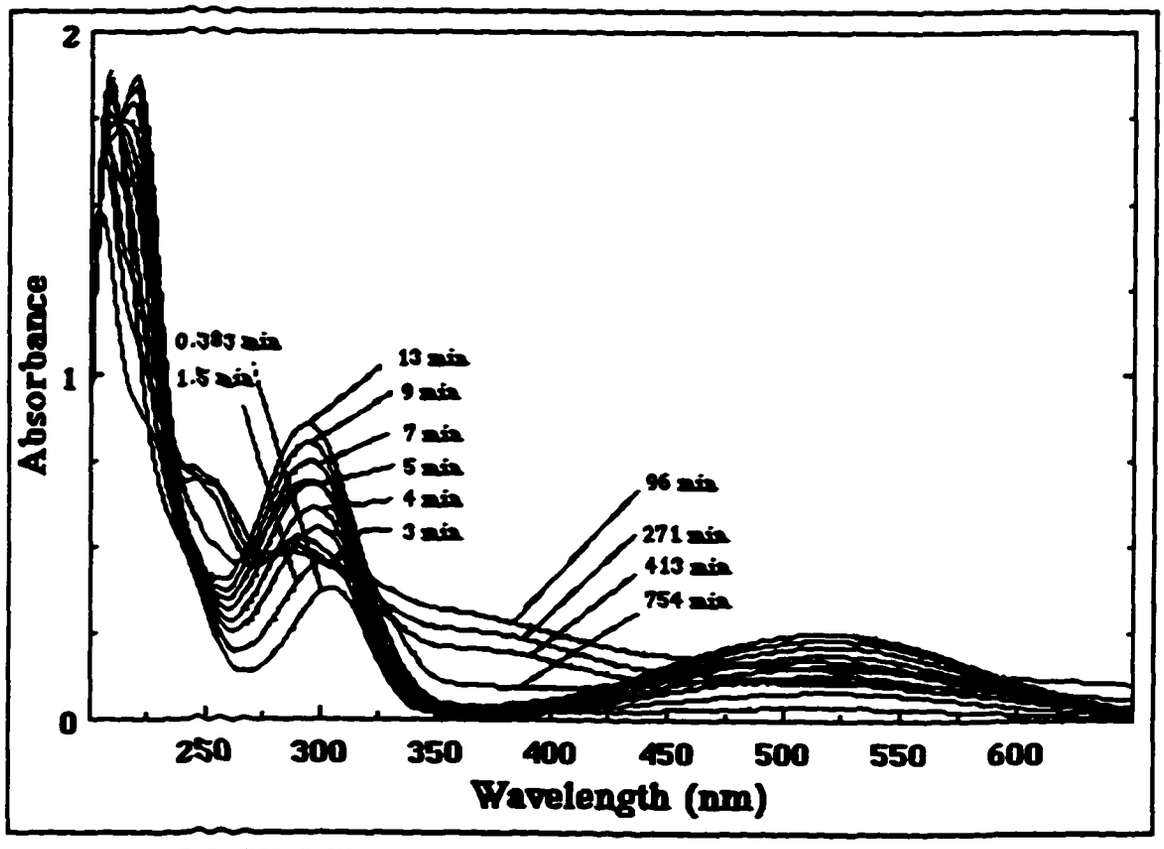

Figure 7-2. UV-VIS spectra of 6,7-ADTQ autoxidation at pH 5.4 and 25°C.

Since the UV spectroscopy employed was not adequate to monitor the initial stages of the autoxidation process at 37°C, we primarily relied upon the oxygen electrode system. Using the oxygen electrode, we initially determined the autoxidation reaction orders with respect to toxin, O_2, and H^+. To determine toxin reaction order, the initial oxygen concentration was held constant at 248 μM and the pH at 7.4. The toxin concentrations used were 98, 147, 196, and 245 μM. Autoxidation appeared to be first order with respect to toxin, as graphically shown in Figure 7-3. To determine the oxygen reaction order, the pH was fixed at 7.4, the initial toxin concentration was fixed at 196 μM, and the O_2 concentration was varied between 165 and 370 μM. The reaction order for oxygen was found to be approximately 3/4, as seen in Figure 7-4. The H^+ reaction order was determined with the initial O_2 concentration fixed at 248 μM, the toxin

concentration fixed at 196 μM, and using pH values of 5.4, 6.4, 7.4, and 8.4. The reaction order was found to be approximately -1/2, as seen in Figure 7-5. The overall rate constant extracted from the data in Figures 7-3 to 7-5 was k = 0.0010 ± 0.0005 $M^{-1/4}sec^{-1}$, and the rate expression was:

$$rate = k[tox][O_2]^{0.75}[H^+]^{-0.5}$$

These results are summarized in Table 7-2.

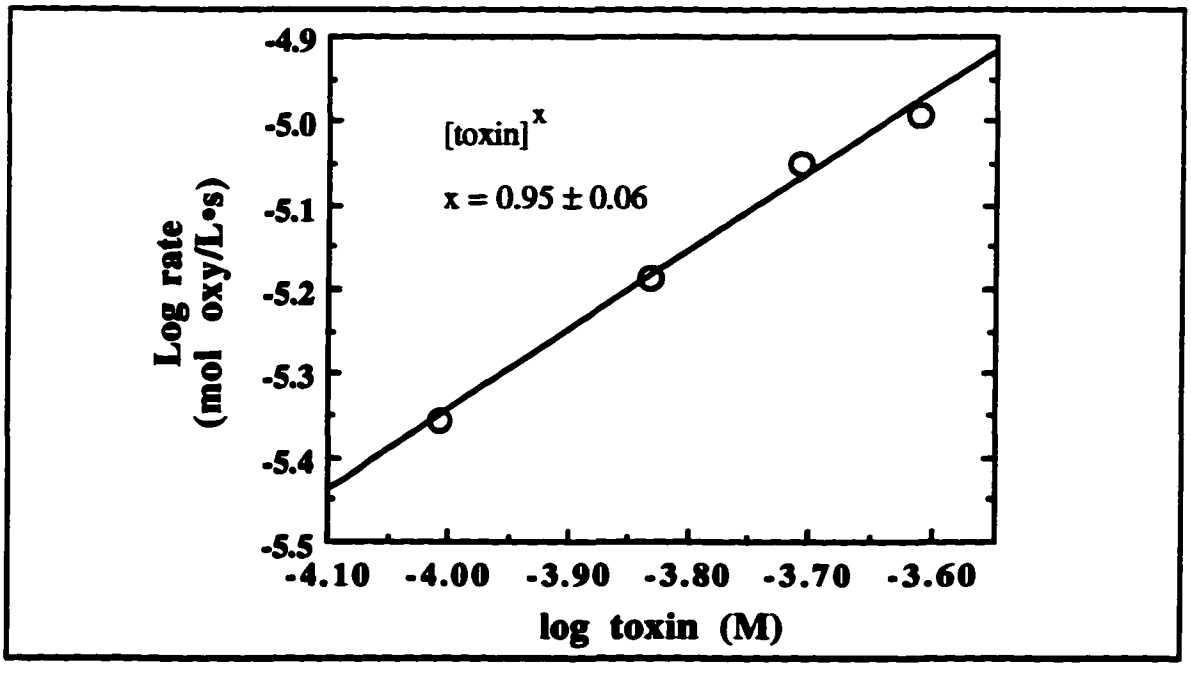

Figure 7-3. Toxin concentration effects on 6,7-ADTQ autoxidation.

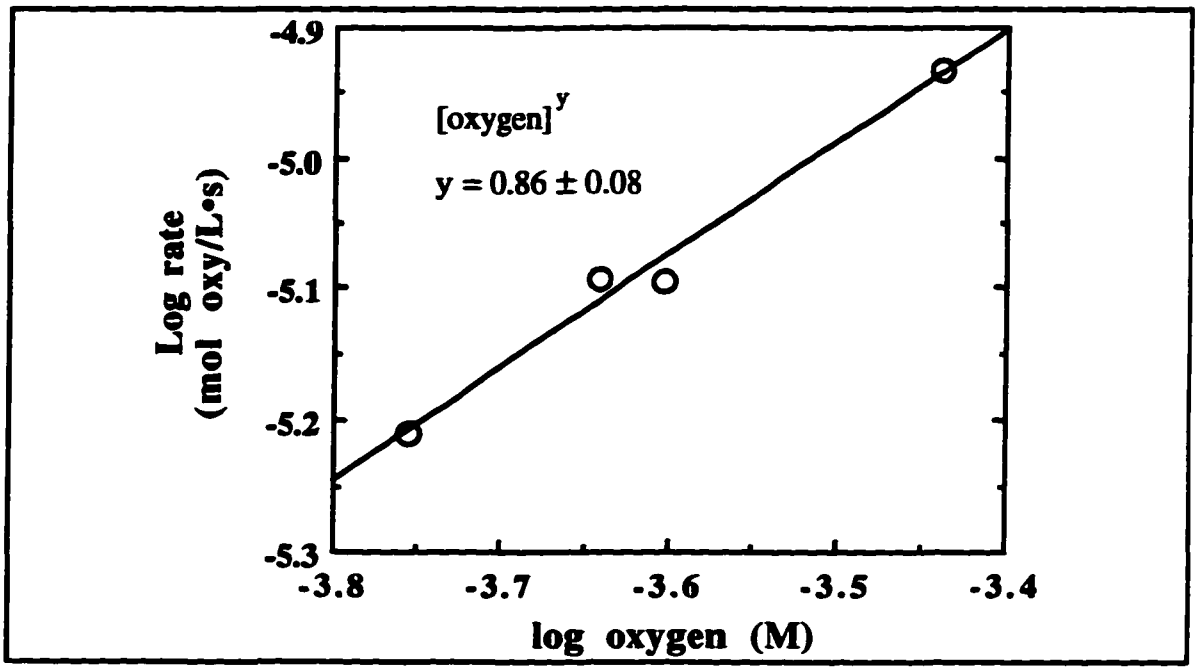

Figure 7-4. Oxygen concentration effects on 6,7-ADTQ autoxidation.

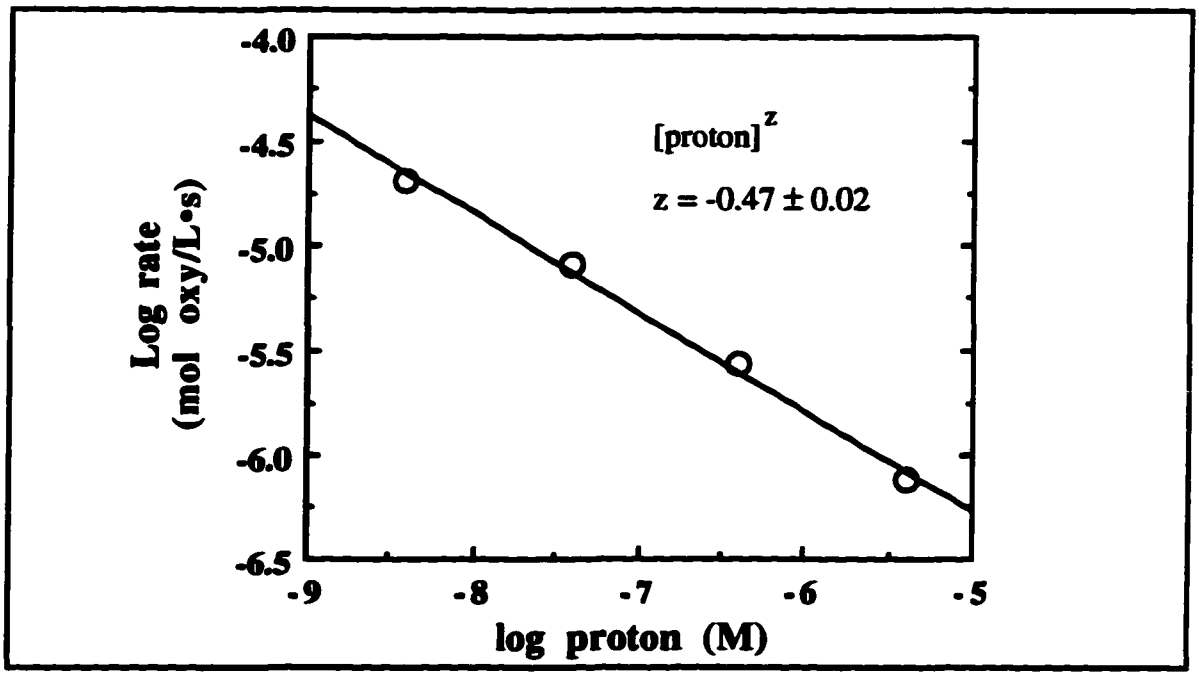

Figure 7-5. The effects of pH on 6,7-ADTQ autoxidation rate.

Table 7-2. 6,7-ADTQ autoxidation reaction orders with respect to individual components.

6,7-ADTQ Reaction Orders	
rate = $k[tox]^x[O_2]^y[H^+]^z$	
x	0.95 ± 0.06
y	0.86 ± 0.08
z	-0.47 ± 0.02
k	0.0010 ± 0.0005 $M^{-0.34}sec^{-1}$

Autoxidation rates of 6,7-ADTQ in the presence of various stimulating and/or inhibiting agents are shown in Table 7-3. Furthermore, the percent oxygen consumed during autoxidation leading to the production of H_2O_2 and $\bullet O_2^-$ is presented in Table 7-4. The average initial oxygen concentration prior to autoxidation was 8 mg/L or 250 μM, the pH was 7.4, the temperature was 37°C, and the toxin concentration was 196 μM.

Autoxidation of ca. 200 μM 6,7-ADTQ in the absence of any added substances was completed in less than 40 seconds and showed an initial oxygen consumption rate of 484 μmol O_2/L•min. The k_{app} determined from preliminary UV-VIS spectroscopy for autoxidation of 200 μM 6,7-ADTQ was k_{app}=11.7 ± 0.7 min^{-1} (100 ± 6%, λ=294 nm). Upon addition of catalase following the completion of autoxidation, 41% of the oxygen consumed was returned to the solution. Therefore, a minimum of 82% of the oxygen consumed went to form H_2O_2. However, due to the possible participation of H_2O_2 in toxin oxidation, the ability of H_2O_2 to participate in Fenton and Haber-Weiss reactions,[44,45,48,169] and the modest innate instability of H_2O_2 in aqueous solutions, it is likely that more H_2O_2 was ultimately produced. Thus, the majority of the oxygen consumed during ADTQ autoxidation was converted to H_2O_2.

Table 7-3. 6,7-ADTQ autoxidation, initial rate of oxygen consumption.

Added Component(s)	Initial O_2 Consumption		
	N	rate ± SEM (μmol O_2 / L•min)	rate ± SEM % controls
none	4	484 ± 1	100 ± 0.2
Fe^{2+} 1.0×10^{-4} M	4	628 ± 2	130 ± 0.3***
Fe^{2+} 1.0×10^{-5} M	4	551 ± 0.6	114 ± 0.1***
Cu^{2+} 1.0×10^{-5} M	4	1133 ± 12	234 ± 2***
Cu^{2+} 1.0×10^{-6} M	4	534 ± 0.3	110 ± 0.1***
Fe^{2+}/EDTA 1.0×10^{-4} M	4	592 ± 2	122 ± 0.3***
DTPA 1.0×10^{-3} M	4	408 ± 18	84 ± 3**
H2O2 2.5×10^{-4} M	3	445 ± 8	92 ± 1**
catalase 200 units/mL	2	325 ± 7	67 ± 1
SOD 100 units/mL	2	577 ± 1	119 ± 0.2***

Significant differences compared to control values (*t* test): $^{**}P < 0.01$, $^{***}P < 0.001$.

There are numerous reports showing that transition metal ions stimulate autoxidation of catechol-type compounds.[171-173] Hence, it was of interest to determine the effects that transition metal ions exert, if any, on the autoxidation of 6,7-ADTQ. We first tested Fe^{+2} at two concentrations with a toxin concentration of 200 μM. The Fe^{+2} was prepared for each experiment 10 min prior to use. There was no noticeable oxygen consumption due to Fe^{+2} alone. A reaction solution containing 10^{-4} M Fe^{+2} stimulated 6,7-ADTQ autoxidation significantly to 130% of controls. At 10^{-5} M Fe^{+2}, autoxidation was stimulated, yet not to the degree seen at 10^{-4} M Fe^{+2}. Interestingly, upon addition of

catalase following this reaction, the oxygen liberated decreased with increasing concentrations of Fe^{+2}. The percent oxygen consumed during autoxidation attributable to the H_2O_2 formation was 59% for 10^{-5} M Fe^{+2} and 53% for 10^{-4} M Fe^{+2}.

Table 7-4. 6,7-ADTQ autoxidation, H_2O_2 and $\bullet O_2^-$ produced.

Added Component(s)	Percent O_2 Consumed which was Liberated Upon Addition of:				Percent O_2 Consumed by Pathway Leading to:	
	Catalase		SOD		H_2O_2	$\bullet O_2^-$
	N	% O_2 ± SEM	N	% O_2	% O_2 ± SEM	% O_2
none	3	40.8 ± 0.7	1	1	82 ± 1	2
Fe^{+2} 1.0 x 10^{-4} M	3	26 ± 1	1	2	53 ± 2	3
Fe^{+2} 1.0 x 10^{-5} M	3	30 ± 3	1	1	59 ± 6	2
Cu^{+2} 1.0 x 10^{-5} M	3	35.6 ± 0.8	1	0	71 ± 2	0
Cu^{+2} 1.0 x 10^{-6} M	3	38 ± 2	1	2	77 ± 3	3
Fe^{+2}/EDTA 1.0 x 10^{-4} M	3	2.0 ± 0.4	1	0	3.9 ± 0.8	0
DTPA 1.0 x 10^{-3} M	3	40 ± 4	1	0	80 ± 7	0

We also conducted similar studies with Cu^{+2}. At 10^{-5} M Cu^{+2}, 6,7-ADTQ autoxidation was dramatically stimulated to 1133 μmol O_2/L•min, or 234% of controls. The majority of 6,7-ADTQ autoxidation under these conditions was complete in less than 10 seconds. At 10^{-6} M Cu^{+2}, however, the rate was only slightly stimulated to 110% of controls. Upon addition of catalase, the oxygen liberated decreased with increasing concentrations of Cu^{+2}, but not to the extent seen with Fe^{+2}. The percent of oxygen

consumed during autoxidation which remained as H_2O_2 was 71% and 77% for 10^{-5} M and 10^{-6} M Cu^{+2}, respectively.

While Fe^{+2} alone increases the autoxidation rate of catecholamines and 6-HDA related toxins, Fe^{+2} complexed with EDTA has been reported to stimulate autoxidation to an even greater.[36,38,165,173] Thus, we investigated 6,7-ADTQ autoxidation in the presence of 10^{-4} M Fe^{+2}/EDTA. Fe^{+2}/EDTA was prepared 10 min prior to use, and no noticeable oxygen consumption was observed with Fe^{+2}/EDTA alone. Fe^{+2}/EDTA stimulated the 6,7-ADTQ autoxidation rate to 122% of controls, which was approximately equal to that seen at 10^{-4} M Fe^{+2}. Therefore, Fe^{+2}/EDTA did not appear to have any different effect on autoxidation than did Fe^{+2} alone. However, upon addition of catalase following autoxidation, surprisingly little oxygen was liberated. The oxygen returned to the solution was only 2% of the oxygen consumed. And, there was no detectable $\cdot O_2^-$.

It has been suggested that 6-HDA related compounds cannot reduce molecular oxygen directly, but require a co-reductant such as a transition metal ion.[172] Additionally, it has been shown that, by effectively chelating all available metal ions, the rate of autoxidation of 6-HDA analogs is dramatically inhibited,[38,173] and their neurotoxic capabilities are retarded.[174] Thus, we investigated this hypothesis by incorporating diethylenetriaminepentacetic acid (DTPA). At 10^{-3} M, DTPA did, indeed, inhibit the autoxidation rate of 200 μM 6,7-ADTQ, but only slightly. The resultant rate was 84% of controls. Furthermore, the percent oxygen consumed leading the production of H_2O_2 was 80%, which was approximately equal to that of 6,7-ADTQ alone.

Since H_2O_2 was the major product of 6,7-ADTQ autoxidation, we investigated the effects of H_2O_2 on 6,7-ADTQ autoxidation rate. With 250 μM H_2O_2 in the reaction solution, the rate of autoxidation was inhibited to 92% of controls. Following this apparent inhibition of autoxidation by H_2O_2, we decided to effectively remove all H_2O_2 produced during autoxidation and see what effect that had. This was accomplished by the

addition of catalase to the reaction solution prior to autoxidation, with a final concentration of 200 unit/mL. The resulting rate was 67% of controls. If all of the oxygen consumed goes to produce H_2O_2, then the observed rate measured by the oxygen electrode in the presence of catalase should be 50% of controls. However, we found that 82% of the oxygen consumed with 6,7-ADTQ went to produce H_2O_2. Therefore, if catalase had no stimulatory or inhibitory effects, the observed rate in the presence of catalase should have been approximately 59% of controls. But we found the rate to be 67% of controls and thus, it appears that catalase has a slight stimulatory effect on 6,7-ADTQ autoxidation. This stimulatory effect was further substantiated by UV-VIS spectroscopy ($k_{app} = 14 \pm 1$ min^{-1}, 120 ± 8% of the control k_{app}, λ=294 nm). Whether this stimulation is due to catalase itself, or the removal of H_2O_2, is not known. But the results from this study suggest that it is from the removal of H_2O_2.

Spin restrictions dictate that, whether by direct reduction of molecular oxygen or by use of a co-reductant, electrons are transferred to oxygen one at a time.[41,167] Therefore, autoxidation must generate $\bullet O_2^-$. However, this may not be "free" $\bullet O_2^-$ and/or may be extremely short lived due to the kinetics of electron transfer with 6,7-ADTQ. The mechanism of autoxidation of 6-HDA and some related analogs depend on the presence of $\bullet O_2^-$, and by removing $\bullet O_2^-$ from the reaction medium, autoxidation is inhibited. On the other hand, autoxidation of other 6-HDA analogs, in particular 6-ADA, proceeds by pathways unaffected by the removal of $\bullet O_2^-$, thereby suggesting very rapid electron transfer kinetics. Therefore, we conducted 6,7-ADTQ autoxidation in the presence of 100 units/mL SOD. Not only was 6,7-ADTQ not inhibited by SOD, but the rate was actually stimulated to 119% of controls. This stimulatory effect was also observed by UV-VIS spectroscopy ($k_{app} = 13.9 \pm 0.7$ min^{-1}, 119 ± 5% of the control k_{app}, λ=294 nm).

B. 6,7-AMDTQ

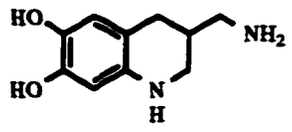

In a pH 7.4 phosphate buffer, 6,7-AMDTQ rapidly forms a pink-purple colored solution. A UV-VIS spectrum of reduced 6,7-AMDTQ initially displays bands at λ_{max} = 218 nm, 284 nm, and 350 nm. The UV-VIS spectral changes that accompany autoxidation of 100 μM 6,7-AMDTQ at pH 7.4 and 25°C are shown in Figure 7-6. Spectral changes occurring at 37°C are the same as that seen at 25°C, however, they occur much faster. During autoxidation, the band at 284 nm rapidly grew and shifted to longer wavelengths with a final absorbance maxima at 300 nm. Corresponding to this increase, there was a decrease in the absorption band at 218 nm, a growth and shift to a shorter wavelength (344 nm) of the band at 350 nm, and the appearance of a new band at 518 nm. At the completion of autoxidation, the bands at 518 nm and 300 nm began to decrease, the 344 nm band continued to increase, and a new band appeared at 244 nm. Interestingly, there was an absence of an overall baseline increase with time, suggesting the absence of polymerization. The rate of autoxidation was pH dependent, as was expected. Surprisingly, even at pH 2.4 autoxidation occurs; however, there was approximately a 10 minute lag period prior to the initiation of autoxidation.

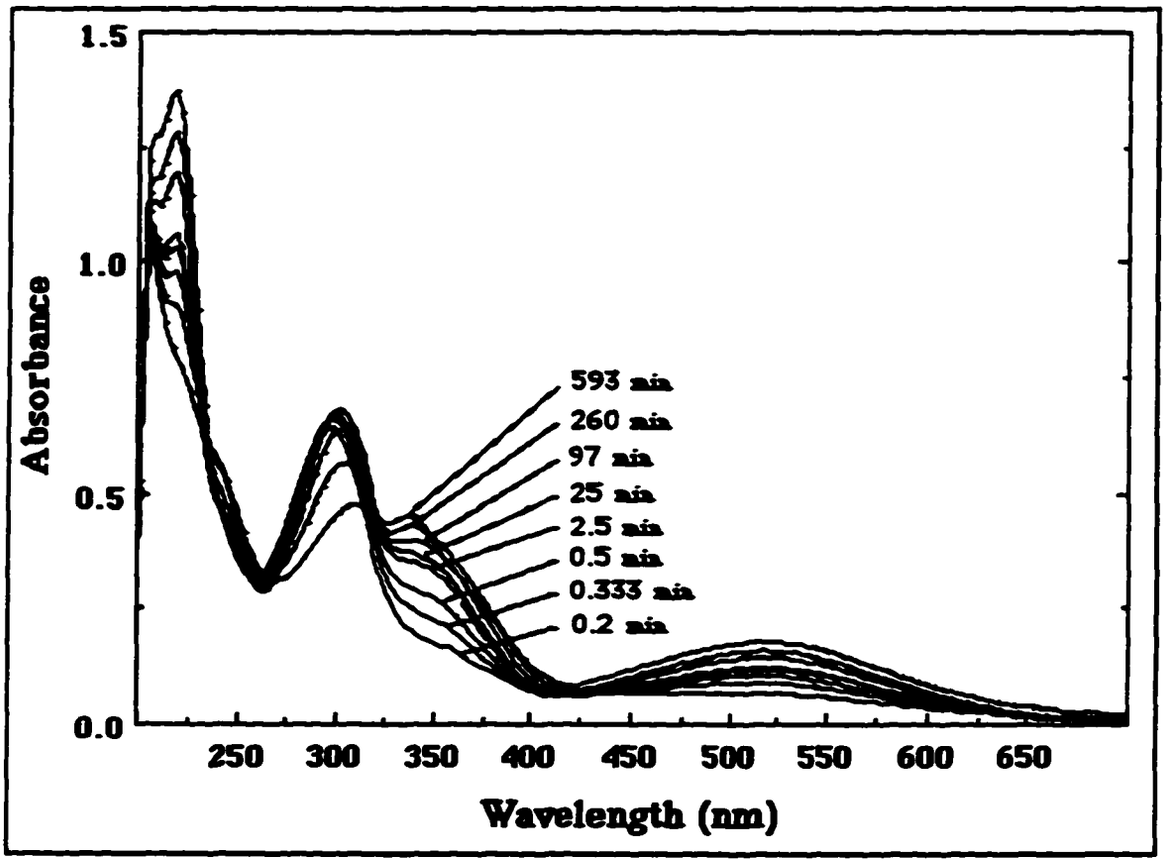

Figure 7-6. UV-VIS spectra of 6,7-AMDTQ autoxidation at pH 7.4 and 25°C.

Autoxidation reaction orders were determined using the oxygen electrode for each of toxin, O_2, and H^+. The conditions under which the reaction order for 6,7-AMDTQ 6,7-AMDTQ was found were: 246 μM oxygen, pH 7.4, and toxin concentrations of 98, 147, 196, and 246 μM. This is shown in Figure 7-7. It was found that autoxidation is approximately first order with respect to 6,7-AMDTQ. With the toxin concentration and the pH fixed at 196 μM and 7.4, respectively, the concentration of O_2 was varied between 132 and 488 μM to determine the reaction order for oxygen. Surprisingly, the reaction order was found to be approximately 1/2, as shown in Figure 7-8. By holding the initial oxygen and toxin concentrations constant and using pH values of 5.4, 6.4, 7.4, and 8.4, the reaction order for H^+ was determined to be -1/4. This is shown in Figure

7-9. From the above data, the autoxidation rate constant for 6,7-AMDTQ was found to be $k = 0.0485 \pm 0.0009\ M^{-1/4}sec^{-1}$, and the rate expression was:

$$rate = k[tox][O_2]^{0.5}[H^+]^{0.25}$$

These results are summarized in Table 7-5.

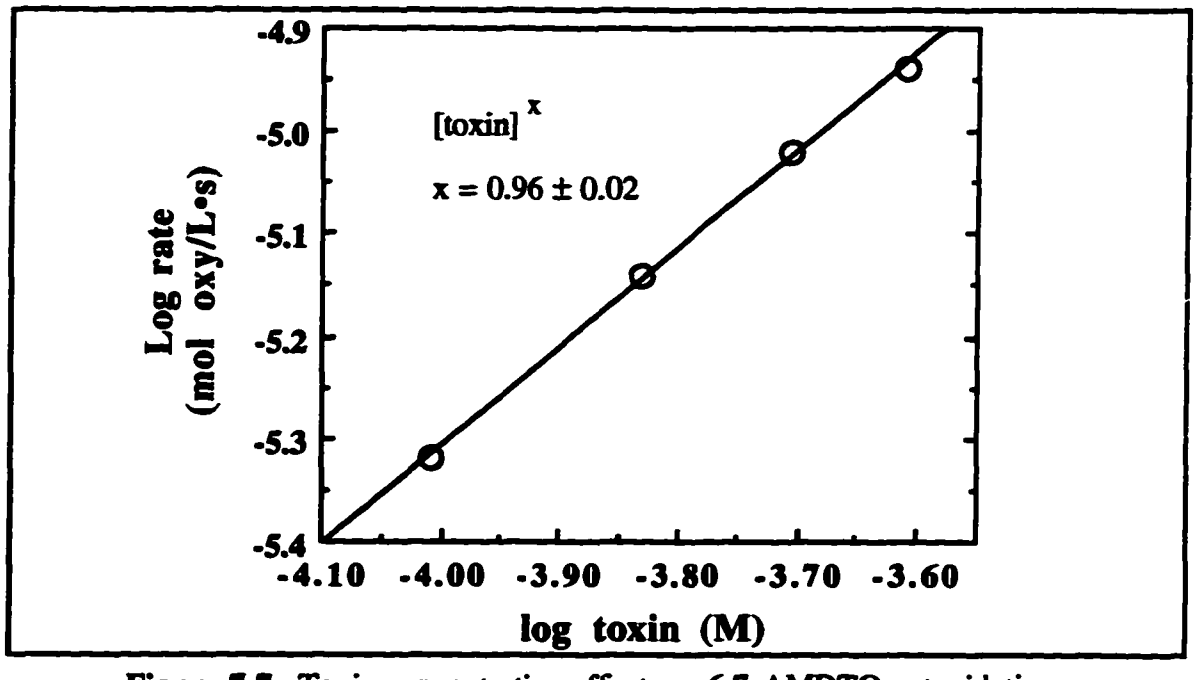

Figure 7-7. Toxin concentration effects on 6,7-AMDTQ autoxidation.

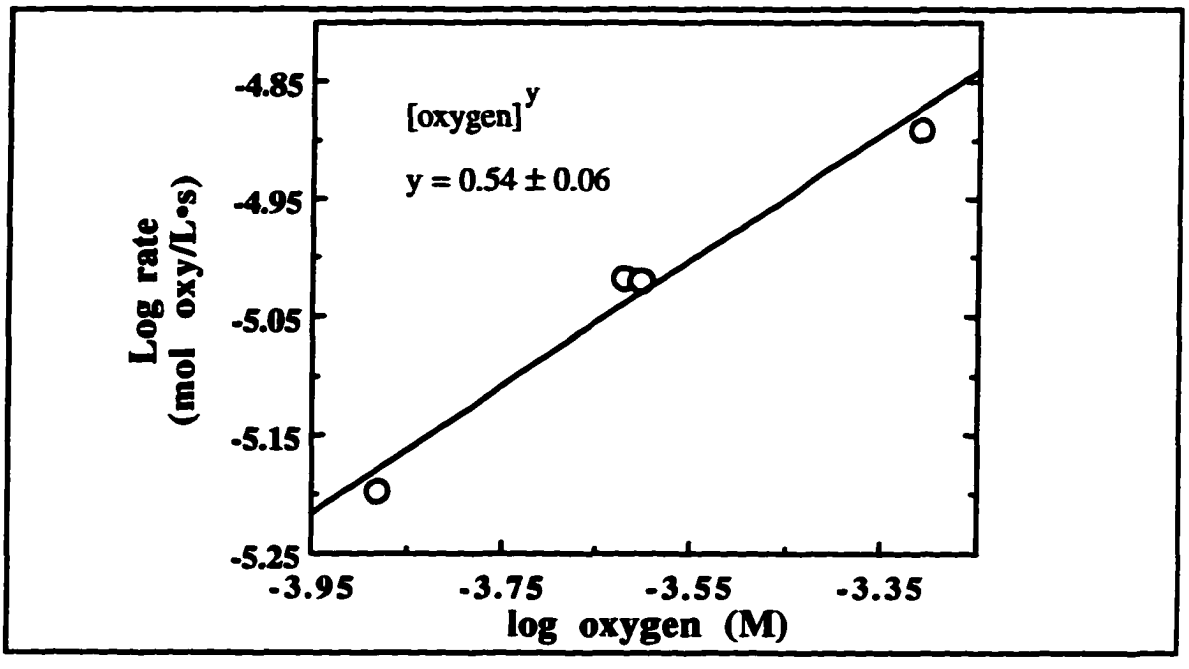

Figure 7-8. Oxygen concentration effects on 6,7-AMDTQ autoxidation.

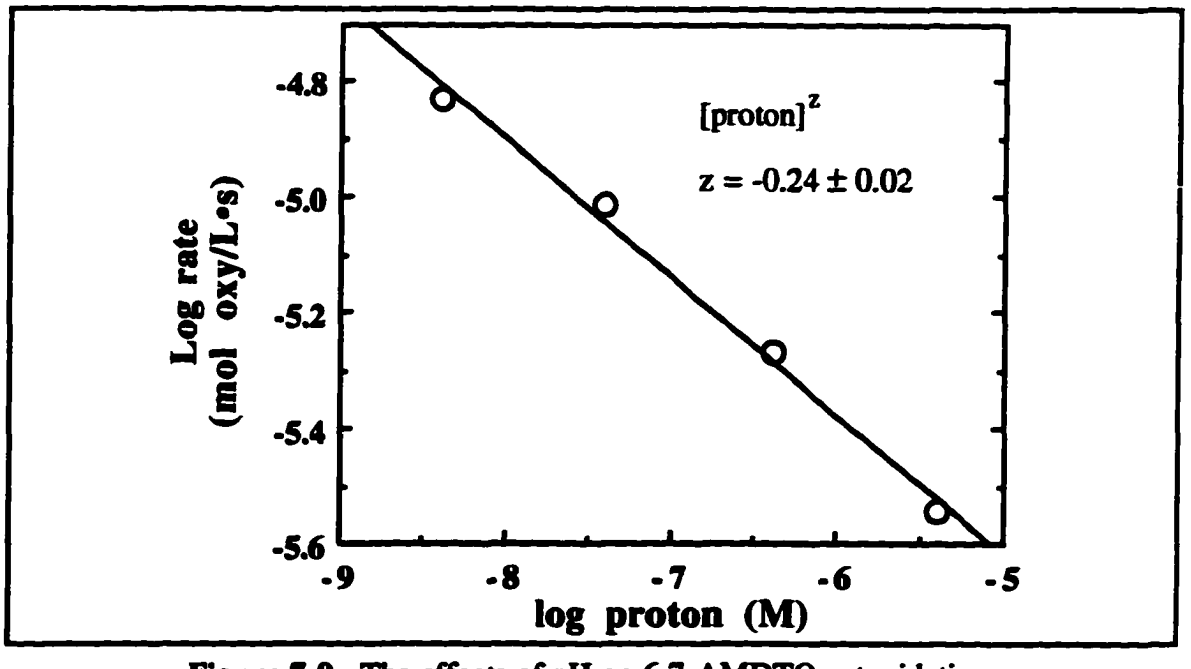

Figure 7-9. The effects of pH on 6,7-AMDTQ autoxidation.

Table 7-5. 6,7-AMDTQ autoxidation reaction orders with respect to individual components.

Reaction Orders	
rate = $k[tox]^x[O_2]^y[H^+]^z$	
x	0.96 ± 0.03
y	0.54 ± 0.06
z	-0.24 ± 0.02
k	0.0485 ± 0.0009 $M^{-0.26}sec^{-1}$

6,7-AMDTQ autoxidation rates in the absence and presence of various metal ions, chelating agents, and enzymes are shown in Table 7-6. Additionally, the percent oxygen consumed during 6,7-AMDTQ autoxidation leading to the production of H_2O_2 and superoxide is presented in Table 7-7. Throughout these studies, the concentration of 6,7-AMDTQ was 196 μM, the initial concentration of O_2 was approximately 250 μM, and the pH was 7.4.

Autoxidation of 6,7-AMDTQ in the absence of any added substances was completed in less than 25 seconds and showed an oxygen consumption rate of 583 μmol O_2/L•min. The k_{app} determined from UV-VIS spectroscopy for 200 μM 6,7-AMDTQ was 4.8 ± 0.1 (100 ± 2%, λ=518 nm). Upon addition of catalase to the oxygen electrode reaction cell following completion of the reaction, 47% of the oxygen consumed was returned to the solution. Therefore, a minimum of 94% of the oxygen consumed during autoxidation went to produce H_2O_2. There was little oxygen liberated (1%) upon SOD addition. Therefore, the majority of oxygen consumed was accounted for by the production of H_2O_2.

Table 7-6. 6,7-AMDTQ autoxidation, initial rate of oxygen consumption.

Added Component(s)	Initial O_2 Consumption		
	N	rate ± SEM (μmol O_2 / L•min)	rate ± SEM % controls
none	6	583 ± 3	100 ± 0.6
Fe^{2+} 1.0 x 10^{-4} M	4	711 ± 7	122 ± 1***
Fe^{2+} 1.0 x 10^{-5} M	4	634 ± 17	109 ± 3*
Cu^{2+} 1.0 x 10^{-5} M	4	1130 ± 2	194 ± 0.3***
Cu^{2+} 1.0 x 10^{-6} M	4	622 ± 9	107 ± 2**
Fe^{2+}/EDTA 1.0 x 10^{-4} M	4	765 ± 7	131 ± 1***
DTPA 1.0 x 10^{-3} M	4	508 ± 6	87 ± 1***
H2O2 2.5 x 10^{-4} M	2	522 ± 1	90 ± 0.2***
catalase 200 units/mL	2	492 ± 2	84 ± 0.3
SOD 100 units/mL	2	614 ± 1	105 ± 0.2***

Significant differences compared to control values (*t* test): $*P < 0.05$; $**P < 0.01$, $***P < 0.001$.

We then investigated the effects of Fe^{2+} on 6,7-AMDTQ autoxidation. 6,7-AMDTQ autoxidation in the presence of 10^{-4} M Fe^{2+} exhibited an oxygen consumption rate which was stimulated to 122% of the control values. While stimulation was also observed at 10^{-5} M Fe^{2+}, it was relatively minimal, being only 109% of controls. It was found that 80% and 81% of the oxygen consumed led to the production of H_2O_2 when in the presence of 10^{-4} M and 10^{-5} M Fe^{2+}, respectively. And, upon addition of SOD following autoxidation, 7% of the oxygen consumed for the Fe^{2+} case was returned to the solution, which correlates to a minimum of 14% of the oxygen consumed being converted to $\bullet O_2^-$.

Table 7-7. 6,7-AMDTQ autoxidation, H_2O_2 and $\bullet O_2^-$ produced.

Added Component(s)	Percent O_2 Consumed which was Liberated Upon Addition of:				Percent O_2 Consumed by Pathway Leading to:	
	Catalase		SOD		H_2O_2	$\bullet O_2^-$
	N	% O_2 ± SEM	N	% O_2	% O_2 ± SEM	% O_2
none	3	47 ± 0.4	1	1	94 ± 1	2
Fe^{2+} 1.0×10^{-4} M	3	40 ± 2	1	7	80 ± 3	14
Fe^{2+} 1.0×10^{-5} M	3	40 ± 2	1	0	81 ± 4	0
Cu^{2+} 1.0×10^{-5} M	3	43 ± 1	1	1	86 ± 2	3
Cu^{2+} 1.0×10^{-6} M	3	50 ± 3	1	4	100 ± 5	8
Fe^{2+}/EDTA 1.0×10^{-4} M	3	7.5 ± 0.5	1	2	15 ± 1	4
DTPA 1.0×10^{-3} M	3	44 ± 1	1	1	88 ± 2	2

At 10^{-5} M Cu^{2+}, 6,7-AMDTQ autoxidation was stimulated to 197% of controls. The 10^{-6} M Cu^{2+} had very little effect on the rate, and only increased it to 107% of controls. Unlike Fe^{2+}, Cu^{2+} did not substantially effect the resultant H_2O_2. The percent of oxygen consumed leading to the production of H_2O_2 was 86% and 100% for 10^{-5} M and 10^{-6} M Cu^{2+}, respectively. And the O_2 liberated upon addition of SOD in the Cu^{2+} experiments was minimal, yet detectable.

As mentioned earlier, Fe^{2+}/EDTA has been reported to increase the rate of autoxidation of some neurotoxins above that of Fe^{2+} alone. At 10^{-4} M Fe^{2+}/EDTA, 6,7-AMDTQ autoxidation was stimulated to 131% of controls, only slightly above the

121% of controls observed with Fe^{2+} alone. However, the percent oxygen recovered following the addition of catalase in the Fe^{2+}/EDTA case was only 7%, which signifies 14% of the oxygen consumed led to the production of and/or remained as H_2O_2. And small, yet detectable amounts of $\bullet O_2^-$ were found upon SOD addition to the Fe^{2+}/EDTA combination.

Autoxidation in the absence of any available metal ions was conducted using the strong chelating agent, DTPA. At 10^{-3} M, DTPA inhibited 6,7-AMDTQ autoxidation to only 87% of controls. Addition of catalase following this reaction that the percent of oxygen leading to the production of H_2O_2 was a substantial 88% of the oxygen consumed.

H_2O_2 was the major byproduct in the autoxidation of 6,7-AMDTQ alone. Thus, we were interested in determining if H_2O_2 participated in, or had any effect on, autoxidation. At 250 μM H_2O_2, the rate was inhibited to 90% of controls. This concentration of H_2O_2, by itself, had no effect on oxygen concentrations monitored. With H_2O_2 displaying an inhibitory effect, we decided to add catalase, thereby effectively removing all H_2O_2 produced during 6,7-AMDTQ autoxidation. At 200 units/mL catalase, the rate was found to be 84% of controls. If catalase exerted no effect on autoxidation, the rate should have been 53% of controls. Therefore, catalase either directly or indirectly, through the removal of H_2O_2, stimulated the rate of 6,7-AMDTQ autoxidation. This stimulation was verified with UV-VIS spectroscopy, showing a stimulation to 121% of controls ($k_{app} = 5.8 \pm 0.2$ min^{-1}, λ=518 nm).

We also wanted to determine if $\bullet O_2^-$ played an active role in the mechanism of 6,7-AMDTQ autoxidation. For this, the reaction cell contained 100 units/mL of SOD. The resulting rate was found to be slightly stimulated to 105% of controls. Again, this stimulation was observed with UV-VIS spectroscopy ($k_{app} = 5.8 \pm 0.2$ min^{-1}, 121 ± 4% of controls, λ=518 nm).

C. 6,8-ADTQ

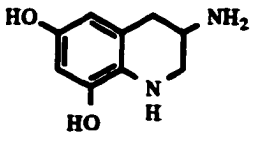

6,8-ADTQ readily undergoes autoxidation at pH 7.4. A UV-VIS spectrum of 200 μM 6,8-ADTQ in the reduced form at pH 7.4 initially shows absorbance maxima at 276 nm and 300 nm (sh). The spectral changes that accompany 6,8-ADTQ autoxidation are shown in Figure 7-10. Upon autoxidation, the band at 276 nm grew and shifted to longer wavelengths (280 nm). Correspondingly, there was an appearance and growth of bands at 460 nm (sh) and 232 nm, and a baseline increase between the bands at 280 nm and 460 nm. At the completion of autoxidation, the band at 280 nm began to decrease and shift to longer wavelengths and the overall baseline began to increase. This general increase in absorbance throughout the spectrum corresponded to the appearance of dark precipitates in the solution, presumably indicating polymerization. Similar spectral changes occurred at higher and lower pH values, with the resultant rate being proportional to pH. As we would expect, there was no observed oxidation at pH values below 3.4.

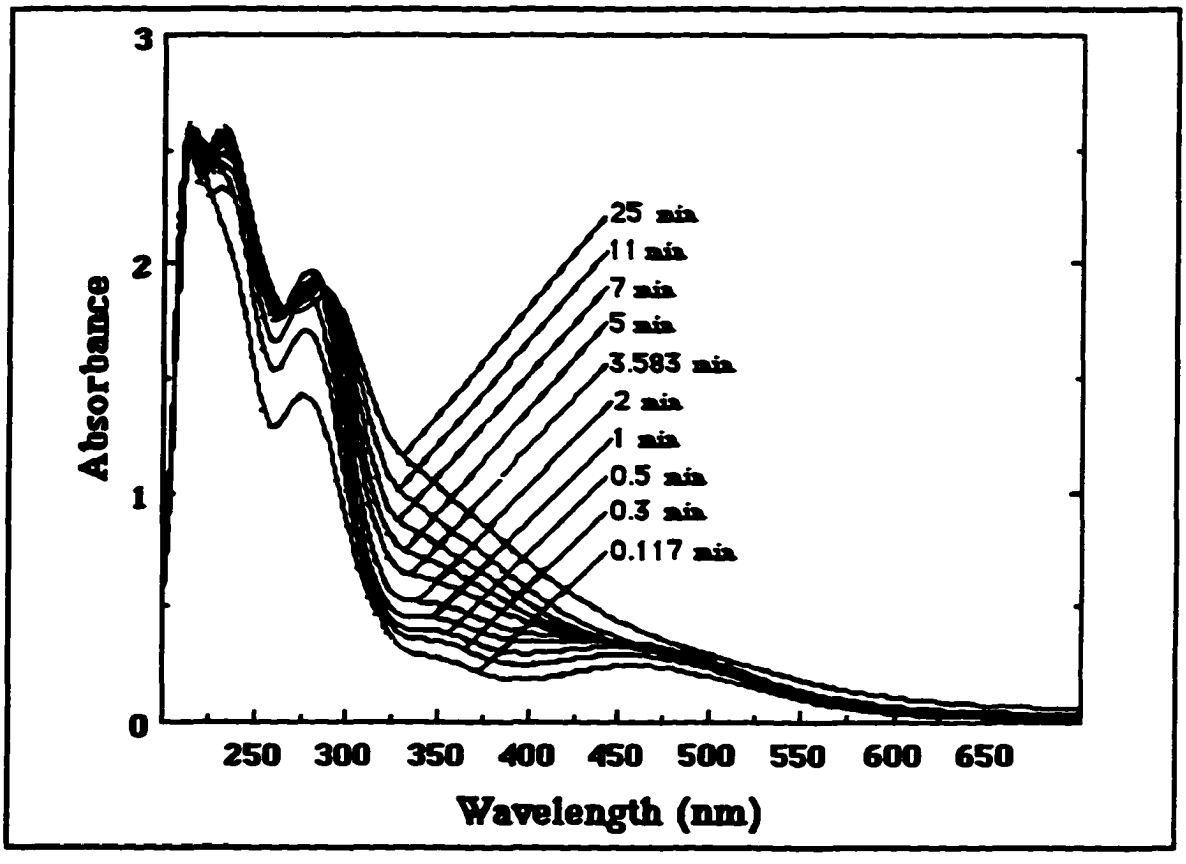

Figure 7-10. UV-VIS spectra of 6,8-ADTQ autoxidation at pH 7.4 and 37°C.

Autoxidation reaction orders were determined using the oxygen electrode for each of 6,8-ADTQ, O_2, H^+. Using 6,8-ADTQ concentrations of 98, 147, 196, and 246 μM, an initial O_2 concentration of 248 μM, and a pH of 7.4, the autoxidation reaction order for 6,8-ADTQ was found to be approximately 1.0, as shown in Figure 7-11. Holding the initial toxin concentration at 196 μM and the pH at 7.4, and varying the concentration of O_2 between 160 and 563 μM, the oxygen reaction order was determined to be approximately 3/4, as shown in Figure 7-12. Keeping the initial O_2 and 6,8-ADTQ concentrations constant and using pH values of 5.4, 6.4, 7.4, and 8.4, the reaction order with respect to H^+ was approximately -1/2, as shown in Figure 7-13. Extracted from the

data in Figures 7-11 to 7-13, the rate constant for 6,8-ADTQ autoxidation at 37°C was found to be $k = 0.0048 \pm 0.0003\ M^{-1/4}sec^{-1}$, and the rate expression was:

$$rate = k[tox][O_2]^{0.75}[H^+]^{0.5}$$

These results are summarized in Table 7-8.

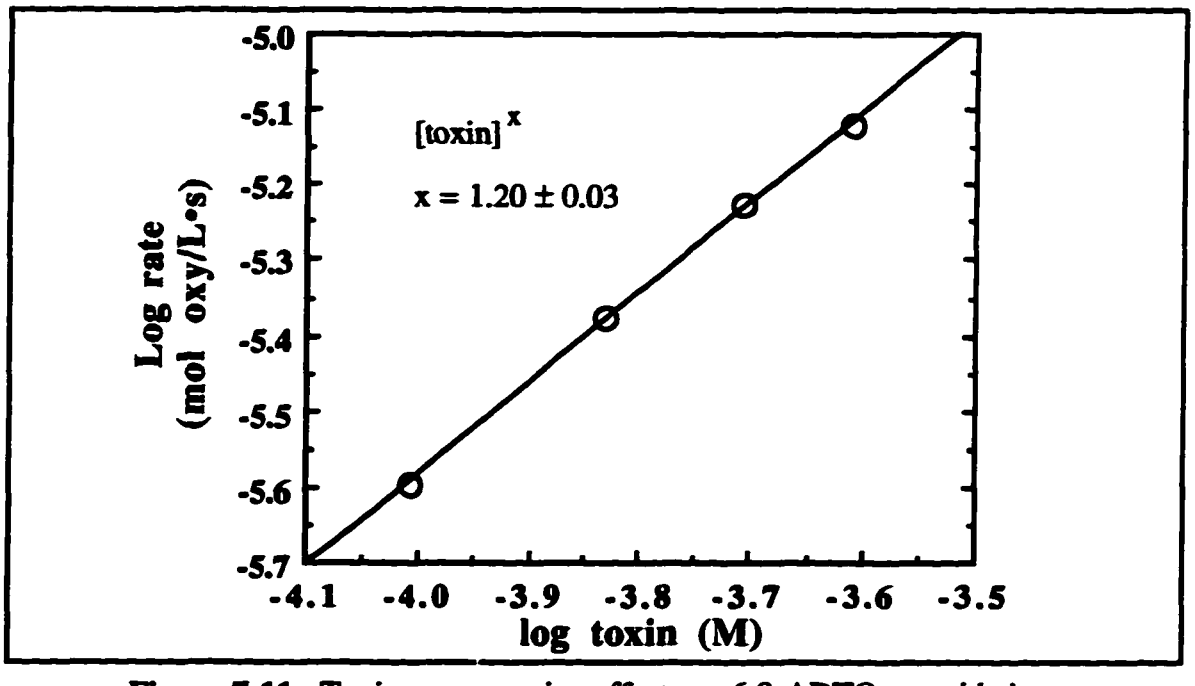

Figure 7-11. Toxin concentration effects on 6,8-ADTQ autoxidation.

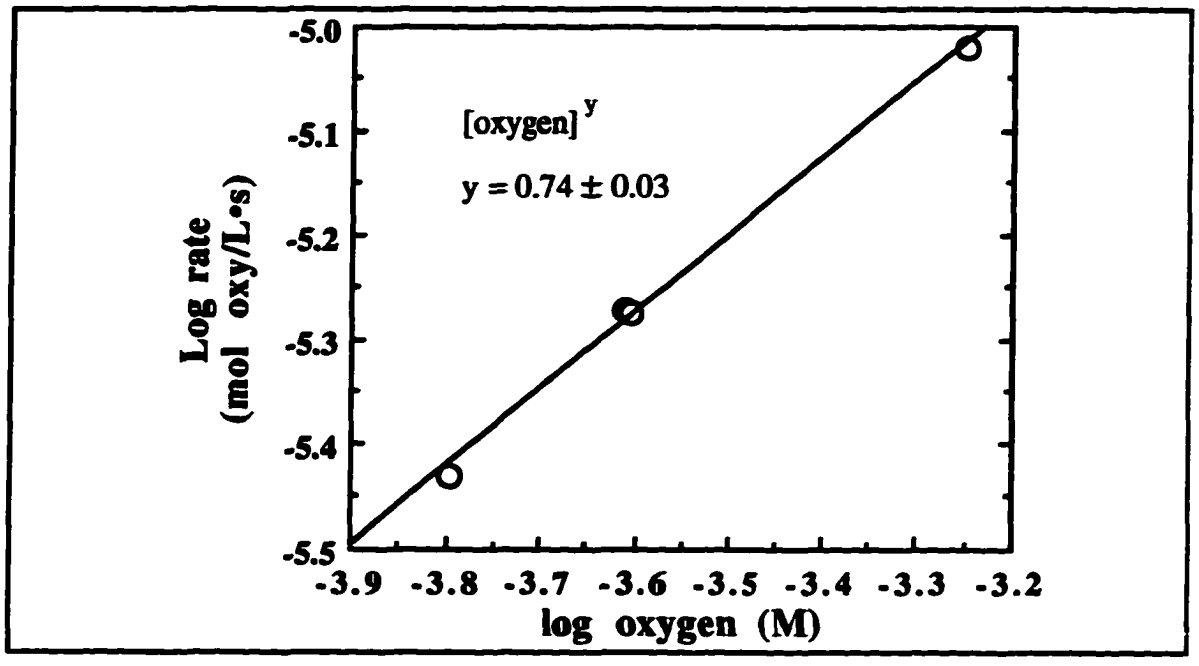

Figure 7-12. Oxygen concentration effects on 6,8-ADTQ autoxidation.

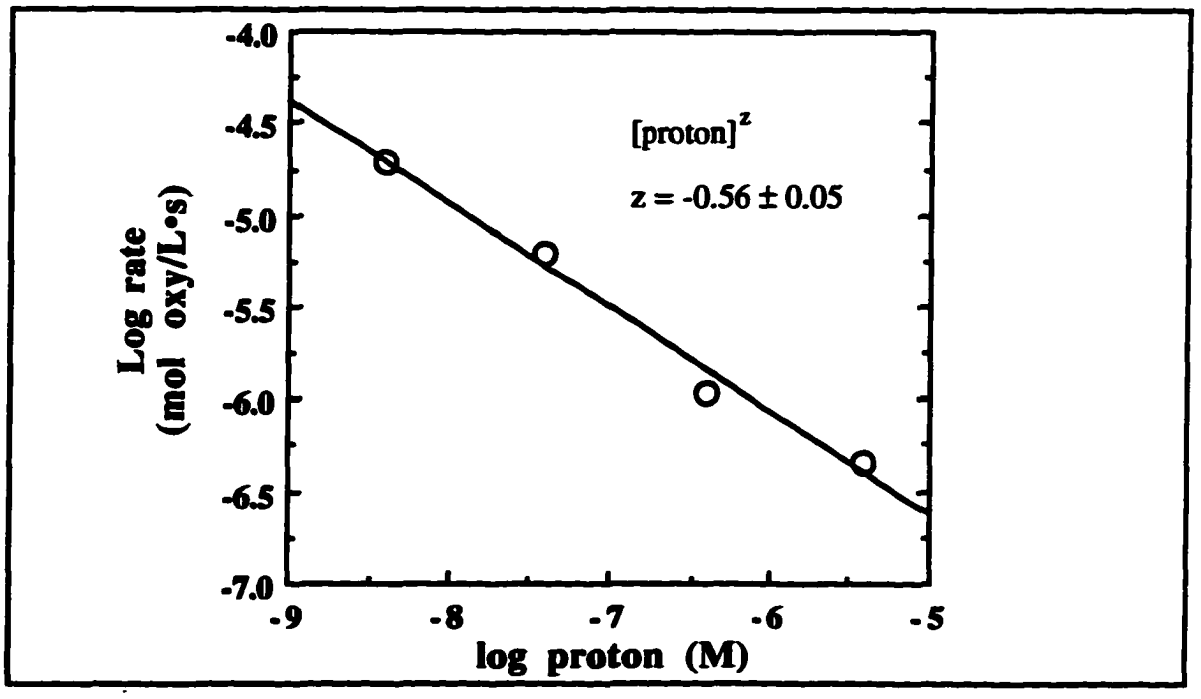

Figure 7-13. The effects of pH on 6,8-ADTQ autoxidation.

Table 7-8. 6,8-ADTQ autoxidation reaction orders with respect to individual components.

Reaction Orders	
rate = $k[tox]^x[O_2]^y[H^+]^z$	
x	1.20 ± 0.03
y	0.74 ± 0.03
z	-0.56 ± 0.05
k	0.0048 ± 0.0003 $M^{-0.38}sec^{-1}$

6,8-ADTQ autoxidation rates in the absence and presence of various stimulating and/or inhibiting agents are presented in Table 7-9. The percentage of oxygen consumed during 6,8-ADTQ autoxidation leading to the production of H_2O_2 and superoxide is presented in Table 7-10. In these studies, the concentration of 6,8-ADTQ was 196 μM, the initial concentration of O_2 was approximately 250 μM, and the pH was 7.4. Stimulating and/or inhibiting agents added to the reaction mixture in this study showed no oxygen effects when presented by themselves.

Autoxidation of 6,8-ADTQ in the absence of any added substances was complete in less than 1.2 min and showed an initial rate consumption rate of 344 μmol O_2/L•min (UV-VIS spectroscopy determined k_{app} = 3.6 ± 0.2 min^{-1}, λ=276 nm). Surprisingly, the oxygen liberated upon addition of catalase following autoxidation was considerably less than expected, being 30% of oxygen consumed. The percent oxygen consumed leading to the production of H_2O_2, therefore, was 60%. The oxygen liberated by the addition of SOD was 2% of the oxygen consumed during autoxidation.

Table 7-9. 6,8-ADTQ autoxidation, initial rate of oxygen consumption.

Added Component(s)	Initial O_2 Consumption		
	N	rate ± SEM (μmol O_2 / L•min)	rate ± SEM % controls
none	7	344 ± 6	100 ± 2
Fe^{2+} 1.0 x 10^{-4} M	4	437 ± 7	127 ± 2***
Fe^{2+} 1.0 x 10^{-5} M	4	392 ± 6	114 ± 2***
Cu^{2+} 1.0 x 10^{-5} M	5	591 ± 10	173 ± 3***
Cu^{2+} 1.0 x 10^{-6} M	4	348 ± 6	101 ± 2
Fe^{2+}/EDTA 1.0 x 10^{-4} M	4	622 ± 6	181 ± 2***
DTPA 1.0 x 10^{-3} M	4	366 ± 3	106 ± 1*
H2O2 2.5 x 10^{-4} M	3	438 ± 1	127 ± 0.3***
catalase 200 units/mL	2	264 ± 1	77 ± 0.2
SOD 100 units/mL	2	363 ± 1	106 ± 0.1*

Significant differences compared to control values (*t* test): $*P < 0.05$; $***P < 0.001$.

In our investigation of transition metal ion effects on 6,8-ADTQ autoxidation, we began with Fe^{2+}. A 10^{-4} M Fe^{2+} solution stimulated the observed rate to 127% of controls. A 10^{-5} M Fe^{2+} solution also showed a stimulation in rate to 114% of controls. There was a dramatic decrease in the oxygen liberated upon the addition of catalase which was related to the Fe^{2+} concentration. The percent oxygen consumed which returned to the solution was 4.4% for 10^{-4} M Fe^{2+} and 18% for 10^{-5} M Fe^{2+}. And while there was no $\bullet O_2^-$ detected at 10^{-5} M Fe^{2+} following SOD addition, 4% of the oxygen consumed during autoxidation was returned to the solution at 10^{-4} M Fe^{2+}.

Table 7-10. 6,8-ADTQ autoxidation, H_2O_2 and $\bullet O_2^-$ produced.

Added Component(s)	Percent O_2 Consumed which was Liberated Upon Addition of:				Percent O_2 Consumed by Pathway Leading to:	
	Catalase		SOD		H_2O_2	$\bullet O_2^-$
	N	% O_2 ± SEM	N	% O_2	% O_2 ± SEM	% O_2
none	5	30 ± 1	1	2	60 ± 3	3
Fe^{2+} 1.0×10^{-4} M	3	4.4 ± 0.5	1	4	9 ± 1	8
Fe^{2+} 1.0×10^{-5} M	4	18 ± 2		NA	37 ± 4	NA
Cu^{2+} 1.0×10^{-5} M	4	22 ± 0.6	1	0	46 ± 1	0
Cu^{2+} 1.0×10^{-6} M	3	24 ± 1	1	6	46 ± 2	12
Fe^{2+}/EDTA 1.0×10^{-4} M	3	1.3 ± 0.2	1	1	2.6 ± 0.4	3
DTPA 1.0×10^{-3} M	3	33 ± 0.3	1	1	66 ± 0.6	2

We then looked at Cu^{2+} effects on autoxidation. We observed stimulatory effects at 10^{-5} M Cu^{2+} to 172% of controls. But, at 10^{-6} M Cu^{2+} there was no stimulation present. The percent oxygen consumed during autoxidation leading to H_2O_2 was decreased to 46% at 10^{-5} M Cu^{2+}. Interestingly, 10^{-6} M Cu^{2+} had no effect on rate, but the amount of oxygen liberated by the addition of catalase was the same as that seen with 10^{-5} M Cu^{2+}.

Fe^{2+} complexed with EDTA, as previously mentioned, stimulates autoxidation of 6-HDA type compounds to a higher degree than does Fe^{2+} alone. The rate of 6,8-ADTQ autoxidation was stimulated substantially over that of Fe^{2+} alone. And, the oxygen returned to the solution following the addition of catalase was decreased compared to that

found with Fe^{2+} alone. The oxygen liberated by catalase was 1.3% of the oxygen consumed. That is to say, the percent oxygen consumed during autoxidation which led to and/or remained as H_2O_2 was 2.6%. Furthermore, an equal amount of oxygen was returned upon the addition of SOD, thus, indicating the presence of $\bullet O_2^-$.

By incorporating DTPA, we were able to investigate the rate of 6,8-ADTQ autoxidation in the absence of, essentially, all metal ions. At 10^{-3} M, DTPA showed no inhibitory effects on the rate, but surprisingly displayed the opposite. DTPA slightly stimulated 6,8-ADTQ autoxidation to a value of 106% of controls. Additionally, the H_2O_2 produced accounted for 66% of the oxygen consumed.

It is apparent that H_2O_2 is not the sole reduced oxygen by-product resulting from 6,8-ADTQ autoxidation; however, it is the major species resulting when in the absence of metal ions. Therefore, we were interested in determining if H_2O_2 was intimately involved in the autoxidation reaction or if it was just a simple by-product. In the presence of 250 μM H_2O_2, the rate of 6,8-ADTQ autoxidation was stimulated to 127% of controls. This stimulation was substantiated from UV-VIS investigations (k_{app}=4.2 ± 0.1 min^{-1}, 118% of controls, λ=276 nm). Thus, it appears that H_2O_2 plays a role in the overall autoxidation process of 6,8-ADTQ. We further investigated this by conducting autoxidation in the presence of 200 units/mL catalase. The corresponding rate was 76% of controls. Since 30% of the oxygen consumed was returned to the solution following the addition of catalase with 6,8-ADTQ alone, one would expect the rate in the presence of catalase, assuming no effects, to be approximately 70% of controls. Furthermore, since H_2O_2 stimulates 6,8-ADTQ autoxidation, by eliminating all produced H_2O_2 during autoxidation we would expect the rate to be even less. However, this was not the case. Therefore, it appears that catalase itself stimulates the autoxidation of 6,8-ADTQ. The stimulation by catalase was further verified by UV-VIS spectroscopy, showing the k_{app} to be 121% of controls (k_{app} = 4.3 ± 0.2 min^{-1}, 276 nm).

Superoxide has been suggested to play a role in the mechanism of autoxidation for toxins similar to 6,8-ADTQ. By conducting 6,8-ADTQ autoxidation in the presence of SOD, all "free" $\bullet O_2^-$ produced during autoxidation should effectively be removed. Using 100 units/mL SOD, we found the rate actually increased to 106% of controls. The increase was also observed using UV-VIS spectroscopy, with a stimulation to 115% of controls ($k_{app} = 4.1 \pm 0.1$ min^{-1}, 276 nm).

D. 6-HDA

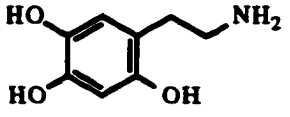

Autoxidation of 6-HDA and its production of reactive oxygen species have been extensively studied and will be elaborated upon in the discussion section. In our studies we have incorporated 6-HDA for (1) comparative purposes, (2) to verify and clarify literature results, and (3) to possibly add new information and insight to the already existing vast base of knowledge on 6-HDA chemistry.

6-HDA readily undergoes autoxidation at pH 7.4 in an air saturated phosphate buffer, forming a pink-red colored solution. A UV-VIS spectrum of reduced 6-HDA initially displays band maxima at 214 nm and 284 nm. Spectral changes that accompany 200 μM 6-HDA autoxidation at a pH of 7.4 and 37°C are shown in Figure 7-14. Upon initiation of autoxidation, the band at 284 nm grew and shifted to shorter wavelengths (268 nm), in the process yielding isobestic points at 292 nm and 312 nm. Correspondingly, the band at 214 nm grew and shifted to longer wavelengths (218 nm) and a new band appeared at 486 nm. The new band at 486 nm accounts for the pink-red color acquired by the solution as 6-HDA autoxidizes. All bands continued to grow until

completion of autoxidation, at which point absorbances stabilized. At extended times following autoxidation, the absorbance bands began to decrease and the baseline increased. These observed changes were both pH and temperature dependent.

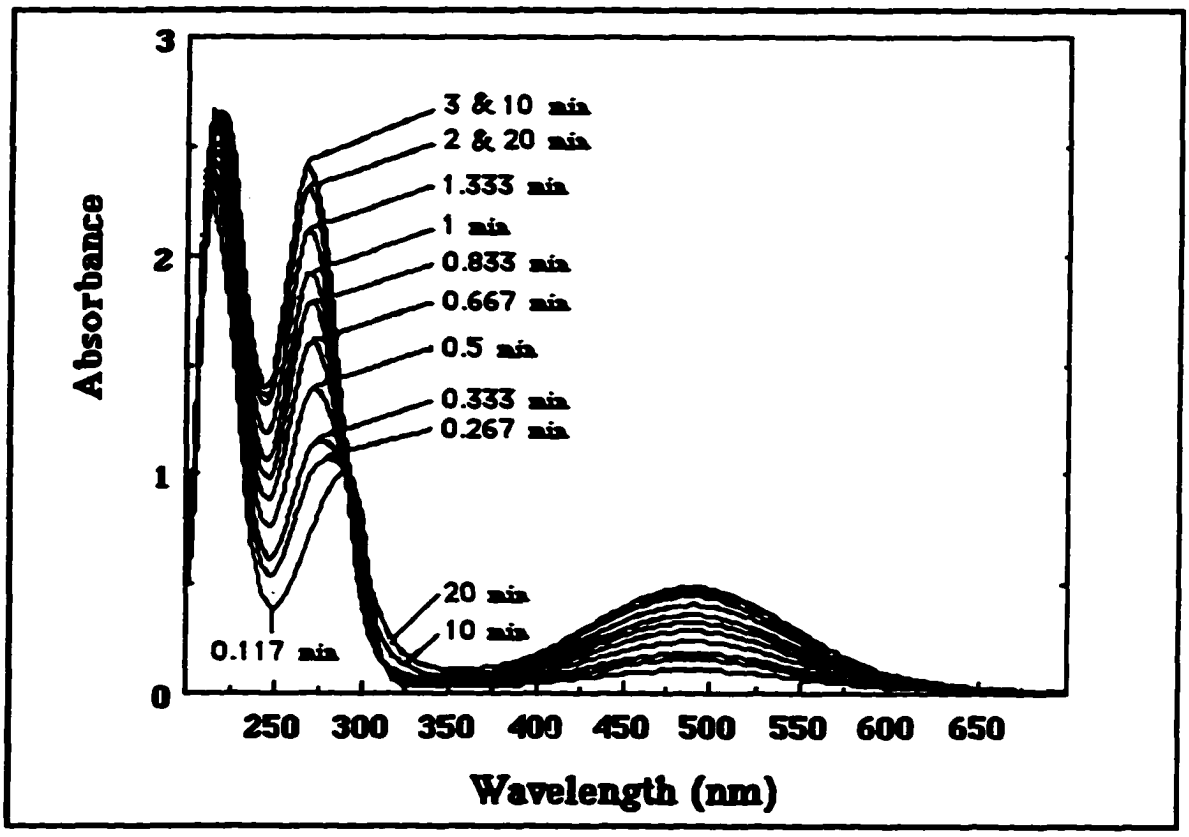

Figure 7-14. UV-VIS spectra of 6-HDA autoxidation at pH 7.4 and 37°C.

Autoxidation reaction orders with respect to 6-HDA, O_2, and H^+ were determined utilizing an oxygen electrode. While at 25°C 6-HDA shows first order reaction kinetics with respect to the toxin (data not shown), at 37°C the reaction order changed. By determining the rate of oxygen consumption during autoxidation of 147, 196, 245, and 294 μM 6-HDA, using a fixed pH of 7.4, and an initial O_2 concentration of 247 μM, the reaction order for 6-HDA at 37°C was determined to be approximately 3/2, as shown in

Figure 7-15. At a pH of 7.4 and an initial 6-HDA concentration of 196 μM, the initial concentration of O_2 was varied between 114 and 553 μM to obtain the plot presented in Figure 7-16. Using this plot, the O_2 reaction order was determined to be approximately 1/3. Employing pH values of 5.4, 6.4, 7.4, and 8.4, the proton reaction order was found to be -1/3 and is graphically displayed in Figure 7-17. Using the information in Figures 7-15 to 7-17, the overall reaction rate constant was calculated to be $k = 0.031 \pm 0.003\ M^{-1/2}sec^{-1}$, and the rate expression was:

$$rate = k[tox]^{1.5}[O_2]^{0.33}[H^+]^{-0.33}$$

These results are summarized in Table 7-11.

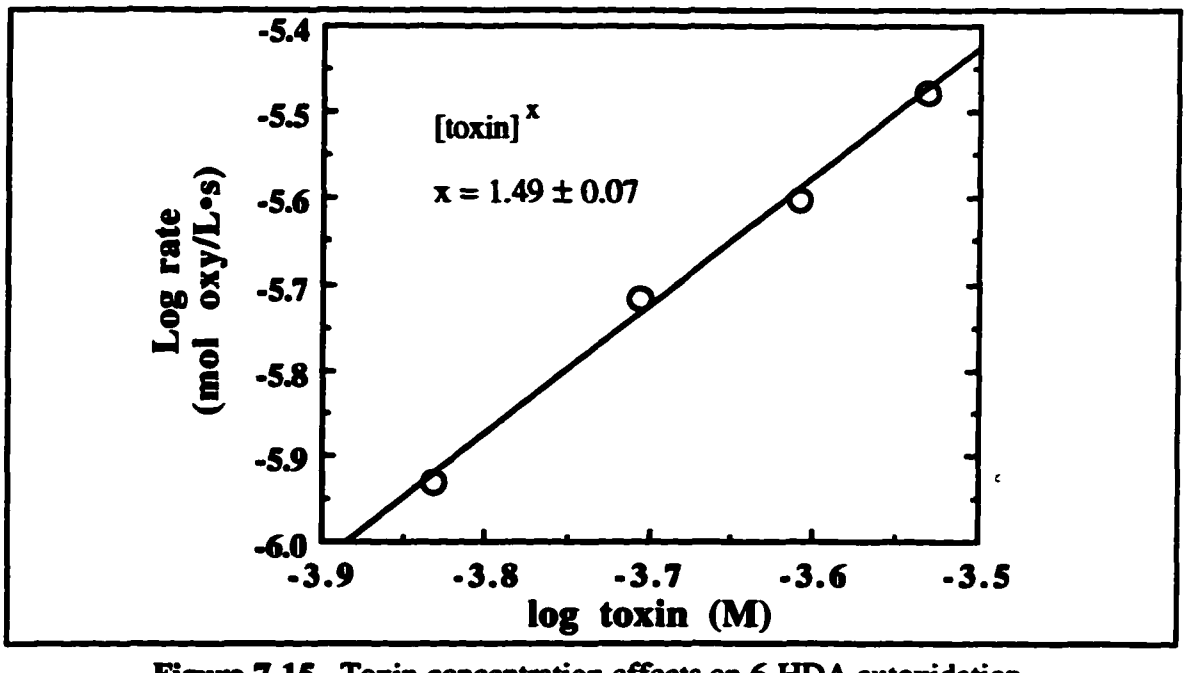

Figure 7-15. Toxin concentration effects on 6-HDA autoxidation.

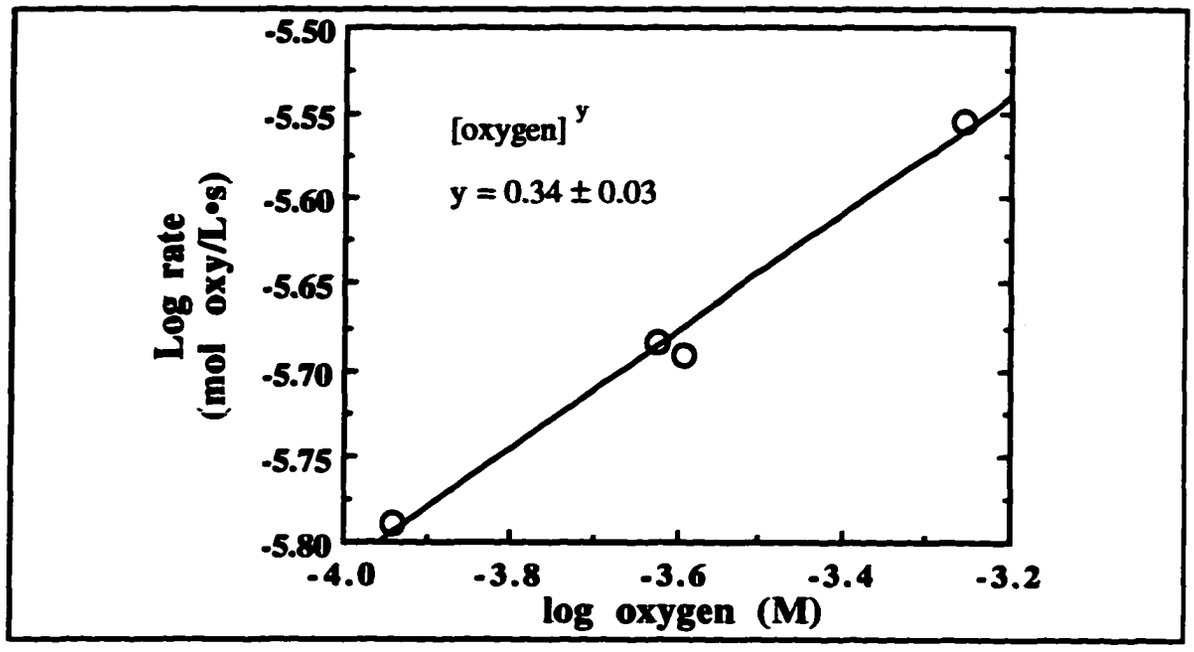

Figure 7-16. Oxygen concentration effects on 6-HDA autoxidation.

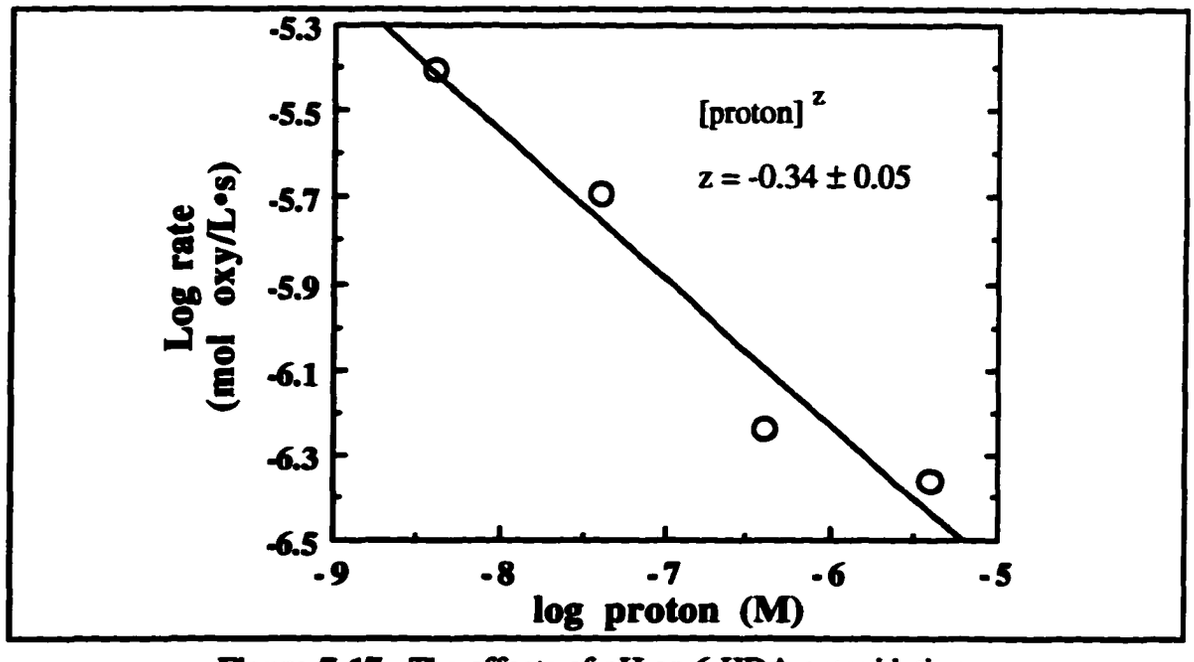

Figure 7-17. The effects of pH on 6-HDA autoxidation.

Table 7-11. 6-HDA autoxidation reaction orders with respect to individual components.

Reaction Orders	
rate = $k[tox]^x[O_2]^y[H^+]^z$	
x	1.49 ± 0.07
y	0.34 ± 0.03
z	-0.34 ± 0.05
k	0.031 ± 0.003 $M^{-0.49}sec^{-1}$

The rate of 6-HDA autoxidation alone and in the presence of various catalysts and/or inhibitors of this reaction are presented in Table 7-12. Furthermore, the percent oxygen consumed during autoxidation leading to the production of H_2O_2 and $\bullet O_2^-$ is given in Table 7-13. In the following studies the initial concentration of O_2 was approximately 250 μM, the 6-HDA concentration was 196 μM, and the pH was 7.4.

Autoxidation of 6-HDA in the absence of any catalysts or inhibitors was completed in less than two minutes and displayed an initial rate of 123 μmol O_2/L•min. From UV-VIS spectroscopic studies, the rate showed a k_{app} = 1.35 ± 0.02 min^{-1} (λ = 486 nm). Following the completion of autoxidation, when employing the oxygen electrode, the addition of catalase returned 40% of the oxygen consumed back to the solution. Therefore, the majority of the oxygen consumed (minimum of 80%) during 6-HDA autoxidation was accounted for by the production of H_2O_2. These results correlate well with those of the literature.[33,34,37]

Table 7-12. 6-HDA autoxidation, initial rate of oxygen consumption.

Added Component(s)	Initial O_2 Consumption		
	N	rate ± SEM (μmol O_2 / L•min)	rate ± SEM % controls
none	5	123 ± 3	100 ± 2
Fe^{2+} 1.0 x 10^{-4} M	3	324 ± 3	264 ± 3***
Fe^{2+} 1.0 x 10^{-5} M	3	187 ± 1	153 ± 1***
Cu^{2+} 1.0 x 10^{-5} M	4	1012 ± 10	825 ± 8***
Cu^{2+} 1.0 x 10^{-6} M	4	169 ± 2	137 ± 2***
Fe^{2+}/EDTA 1.0 x 10^{-4} M	4	1176 ± 12	958 ± 10***
DTPA 1.0 x 10^{-3} M	4	123 ± 2	100 ± 2
H2O2 2.5 x 10^{-4} M	2	114 ± 1	93 ± 1*
catalase 200 units/mL	2	11 ± 2	9 ± 1
SOD 100 units/mL	2	10.0 ± 0.2	8.2 ± 0.1***

Significant differences compared to control values (*t* test): $*P < 0.05$; $***P < 0.001$.

It has been reported that the rate of 6-HDA autoxidation is stimulated in the presence of transition metal ions.[36,165,171-173] We also found this to be so. At 10^{-4} M Fe^{2+} autoxidation was increased to 264% of controls, while at 10^{-5} M Fe^{2+} the rate was increased to 153% of controls. The H_2O_2 produced from or, at least, available at the completion of the autoxidation decreased in an Fe^{2+} concentration dependent manner. The percent oxygen consumed that was liberated upon the addition of catalase was 12% and 25% for 10^{-4} M and 10^{-5} M Fe^{2+}, respectively. Therefore, in the presence of Fe^{2+} there is a significant decrease in the production or availability of H_2O_2 following 6-HDA autoxidation. This has also previously been observed.[165]

Table 7-13. 6-HDA autoxidation, H_2O_2 and $\bullet O_2^-$ produced.

Added Component(s)	Percent O_2 Consumed which was Liberated Upon Addition of:				Percent O_2 Consumed by Pathway Leading to:	
	Catalase		SOD		H_2O_2	$O_2^{-\bullet}$
	N	% O_2 ± SEM	N	% O_2	% O_2 ± SEM	% O_2
none	3	40 ± 2	1	4	80 ± 4	8
Fe^{2+} 1.0×10^{-4} M	3	12.3 ± 0.4	1	6	25 ± 1	12
Fe^{2+} 1.0×10^{-5} M	3	25 ± 1		NA	50 ± 2	NA
Cu^{2+} 1.0×10^{-5} M	3	40 ± 1	1	5	81 ± 2	9
Cu^{2+} 1.0×10^{-6} M	3	36 ± 2	1	4	71 ± 4	8
Fe^{2+}/EDTA 1.0×10^{-4} M	3	5.9 ± 0.5	1	5	12 ± 1	9
DTPA 1.0×10^{-3} M	3	49 ± 2	1	4	97 ± 3	8

In the presence of 10^{-5} M Cu^{2+}, 6-HDA autoxidation rate was amazingly increased to 825% of controls. At 10^{-6} M Cu^{2+}, however, the rate was stimulated to only 137% of controls. And, the percent oxygen consumed which led to the production of H_2O_2 was not significantly different from that found for controls. Therefore, while Cu^{2+} stimulates 6-HDA autoxidation dramatically, it does not appear to alter the resultant reduced oxygen species.

Fe^{2+}/EDTA has been reported to enhance the rate of 6-HDA autoxidation over that found with Fe^{2+} alone.[36,38,173] We found that at 10^{-4} M Fe^{2+}/EDTA, autoxidation was dramatically stimulated to a rate of 1176 μmol O_2/L•min, which was 958% of

controls. Furthermore, the percent oxygen returned to the solution following catalase addition was substantially lowered (6%) in comparison to that observed with Fe^{2+} (12%).

It has been proposed by various research groups that 6-HDA autoxidation is metal ion mediated.[38,172] Furthermore, in the presence of an effective chelating agent, the rate of 6-HDA autoxidation has been reported to substantially decrease.[38,173] However, this inhibition of autoxidation by a chelator alone has met with some disagreement.[36,165,172] Therefore, we were interested in investigating the effects of strong metal chelation on autoxidation. At 10^{-3} M DTPA, 6-HDA autoxidation displayed no difference in rate from that of controls. Interestingly, upon addition of catalase following this reaction, the percent oxygen consumed leading to H_2O_2 was nearly quantitative in nature, being 97% of controls. Therefore, while effective metal chelation did not appear to affect autoxidation rates, it did either enhance the production of H_2O_2 or inhibit the follow-up reactions of H_2O_2 with various metal ions, i.e., Fenton and Haber-Weiss chemistry.

The major byproduct of 6-HDA autoxidation is H_2O_2. H_2O_2, itself, has the ability to oxidize 6-HDA.[162] Therefore, we wanted to investigate the active participation, if any, of H_2O_2 on 6-HDA autoxidation. At 250 μM H_2O_2, autoxidation was slightly inhibited to 93% of controls. In order to further investigate this H_2O_2 effect, catalase was employed. At 200 units/mL catalase, the initial rate of autoxidation was significantly inhibited to 9% of controls. This effect was interesting, yet inhibition has been reported by other researchers.[36,65,165] Using UV-VIS spectroscopy, we again found an inhibition by catalase. However, we observed an initial lag period which was followed by a more rapid rate of autoxidation. The inhibition apparently measured with the oxygen electrode system actually corresponded to the initial lag period. Following this lag period, UV studies showed an inhibition of 6-HDA autoxidation by catalase to 47% of controls ($k_{app} = 0.641 \pm 0.009$ min^{-1}, $\lambda = 486$ nm).

There is a large amount of research showing that SOD greatly inhibits 6-HDA autoxidation.[34,35,65,164] Conversely, it has also been demonstrated that SOD has very little effect on 6-HDA autoxidation except in the presence of strong metal chelating agents.[36,38,175] Therefore, we incorporated SOD in the initial autoxidation reaction mixture and found a dramatic inhibition of rate. The rate was found to be 8% of controls. From UV studies we again found this dramatic inhibition seen with the oxygen electrode to be the lag period rate. However, following the lag period, 6-HDA inhibition was still observed at 29% of controls ($k_{app} = 0.39 \pm 0.02$ min^{-1}, $\lambda = 486$ nm).

V. Discussion

A. Rates of Autoxidation

1. Toxin Autoxidation Rates

The ability of molecular oxygen to oxidize 6,7-ADTQ, 6,7-AMDTQ, 6,8-ADTQ, and 6-HDA was followed by both oxygen consumption and UV-VIS absorbance changes. Figure 7-18 summarizes the rates of autoxidation of the various agents obtained using an oxygen electrode. We see that autoxidation rates under the tested conditions decrease in the order of 6,7-AMDTQ > 6,7-ADTQ > 6,8-ADTQ > 6-HDA. A summary of the determined reaction orders and the rate constants is presented in Table 7-14.

From the UV-VIS spectroscopic results, it appears that, while none of the oxidized forms of the compounds are completely stable, oxidized 6,7-ADTQ and 6,8-ADTQ rapidly undergoe some form of follow-up polymerization. Oxidized 6,7-AMDTQ and 6-HDA display slow spectral changes with time; however, these changes, which occur up to 15 hours, do not appear to be associated with polymerization due to the fact that there is an absence of an overall baseline absorption increase.

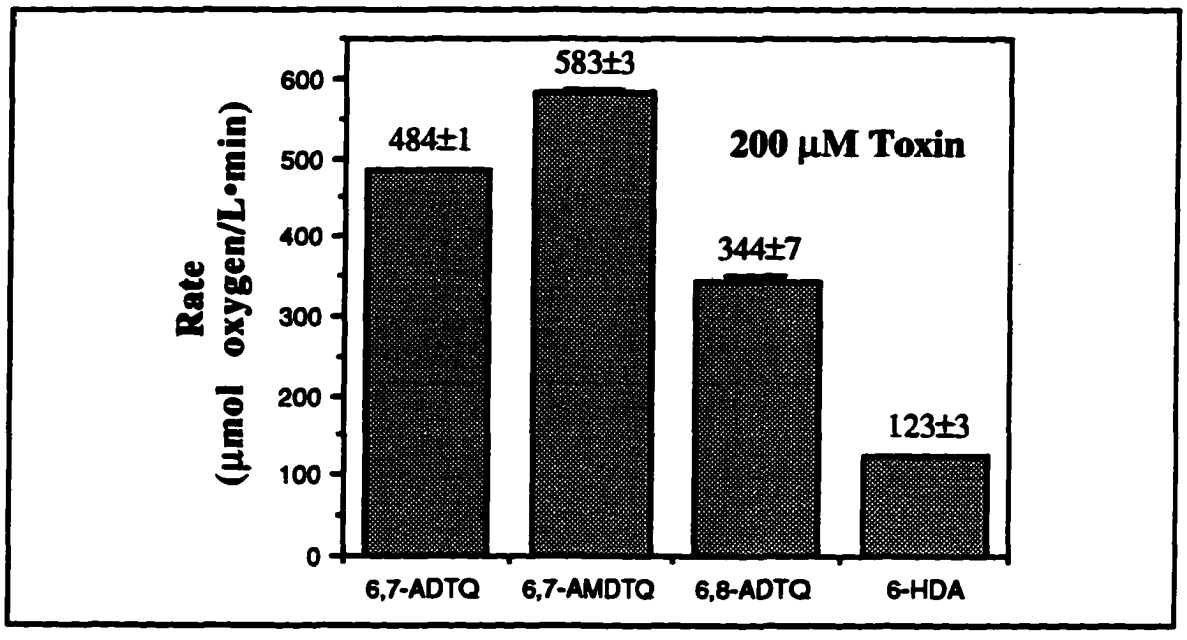

Figure 7-18. Rates of autoxidation of the quinoline agents and 6-HDA.

Table 7-14. A toxin comparison of autoxidation reaction orders and rate constants.

Reaction Orders				
rate = $k[tox]^x[O_2]^y[H^+]^z$				
Agents	x	y	z	k ($M^{(1-x-y-z)}sec^{-1}$)
6,7-ADTQ	0.95 ± 0.06	0.86 ± 0.08	-0.47 ± 0.02	0.0010 ± 0.0005
6,7-AMDTQ	0.96 ± 0.03	0.54 ± 0.06	-0.24 ± 0.02	0.0485 ± 0.0009
6,8-ADTQ	1.20 ± 0.03	0.74 ± 0.03	-0.56 ± 0.05	0.0048 ± 0.0003
6-HDA	1.49 ± 0.07	0.34 ± 0.03	-0.34 ± 0.05	0.031 ± 0.003

2. Effects of SOD, Catalase, and H_2O_2

As noted earlier, SOD effectively removes any "free" $\bullet O_2^-$ and produces singlet oxygen, O_2^*, and H_2O_2. Catalase eliminates H_2O_2 to produce oxygen and water. Therefore, by individually including these enzymes in the reaction cell with our compounds, we were able to determine autoxidation dependence, if any, on these reduced oxygen species.

Spin restrictions dictate that, whether by direct reduction of molecular oxygen or by way of a co-reductant, electrons are transferred to oxygen one at a time. Therefore, autoxidation must generate $\bullet O_2^-$. However, this may not be "free" $\bullet O_2^-$ and/or may be extremely short lived due to rapid electron transfer kinetics. The mechanism of autoxidation of 6-HDA and some related analogs depends on the presence of $\bullet O_2^-$, where as other 6-HDA analogs, in particular 6-ADA, proceed by pathways unaffected by the removal of $\bullet O_2^-$, suggesting very rapid electron transfer kinetics.

We found that SOD, at 100 units/mL, actually stimulated autoxidation of the quinoline analogs, while inhibiting that of 6-HDA. This inhibition of 6-HDA autoxidation has been reported by many research groups.[34,35,65,164,165] It has recently been shown, however, that small, catalytic amounts of SOD (<10 units/mL) have no major effect on 6-HDA autoxidation except in the presence of strong metal chelators.[36,38,175] This suggests that in the absence of metal chelation, 6-HDA produces a toxin•metal•oxygen complex by which no "free" $\bullet O_2^-$ is produced. However, in the presence of a metal chelator or high concentrations of SOD, which has been established to effectively chelate metal ions,[38] 6-HDA oxidation mechanism changes to produce "free" $\bullet O_2^-$, which then participates in the overall oxidation reaction and is shown in Figure 7-19.

$$6\text{-HDA} + O_2 \longrightarrow {}^{\bullet}SQ + {}^{\bullet}O_2^- + H^+$$

$$6\text{-HDA} + {}^{\bullet}O_2^- + H^+ \longrightarrow {}^{\bullet}SQ + H_2O_2$$

$${}^{\bullet}SQ + O_2 \longrightarrow Q + {}^{\bullet}O_2^- + H^+$$

$${}^{\bullet}SQ + {}^{\bullet}O_2^- \longrightarrow Q + H_2O_2$$

$${}^{\bullet}SQ + {}^{\bullet}SQ \longrightarrow Q + 6\text{-HDA}$$

overall summary $\quad 6\text{-HDA} + O_2 \longrightarrow Q + H_2O_2$

Figure 7-19. Possible autoxidation mechanisms of 6-HDA.

At SOD concentration used in our studies, we observed no inhibition of quinoline analog autoxidation and, in fact, we observed a stimulation. This may partially be explained from the fact that H_2O_2 inhibits the quinoline autoxidation rates, and by removing ${}^{\bullet}O_2^-$ with SOD, little or no H_2O_2 can be formed. This suggests that the mechanism by which our toxins autoxidize is different than that of 6-HDA, i.e., ${}^{\bullet}O_2^-$ independent. However, another plausible explanation for this observance, which does not explain the stimulation, is that our toxins may form tighter complexes with metal ions than does 6-HDA, thereby not allowing SOD to chelate all of the metal ions, forcing the existence of "free" ${}^{\bullet}O_2^-$. Furthermore, the electron transfer kinetics of our toxins may be such, that both electrons are transferred almost instantaneously, thus, not allowing time for SOD to exert its effects.

Catalase exerted stimulatory effects on autoxidation of the quinoline analogs and inhibited 6-HDA autoxidation. It was found that H_2O_2, added to the reaction solution, actually inhibited autoxidation of 6,7-ADTQ, 6,7-AMDTQ, and 6-HDA to some degree. Therefore, the stimulation elicited by catalase is most likely due to the removal of H_2O_2 from the reaction medium. This, however, does not explain the effects observed with 6,8-ADTQ in which there is a stimulation in rate with both H_2O_2 and catalyst.

The inhibition of 6-HDA by catalase has been reported previously.[65,165] However, recent reports suggest that catalase, itself, does not exert the inhibitory effects, but rather the inhibition is due to the trace contamination of catalase with SOD.[38] We find this SOD contamination theory insufficient to explain the massive inhibition observed with catalyst on 6-HDA. Even assuming 5% contamination in our study, there would only be 10 units/mL SOD in the reaction cell. And this concentration of SOD has been shown to produces little 6-HDA inhibition (approx. 7% inhibition).[38]

3. Role of Metal Ions in Autoxidation

It has been proposed that the oxidation of 6-HDA and related agents is mediated by a co-reductant, such as transition metal ions.[38,172] Various research groups have reported some degree of inhibition of 6-HDA autoxidation in response to complete metal chelation by desferrioxamine[38,173] and DTPA.[36,65,173] Our current results indicate that autoxidation of our compounds and 6-HDA are, at least in part, metal ion mediated and/or catalyzed.

Autoxidation rates of our toxins were stimulated by Fe^{2+} and Cu^{2+} in a concentration dependent manner, and is exemplified in Figure 7-20 for 100 μM Fe^{2+} and in Figure 7-21 for 10 μM Cu^{2+}. However, in the presence of DTPA (1 mM), autoxidation rates of the quinoline agents were not dramatically effected (see Figure 7-23). And, as mentioned previously, SOD inhibited only 6-HDA autoxidation, while actually stimulating autoxidation of the ADTQ analogs. This inhibition of 6-HDA autoxidation by SOD has been previously discussed and is believed to dependent on both the SOD activity and the ability of SOD to chelate metal ions at the concentrations used.

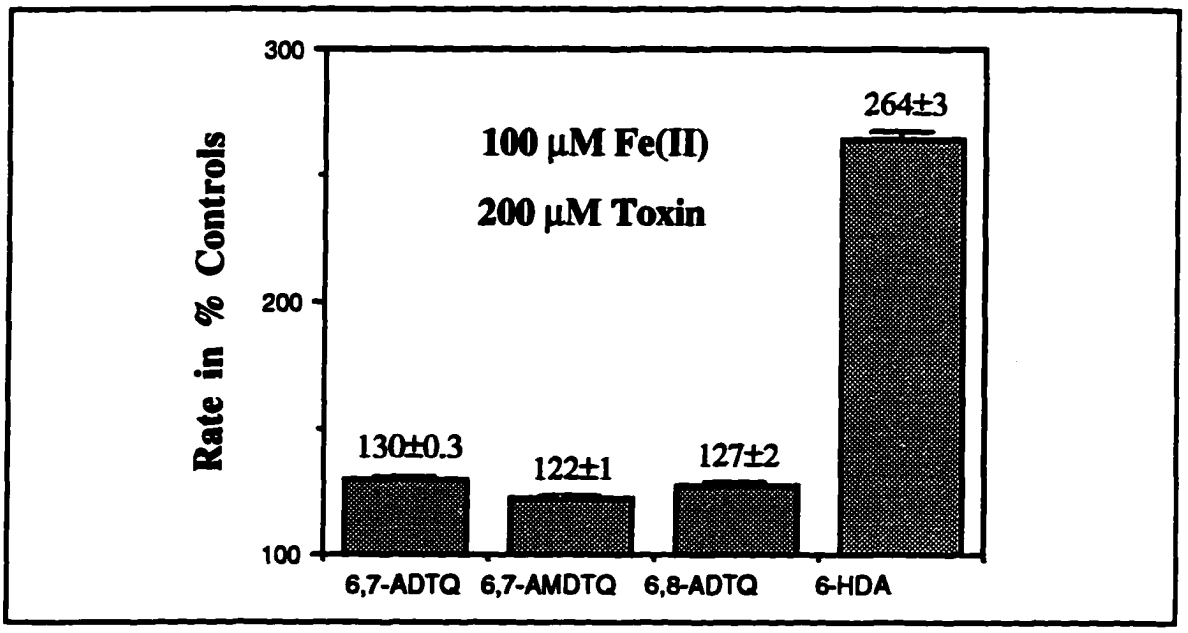

Figure 7-20. A toxin comparison of the rates of autoxidation in the presence of 100 μM Fe^{2+} in % controls. Rates presented in this graph are not reflective of direct comparisons, but are in percent of their corresponding control group.

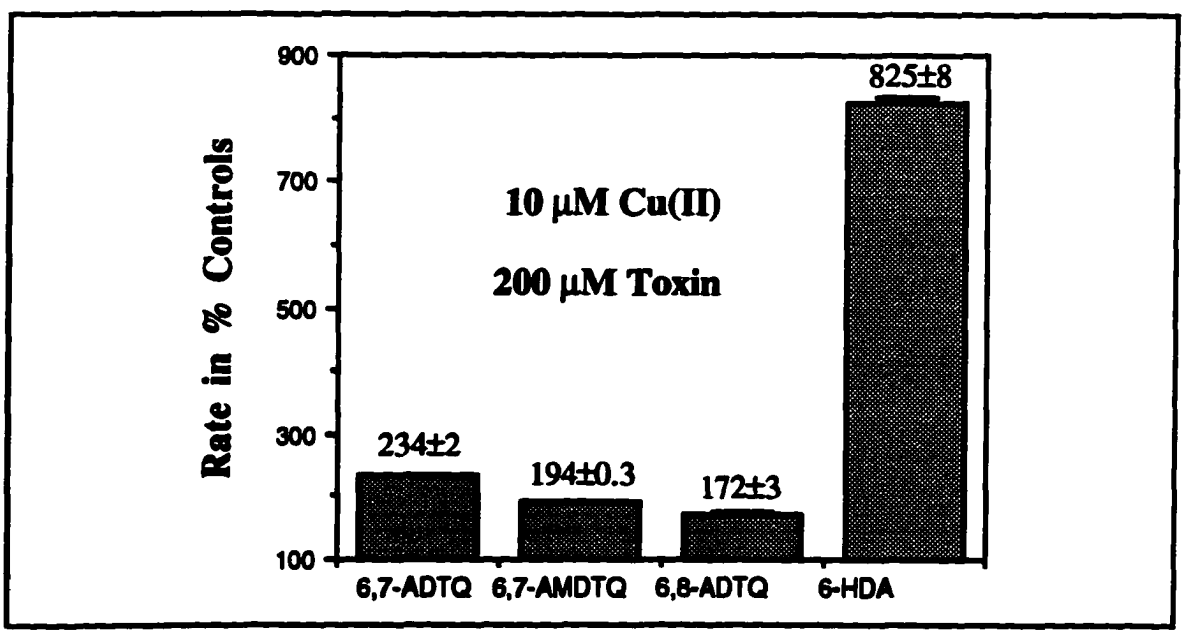

Figure 7-21. A toxin comparison of the rates of autoxidation in the presence of 10 μM Cu^{2+} in % controls. Rates presented in this graph are not reflective of direct comparisons, but are in percent of their corresponding control group.

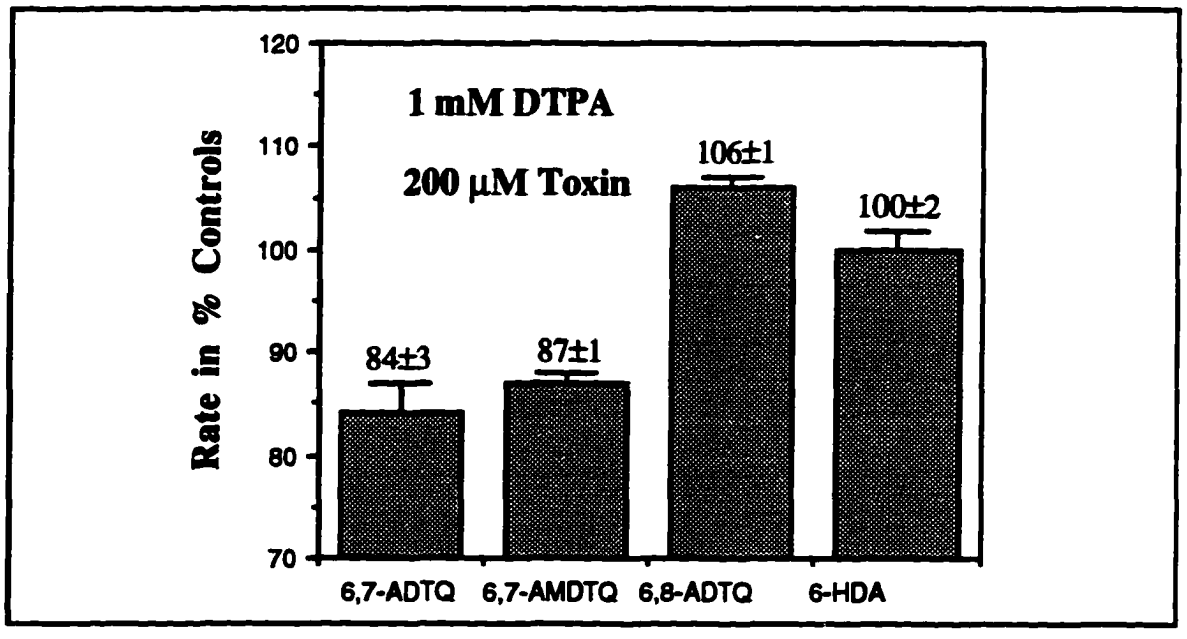

Figure 7-22. A toxin comparison of the rates of autoxidation in the presence of 10^{-3} M DTPA in % controls. Rates presented in this graph are not reflective of direct comparisons, but are in percent of their corresponding control group.

This observed stimulation of quinoline analog autoxidation by metal ions, and lack of inhibition by SOD, suggests a reaction mechanism by which there exists a ternary complex between toxin•metal•oxygen similar to that proposed for 6-HDA.[25,38] In such a complex, electrons are sequentially passed to oxygen without the existence of "free" $\bullet O_2^-$ *via* innersphere electron transfer. Furthermore, from the absence of SOD inhibition on our quinoline analogs, (1) the electron transfer kinetics must be very fast, and/or (2) the quinoline agents may chelate metal ions more strongly than that of agents inhibited by SOD, such as 6-HDA. This ternary complex idea is shown in the following scheme.

$$\text{Toxin} + M^{n+} + \text{oxygen} \longrightarrow [\text{Toxin}\bullet M^{n+}\bullet\text{oxygen}] \longrightarrow \text{p-Q} + M^{n+} + H_2O_2$$

This could explain not only the lack of inhibition by SOD, but also the stimulation observed with metal ions.

4. Effects of Fe^{2+}/EDTA

EDTA in the presence of Fe^{2+} has previously been shown to accelerate 6-HDA autoxidation.[38,173] Additionally, EDTA, both in the presence of and absence of Fe^{2+}, has also been reported to increase the inhibition of SOD on 6-HDA autoxidation.[38] This suggests that EDTA changes the mechanism by which 6-HDA autoxidation occurs, making the formation of the ternary 6-HDA•metal•oxygen complex difficult; thus, more dependent on a "free" $\bullet O_2^-$ mechanism(s). The stimulation in autoxidation seen with EDTA is believed to be associated with the seventh binding site of Fe^{2+} in the Fe^{2+}/EDTA complex.[38,176] The seventh binding site, while normally being occupied by water, can be occupied by O_2 and $\bullet O_2^-$. This allows for rapid electron transfer to occur due to the conformational arrangement of the metal ion and O_2.

Our results show an overall stimulation of toxin autoxidation in the presence of 100 μM Fe^{2+}/EDTA. 6-HDA was accelerated to approximately 1000% of controls. However, while our quinoline analogs also displayed stimulation of their autoxidation rates, they were similar to the rates observed at equal concentration of Fe^{2+} alone. This lack of substantial rate increase seen with the quinoline analogs suggests that the reduction of the metal ion is the rate limiting step in the quinoline analog autoxidation.

B. Production of H_2O_2 From Autoxidation

The sequential reduction of oxygen by one electron transfer is shown below:

$$O_2 \xrightarrow{+1e^-} \cdot O_2^- \xrightarrow{+1e^-} H_2O_2 \xrightarrow{+1e^-} \cdot OH\ (+\ OH^-) \xrightarrow{+1e^-} H_2O$$

1. Toxin effects

Autoxidation of 6-HDA has been reported to produce H_2O_2 in close to stoichiometric amounts.[33,34,37,165] Our results concur with these reports. The percent oxygen consumed during our quinoline analog and 6-HDA autoxidations which led to the production of H_2O_2 is presented in Figure 7-23. For 6,7-ADTQ, 6,7-AMDTQ, and 6-HDA, the majority of oxygen consumed during autoxidation went to produce H_2O_2. While the conversion of O_2 to H_2O_2 appears to be less than 100% for all of the agents, this may be attributed to the H_2O_2 (1) participating in toxin oxidation, thereby producing H_2O, (2) participating in •OH formation through Fenton and Haber-Weiss chemistry, resulting from trace metal ions which exist in the solutions or the reagents, (3) reaction of H_2O_2 with various components in the reaction cell and the reaction cell itself, and (4) the innate instability of H_2O_2 in aqueous systems. Interestingly, 6,8-ADTQ only showed a 60% conversion of O_2 to H_2O_2. This could be a result of the above mentioned reactions, but doubtful in that this was not observed with the other toxins. An alternative answer could be that oxygen is incorporated directly into the molecular structure of 6,8-ADTQ, similar to that seen with 5,7-DHT,[85,89] *via* a methide[177] or carbanion[85] radical mechanism.

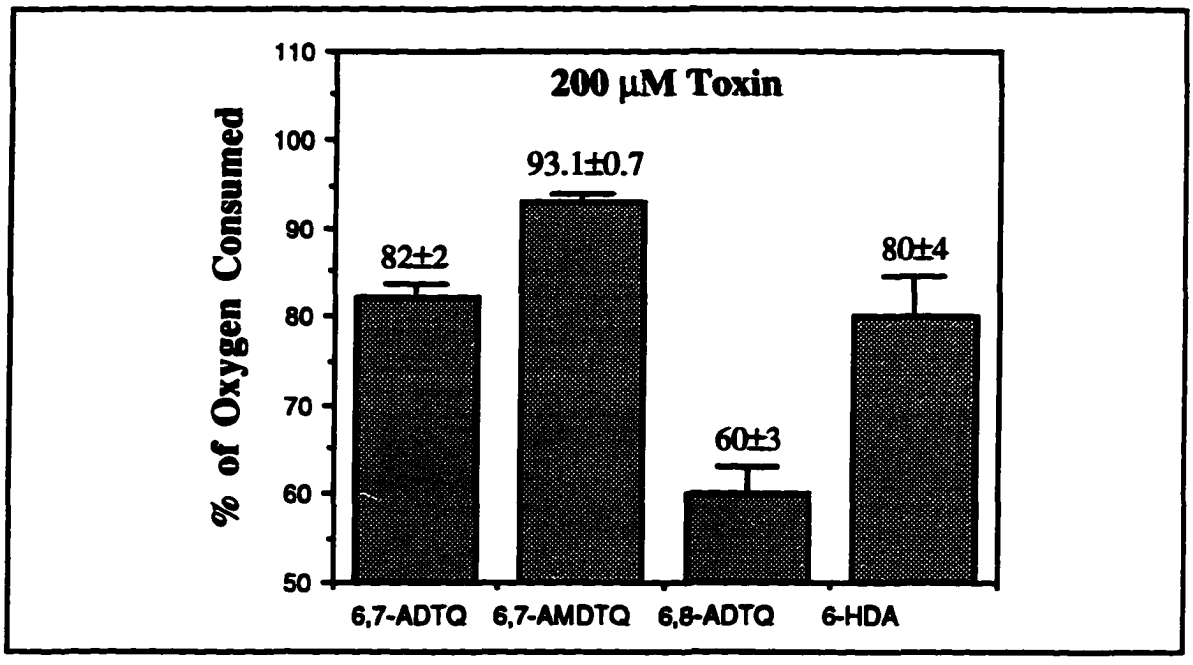

Figure 7-23. Oxygen consumed during autoxidation leading to the production of H_2O_2.

2. DTPA Effects

In order to eliminate trace metal ion interactions with H_2O_2 produced during autoxidation, *via* Fenton chemistry, DTPA was used to effectively remove any participatory ions. In the presence of DTPA, the H_2O_2 produced from 6-HDA autoxidation accounted for almost 100% of the oxygen consumed. However, 6,7-ADTQ, 6,7-AMDTQ, and 6,8-ADTQ showed relatively no change in the H_2O_2 produced from that of their respective controls. Therefore, it does not appear that trace metal ion contaminants in the buffer solutions effect, to any substantial degree, the resulting H_2O_2 *via* •OH production.

3. Metal Ion Effects

H_2O_2 and $\bullet O_2^-$, in the presence of metal ions, can produce •OH through Fenton and Haber-Weiss processes. The Fenton reaction is shown below. The Haber-Weiss

reaction is similar to the Fenton reaction with the addition of $\bullet O_2^-$ recycling of Fe^{3+} to Fe^{2+}, and is also shown below.

$$Fe^{2+} + H_2O_2 \longrightarrow Fe^{3+} + \bullet OH + OH^- \quad \text{(Fenton reaction)}$$

$$\bullet O_2^- + H_2O_2 \xrightarrow{Fe^{3+}/Fe^{2+}} \bullet OH + OH^- + O_2^{\bullet} \quad \text{(Haber-Weiss reaction)}$$

As we saw earlier, metal ions accelerated the autoxidation of all compounds tested. Paralleling this increase in rate was a metal ion concentration dependent decrease in the recoverable H_2O_2 at the completion of autoxidation. These effects were observed with Fe^{2+} and Fe^{2+}/EDTA, and, to a much lesser extent, Cu^{2+}. At high concentration of Cu^{2+} (10^{-5} M) the available H_2O_2 resulting from the autoxidation of 6,7-ADTQ and 6,8-ADTQ decrease slightly; however, no significant change in H_2O_2 production was observed for 6,7-AMDTQ or 6-HDA. While Cu^{2+} can participate in free radical production, it does so to a much lesser extent than iron.

Iron participates readily in $\bullet OH$ formation through Fenton and Haber-Weiss mechanisms. In the presence of Fe^{2+}, it has been reported that 6-HDA produces $\bullet OH$, which is paralleled by a decrease in H_2O_2 available at the completion of autoxidation.[165] Our study of 6-HDA with Fe^{2+} also showed a decrease in available H_2O_2 following the completion of autoxidation, which we presume is due to formation of the $\bullet OH$ through Fenton type chemistry. The percent oxygen consumed during autoxidation of the quinoline compounds, in the presence of 100 μM Fe^{2+}, remaining as H_2O_2 is presented in Figure 7-24. We found with both 6,8-ADTQ and 6-HDA that the majority of oxygen consumed was unaccounted for by the remaining H_2O_2 in solution. 6,7-ADTQ also showed a substantial, but lesser, decrease in recoverable oxygen related to the remaining H_2O_2 following autoxidation. 6,7-AMDTQ showed a significant, yet not substantial,

decrease in the available H_2O_2 produced during autoxidation when in the presence of Fe^{2+}. These decreases in recoverable oxygen from H_2O_2 are believed to result from H_2O_2 and Fe^{2+} participation in •OH formation. Furthermore, preliminary studies currently being conducted on these compounds do show •OH production when autoxidation is carried out in the presence of Fe^{2+}. However, this does not explain why there is more •OH production, through the above described processes, with any one toxin vs. the others.

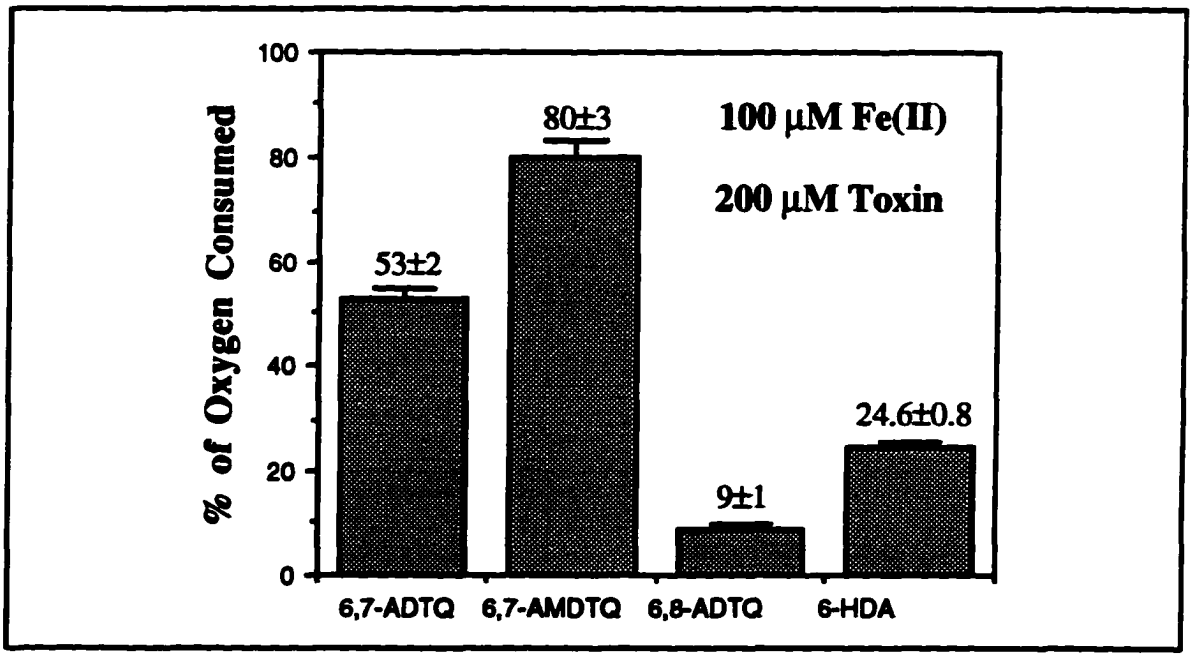

Figure 7-24. Oxygen consumed during toxin autoxidation, in the presence of 10^{-4} M Fe^{2+}, leading to the production of H_2O_2.

Fe^{2+}/EDTA with H_2O_2 is a classic •OH generating system.[40,41,104] There was dramatic decreases in the remaining H_2O_2 following toxin autoxidation when in the presence of 100 μM Fe^{2+}/EDTA. This is shown in Figure 7-25. The majority of the oxygen consumed during autoxidation, of all of the toxins studied, was unaccounted for by the H_2O_2 remaining following this process. This disappearance or lack of generation

of H_2O_2, from toxin autoxidation in the presence of Fe^{2+}/EDTA, suggests strongly the production of •OH from H_2O_2. Furthermore, it has been shown with 6-HDA and related analogs, that the loss of H_2O_2 was accounted for by the formation of •OH.[165]

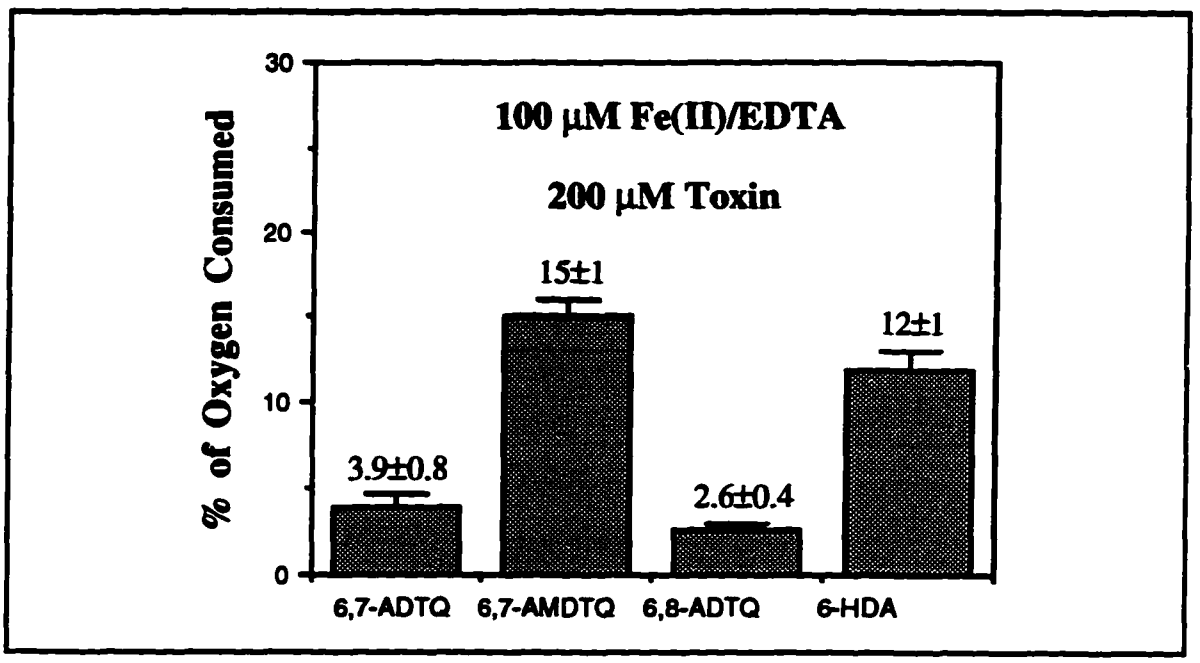

Figure 7-25. Oxygen consumed during autoxidation, in the presence of 10^{-4} M Fe^{2+}/EDTA, leading to the production of H_2O_2.

VI. Conclusions

It is apparent from the preceding autoxidation studies that our toxins have the capability to rapidly autoxidize when in aqueous solutions at physiological pH. We believe this autoxidation to be a prerequisite for our toxin-induced neuronal damage and/or degeneration. From the effects observed, it appears that metal ions serve as an electron transfer catalyst in the autoxidation process. This may be envisioned to involve

the formation of a ternary toxin•metal•oxygen complex, thereby promoting inner-sphere electron transfer. The complex most likely facilitates electron transfer to molecular oxygen by two sequential and coupled one-electron steps, resulting in the formation of H_2O_2 and absence of "free" intermediate $\bullet O_2^-$. Additionally, as metal ion concentrations increase, there is a decrease in available H_2O_2 following toxin autoxidation, which is suggestive of •OH production *via* Fenton and/or Haber-Weiss mechanisms.

The absence of inhibition by SOD on the autoxidation of the quinoline analogs suggests a $\bullet O_2^-$ independent oxidation mechanism. The stimulation in rate observed in the presence of catalase and SOD, individually, along with the general decrease in rate seen in the presence of H_2O_2, implies that H_2O_2 inhibits the preferred mechanism of oxidation of the quinoline agents.

Two of the toxins tested, 6,7-ADTQ and 6,8-ADTQ, rapidly underwent some form of polymerization following autoxidation. This suggests that they would readily react with nucleophiles in the cellular milieu.

All of the agents tested have been shown to elicit considerable neurodestruction in the CNS. From our findings in this chapter, it is not unreasonable to suggest multiple possibilities which could result in neuronal damage and/or destruction. These would include, but are not limited to: (1) production of damaging reactive oxygen species; (2) binding of oxidized toxin to essential proteins and enzymes; (3) neuronal hypoxia *via* toxin redox cycling; and (4) depletion of cellular antioxidant defenses.[43]

Mode of Action IV: Disruption of Mitochondrial Oxidative Phosphorylation

Chapter 8

I. Introduction

Adenosine triphosphate (ATP) plays a fundamental role in the proper functioning of neurons in the brain. ATP is produced almost exclusively in the mitochondria by oxidative phosphorylation; thus, the primary role of mitochondria is to furnish the cell with energy.[178-183] A disruption in energy production within a neuron generally results in neuronal dysfunction and/or death. There is a large body of evidence suggesting that numerous mental disorders are a result of energy metabolism dysfunctions, including

Parkinson's and Alzheimer's diseases.[78,184] Furthermore, it has been shown that a substantial number of drug-induced toxicities result from the interference of energy production in the brain.[185]

As discussed in Chapter 1, MPTP induced neurotoxicity is believed to be a result of inhibition of electron transport at the level of complex I.[69,72,73] It has been suggested that 5,6-DHT and 5,7-DHT interfere with electron transport.[82,86] Researchers have proposed that 6-HDA produces its neurotoxicity, at least in part, by uncoupling of oxidative phosphorylation[57,60,165] and by inhibiting electron transport.[58,59] Additionally, 6-HDA has been shown to cause a disruption mitochondrial Ca^{2+} homeostasis.[43,61,62] Further, when brain tissue homogenates of ^{3}H-6-HDA, ^{14}C-5,6-DHT and ^{14}C-5,7-DHT treated rats were separated on a discontinuous sucrose gradient, most of the radioactivity was found to be located in the mitochondrial fraction.[26]

When considering that all of the above mentioned toxins elicit some degree of dysfunction in mitochondrial oxidative phosphorylation, it is not unreasonable to suggest that impairment of mitochondrial function may be a common underlying mechanism by which many neurotoxins produce their damaging effects. Therefore, it was of interest to us to evaluate the effects of our fixed side chain toxins, along with 6-HDA, for possible mitochondrial interactions.

II. Background

The viability of mitochondria are frequently discussed in terms of how tightly or loosely mitochondria are coupled, or, how well the flow of electrons through the respiratory chain is reflected in the phosphorylation of ADP to ATP. Mitochondrial

coupling is most generally expressed quantitatively in two ways; the respiratory control ratio (RCR) and the P/O ratio.[178,179,183,186] Both of these ratios can be determined by monitoring the amount and rate of oxygen consumption a solution containing mitochondria and an electron donating substrate in the absence (state 4) and presence (state 3) of the phosphate acceptor, ADP. Substances added, states observed, and quantities measured for the determination of the ratios are exhibited on the typical oxygen trace shown in Figure 8-1 for a mitochondrial preparation.

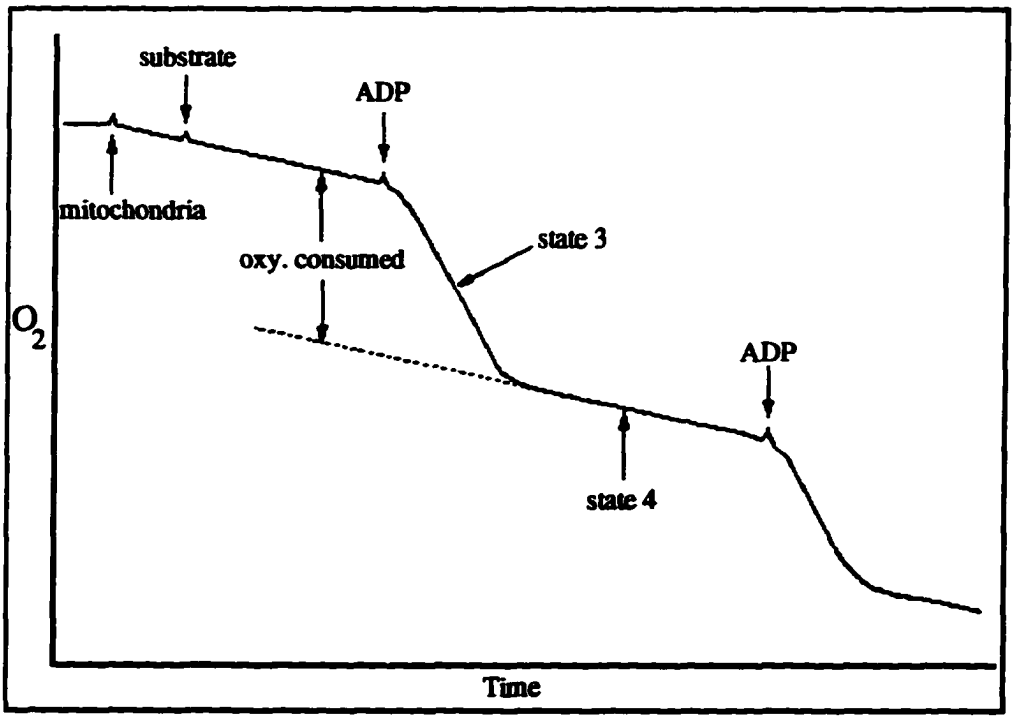

Figure 8-1. Typical O_2 trace showing stimulated and non-stimulated mitochondrial respiration.

The mitochondrial respiratory control ratio (RCR) is defined as the respiration rate in the presence of ADP divided by the respiration rate in the absence of ADP. In Figure 8-1 we see this corresponds to (state 3 rate)/(state 4 rate). High RCR values indicate a

tight coupling or a good energy-conversion capability. Low RCR values indicate loose coupling and a damaged or poorly functioning mitochondria.

The P/O ratio is defined as the number of ATP molecules produced in oxidative phosphorylation per oxygen atom consumed. In a tightly coupled NAD-linked pathway, approximately 3 ATP are produced per oxygen atom converted to water, and in a tightly coupled succinate-linked system, 2 ATP are produced per oxygen atom converted to water. Thus, by making ADP the limiting reactant and measuring the oxygen consumed, the P/O ratio can easily be calculated. This is mathematically expressed as P/O = (mol ADP added)/(mol oxygen atoms consumed).

Another important parameter in mitochondrial oxidative phosphorylation is the state 4 respiration rate. In a highly coupled system, oxygen consumption is very low in the absence of a phosphate acceptor. While a small amount of oxygen consumption will exist in the absence of ADP due to endogenous phosphorylatable substrates and residual energy leakage, a large state 4 rate indicates massive energy leakage from the electron chain and, hence, a non-viable mitochondrial preparation.

Toxins may elicit their neurodestructive action by interfering with the proper functioning of mitochondrial oxidative phosphorylation. The two most prominent ways in which an agent could produce an energy deficit are (1) inhibition of the electron transport chain, and (2) uncoupling of oxidative phosphorylation.

Inhibitors prevent production of ATP by blocking the flow of electrons through the respiratory chain. Inhibitors, thus, cause the rate of oxygen consumption to return to that of state 4. This is exemplified in Figure 8-2. Inhibitors are generally lipophilic molecules; however, there are no obvious functional or structural properties which they all possess to describe or characterize them as a group. Classic inhibitors of oxidative phosphorylation are antimycin and cyanide.[187]

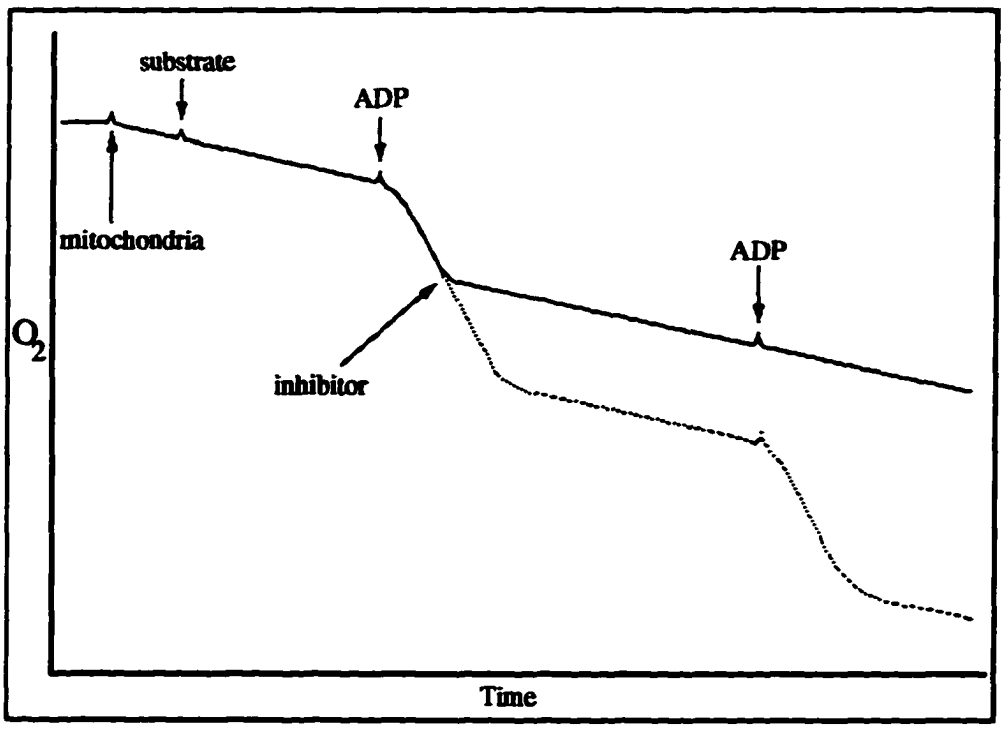

Figure 8-2. Typical effects of an inhibitor (solid line) on ADP stimulated respiration (broken line).

Uncouplers also prevent production of ATP, but by a completely different mechanism than that of inhibitors. Uncouplers are believed to elicit their action by breaking down the transmembrane proton gradient. They are generally lipid soluble weak acids. The weak acid characteristic allows an uncoupler to be protonated outside of the mitochondrial intermembrane, shuttle inside as the protonated form, become deprotonated, and then shuttle back out again in the deprotonated form. The mitochondrial proton gradient is built up by the passage of electrons down the respiratory chain and is essential for the production of ATP. In the absence of ADP, the proton gradient inhibits the further flow of electrons through the chain, therefore stopping the consumption of oxygen. When this proton gradient is dissipated, electrons flow through the respiratory chain and oxygen is consumed with little or no regulation. Thus, uncouplers not only eliminate production of ATP, but also produce a hypoxic state within the mitochondria and the cell.

Uncouplers display the ability to release state 4 respiration in the absence of a phosphate acceptor, resulting in a rate which approaches that of state 3. This release continues until all available oxygen is depleted. The effect of an uncoupler is depicted in Figure 8-3. 2,6- and 2,4-Dinitrophenol (2,4-DNP) are classic oxidative phosphorylation uncouplers[187] which are still commonly employed.

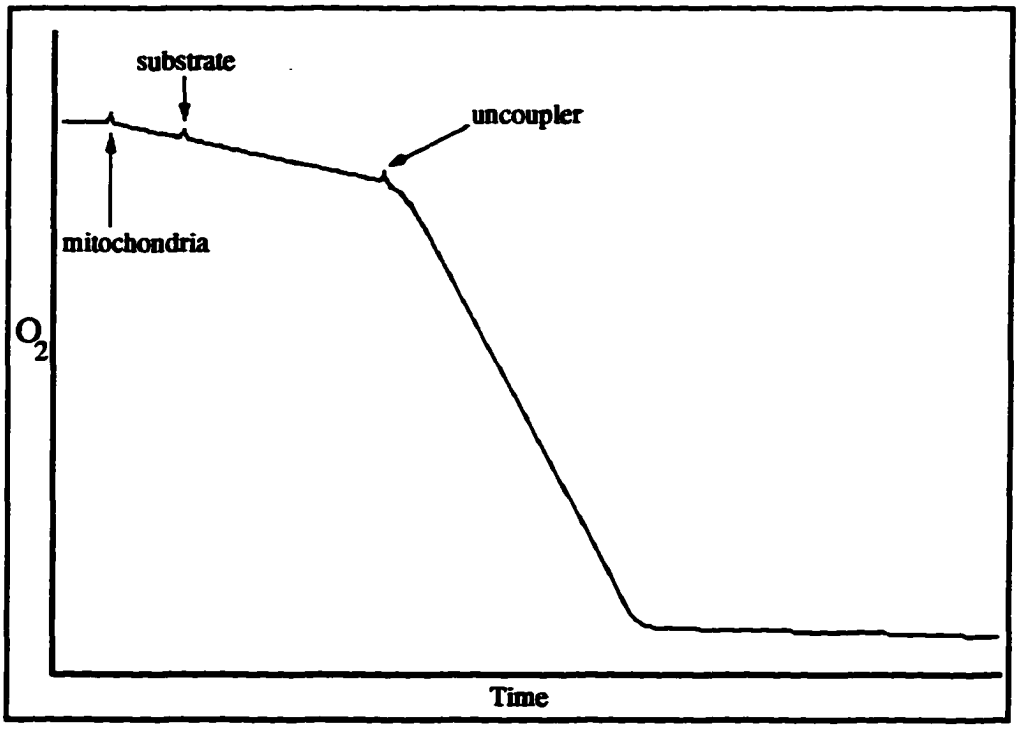

Figure 8-3. The effects of an uncoupler on non-ADP stimulated respiration.

III. Methods and Materials

A. Chemicals and Solutions

1. Chemicals

All aqueous solutions employed 18 MΩ distilled/deionized water which was prepared by passing distilled water through a Milli-Q Reagent Water System (Millipore, Continental Water Systems, El Paso, TX).

Chemicals listed below were purchased through Sigma Chemical Company (St. Louis, Mo.) in high purity and used without further purification. All other chemicals were obtained and used as described in previous chapters.

ethyleneglycol-bis-(ß-aminoethylether)-N,N,N',N'-tetraacetic acid (EGTA), 98%

3-(N-morpholino)-propanesulfonic acid, sodium salt (MOPS)

bovine serum albumin (BSA), fatty acid free, 99%

L-glutamic acid monosodium, 99%

L-malic acid monosodium, 98%

adenosine-5'-diphosphate (ADP), sodium salt, 96%

2. Homogenization Buffer

The homogenization solution was 0.30 M sucrose. This buffer was stored at 2°C and discarded after seven days. Component additions and solution adjustments were performed sequentially as shown in Table 8-1.

Table 8-1. Homogenization buffer preparation.

Compound	Amount	Final concentration
sucrose	51.35 g	0.30 M
EGTA	190.2 mg	1.0 mM
MOPS	523.3 mg	5.0 mM
K_2HPO_4	340.3 mg	5.0 mM
BSA	50.0 mg	0.10 %
add 475 mL water and adjust to pH 7.4 with conc. KOH		
dilute to a final volume of 500 mL		

3. Mitochondrial Incubation Buffer

The incubation buffer was the same as homogenization buffer except EGTA and BSA were excluded. This buffer was also stored at 2°C and discarded after 7 days.

4. Mitochondrial Substrate Solution

The mitochondria substrate solution was a malate/glutamate mixture. This solution was stored at 2°C until use and was discarded after 7 days. Component additions and solution adjustments were performed sequentially as shown in Table 8-2.

Table 8-2. Mitochondrial substrate solution preparation.

Malate/Glutamate Solution[181]		
Compound	Amount	Final concentration
L-malic acid, Na^+	134.1 mg	0.10 M
L-glutamic acid, Na^+	294.2 mg	0.20 M
add 3 mL water		
add 50 µL conc. HCl (aids in dissolving substrate)		
adjust to pH 7.4 with KOH		
dilute to 10 mL with homogenization buffer		

5. ADP Stock Solution

The ADP stock solution was prepared by dissolving 123 mg ADP (96%) in 5 mL homogenization buffer to give a concentration of 55.3 mM. This was divided into 0.5 mL aliquots and stored at -20°C until use. Samples were thawed only once then discarded.

6. Toxin Stock Solution

A stock toxin solution was made by dissolving a desired amount of toxin in an appropriate volume of degassed homogenization solution, typically 500-700 µL, to yield a concentration of 10 mM. This solution was stored on ice. For the experiment, 10, 40, or 80 µL of the stock solution was injected into the 2.036 mL incubation cell to yield a final incubation concentration of 50, 200, or 400 µM, respectively. The stock toxin solution was stable in excess of 8 h. When needed, the toxin was converted to its oxidized form just prior to injection into the incubation mixture by bubbling with oxygen for 3-5 min.

B. Experimental

1. Animals

Animals used in mitochondrial studies were male Sprague-Dawley rats (Harlan Sprague Dawley, Indianapolis, IN). The typical rat weighed 350 to 420 g, and a typical liver weight was 15 to 25 g.

2. Liver Homogenate

Since mitochondrial preparations are only viable for 3 to 4 hours, time is critical in the homogenization, isolation, and utilization of such preparations.

The rat was deprived of food for 15-20 h prior to the experiment to decrease the fatty acid and glycogen content of the liver. The animal was then sacrificed by decapitation without anesthesia. The liver was rapidly excised, and all fat and connective tissue were removed. The liver was weighed and placed into 30 mL of ice-cold homogenization buffer. All subsequent steps were completed at 0°C in order to enhance survival of the mitochondria. All solutions, glassware, homogenizing equipment, and centrifuges were maintained at 0°C throughout the experimental procedures.

While in the buffer solution, the liver tissue was chopped into approximately 1 mm cubes with scissors. The chopped tissue was rinsed three times with clean buffer during the chopping procedure to remove blood. Tissue chopping was completed within 3 min. The tissue mixture was drained and resuspended in homogenizing buffer, using 2 mL of fresh buffer per gram of original tissue. The mixture was then divided into four approximately equal parts which were transferred, one at a time, to the homogenization mortar. With the homogenization mortar in ice, the tissue was homogenized at a pestle rotation of 100 to 120 rpm using 5 complete up and down strokes. Caution was taken not to apply excessive pressure or to pull a vacuum, which caused damage to the integrity of the mitochondria. The four individual homogenates were subsequently combined,

mixed, and then equally divided between two 50 mL polycarbonate centrifuge tubes. The final homogenate was a reddish-brown color. The homogenization process was completed within 10 to 15 min after sacrifice.

3. Isolation of Mitochondria[179,183,188]

All centrifuge steps were carried out at 0°C. The homogenate was centrifuged using a model RC-5B Sorvall (DuPont Instruments, Newtown, CT) superspeed centrifuge with a model SM-24 rotor at 3,000 rpm (1,000g) for 5 min. This step separated cellular debris from the suspended mitochondria. Three layers resulted from this initial centrifugation: a top, milky white layer which consisted of fats; a middle layer, which was the desired layer; and a bottom layer, which was a pellet of cellular debris and blood. The middle layers of each tube were collected using a Pasteur pipette, combined, and put on ice. Throughout this collection, caution was used to avoid gathering any of the white milky material at the top or the sediment at the bottom, since these materials would contaminate the preparation. After discarding the remaining upper layer, the resultant pellets were combined, resuspended in 20 mL of homogenization buffer, and centrifuged again at 3,000 rpm (1,000g) for 5 min. The middle layer was again isolated and combined with the previously collected material. The remaining top and bottom layers were discarded. The combined middle layers were centrifuged at 12,000 rpm (15,000g) for 10 min. The resultant supernatant was discarded. Any white material present on the tube walls was wiped away. The pellet was resuspended in 20 mL homogenization buffer and centrifuged again at 12,000 rpm (15,000g) for 5 min. Following the final centrifugation, the supernatant was discarded and the remaining pellet saved. The pellet was light brown in color and was composed of the desired mitochondria. This pellet was resuspended in 1.0 mL of homogenization buffer and stored on ice. To ensure homogeneity of the final mitochondrial mixture, two complete manual revolutions of the pestle were employed. The entire isolation procedure required

approximately one hour to complete. A typical rat liver preparation yielded 2 mL of final mitochondrial suspension.

4. RCR Ratio, P/O Ratio & State 4 Rate

Viability of the preparation and coupling of the mitochondria in a typical preparation was assessed by measuring the RCR and P/O ratios and the state 4 oxygen consumption rate.

A model 58 YSI dissolved oxygen meter outfitted with a model 5739 YSI dissolved oxygen probe (Yellow Springs Instrument Co., Yellow Springs, OH) was equipped with fresh internal KCl solution, a new 0.001" standard electrode membrane, and calibrated prior to each complete experiment. The reaction cell used for all experiments was a 2.036 mL temperature regulated, water jacketed cell that fit tightly over the end of the O_2 probe. The temperature was held at 37°C for all experiments. The oxygen trace was recorded on a model 156 Cole/Parmer chart recorder. Stirring of the solution inside the cell was held constant at a setting of 4 on a model 120M Fisher magnetic stirrer. Stock incubation buffer was kept at 37°C during the experiment. The cell was filled with the incubation buffer using a 5 mL plastic syringe, being careful to eliminate any oxygen bubbles inside the reaction cell. The temperature was then allowed to equilibrate 1 min. A 100 µL aliquot of the mitochondria suspension was injected into the cell and, then, 100 µL of the malate/glutamate solution was injected. This was allowed to equilibrate until a steady oxygen trace was achieved. A 10 µL aliquot of 55.3 mM ADP was then injected into the cell with a resultant oxygen consumption rate increase. Upon mitochondrial utilization of all available ADP, the oxygen consumption rate slowed and gave a steady, non-phosphorylation respiratory state. This state was then observed for approximately 1 min, followed by another 10 µL injection of ADP. Using this approach, mitochondria integrity was evaluated and experimental control values obtained.

When investigating the interaction of the toxin with mitochondria, the same experimental approach as described immediately above was conducted with the addition of one step. An appropriate amount of 10 mM toxin in either the reduced or the oxidized form (10, 40, 80 μL) was added to the reaction cell following the addition of the mitochondria. For the majority of the studies, the oxidized form of the toxin was employed unless otherwise noted. This was done in order to eliminate any mitochondrial damage resulting from possible short-lived reactive by-products of toxin autoxidation, and to eliminate changes in oxygen concentrations resulting from toxin autoxidation. Additionally, since these toxins are most likely in their oxidized form in the brain, it seems only logical that the oxidized form be used in these investigations. For investigation of the effect of toxin autoxidation process on mitochondrial function, the reduced toxin was injected immediately following mitochondria. In these studies, the dissolved oxygen content in the cell was increased prior to the experiment to compensate for the initial, large oxygen consumption *via* toxin oxidation. The mitochondria-toxin autoxidation studies are denoted in tables and figures by a superscript ^{aut}.

Typically, each toxin condition had an N value of 3 to 4, and control values had N of 5 to 6. All values presented in tables and figure are reported as the mean ± SEM. Typical RCR and P/O ratio values were found to be 3.5 to 6.0 and 2.7 to 3.1, respectively.

IV. Results and Discussion

A. 6,7-ADTQ

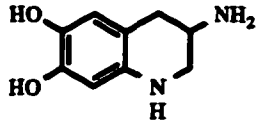

The mitochondrial interactions observed with 6,7-ADTQ are presented in Table 8-3 and Figures 8-4 through 8-6. At 50 μM preoxidized 6,7-ADTQ (ox-6,7-ADTQ) the RCR showed a marked decrease (31% inhibition). Along with this decrease, state 4 respiration, i.e., release, was stimulated to 165% of control.

Table 8-3. 6,7-ADTQ effects on mitochondrial function.

	Respiration values in % control ± SEM		
Conc. (μM)	RCR	P/O	State 4 rate
controls[a]	100 ± 1	100 ± 2	100 ± 2
50	69 ± 2***	96 ± 1	165 ± 11***
200	64 ± 1***	86 ± 2**	185 ± 8***
400	56 ± 1***	80 ± 0.6***	227 ± 9***
200 aut	61 ± 1***	88 ± 3**	190 ± 3***

Significant differences compared to control values (*t* test): $*P < 0.05$; $**P < 0.01$, $***P < 0.001$.

[a] Control values (mean ± SEM): RCR, 3.45 ± 0.03; P/O, 2.87 ± 0.06.

At 200 μM, ox-6,7-ADTQ caused decreases in the RCR and P/O values to 64% and 86% of controls, respectively. Additionally, state 4 respiration was stimulated to 185% of controls. At 400 μM, ox-6,7-ADTQ further decreased RCR and P/O values and state 4 respiration was simulated to 227% of control values. In fact, the state 4 release effects almost quantitatively accounted for the corresponding RCR effects. Likewise, the P/O effects are at least partially attributed to the state 4 effects.

To ensure that the observed concentration dependent effects were a result of stimulated mitochondrial oxygen consumption, i.e., state 4 release, and not any residual autoxidation of the toxin, similarly prepared, pre-oxidized toxin was introduced into the reaction cell containing only the incubation buffer. No oxygen consumption was observed in these experiments, and in fact, there was a slight increase observed in the oxygen level of the reaction cell, which resulted from the slightly higher oxygen content of the oxidized toxin solution.

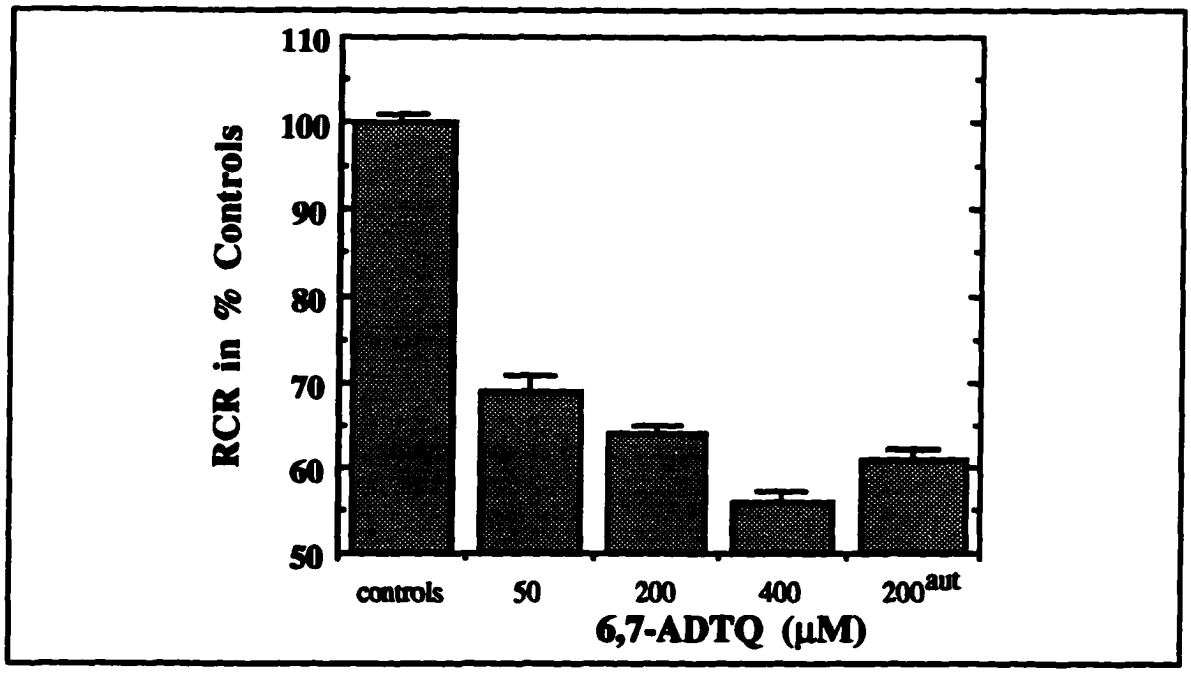

Figure 8-4. 6,7-ADTQ effects on RCR. ^{aut} indicates toxin not pre-oxidized.

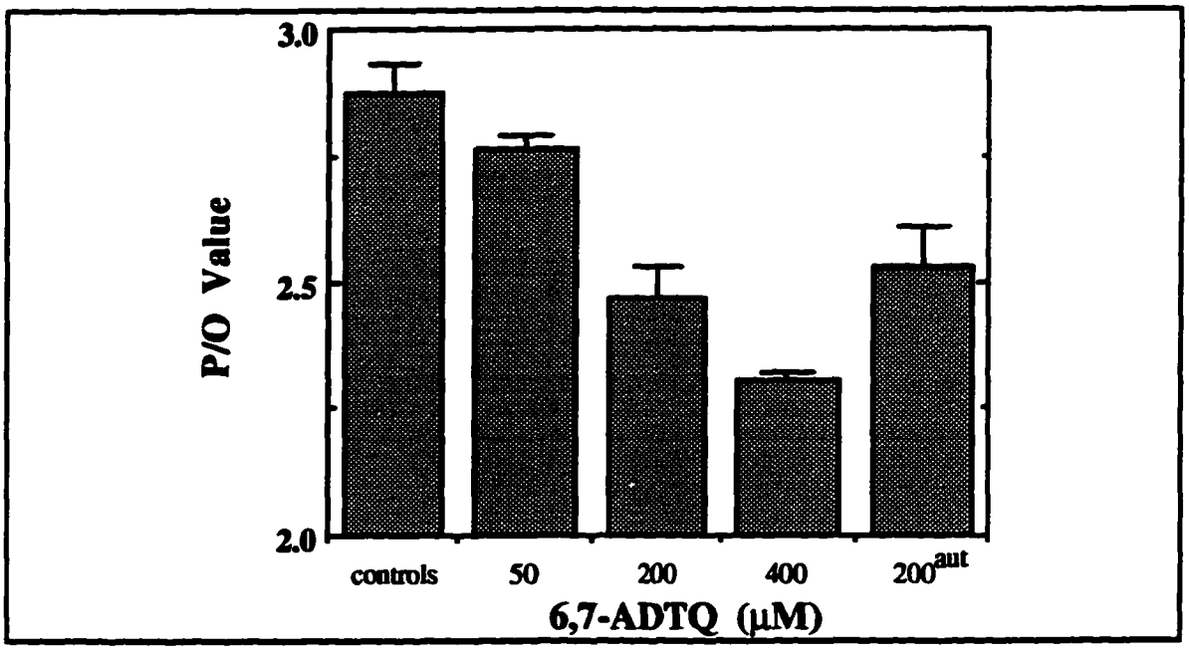

Figure 8-5. 6,7-ADTQ effects on P/O ratio. [aut] indicates toxin not pre-oxidized.

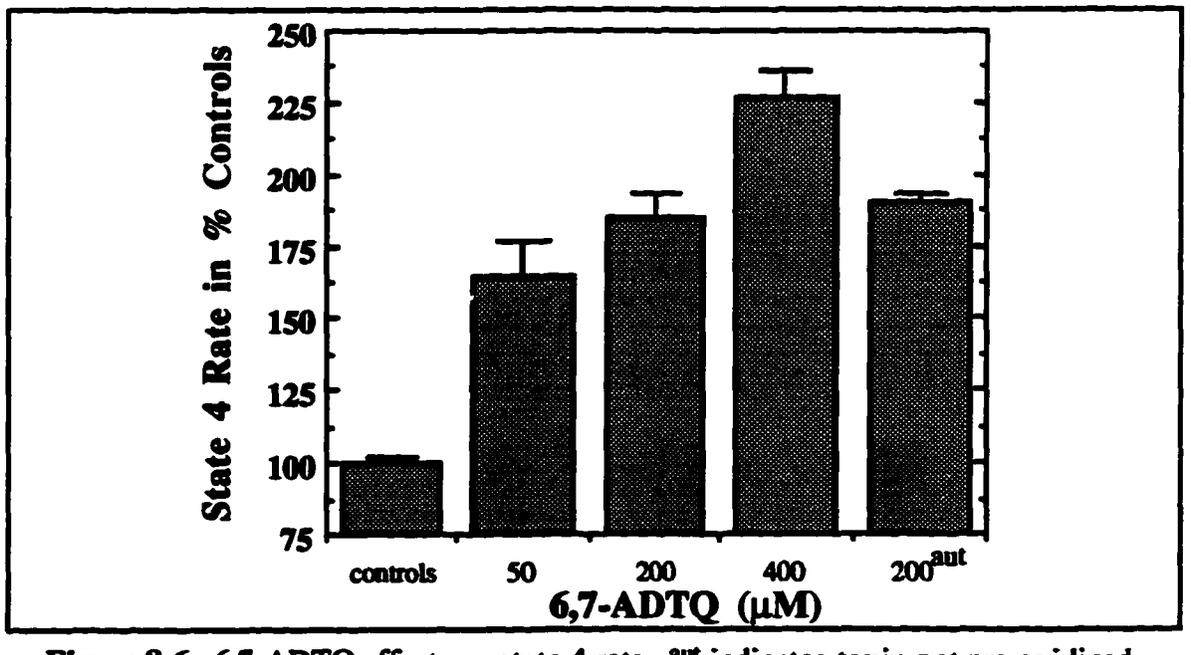

Figure 8-6. 6,7-ADTQ effects on state 4 rate. [aut] indicates toxin not pre-oxidized.

We then investigated the effects of the 6,7-ADTQ autoxidation process on mitochondrial function. 6,7-ADTQ, in its reduced form, was introduced to the reaction cell containing mitochondria and subsequently underwent autoxidation. Once steady state oxygen consumption was observed, the mitochondria were tested for their resultant possible functional impairment. The determined RCR and P/O values were significantly lower than controls, but were no different than those observed in the corresponding 200 μM ox-6,7-ADTQ group. The same was seen for state 4 respiration stimulation. These results indicate that autoxidation of 6,7-ADTQ does not substantially impair mitochondrial function.

In these studies, we found significant mitochondrial interaction over a broad toxin concentration range. ox-6,7-ADTQ demonstrates a potent uncoupling effect, as seen by its ability to release state 4 respiration. If there exists any respiratory inhibition effects, they are minimal as both the RCR and P/O inhibition can be attributed to the release in state 4 respiration.

B. 6,7-AMDTQ

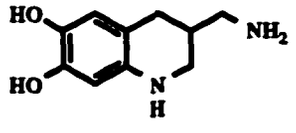

The effects exerted by 6,7-AMDTQ on mitochondrial function are presented in Table 8-4 and Figures 8-7 to 8-9. At the lowest concentration of 6,7-AMDTQ tested, 50 μM, there was a 20% decrease in the RCR. This was also seen in the P/O value. These decreases were paralleled by, and may be easily attributed to, a 22% stimulation in the state 4 respiration, suggesting uncoupling.

Table 8-4. 6,7-AMDTQ effects on mitochondrial function.

	Respiration values in % control ± SEM		
Conc. (μM)	RCR	P/O	State 4 rate
controls[a]	100 ± 2	100 ± 3	100 ± 5
50	80 ± 0.1***	83 ± 2**	122 ± 1**
200	73 ± 1***	74 ± 2***	123 ± 6*
400	67 ± 4***	75 ± 2***	128 ± 12
200 [aut]	60 ± 1***	80 ± 2**	142 ± 1***

Significant differences compared to control values (*t* test): $*P < 0.05$; $**P < 0.01$, $***P < 0.001$.

[a] Control values (mean ± SEM): RCR, 4.49 ± 0.08; P/O, 2.74 ± 0.09.

At 200 μM oxidized toxin, further lowering of RCR and P/O values were observed. However, the release of state 4 respiration, while being 123% of controls, was approximately the same as that observed at 50 μM ox-6,7-AMDTQ. At 400 μM, ox-6,7-AMDTQ produced RCR and P/O values similar to those at 200 μM. Additionally, state 4 release was observed, but the release was not significantly different from that observed at 50 μM and 200 μM. At the two higher toxin concentrations, state 4 respiration release did not completely account for the decreases seen in RCR and P/O values. These results suggest that at low concentrations, ox-6,7-AMDTQ acts primarily as an uncoupler, while at higher concentrations it may act as both an uncoupler and weak inhibitor.

The effects of 6,7-AMDTQ autoxidation on mitochondrial function showed interactions greater than those seen with ox-6,7-AMDTQ. RCR values decreased a further 13% below that observed for the corresponding 200 μM preoxidized group.

Moreover, state 4 respiration was stimulated to 142% of control, which was 19% above that found in the preoxidized group. These potentiated mitochondrial effects suggest that reactive oxidation intermediates and/or by-products interfere with and/or damage mitochondrial function above and beyond that of the oxidized form of the toxin.

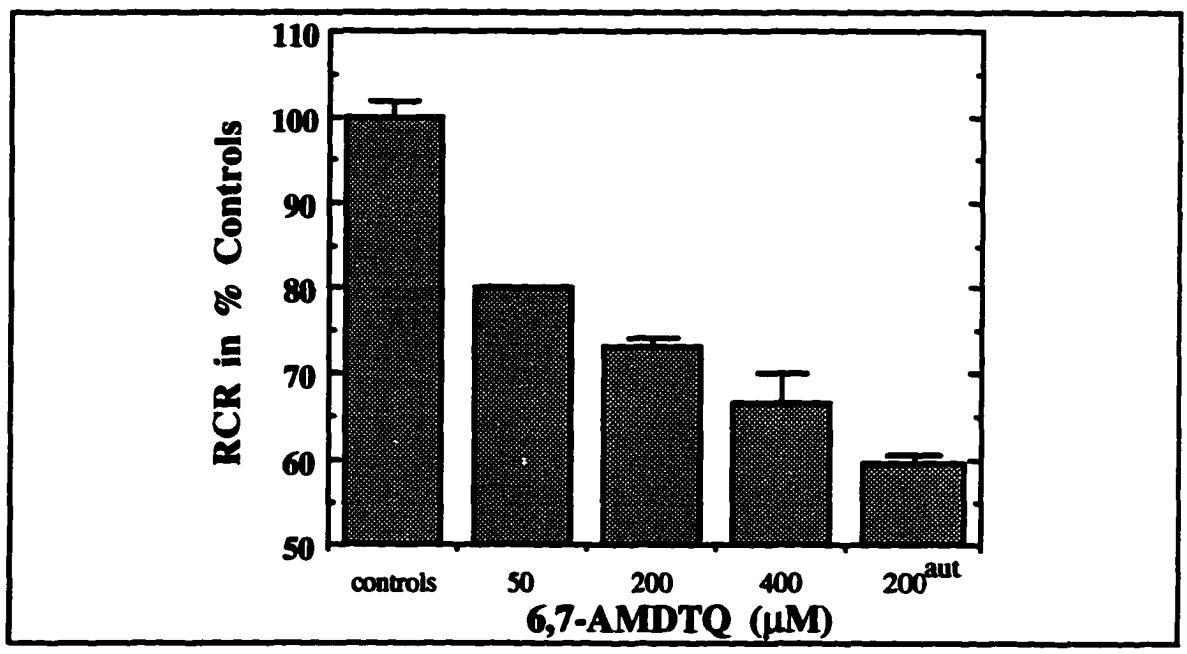

Figure 8-7. 6,7-AMDTQ effects on RCR. ^{aut} indicates toxin not pre-oxidized.

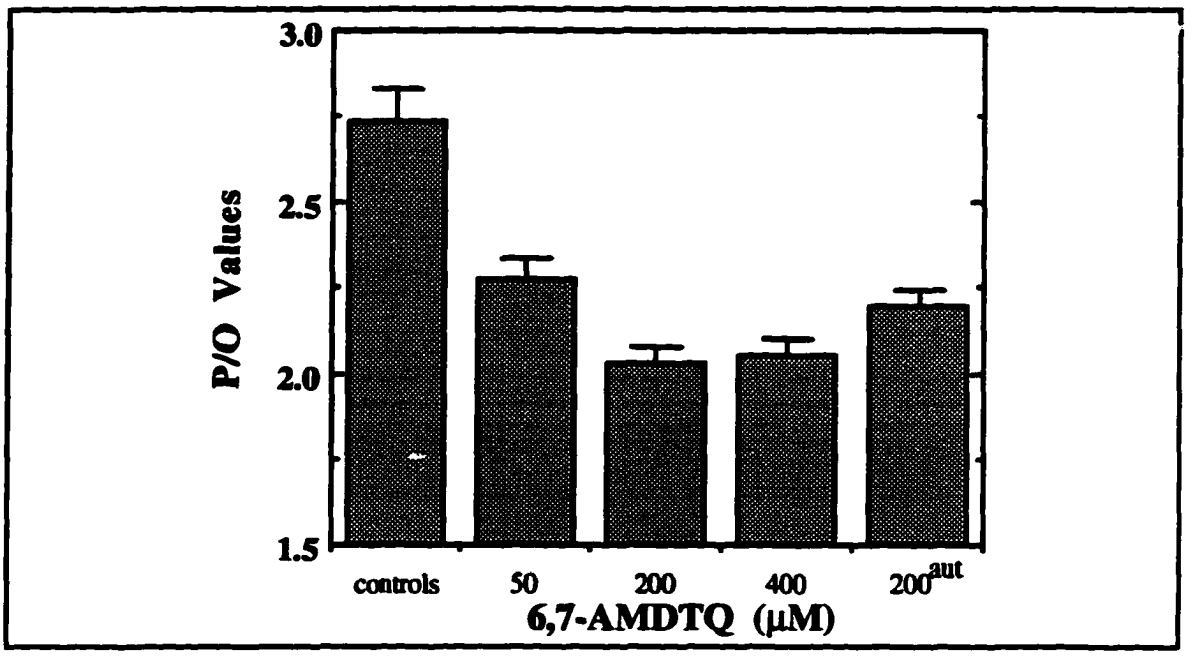

Figure 8-8. 6,7-AMDTQ effects on P/O ratio. [aut] indicates toxin not pre-oxidized.

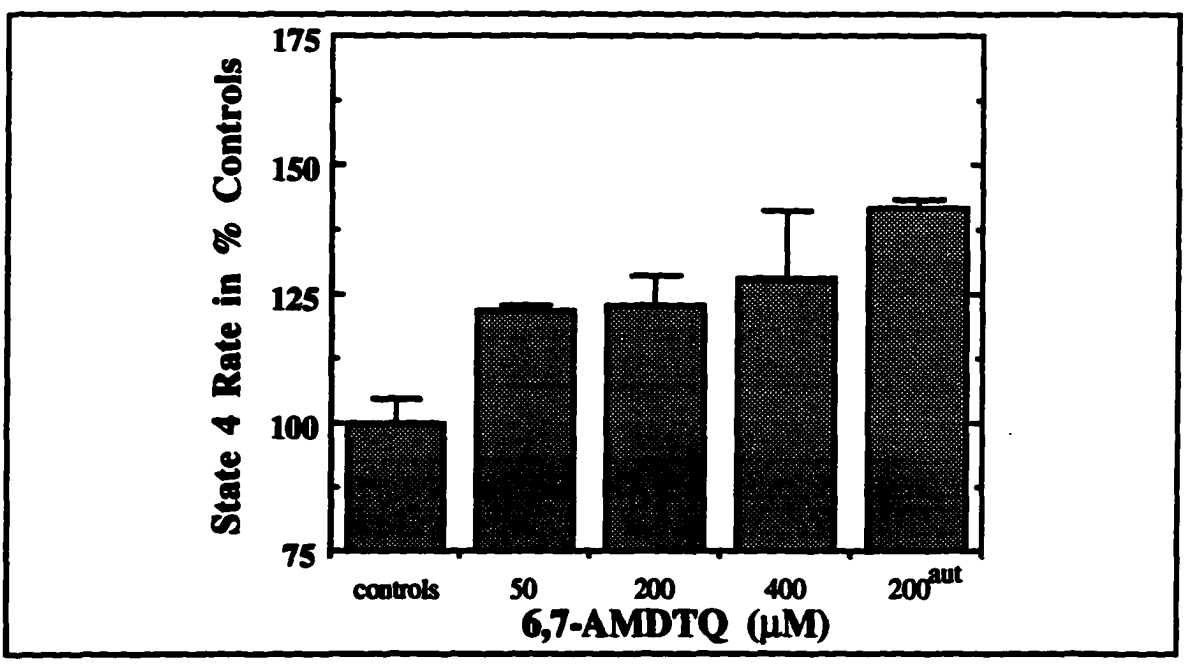

Figure 8-9. 6,7-AMDTQ effects on state 4 rate. [aut] indicates toxin not pre-oxidized.

Stimulation of state 4 respiration directly indicates uncoupling produced by ox-6,7-AMDTQ. However, at high concentrations of ox-6,7-AMDTQ, stimulation of state 4 respiration does not appear to account for the total decrease in RCR or P/O values. Thus, 6,7-AMDTQ may also be partially acting as a weak inhibitor of oxidative phosphorylation. Further studies have not been conducted to investigate the exact nature of this possible action. Toxin autoxidation in the presence of mitochondria displayed potentiated effects compared to preoxidized toxin. This is believed to result from reactive oxidation intermediates or, more likely, reactive oxygen species damaging mitochondrial membranes and/or enzyme integrity.

C. 6,8-ADTQ

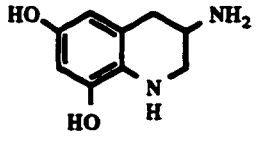

The mitochondrial interactions displayed by 6,8-ADTQ are presented in Table 8-5 and Figures 8-10 to 8-12. The interactions produced at 50 μM were minimal, yet significant. The RCR was lowered by approximately 13% and the P/O by 8%. Furthermore, state 4 respiration was stimulated to 115% of controls. Thus, the reductions in RCR and P/O values were primarily attributed to uncoupling.

Oxidized 6,8-ADTQ (ox-6,8-ADTQ) at 200 μM produced a further decrease in the RCR to 81% of control, while P/O values exhibited relatively no change from those produced at 50 μM. Additionally, state 4 respiration showed a concentration dependent effect with an increase in oxygen consumption to 129% of control.

Table 8-5. 6,8-ADTQ effects on mitochondrial function.

	Respiration values in % control ± SEM		
Conc. (μM)	RCR	P/O	State 4 rate
controls[a]	100 ± 1	100 ± 1	100 ± 3
50	87 ± 2***	92 ± 2**	115 ± 3*
200	81 ± 1***	92 ± 1**	129 ± 3***
400	77 ± 0.3***	90 ± 1***	136 ± 7**
200 aut	69 ± 2***	96 ± 2*	125 ± 6*

Significant differences compared to control values (*t* test): $*P < 0.05$; $**P < 0.01$, $***P < 0.001$.

[a] Control values (mean ± SEM): RCR, 4.99 ± 0.04 ; P/O, 2.91 ± 0.04.

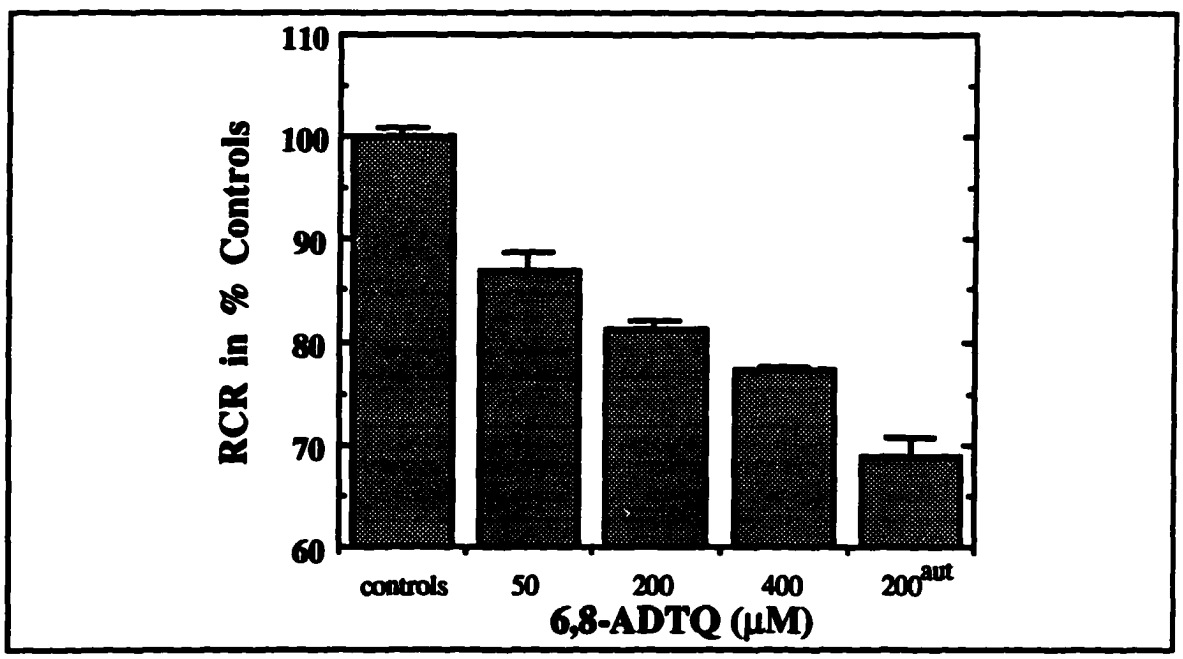

Figure 8-10. 6,8-ADTQ effects on RCR. [aut] indicates toxin not pre-oxidized.

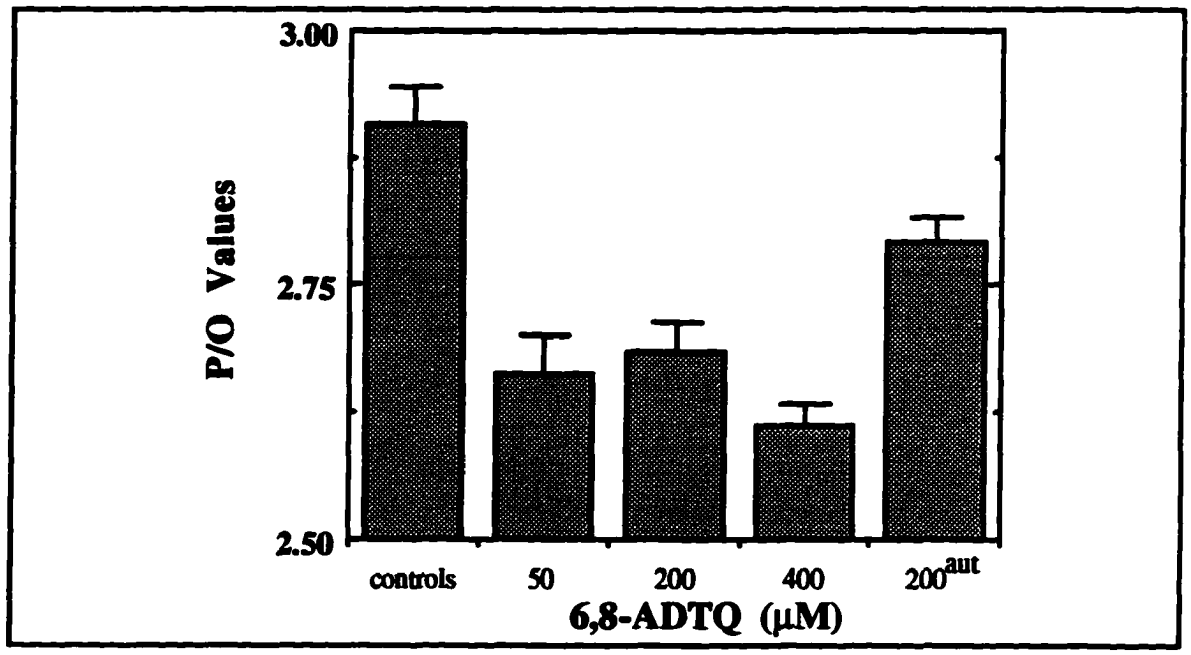

Figure 8-11. 6,8-ADTQ effects on P/O ratio. [aut] indicates toxin not pre-oxidized.

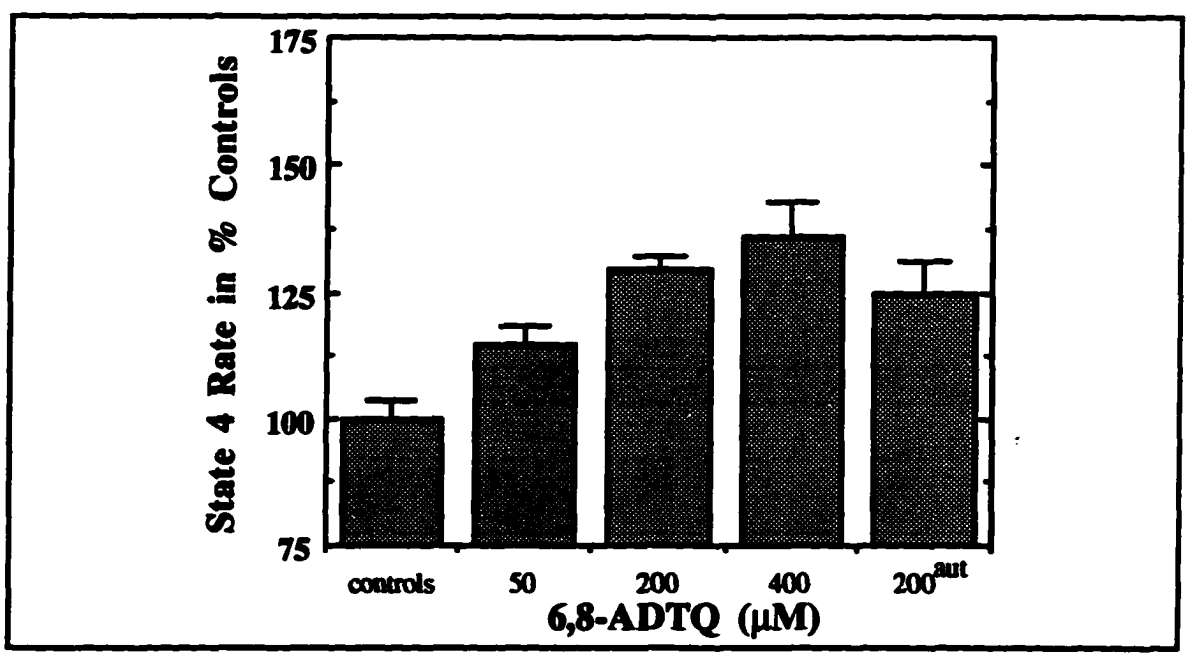

Figure 8-12. 6,8-ADTQ effects on state 4 rate. [aut] indicates toxin not pre-oxidized.

Oxidized 6,8-ADTQ at 400 μM resulted in a state 4 release to 36% above controls. This was reflected in the RCR, which was lowered to 77%. Interestingly, at all concentrations tested, the P/O values remained approximately unchanged at 90% of control. It is possible, however, that this may be a result of experimental error in the measurement of absolute oxygen consumption. Since state 4 release was reflected in and primarily accounted for by the decrease in RCR values, the results suggest this compound acts predominantly as an uncoupler.

Additionally, we investigated the effects of 6,8-ADTQ autoxidation on mitochondrial function. At 200 μM we observed a decrease in the RCR below that seen in the preoxidized 200 μM group. However, P/O values remained statistically unchanged from the corresponding preoxidized group, as did state 4 respiration rates. Thus, it appears there is little to no substantial effect produced by 6,8-ADTQ autoxidation itself beyond that elicited by the oxidized form of the toxin.

The RCR inhibition and state 4 stimulation occurred in a concentration dependent manner. And for the most part, the decrease observed in RCR was accounted for by the state 4 release. No substantial effects are produced by the toxin autoxidation process beyond those found with ox-6,8-ADTQ. Thus, we have concluded that 6,8-ADTQ acts primarily as an uncoupler of oxidative phosphorylation.

D. 6-HDA

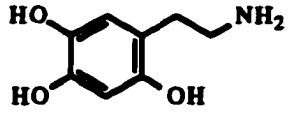

The results of 6-HDA interactions with mitochondria are presented in Table 8-6 and Figures 8-13 to 8-15. In studies using 50 μM oxidized 6-HDA (ox-6-HDA), we

observed a general lowering of RCR and P/O values and an increase in state 4 respiration, but none to a significant extent. In the presence of higher concentrations of ox-6-HDA, however, significant mitochondrial interference was observed.

Table 8-6. 6-HDA effects on mitochondrial function.

	Respiration values in % control ± SEM		
Conc. (μM)	RCR	P/O	State 4 rate
controls[a]	100 ± 3	100 ± 3	100 ± 3
50	94 ± 1	96 ± 6	111 ± 9
200	79 ± 1**	87 ± 2**	116 ± 2*
400	69 ± 1***	70 ± 5**	137 ± 3**
200 aut	62 ± 2***	89 ± 2*	162 ± 7***

Significant differences compared to control values (*t* test): $*P < 0.05$; $**P < 0.01$, $***P < 0.001$.

[a] Control values (mean ± SEM): RCR, 3.26 ± 0.11; P/O, 2.59 ± 0.08.

Using 200 μM ox-6-HDA, the RCR inhibition was approximately 21%. At this concentration, the P/O value was found to be 87% of controls. Furthermore, state 4 respiration was stimulated to 116% of control. The stimulation of state 4 respiration indicates uncoupling and can account for the majority of the decrease in RCR and P/O values. However, some slight respiratory chain inhibition effects may be indicated. Both uncoupling and inhibition by 6-HDA has been reported in the literature.[57-60,165]

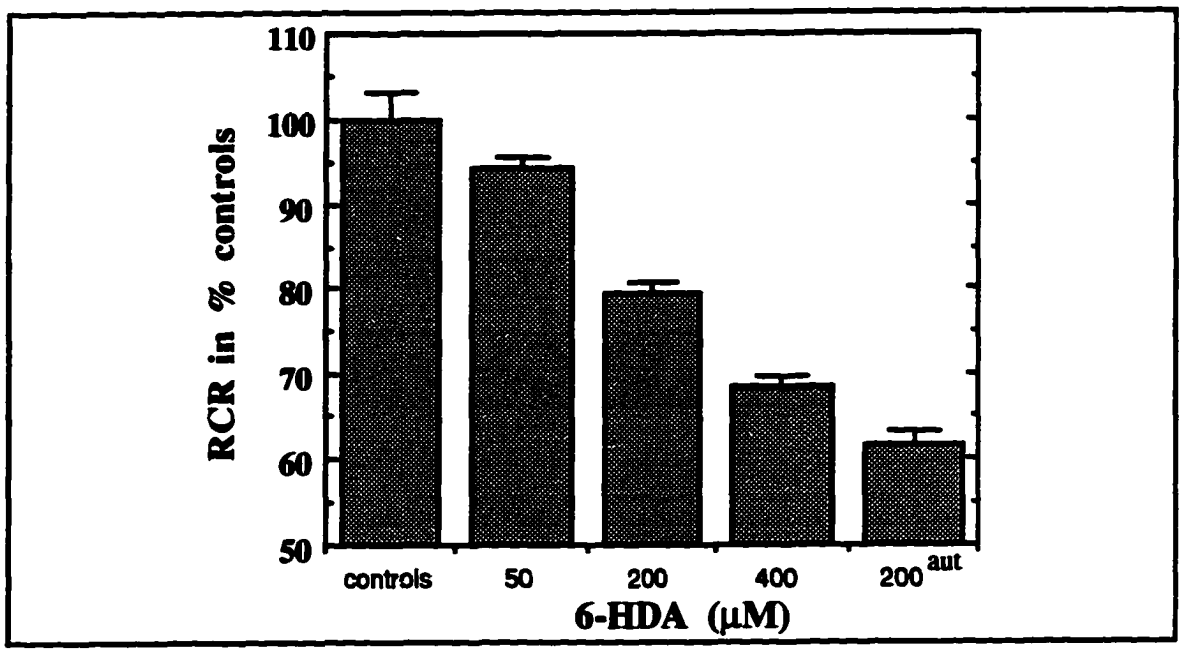

Figure 8-13. 6-HDA effects on RCR. aut indicates toxin not pre-oxidized.

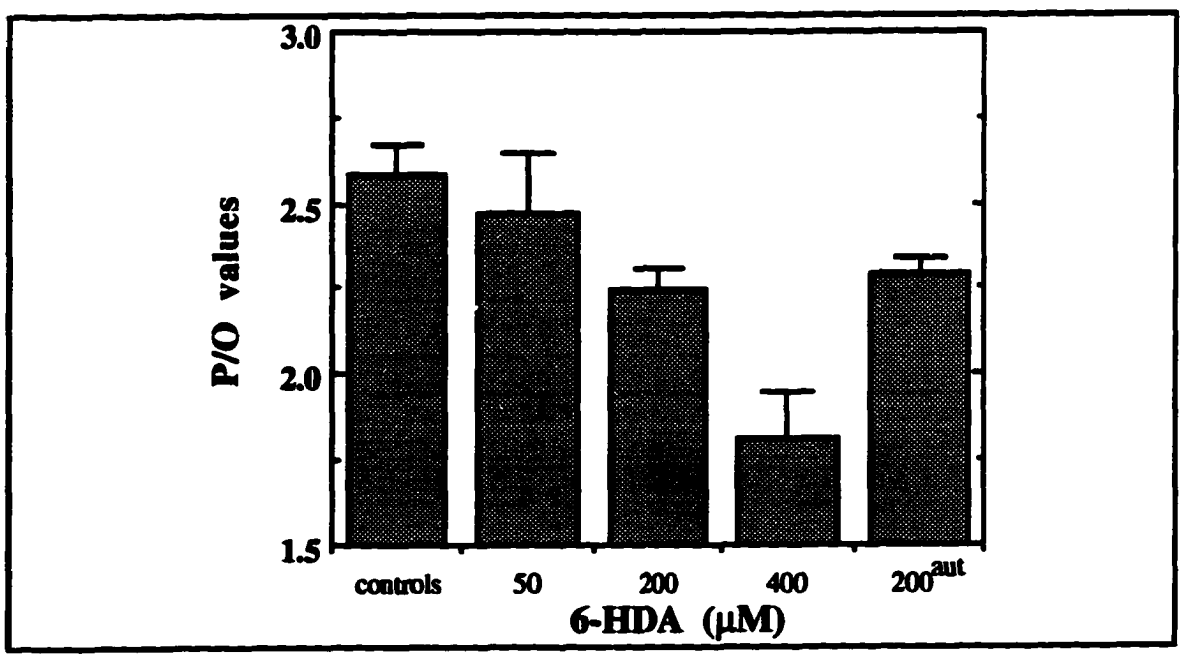

Figure 8-14. 6-HDA effects on P/O ratio. aut indicates toxin not pre-oxidized.

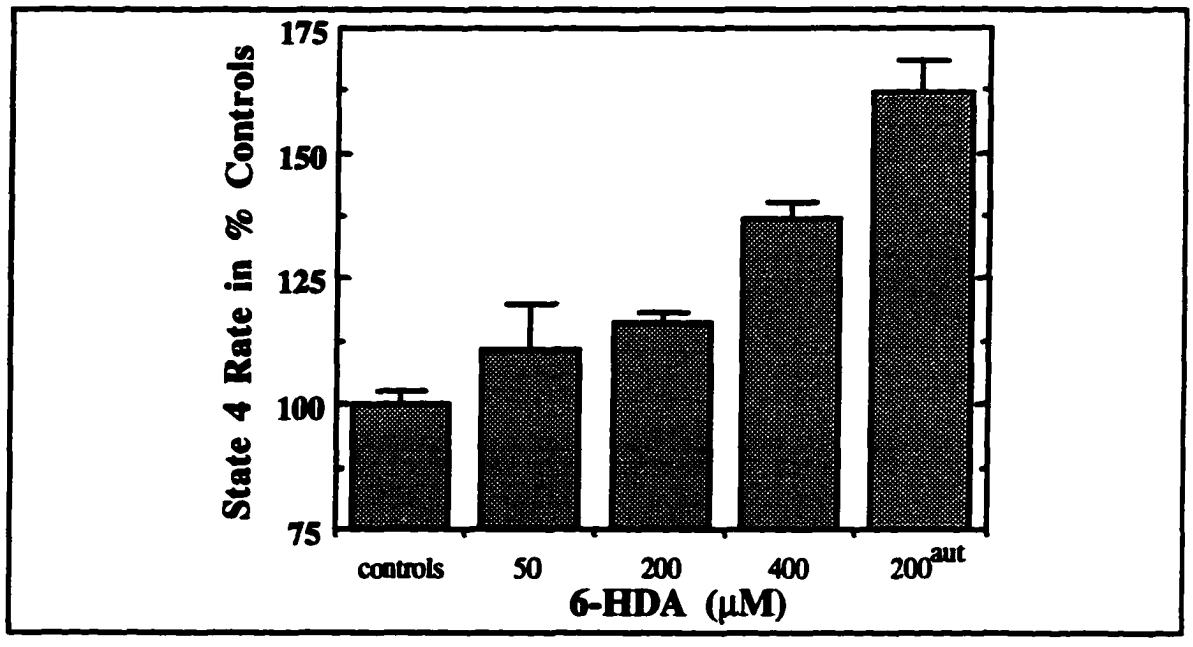

Figure 8-15. 6-HDA effects on state 4 rate. ^{aut} indicates toxin not pre-oxidized.

At 400 μM ox-6-HDA, we observed a concentration dependent increase in mitochondrial interaction. Both RCR and P/O values were inhibited by approximately 30%. State 4 respiration was stimulated to 137% of controls, which, for the most part, accounted for the lowering of the RCR and P/O values. However, again it appears that there may exist a very small degree of respiratory chain inhibition.

Investigating the effects of 6-HDA autoxidation on mitochondrial function yielded significantly different results than were found with the 200 μM preoxidized group. RCR values were 17% of control lower than observed with the preoxidized group. Furthermore, autoxidation resulted in an apparent increase in state 4 respiration to 162% of control, 46% of control higher than the preoxidized group. The potentiation in mitochondrial dysfunction resulting from toxin autoxidation suggests reactive intermediates and/or by-products that possibly disrupt mitochondrial membrane integrity, allowing respiration to occur at a higher, more uninhibited rate.

The decreases found in RCR and P/O values suggest either oxidative phosphorylation uncoupling or inhibition. However, stimulation of state 4 respiration is strongly indicative of uncoupling. The release of state 4 respiration by 6-HDA appears to account for the majority of the decreases observed in RCR and P/O values. The results found in our studies are in good agreement with those reported elsewhere.[57,60,165] Thus, it is our conclusion that 6-HDA, while possibly eliciting slight inhibition of the respiratory chain, acts primarily as a mitochondrial oxidative phosphorylation uncoupler.

E. Toxin Effects on Mitochondria, A Toxin Comparison

1. Respiratory Control Ratios (RCR)

Our studies indicate that there exists strong mitochondrial interactions with all of the quinoline toxins as well as 6-HDA. The RCR results are summarized in Table 8-7.

Table 8-7. RCR values of various toxins.

	RCR values in % control ± SEM				
Compound	Controls	50 μM	200 μM	400 μM	200 μM^{aut}
6,7-ADTQ	100 ± 1	69 ± 2***	64 ± 1***	56 ± 1***	61 ± 1***
6,7-AMDTQ	100 ± 2	80 ± 0.1***	73 ± 1***	67 ± 4***	60 ± 1***
6,8-ADTQ	100 ± 1	87 ± 2***	81 ± 1***	77 ± 0.3***	69 ± 2***
6-HDA	100 ± 3	94 ± 1	79 ± 1**	69 ± 1***	62 ± 2***

Significant differences compared to control values (*t* test): *$P < 0.05$; **$P < 0.01$, ***$P < 0.001$.

As we see in Table 8-7, these toxins elicit substantial decreases in the RCR values, of intact mitochondria, which correlates to serious oxidative phosphorylation interference. Moreover, the RCR values were found to consistently decrease in a toxin concentration-dependent manner. 6-HDA was included in these studies for comparative purposes, and the results obtained for this toxin agreed well with those reported in the literature.[57,60,165]

At all concentrations tested, 6,7-ADTQ produced the greatest decreases in RCR values, ranging from 31% inhibition in RCR at 50 μM to 46% at 400 μM. 6,7-AMDTQ showed the same trend as 6,7-ADTQ, but gave RCR values that were consistently approximately 10% higher than those of 6,7-ADTQ. 6,8-ADTQ also displayed the same trend, yet was even less potent in its ability to lower RCR values. 6-HDA did not tightly parallel the trend observed with the other compounds in that it produced very little RCR effects at 50 μM and only a 31% decrease in RCR values at 400 μM.

While we were primarily interested in the effects of the oxidized toxins on mitochondrial respiration, we were also curious to see if the process of toxin autoxidation had any additional effects on mitochondrial function. Not expecting to see any major differences between the pre-oxidized and the autoxidized 200 μM groups, we were quite surprised when differences appeared. 6,7-ADTQ^{aut} was the only toxin that did not display a substantial and significant decrease in the RCR value from that of its pre-oxidized group (64% vs. 61%^{aut} of controls). 6,7-AMDTQ^{aut} showed a significant 13% drop in its RCR below that of the pre-oxidized group, to 60% of control. 6,8-ADTQ^{aut} also showed significantly lower RCR values than the pre-oxidized group. 6-HDA^{aut} produced the most dramatic drop in RCR values, from the pre-oxidized group value of 79% to 62% of control values.

The pre-oxidized toxins showed a significant and substantial inhibition of the RCR, which was concentration dependent. This overall inhibition, occurring with the oxidized forms of the toxins, indicates either moderate inhibition or uncoupling of

oxidative phosphorylation. The further lowering of RCR values resulting from toxin autoxidation process suggests that there are reactive oxidation intermediates which interact with and/or damage the mitochondria, independent from the effects of the oxidized form of the toxin. This observed potentiation may also be a result of reactive oxygen species produced during toxin autoxidation.

2. P/O Ratios

For comparative purposes, P/O values are summarized in Table 8-8. 6,7-ADTQ and 6-HDA displayed a similar concentration-dependent reduction in P/O values, much like the trend seen with their RCR values. At 200 μM they both lower P/O values by approximately 14%, while at 400 μM P/O values were decreased by 20% and 30%, respectively. It appears that 6,7-AMDTQ exerted its maximal P/O effects of approximately 25% inhibition, over the entire concentration range tested. 6,8-ADTQ shows the least potency in lowering the P/O ratio, which parallels its effects on RCR values. 6,8-ADTQ, while not eliciting large decreases in P/O ratios, resulted in a consistent 10% RCR decrease from the lowest to the highest toxin concentration tested.

Table 8-8. P/O values of various toxins.

	P/O values in % controls ± SEM				
Compound	Control	50 μM	200 μM	400 μM	200 μM^{aut}
6,7-ADTQ	100 ± 2	96 ± 1	86 ± 2**	80 ± 0.6***	88 ± 3**
6,7-AMDTQ	100 ± 3	83 ± 2**	74 ± 2***	75 ± 2***	80 ± 2**
6,8-ADTQ	100 ± 1	92 ± 2**	92 ± 1**	90 ± 1***	96 ± 2*
6-HDA	100 ± 3	96 ± 6	87 ± 2**	70 ± 5**	89 ± 2*

Significant differences compared to control values (*t* test): *$P < 0.05$; **$P < 0.01$, ***$P < 0.001$.

When looking at the effects of the toxin autoxidation process on P/O ratios, we expected to observe similar trends as with the overall lowering in the RCR values, or at least equivalent P/O values to those found with the 200 μM pre-oxidized toxin group. Surprisingly, however, the P/O values observed with toxin autoxidation did not parallel the increased RCR^{aut} inhibition effects. And in fact, P/O^{aut} values were slightly larger than those of their corresponding 200 μM pre-oxidized toxin group. However, these results were not substantial nor significant in comparison to that of the pre-oxidized test group, except in the case of 6,8-ADTQ.

Lowering of the P/O value, while possibly occurring in multiple mitochondrial dysfunctions, is most suggestive of oxidative phosphorylation uncoupling. 6-HDA has previously been reported by many researchers to act primarily as an uncoupler.[57,60,165] Additionally, 6-HDA has been suggested to possess possible respiratory chain inhibitor activities.[58,59] Our toxic agents demonstrated equal or greater mitochondrial interactions than was observed with 6-HDA. All toxins tested displayed substantial enough decreases in P/O values that one could suggest their neurotoxic effects could be attributed, at least in part, to the associated mitochondrial interactions.

3. State 4 Respiration Rates

State 4 oxygen consumption rates were investigated to determine the ability of these toxins to release state 4 respiration. For comparative purposes, the results are summarized in Table 8-9.

6-HDA was found to release state 4 respiration to 116% of control at 200 μM and 137% at 400 μM, presumably by uncoupling oxidative phosphorylation. This correlates well with its ability to decrease RCR and P/O values and is further substantiated by reports of uncoupling in the literature.[57,60,165] The increase in state 4 rate produced by 6,8-ADTQ was very similar to 6-HDA. 6,7-AMDTQ was also much like 6-HDA and

6,8-ADTQ in that it increased state 4 respiration, at 200 μM, to 23% above controls. Interestingly, yet somewhat expected from its RCR values, 6,7-ADTQ resulted in a substantial state 4 release, to 185% of controls at 200 μM and 227% at 400 μM.

Table 8-9. State 4 respiration rates of various toxins.

	State 4 rate[a] in % controls ± SEM				
Compound	Controls	50 μM	200 μM	400 μM	200 μM[aut]
6,7-ADTQ	100 ± 2	165 ± 11**	185 ± 8***	227 ± 9***	190 ± 3***
6,7-AMDTQ	100 ± 5	122 ± 1**	123 ± 6*	128 ± 12	142 ± 1***
6,8-ADTQ	100 ± 3	115 ± 3*	129 ± 3***	136 ± 7**	125 ± 6*
6-HDA	100 ± 3	111 ± 9	116 ± 2*	137 ± 3**	162 ± 7***

Significant differences compared to control values (*t* test): $*P < 0.05$; $**P < 0.01$, $***P < 0.001$.

[a] Typical control state 4 oxygen consumption rates were 31 ± 1 (μmol O_2 / L•min).

The effects of toxin autoxidation on state 4 respiration were also investigated. For 6,7-ADTQ and 6,8-ADTQ, state 4 rates were similar to those of their pre-oxidized toxin values. 6,7-AMDTQ autoxidation resulted in an increase of 19% in state 4 respiration over the corresponding pre-oxidized group, but this was not significant. Autoxidation of 6-HDA showed a greater ability to release state 4 than was shown by its pre-oxidized counterpart, resulting in a stimulation to approximately 162% of control. Thus, 6-HDA appears to produce some oxidation intermediate and/or reactive by-product by which more complete mitochondrial uncoupling, damage, and/or inhibition is produced than by its oxidized form alone.

The ability of a compound to release state 4 respiration positively identifies it as an uncoupler. Therefore, our results show all of these toxic agents to be uncouplers to at

least some degree. While all toxins tested displayed uncoupling substantial enough to elicit mitochondrial dysfunction, 6,7-ADTQ was found to be the most potent in its uncoupling effects. 6,7-ADTQ, at 200 to 400 μM, displayed state 4 rates approaching those seen for state 3 respiration.

V. Conclusions

There must exist an adequate electron flow through the respiratory chain, sufficient oxygen delivery, and efficient coupling between the electron transport and oxidative phosphorylation in order to maintain the balance between ATP production and utilization in mitochondria. Our toxins have demonstrated the ability to interfere with production of ATP through what appears to be predominantly an uncoupling mechanism. The release in state 4 respiration produced by our toxins most likely results from the collapse of the mitochondrial proton gradient, thus allowing electrons to move through the respiratory chain with only limited regulation until all available oxygen is depleted. This hyperactive respiration could lead to the production of reactive oxygen species, hypoxia, reduced cytochrome activities, and a decrease in ATP levels. Many neuronal functions depend heavily on ATP and, when exposed to such disruptions, would be expected to be severely stressed. For example, one of the early results of ATP depletion is the impairment of the neuronal membrane ATP-linked Na^+/K^+ pump. Increases in extracellular K^+ depolarize voltage sensitive Ca^{2+} channels allowing Ca^{2+} to enter the cell, which in turn results in cell death.[63,64]

All toxins tested displayed a substantial lowering of RCR and P/O values and a release of state 4 respiration. Of these toxins, 6,7-ADTQ showed the highest potency for uncoupling oxidative phosphorylation, followed by 6,7-AMDTQ and 6-HDA, then 6,8-ADTQ. And, as shown in chapter four, 6,7-ADTQ was the most potent depleting

agent of the dihydroxytetrahydroquinoline derivatives. Thus, the mitochondrial effects at least correspond qualitatively to the observed neurodegenerative effects.

The pK_a values determined for the oxidized forms of these compounds were discussed in chapter six and are presented in Table 8-10. 2,6- and 2,4-DNP, classic mitochondrial oxidative phosphorylation uncouplers, are additionally included in Table 8-10 for comparative purposes. The pK_a values of the oxidized toxins are well within a reasonable range to act as uncouplers. While simple charged atoms and molecules cannot cross the mitochondrial inner membrane without specific carrier systems, charged molecules with an extended lipophilic structure and/or the ability to substantially delocalize charge are capable of passive transport.[72] Our toxins may, thus, produce uncoupling by this acid/base/transport phenomenon.

Table 8-10. pKa values of oxidized toxins and standard uncoupling agents.

Agent	pK_a
ox-6,7-ADTQ	6.61 ± 0.17
ox-6,7-AMDTQ	7.57 ± 0.03
ox-6,8-ADTQ	4.32 ± 0.09
ox-6-HDA	3.87 ± 0.04
2,4-DNP[179]	3.96
2,6-DNP[179]	5.63

While the toxin concentrations used in the current investigations may seem quite high, they are actually much lower than expected intraneuronally upon CNS injection. Studies have shown for 6-HDA that the intraneuronal threshold concentration, i.e., the

concentration which must be reached in order to initiate neurodestruction, is 30-100 mM.[27] Thus, the mitochondrial effects described above would be increased substantially in a neuron experiencing a neurotoxin insult.

Whether the impairment of mitochondrial function is a major factor in the neurotoxic mode of action of our toxins remains to be shown. However, the fact that our toxins all produce alterations in mitochondrial oxidative phosphorylation suggests that impairment of mitochondrial function is certainly a common, underlying property of 6-HDA and related neurotoxins.

References

1. Cooper, J.R., Bloom, F.E. and Roth, R.H. *The Biochemical Basis of Neuropharmacology*, New York:Oxford University Press, 1991. Ed. 6

2. Shepherd, G.M. *Neurobiology*, Nwe York:Oxford University Press, 1988. Ed. 2

3. Feldman, R.S. and Quenzer, L.F. *Fundamentals of Neuropsychopharacology*, Sunderland, Mass.:Sinauer Associates, Inc., 1984.

4. Kandel, E.R. and Schwartz, J.H. *Principles of Neural Science*, New York:Elsevier Science Publishing, 1985. Ed. 2

5. Gilman, A.G., Rall, T.W., Nies, A.S. and Taylor, P. *The Pharmacological Basis of Therapeutics*, New York:Pergamon Press, 1991. Ed. 8

6. Francis, C.A. *Synthesis of a Hydrocarbon-Nucleoside Adduct using Activated Purine Nucleosides, and the Synthesis and Bological Testing of Novel Serotonergic Neurotoxins*, Dissertation, University of Oklahoma, 1996.

7. Liebson, E. and Albert, M.L. Cognitive Changes in Dementia of the Alzheimers Type. In: *Neurodegenerative Diseases*, edited by Calne, D.B. Philadelphia, Pennsylvania: W.B. Saunders Co., 1994.

8. Rajput, A.H. Clinical Features and Natural History of Parkinson's Disease. In: *Neurodegererative Diseases*, edited by Calne, N.B. Philadelphia, Pennsylvania: W.B. Saunders Co., 1994.

9. Stinson, S.C. Frontiers in Modern Science. *Chem.Engin.News* 68:33, 1990.

10. Whyte, S., Beyreuther, K. and Masters, C.L. Rational Therapeutic Strategies for Alzheimer's Disease. In: *Neurodegenerative Diseases*, edited by Calne, D.B. Philadelphia, Pennsylvania: W.B. Saunders Co., 1994.

11. Braak, H. and Braak, E. Pathology of Alzheimer's Disease. In: *Neurodegenerative Diseases*, edited by Calne, D.B. Philadelphia, Pennsylvania: W.B. Saunders Co., 1994.

12. Hedera, P. and Whitehouse, P.J. Neurotransmitters in Neurodegeneration. In: *Neurodegenerative Diseases*, edited by Calne, D.B. Philadelphia: W. B. Saunders Co., 1994, p. 97-117.

13. Tsui, J.K.C. Treatment of Parkinson's Disease. In: *Neurodegenerative Diseases*, edited by Calne, D.B. Philadelphia, Pennsylvania: W.B. Saunders Co., 1994,

14. Fearnley, J. and Lees, A. Pathology of Parkinson's Disease. In: *Neurodegenerative Diseases*, edited by Calne, D.B. Philadelphia, Pennsylvania: W.B. Saunders Co., 1994.

15. Coopen, A., Prange, A.J., Whybrow, P.C. and Noguera, R. Abnormalities of the Indolamines in Affective Disorders. *Arch.Gen.Psychiat.* 26:474-478, 1972.

16. Coopen, A., Whybrow, P.C., Noguera, R., Maggs, R. and Prange, A.J. The Comparative Antidepressent Value of L-Tryptaphan and Imipramine With and Without Attempted Potentiation by Biothyronine. *Arch.Gen.Psychiat.* 26:234-241, 1972.

17. Dencker, S.J., Malm, U., Roos, B.E. and Werdinius, B. Acid Monoamine Metabloites Of Cerebrospinal Fluid in Mental Depression and Mania. *J.Neurochem.* 13:1545-1548, 1966.

18. Senoy, S., Creveling, C.R., Udenfriend, S. and Witkop, B. Chemical, Enzymatic and Metabolic Studies on the Mechanism of Oxidation of Dopamine. *J.Am.Chem.Soc.* 81:6236-6240, 1959.

19. Porter, C.C., Totaro, J.A. and Stone, C.A. Effect of 6-Hydroxydopamine and Some Other Compounds on the Concentration of Norepinephrine in the Hearts of Mice. *J.Pharacol.Exp.Ther.* 140:308-315, 1963.

20. Siggins, G.R., Forman, D.S., Bloom, F.E. and Sims, K.L. Degenerative Effects of 6-Hydroxydopamine on Peripheral and Central Adrenergic Nerves. In: *Chemical Tools in Catecholamine Research, Vol. 1*, edited by Jonsson, G., Malmfors, T. and Sachs, C. Amsterdam: North-Holland, 1975, p. 51-57.

21. Thoenen, H. and Tranzer, P. Chemical Sympathectomy by Selective Destruction of Adrenergic Nerve Endings with 6-Hydroxydopamine. *Naunyn Schmeidebergs Arch.Pharacol.* 261:271-288, 1968.

22. Johansson, B.B. Protective Barriers in the Nervous System Against Neurotoxic Agents: The Blood-Brain Barrier. In: *Handbook of Experimental Pharmacology Vol. 101/102, Selective Neurotoxicity*, edited by Herken, H. and Hucho, F. New York: Springer-Verlag, 1992, p. 67-80.

23. Lin, L.A. *Catecholamine and Indoleamine Neurotoxins*, Dissertation, University of Oklahoma, 1986.

24. Ma, S., Lin, L., Raghavan, R., Cohenour, P., Lin, P.Y.T., Bennett, J., Lewis, R.J., Enwall, E.L., Kostrzewa, R., Lehr, R.E. and Blank, C.L. In Vivo and In Vitro Studies on the Neurtoxic Potential of 6-Hydroxydopamine Analogs. *J.Med.Chem.* 38:4087-4097, 1995.

25. Blank, C.L., Lewis, R.J. and Lehr, R.E. 6-Hydroxydopamine and Related Catecholaminergic Neurotoxins: Molecular Mechanisms. In: *Highly Selective Neurotoxins: Basic and Clinical Applications*, edited by Kostrzewa, R.M. Clifton, NJ: Humana Press, 1996, in press.

26. Baumgarten, H.G., Bjorklund, A. and Bogdanski, D.F. Similarities and Differences in the Mode of Action of 6-Hydroxydopamine and Neurotoxic Indolamines. In: *Chemical Tools in Catecholamine Research, Vol. 1*, edited by Jonsson, G., Malmfors, T. and Sachs, C. Amsterdam: North-Holland, 1975, p. 59-66.

27. Jonsson, G. and Sachs, C. On the Mode of Action of 6-Hydroxydopamine. In: *Chemical Tools in Catecholamine Research, Vol. 1*, edited by Jonsson, G., Malmfors, T. and Sachs, C. Amsterdam: North-Holland, 1975, p. 41-50.

28. Sachs, C. and Jonsson, G. Mechanisms of Action of 6-Hydroxydopamine. *Biochem.Pharmac.* 24:1-8, 1975.

29. Langston, J.W. and Irwin, I. Organic Neurotoxicants. In: *Neurodegenerative Diseases*, edited by Calne, D.B. Philadelphia: W. B. Saunders Co., 1994, p. 225-240.

30. Baumgarten, H.G. and Ziggermann, B. Neurotoxic Phenylethylamines and Indolamines. In: *Handbook of Experimental Pharmacology*, edited by Herken, H. and Hucho, F. New York: Springer-Verlag, 1992.

31. Jonsson, G. and Sachs, C. Actions of 6-Hydroxydopamine Quinones on Catecholamine Neurons. *J.Neurochem.* 25:509-516, 1975.

32. Evans, J. and Cohen, G. Catecholamine Uptake Inhibitors Elevate 6-Hydroxydopamine in Brain after Administration of 6-Hydroxydopa. *Eur.J.Pharacol.* 232:241-245, 1993.

33. Cohen, G. and Heikkila, R.E. The Generation of Hydrgen Peroxide, Superoxide Radical, and Hydroxyl Radical by 6-Hydroxydopamine, Dialuric Acid, and Related Cytotoxic Agents. *J.Biol.Chem.* 249:2447-2452, 1974.

34. Heikkila, R.E. and Cohen, G. Cytotoxic Aspects of the Interaction of Ascorbic Acid with Alloxan and 6-Hydroxydopamine. *Ann.N.Y.Acad.Sci.* 258:221-230, 1975.

35. Heikkila, R.E. and Cohen, G. 6-Hydroxydopamine: Evidence for Superoxide Radical as an Oxidative Intermediate. *Science* 181:456-457, 1973.

36. Sullivan, S.G. and Stern, A. Effects of Superoxide Dismutase and Catalase on 6-Hydroxydopamine and 6-Aminodopamine Autoxidation by Iron and Ascorbate. *Biochem.Pharmac.* 30(16):2279-2285, 1981.

37. Heikkila, R. and Cohen, G. Further Studies on the Generation of Hydrogen Peroxide by 6-Hydroxydopamine. *Mol.Pharmacol.* 8:241-248, 1972.

38. Bandy, B. and Davison, A.J. Interaction Between Metals, Ligands, and Oxygen in the Autoxidation of 6-Hydroxydopamine: Mechanisms by which Metal Chelation Enhances Inhibition by Superoxide Dismutase. *Arch.Biochem.Biophys.* 259(2):305-315, 1987.

39. Palomba, L., Brambilla, L., Brandi, G., Sestili, P., Cattabeni, F. and Cantoni, O. Low Levels of Hydrogen Peroxide and L-Histidine induce DNA Double-Strand Breakage and Apoptosis. *Eur.J.Pharacol.* 318:167-173, 1996.

40. Simic, M.G. *Oxygen Radicals in Biology and Medicine*, New York:Plenum Press, 1988.

41. Cohen, G. and Werner, P. Free Radicals, Oxidative Stress, and Neurodegeneration. In: *Neurodegenerative Diseases*, edited by Calne, D.B. Philadelphia, Pennsylvania: W.B. Saunders Co., 1994.

42. Borg, D.C., Schaich, K.M., Elmore, Jr.,J.J. and Bell, J.A. Cytotoxic Reactions of Free Radical Species of Oxygen. *Photochem.Photobiol.* 28:887-907, 1978.

43. Kumar, R., Agarwal, A.K. and Seth, P.K. Free Radical-Generated Neurotoxicity of 6-Hydroxydopamine. *J.Neurochem.* 64:1703-1707, 1995.

44. Graf, E., Mahoney, J.R., Bryant, R.G. and Eaton, J.W. Iron-Catalyzed Hydroxyl Radical Formation. *J.Bio.Chem.* 259:3620-3624, 1984.

45. Floyd, R.A. Direct Demonstration that Ferrous Ion Complexes of Di- and Triphosphate Nucleotides Catalyze Hydroxyl Free Radical Formation from Hydrogen Peroxide. *Arch.Biochem.Biophys.* 225(1):263-270, 1983.

46. Butler, J. and Halliwell, B. Reaction of Iron-EDTA Chelates with the Superoxide Radical. *Arch.Biochem.Biophys.* 218(1):174-178, 1982.

47. Gutteridge, J.M.C., Richmond, R. and Halliwell, B. Inhibition of the Iron-Catalyzed Formation of Hydroxyl Radicals from Superoxide and of Lipid Peroxidation by Desferrioxamine. *J.Biochem.* 184:469-472, 1979.

48. Walling, C. Fenton's Reagent Revised. *Acc.Chem.Res.* 8:125-131, 1975.

49. Abad, F., Maroto, R., Lopaz, M.G., Garcia, P.S. and Garcia, A.G. Pharacological Protection Against the Cytotoxicity Induced by 6-Hydroxydopamine and Hydrogen Peroxide in Chromaffin Cells. *Eur.J.Pharacol.* 293:55-64, 1995.

50. Nappi, A.J. and Vass, E. The Effects of Glutathione and Ascorbic Acid on the Oxidation of 6-Hydroxydopa and 6-Hydroxydopamine. *Biochim.Biophys.Acta* 1201:498-504, 1994.

51. Creveling, C.R., Rotman, A. and Daly, J.W. Interactions of 6-Hydroxydopamine and Related Compounds with Proteins; A Model for the Mechanism of Cytotoxicity. In: *Chemical Tools in Catecholamine Research, Vol. 1*, edited by Jonsson, G., Malmfors, T. and Sachs, C. Amsterdam: North-Holland, 1975, p. 23-32.

52. Borchardt, R.T. Catechol O-Methyltransferase: A Model to Study the Mechanism of 6-Hydroxydopamine Interaction with Proteins. In: *Chemical Tools in Catecholamine Research, Vol. 1*, edited by Jonsson, G., Malmfors, T. and Sachs, C. Amsterdam: North-Holland, 1975, p. 33-40.

53. Liang, Y.O., Wightman, R.M., Plotsky, P. and Adams, R.N. Oxidative Interactions of 6-Hydroxydopamine with CNS Constituents. In: *Chemical Tools in Catecholamine Research, Vol. 1*, edited by Jonsson, G., Malmfors, T. and Sachs, C. Amsterdam: North-Holland, 1975, p. 15-22.

54. Graham, D.G., Tiffany, S.M., Bell, Jr.,W.R. and Gutknecht, W.F. Autoxidation versus Covalent Binding of Quinones as the Mechanism of Toxicity of Dopamine, 6-Hydroxydopamine, and Related Compounds toward C1300 Neuroblastoma Cells in Vitro. *Mol.Pharmacol.* 14:644-653, 1978.

55. Rotman, A., Daly, J.W., Creveling, C.R. and Breakefield, X.O. Uptake and Binding of Dopamine and 6-Hydroxydopamine in Murine Neuroblastoma and Fibroblast Cells. *Biochem.Pharm.* 25:383-388, 1976.

56. Decker, D.E., Althaus, J.S., Buxser, S.E., VonVoigtlander, P.F. and Ruppel, P.L. Competitive Irreversible Inhibition of Dopamine Uptake by 6-Hydroxydopamine. *Res.Com.Chemical Pathol.Pharmacol.* 79:195-208, 1993.

57. Thakar, J.H. and Hassen, M.N. Effects of 6-Hydroxydopamine on Oxidative Phosphorylation of Mitochondria from Rat Striatum, Cortex, and Liver. *Can.J.Physiol.Pharacol.* 66:376-379, 1987.

58. Glinka, Y., Tipton, K.F. and Youdim, M.B.H. Nature of Inhibition of Mitochondrial Respiratory Complex I by 6-Hydroxydopamine. *J.Neurochem.* 66:2004-2010, 1996.

59. Glinka, Y.Y. and Youdim, M.B.H. Inhibition of Mitochondrial Complexes I and IV by 6-Hydroxydopamine. *Eur.J.Pharacol.* 292:329-332, 1995.

60. Wagner, K. and Trendelenburg, U. Effects of 6-HDA on Oxidative Phosphorylation and on Monoamine Oxidase Activity. *Naunyn Schmeidebergs Arch.Pharacol.* 269:112-116, 1971.

61. Frei, B. and Richter, C. N-Methyl-4-Phenylpyridine (MMP+) Together with 6-Hydroxydopamine of Dopamine Stimulates Ca++ Release from Mitochondria. *FEBS* 198(1):99-102, 1986.

62. Reichman, N., Porteous, C.M. and Murphy, M.P. Cyclosporin A Blocks 6-Hydroxydopamine-Induced Efflux of Ca++ from Mitochondria without Inactivating the Mitochondrial Inner-Membrane Pore. *J.Biochem.* 297:151-155, 1994.

63. Jewell, S.A., Bellomo, G., Thor, H., Orrenius, S. and Smith, M.T. Bleb Formation in Hepatocytes During Drug Metabolism is Caused by Disturbances in Thiol and Calcium Ion Homeostasis. *Science* 217:1257-1258, 1982.

64. Bellomo, G., Jewell, S.A., Thor, H. and Orrenius, S. Regulation of Intracellular Calcium Compartmentation: Studies With Isolated Hepatocytes and t-Butyl Hydroperoxide. *Proc.Natl.Acad.Sci.USA* 79:6842-6846, 1982.

65. Monteiro, H.P. and Winterbourn, C.C. 6-Hydroxydopamine Releases Iron from Ferritin and Promotes Ferritin-Depentent Lipid Peroxidation. *Biochem.Pharmac.* 38(23):4177-4182, 1989.

66. Walkinshaw, G. and Waters, C.M. Neurotoxin-Induced Cell Death in Neuronal PC12 Cells is Mediated by Induction of Apootosis. *J.Neurosci.* 63(4):975-987, 1994.

67. Kopin, I.J. Features of the Dopaminergic Neurotoxin MPTP. *Ann.N.Y.Acad.Sci.* 648:96-104, 1992.

68. Langston, J.W., Ballard, P., Tetrud, J.W. and Irwin, I. Chronic Parkinsonism in Humans Due to a Product of Meperidine-Analog Synthesis. *Science* 219:979-980, 1983.

69. Kopin, I.J. Mechanism of 1-Methyl-4-Phenyl-1,2,3,6-Tetrahydropyridine Induced Destruction of Dopaminergic Neurons. In: *Handbook of Experimental Pharmacology*, edited by Herken, H. and Hucho, F. New York: Springer-Verlag, 1992.

70. Sonsalla, P.K., Youngster, S.K., Kindt, M.V. and Heikkila, R.E. Characteristics of 1-Methyl-4-(2'-methylphenyl)-1,2,3,6-tetrahydropyridine-Induced Neurotoxicity in the Mouse. *J.Pharm.Exp.Therap.* 242(3):850-857, 1987.

71. Langston, J.W., Irwin, I., Langston, E.B. and Forno, L.S. Pargyline Prevents MPTP-Induced Parkinsonism in Primates. *Science* 225:1480-1482, 1984.

72. Hoppel, C.L., Greenblatt, D., Kwok, H., Arora, P.K., Singh, M.P. and Sayre, L.M. Inhibition of Mitochondrial Respiration by Analogs of 4-Phenylpyridine and 1-Methyl-4-Phenylpyridinium Cation (MPP+), the Neurotoxic Metabolite of MPTP. *Biochem.Biophys.Res.Commun.* 148:684-693, 1987.

73. Nicklas, W.J., Vyas, I. and Heikkila, R.E. Inhibition of NADH-Linked Oxidation in Brain Mitochondria by 1-Methyl-4-Phenylpyridine, a Metabolite of the Neurotoxin, 1-Methyl-4-Phenyl-1,2,5,6-Tetrahydropyridine. *Life Sci.* 36:2503-2508, 1985.

74. DiMonte, D.A., Jewell, S.A. and Ekstom, G. 1-Methyl-4-Phenyl-1,2,3,6-Tetrahydropyridine (MPTP) and 1-Methyl-4-Phenylpyridine (MPP+) Cause Rapid ATP Depletion in Isolated Hepatocytes. *Biochem.Biophys.Res.Commun.* 137:310-315, 1986.

75. Chan, P., DeLanney, L.E. and Irwin, I. Rapid ATP Depletion by 1-Methyl-4-Phenyl-1,2,3,6-Tetrahydropyridine in Mouse Brain. *J.Neurochem.* 57:348-351, 1991.

76. Tetrud, J.W. and Langston, J.W. The Effects of Deprenyl (slegiline) on the Natural History of Parkinson's Disease. *Science* 245:519-522, 1989.

77. Youdim, M.B.H. and Lavie, L. Selective MAO-A and MAO-B Inhibitors, Radical Scavengers and Nitric Oxide Synthase Inhibitors in Parkinsin's Disease. *Life Sci.* 55(25/26):2077-2082, 1994.

78. Reichmann, H. and Riederer, P. Mitochondrial Disturbances in Neurodegeneration. In: *Neurodegenerative Diseases*, edited by Calne, D.B. Philadelphia, Pennsylvania: W.B. Saunders Co., 1994.

79. Herman, Z.S. and Bonczek, A. Model of Central Chemical 'Serotoninectomy' in Mice. *Pharmacol.* 17:8-14, 1978.

80. Jacoby, J.H., Lytle, L.D. and Nelson, M.F. Long-Term Effects of 5,7-Dihydroxytryptamine on Brain Monoamines. *Life Sci.* 14:909-919, 1974.

81. Liston, D.R., Franz, D.N. and Gibb, J.W. Biochemical Evidence for Alteration of Neostriatal Dopaminergic Function by 5,7-Dihydroxytryptamine. *J.Neurochem.* 38:1329-1335, 1982.

82. Klemm, H.P., Baumgarten, H.G. and Schlossgerger, H.G. Polarographic Measurements of Spontaneous and Mitochondria-Promoted Oxidation of 5,6- and 5,7-Dihydroxytryptamine. *J.Neurochem.* 35(6):1400-1408, 1980.

83. Sinhababu, A.K. and Borchardt, R.T. Mechanism and Products of Autoxidation of 5,7-Dihydroxytryptamine. *J.Am.Chem.Soc.* 107:7618-7627, 1985.

84. Wrona, M.Z., Lemordant, D., Lin, L., Blank, C.L. and Dryhurst, G. Oxidation of 5-Hydroxytryptamine and 5,7-Dihydroxytrypamine. A New Oxidation Pathway and Formation of a Novel Neurotoxin. *J.Med.Chem.* 29:499-505, 1986.

85. Tabatabaie, T. and Dryhurst, G. Chemical and Enzyme-Mediated Oxidation of the Serotonergic Neurotoxin 5,7-Dihydroxytryptamine: Mechanistic Insight. *J.Med.Chem.* 35:2261-2274, 1992.

86. Cohen, G. and Heihhila, R.E. Mechanisms of Action of Hydroxylated Phenylethylamine and Indolamine Neurotoxins. *Ann.N.Y.Acad.Sci.* 305:74-84, 1978.

87. Baumgarten, H.G., Klemm, H.P., Lachenmayer, L., Bjorklund, A., Lovenberg, W. and Schlossberger, H.G. Mode and Mechanism of Action of Neurotoxic Indolamines: A Review and a Progress Report. *Ann.N.Y.Acad.Sci.* 305:3-24, 1978.

88. Klemm, H.P., Baumgarten, H.G. and Schlossberger, H.G. In Vitro Studies on the Interaction of Brain Monoamine Oxidase with 5,6- and 5,7-Dihydroxytryptamine. *J.Neurochem.* 32:111-119, 1979.

89. Tabatabaie, T. *Study of the Oxidation Chemistry and the biochemistry of the Serotonergic Neurotoxin 5,7-Dyhydroxytryptamine in Regard to its Neurodegenerative Action*, Dissertation, University of Oklahoma, 1992.

90. Baumgarten, H.G., Bjorklund, A., Lachenmayer, L., Nobin, A. and Stenevin, U. Long-Lasting Selective Depletion of Brain Serotonin by 5,6-Dihydroxytryptamine. *Acta Physiol.Scand.Suppl.* 373:1-15, 1971.

91. Costa, E., Lefevere, H., Meek, J., Revuelta, A., Spano, F., Strada, S. and Daly, J. Serotonin and Catecholamine Concentrations in Brain of Rats Injected Intracerebrally with 5,6-Dihydroxytryptamine. *Brain Res.* 44:304-308, 1972.

92. Singh, S. and Dryhurst, G. Further Insights into the Oxidation Chemistry and Biochemistry of the Serotonergic Neurotoxin 5,6-Dihydroxytryptamine. *J.Med.Chem.* 33:3035-3044, 1990.

93. Williams, A. Susceptibility to Neurotoxins. In: *Neurodegenerative Diseases*, edited by Calne, D.B. Philadelphia: W. B. Saunders Co., 1994, p. 205-224.

94. Rollema, H., Johnson, E.A., Booth, R.G., Caldera, P., Lampen, P., Youngster, S.K., Trevor, A.J., Naiman, N. and Castagnoli, N. In Vivo Intracerebral Microdialysis in Rats of MPP+ Analogues and Related Charged Species. *J.Med.Chem.* 33:2221-2230, 1990.

95. Wrona, M.Z., Goyal, R.N., Turk, D.J., Blank, C.L. and Dryhurst, G. 5,5'-Dihydroxy-4,4'-Bitryptamine: A Potentially Aberrant Neurotoxic Metabolite of Serotonin. *J.Neurochem.* 59:1392-1398, 1992.

96. Musson, D.G., Karashina, D., Rubiero, H., Melmon, K.L., Cheng, A. and Castagnoli, N. Synthetic and Preliminary Hemodynamic and Whole Animal Toxicity Studies on (R,S)-, and (S)-2-Methyl-3-(2,4,5-Trihydroxyphenyl)Alanine. *J.Med.Chem.* 23:1318-1323, 1980.

97. Cheng, A. and Castagnoli, N. Synthesis and Physicochemical and Neurotoxicity Studies of 1-(4-Substituted-2,5-dihydroxyphenyl)-2-Aminoethane Analogues of 6-Hydroxydopamine. *J.Med.Chem.* 27:513-520, 1984.

98. Jacob, P., Kline, T. and Castagnoli, N. Chemical and Biological Studies of 1-(2,5-Dihydroxy-4-Methylphenyl)-2-Aminopropane, an Analogie of 6-Hydroxydopamine. *J.Med.Chem.* 22:662-670, 1979.

99. Zweig, J.S. and Castagnoli, N. In Vitro O-Demethylation of the Psychotomimetic Amine, 1-(2,5-Dimethoxy-4-Methylphenyl)-2-Aminopropane. *J.Med.Chem.* 20:414-420, 1977.

100. Zweig, J.S. and Castagnoli, N. Chemical Conversion of the Psychotomimetic Amine 1-(2,5-Dimethoxy-4-Methylphenyl)-2-Aminopropane to 5-Hydroxy-2,6-Dimethylindole. *J.Med.Chem.* 17:747-749, 1974.

101. Buchley, T.F.,III and Rapoport, H. Dependence of Aryl Ether Acylation upon Lewis Acid Stoichiometry. *J.Am.Chem.Soc.* 102:9:3056-3062, 1980.

102. Irie, H., Shiina, A., Fushimi, T., Katakawa, J., Fujii, N. and Yajima, H. New Synthesis of Isoquinoline Alkaloids, Thalifoline, Corypalline, and Cherylline. *Chem.Lett.* 875-878, 1980.

103. Lin, P.Y.T., Bulawa, M.C., Wong, P., Lin, L., Scott, J. and Blank, C.L. The Determination of Catecholamines, Indoleamines, Metabolites, and Related Activities using Three Micron Liquid Chromatography Columns. *J.Liq.Chromatogr.* 7(3):509-538, 1984.

104. Ikarashi, I., Blank, C.L., Inoue, H.K. and Maruyama, Y. Measurement of Neurochemical Levels in Ventricular Cerebrospinal Fluid of Parkinson's Patients using Multicolumn, Multielectrode Liquid Chromatography with Electrochemical Detection. *Biogen.Amines* 8(3/4):175-190, 1992.

105. Kissinger, P.T. Amperometric and Coulometric Detectors for High-Performance Liquid Chromatography. *Anal.Chem.* 49(4):447-456, 1977.

106. Mefford, I.N. Application of High Performance Liquid Chromatography with Electrochemical Detection to Neurochemical Analysis: Measurement of Catecholamines, Serotonin and Metabolites in Rat Brain. *J.Neurosci.Meth.* 3:207-224, 1981.

107. Bard, A.J. and Faulkner, L.R. *Electrochemical Methods: Fundamentals and Applications*, New York:John Wiley & Sons, 1980.

108. Adams, R.N. Probing Brain Chemistry with Electroanalytical Techniques. *Anal.Chem.* 48(14):1128-1138, 1976.

109. Blank, C.L. Dual Electrochemical Detector for Liquid Chromatography. *J.Chromatogr.* 117:35-46, 1976.

110. Stulik, K. and Pacakova, V. Electrochemical Detection Techniques in High-Performance Liquid Chromatography. *J.Electroanal.Chem.* 129:1-24, 1981.

111. Ewing, A.G., Mesaros, J.M. and Gavin, P.F. Electrochemical Detection in Microcolumn Separations. *Anal.Chem.* 66:527A-537A, 1994.

112. Kissinger, P.T. Biomedical Applications of Liquid Chromatography-Electrochemistry. *J.Chromatogr.* 488:31-52, 1989.

113. Kissinger, P.T., Burntlett, C.S. and Shoup, R.E. Neurochemical Applications of Liquid Chromatography with Electrochemical Detection. *Life Sci.* 28:455-465, 1981.

114. Buchberger, W. Trends in the Combination of High-Performance Liquid Chromatograpgy and Electrochemical Methods. *Chromatographia* 30:577-581, 1990.

115. Wang, J. Modified Electrodes for Electrochemical Detection in Flowing Systems. *Analytica Chimica Acta* 234:41-48, 1990.

116. Weber, S.G. and Purdy, W.C. The Behaviour of an Electrochemical Detector Used in Liquid Chromatography and Continuous Flow Voltammetry. *Analytica Chimica Acta* 100:531-544, 1978.

117. Prabhu, S. and Anderson, J.L. Flow-Rate and Column-Parameter Dependence of Amperometric Detector Responce in Liquid Chromatography with Electrochemical Detection. *Anal.Chem.* 59:157-163, 1987.

118. Nicholson, R.S. and Shain, I. Theory of Stationary Electrode Polarography. *Anal.Chem.* 36(4):706-723, 1964.

119. Faulkner, L.R.K Understanding Electrochemistry: Some Distinctive Concepts. *J.Chem.Edu.* 60(4):262-264, 1983.

120. Maloy, J.T. Factors Affecting the Shape of Current-Potential Curves. *J.Chem.Edu.* 60(4):285-289, 1983.

121. Giddings, J.C. *Unified Separation Science*, New York:John Wiley & Sons, 1991.

122. Freeman, K., Lin, P.Y.T., Lin, L. and Blank, C.L. Monoamines and metabolites in the brain. In: *High Performance Liquid Chromatography in the Neurosciences, a Monograph in the International Brain Research Organization (IBRO) Handbook Series*, edited by Holman, R.B., Joseph, M.H. and Cross, A.J. London, England: John Wiley & Sons, Ltd., 1993, p. 27-55.

123. Lochmuller, C.H., Breiner, S.J., Reese, C.E. and Koel, M.N. Characterization and Prediction of Retention Behavior in Reversed-Phase Chromatography Usinf Factor Analytical Modeling. *Anal.Chem.* 61:367-375, 1989.

124. Kostrzewa, R.M., Fukushima, H., Morrow, A., Cohenour, P., Hsi, T., Lehr, R.E. and Blank, C.L. a-Methyl-6-aminodopamine:Depletion of Catecholamines in Mouse Brain and Peripheral Tissue. *Life Sci.* 27:2245-2250, 1980.

125. Tranzer, J.P. and Thoenen, H. Selective Destruction of Adrenergic Nerve Terminals by Chemical Analogues of 6-Hydroxydopamine. *Experientia* 29:314-315, 1973.

126. Hogg, R.V. and Tanis, E.A. *Probability and Statistical Inference*, New York:Macmillan, 1988. Ed. 3

127. Skoog, D.A., West, D.M. and Holler, F.J. *Analytical Chemistry*, Philadelphia, Pennsylvania:Saunders College Publishing, 1990. Ed. 5

128. Dixon, W.J. and Mood, A.M. A Method for Obtaining and Analyzing Sensitivity Data. *J.Amer.Statistical Assoc.* 109-126, 1948.

129. Dixon, W.J. The Up-and-Down Method for Small Samples. *J.Amer.Statistical Assoc.* 60:967-978, 1965.

130. Dixon, W.J. Staircase Bioassay: The Up-and-Down Method. *Neurosci.Biobehav.Rev.* 15:47-50, 1991.

131. Blank, C.L., Sasa, S., Isernhagen, R., Meyerson, L.R., Wassil, D., Wong, P., Modak, A.T. and Stavinoha, W.B. Levels of Norepinephrine and Dopamine in Mouse Brain Regions Following Microwave Inactivation - Rapid Post-Mortem Degradation of Striatal Dopamine in Decapitated Animals. *J.Neurochem.* 33:213-219, 1979.

132. Blank, C.L., Abdullah, H., Meyerson, L.R., Modak, A.T. and Stavinoha, W.B. Microwave Heating and Serotonin Determinations. In: *Microwave Irradiation as a Tool to Study Labile Metabolites in Tissue*, edited by Blank, C.L., Stavinoha, W.B. and Maruyama, Y. london, England: Pergamon Press, 1983, p. 63-73.

133. Maruyama, Y., Ikarashi, Y. and Blank, C.L. Evaluation of Various Microwave Instruments for Rapid Inactivation of Brain Enzymes. *Biogen.Amines* 4(1):55-71, 1987.

134. Turk, D.J. and Blank, C.L. Calibration of Microwave Instruments. In: *Microwave Irradiation for Histochemical and Neurochemical Investigations*, edited by Blank, C.L., Howard, S. and Maruyama, Y. Tokyo, Japan: Science Publishers, 1989, p. 103-121.

135. Horn, A.S. Structure Activity Relations for the Inhibition of 5-HT Uptake into Rat Hypothalamic Homogenates by Serotonin and Tryptamine Analogues. *J.Neurochem.* 21:883-888, 1973.

136. Horn, A.S. Structure-Activity Relations for the Inhibition of Catecholamine Uptake into Synaptosomes from Noradrenergic and Dopamineergic Neurones in Rat Brain Homogenates. *Br.J.Pharmac.* 47:332-338, 1973.

137. Horn, A.S. Dopamine Uptake: A Review of Progress in the Last Decade. *Progress in Neurobiology* 34:387-400, 1990.

138. Booth, R.F.G. and Clark, J.B. A Rapid Method for the Preparation of Relatively Pure Metabolically Competent Synaptosomes from Rat Brain. *Biochem.J.* 176:365-370, 1978.

139. Appel, S.H., Day, E.D. and Mickey, D.D. Cellular and Subcellilar Fractionation. In: *General Neurochemistry*, 1987.

140. Iversen, L.L. Role of Transmitter Uptake Mechanisms in Synaptic Neurotransmission. *Br.J.Pharmac.* 41:571-591, 1971.

141. Harris, J.E. and Baldessarin, R.J. Uptake of Catecholamines by Homogenates of Rat Corpus Striatum and Cerebral Cortex: Effects of Amphetamine Analogues. *Neuropharm.* 12:669-679, 1973.

142. Coyle, J.T. and Axelrod, J. Development of the Uptake and Storage of NE in the Rat Brain. *J.Neurochem.* 18:2061-2075, 1971.

143. Cheng, Y.C. and Prusoff, W.H. Relationship Between the Inhibition Constant (Ki) and the Concentration of Inhibitor which causes 50% Inhibition (IC50) of an Enzymatic Reaction. *Biochem.Pharmac.* 22:3099-3108, 1973.

144. Smith, P.K., Kronhn, R.I., Hermanson, G.T., Mallia, A.K., Gartner, F.H., Provenzano, M.D., Fujimoto, E.K., Goeke, N.M., Olson, B.J. and Klenk, D.C. Measurement of Protein Using Bicinchoninic Acid. *Anal.Biochem.* 150:76-85, 1985.

145. Zhang, J.M. and Sieber-Blum, M. Characterization of the Norepinephrine Uptake System and the Role of Norepinephrine in the expression of the Adrenergic Phenotype by Quail Neural Crest Cells in Clonal Culture. *Brain Res.* 570:251-258, 1992.

146. Iversen, L.L. The Uptake of Noradenaline by the Isolated Perfused Rat Heart. *Br.J.Pharmac.* 21:523-537, 1963.

147. Ross, S.B. Synaptic Concentration of Dopamine in the Mouse Striatum in Relationship to the Kinetic Properties of the Dopamine Receptors and Uptake Mechanism. *J.Neurochem.* 56:22-29, 1991.

148. Martin, D.C., Adams, R.J. and Introna, R.P.S. Halothane Inhibits 5-Hydroxytryptamine Uptake by Synaptosomes from Rat Brain. *Neuropharm.* 29, No. 1:9-16, 1990.

149. Martin, D.C., Watkins, C.A., Adams, R.J. and Nason, L.A. Anesthetic Effects on 5-Hydroxytryptamine Uptake by Rat Brain Synaptosomes. *Brain Res.* 455:360-365, 1988.

150. Parsons, L.H., Schad, C.A. and Justice, Jr.,J.B. Co-Administration of the D2 Antagonist Pimozide Inhibits Up-Regulation of Dopamine Release and Uptake Induced by Repeated Cocaine. *J.Neurochem.* 60:376-379, 1993.

151. Nagafugi, T., Koide, T., Miyauchi, T. and Takato, M. An Activation of Synaptosomal Na+, K+-ATPase by a Novel Dibenzoxapine Derivative (BY-1949) in the Rat Brain: Its Functional Role in the Neurotransmitter Uptake System. *J.Neurochem.* 58:362-368, 1992.

152. Komulainen, H., Pietarinen, R. and Tuomisto, J. Increase in Dopamine Uptake in rat Synaptosomes after an Acute in vivo Administration of Organic and Inorganic Lead. *Acta pharmacol.et toxicol.* 52:381-389, 1983.

153. Ahluwalia, P. and Singhal, R.L. Monoamine Uptake Into Synaptosomes From Various Regions of Rat Brain Following Lithium Administration and Withdrawal. *Neuropharm.* 20:483-487, 1981.

154. Odarjuk, J., Hetey, L. and Gross, J. Synaptosomal Uptake and Release of Dopamine in Rat Striatum After Hypoxia. *J.Neurochem.* 48:1115-1120, 1987.

155. Ganellin, C.R. Relative Concentrations of Zwitterionic and Uncharged Species in Catecholamines and the Effect of N-Substitution. *J.Med.Chem.* 20:579-581, 1977.

156. Antikainen, P.J. and Witikainen, U. A Comparative Study on the Ionization of Catechol Amines in Aqueous Solutions. *Acta Chem.Scand.* 27:2075-2082, 1973.

157. Kappe, T. and Armstrong, M.D. Ultraviolet Absorption Spectra and Apparent Acidic Dissociation Constants of some Phenolic Amines. *J.Med.Chem.* 8:368-374, 1965.

158. Martin, R.B. Zwitterion Formation upon Deprotonation in L-3,4-Dihydroxyphenylalanine and Other Phenolic Amines. *J.Phys.Chem.* 75:2657-2661, 1971.

159. Riegelman, S., Strait, L.A. and Fischer, E.Z. Acid Dissociation Constants of Phenylalkanolamines. *J.Phys.Chem.* 51:129-133, 1962.

160. Lewis, G.P. The Importance of Ionization in the Activity of Sympathomimetic Amines. *Brit.J.Pharm.Chemo.* 9:488-493, 1954.

161. Albert, A. Ionization, pH and Biological Activity. *Pharm.Rev.* 4:136-167, 1952.

162. Liang, Y.O., Wightman, R.M. and Adams, R.N. Competitive Oxidation of 6-Hydroxydopamine by Oxygen and Hydrogen Peroxide. *Eur.J.Pharacol.* 36:455-458, 1976.

163. McCreery, R.L., Dreiling, R. and Adams, R.N. Voltammetry in Brain Tissue: the Fate of Injected 6-Hydroxydopamine. *Brain Res.* 73:15-21, 1974.

164. Heikkila, R.E. and Cohen, G. *Chemical Tools in Catecholamine Research, Vol. I,* North-Holland Publishing Co., 1975. pp. 7-14.

165. Ma, S. *University of Oklahoma,* 1995. (UnPub)

166. Halliwell, B. Reactive Oxygen Species and the Central Nervous System. *J.Neurochem.* 59:1609-1623, 1992.

167. Halliwell, B. and Gutteridge, J.M.C. Oxygen Radicals and the Nervous System. *TINS* January:22-26, 1985.

168. Cohen, G. Catalase, Glutathione Peroxidase, Superoxide Dismutase, and Cytochrome P-450. In: *Handbookof Neurochemistry,* Vol. 4, 1997.

169. Buettner, G.R., Doherty, T.P. and Patterson, L.K. The Kinetics of the Reaction of Superoxide Radical with Fe(III) Complexes of EDTA, DETAPAC and HEDTA. *FEBS* 158:143-146, 1983.

170. Winston, G.W., Feierman, D.E. and Cederbaum, A.I. The Role of Iron Chelates in Hydroxyl Radical Production by Rat Liver Microsomes, NADPH-Cytochrome P-450 Reductase and Xanthine Oxidase. *Arch.Biochem.Biophys.* 232:378-390, 1984.

171. Mentasti, E., Pelizzetti, E. and Baiocchi, C. Interactions of Fe(III) with Adrenaline, L-Dopa and Other Catechol Derivatives. *J.inorg.nucl.Chem.* 38:2017-2021, 1976.

172. Gee, P. and Davison, A.J. 6-Hydroxydopamine Does Not Reduce Molecular Oxygen Directly, but Requires a Coreductant. *Arch.Biochem.Biophys.* 231(1):164-168, 1984.

173. Heikkila, R.E. and Cabbat, F.S. Inhibition of Iron-Stimulated Catecholamine Degradation by the Iron-Chelators DETAPAC and DESFERAL. *Biochem.Pharmac.* 30(21):2945-2947, 1981.

174. Shachar, D.B., Eshel, G., Fingerg, J.P.M. and Youdim, M.B.H. The Iron Chelator Desferrioxamine (Desferal) Retards 6-Hydroxydopamine-Induced Degeneration of Nigrostriatal Dopamine Neurons. *J.Neurochem.* 56:1441-1444, 1991.

175. Pilebald, E., Slivka, A., Bratvold, D. and Cohen, G. Studies on the Autoxidation of Dopamine: Interaction with Ascorbate. *Arch.Biochem.Biophys.* 263(2):447-452, 1988.

176. Lind, M.D., Hoard, J.L., Harmor, M.J. and Harmor, J.L. Stereochemistry of Ethylenediaminetetraaceto Complexes. *Inorg.Chem.* 3:34-45, 1964.

177. Li, J. and Christensen, B.M. Effects of pH on the Oxidation Pathway of Dopamine and Dopa. *J.Electroanal.Chem.* 375:219-231, 1994.

178. Tzagoloff, A. *Mitochondria*, New York:Plenum Press, 1982. pp. 131-156.

179. Rickwood, D., Wilson, M.T. and Darley-Usmar, V.M. Isolation and Characteristics of Intact Mitochondria. In: *Mitochondria; a Practical Approach*, edited by Darley-Usmar, V.M., Rickwood, D. and Wilson, M.T. Washington, DC: IRL Press, 1985.

180. Slater, E.C. Energy-Conservation Mechanisms of Mitochondria. *FEBS* 17:205-217, 1969.

181. Wainio, W.W. *The Mammalian Mitochondrial Respiratory Chain*, New York:Academic Press, 1970.

182. Chance, B. and Williams, G.R. The Respiratory Chain and Oxidative Phosphorylation. *Adv.Enzymol.* 17:65-132, 1956.

183. Nedergaard, J. and Cannon, B. Overview-Preparation and Properties of Mitochondria from Different Sources. *Meth.Enzymol.* LV:9-18, 1979.

184. Jenner, P. Clues to the Mechanism Underlying Dopamine Cell Death in Parkinson's Disease. *J.Neurol.Neurosurg.Psych.* Special Supplement:22-28, 1989.

185. Krieglstein, J. and Nuglisch, J. Metabolic Disorders as Consequences of Drug-Induced Energy Deficits. In: *Handbook of Experimental Pharmacology, Vol.102*, edited by Herken, H. and Hucho, F. New York: Springer-Verlag, 1992.

186. Van Dam, K. and Wiechmann, A.H.C.A. Respiratory Control and Oxidative Phosphorylation Measurements in Mitochondria. *Meth.Enzymol.* LV:225-229, 1979.

187. Slater, E.C. Application of Inhibitors and Uncouplers for a Study of Oxidative Phosphorylation. In: *Biochemistry of Mitochondria*, edited by Slater, E.C., Kaiuga, Z. and Wojtczak, L. New York: Academic Press, 1967, p. 48-57.

188. Fleischer, S., McIntyre, J.O. and Vidal, J.C. Large-Scale Preparation of Rat Liver Mitochondria in High Yield. *Meth.Enzymol.* LV:32-39, 1979.